University of São Paulo
"Luiz de Queiroz" College of Agriculture

Iron geochemistry in tropical estuarine soils affected by anthropic and natural disasters

Hermano Melo Queiroz

Thesis presented to obtain the degree of Doctor in Science: Area: Soil and Plant Nutrition

Piracicaba
2021

Hermano Melo Queiroz
Agronomist

Iron geochemistry in tropical estuarine soils affected by anthropic and natural disasters

versão revisada de acordo com a resolução CoPGr 6018 de 2011

Advisor:
Prof. Dr. **TIAGO OSÓRIO FERREIRA**

Thesis presented to obtain the degree of Doctor in Science: Area: Soil and Plant Nutrition

Piracicaba
2021

Dados Internacionais de Catalogação na Publicação
DIVISÃO DE BIBLIOTECA – DIBD/ESALQ/USP

Queiroz, Hermano Melo

Iron geochemistry in tropical estuarine soils affected by anthropic and natural disasters / Hermano Melo Queiroz. - - versão revisada de acordo com a resolução CoPGr 6018 de 2011. - - Piracicaba, 2021.

254 p.

Tese (Doutorado) - - USP / Escola Superior de Agricultura “Luiz de Queiroz”.

1. Mudanças climáticas 2. Manguezais 3. Desastre de Mariana 4. Metais 5. Eutrofização 6. Pedogênese I. Título

To my beloved wife Juliana, to my parents Guaracy Jardel and Ana Maria. Thank you for all your love, trust, inspiration, support, and encouragement towards my career decisions.

I dedicate to you

ACKNOWLEDGMENTS

I would like to thank the following people and institutions who significantly contributed to the success of this work, only through their support this work was possible:

To the University of São Paulo - "Luiz de Queiroz" College of Agriculture (ESALQ-USP) and to the Graduate Program in Soil and Plant Nutrition, for all the support and oportunity to get my Doctor in Science degree.

To University of California, Riverside, Departament of Environmental Sciences, and Dirty Lab for providing infrastructural support during my research internship.

To São Paulo Research Foundation (FAPESP) for my doctorate and research internship abroad (BEPE) scholarships granted (processes: 2018/04259-2 and 2019/17413-2). Also, I thank the Brazilian Federal Agency for the Support and Evaluation of Graduate Education (CAPES) for the national scholarship provided in the beginning of my doctorate and to Espírito Santo Research Foundation (FAPES) for the financial support through project Soils and benthic ecosystems network on the assessment of environmental mine tailing impacts in the Rio Doce estuary, Eastern Brazil.

To my Wife, Juliana Costa who always support me from my undergraduate to a college career, always with comprehension, love, compassion, friendship, and patience. Thank you for the love that you give to me every day. You are a blessing to my life. None of this would have been possible without you here. You inspire me, I LOVE YOU!!

To my parents. Ana Maria my mother, for everything in my life and all their love, my father, Guaracy Jardel who from heaven, I'm sure, is supporting me. Thanks to my brother, Alano, and my sisters-in-law Mariana and Bruna. To my aunties Marlene and Jaci (Nenê) for care, love, and support. I LOVE you all !!

To professor Tiago Osório Ferreira (advisor), an example of a dedicated professor and enthusiastic scientist who became a close friend. You are an inspiration for me as a researcher, professor, and person. I'm more than grateful for all knowledge and patience along all my scientific career since the undergraduate course.

To professor Gabriel Nuto Nóbrega, who always encouraged and supported me in my development as a researcher since fieldwork, laboratory, and writing. My thanks for your enthusiasm, all work together, and for being a great friend! I'm grateful for all knowledge shared since the undergraduate course.

To professor Xosé L. Otero who always encouraged me to the enhancement of my skills as a researcher and always contributed valuably to my scientific progress.

To professor Angelo Fraga Bernardino for the support to develop this work, always encouraged and contributing valuably to my scientific progress.

My supervisor, professor Samantha C. Ying for accepting me as a visiting scholar in your research team. I'm very grateful for your hospitality, patience, friendship, provided infrastructure, and valuable mentorship in my research internship abroad.

To all professors of the Soil Science Departament, especially to Fernando Andreote, Pablo Vidal-Torrado, and Antônio Azevedo.

To all staff of the Soil Departament and Graduate Studies Office, especially to Leandro Goia (Tirolez), Marina Colzato, Rodrigo Alves Pessanha, Paulo Jaoudé, Nivanda, Rossi, Dorival, Sonia Moraes, Luiz Silva, and Ednéia Cristina.

To GEPGeoq members and past members who I still hold dear, Isadora Bragantini, Diego Barcellos, Francisco Ruiz, Laís Jimenez, Elves Barreto, Glêvia Lima, Aaron, Alexys Boim, Beatriz Marchese, Fábio Perlatti, Geraldo, Mateus, Rodolfo Fagundes, Thayana, Verónica Fandiño, Maíra Kanegae, Suzana, and Bárbara Machado. A special thanks to Danilo Romero, Amanda Duim, Renata Bovi, and Lucas Resmini for the companionship during the period in Piracicaba.

To Dirty Lab members, Claudia C. Avila, Leia (the cutest soil scientist, Ph. Dawg), Miranda Aiken, Shuhan Tian, Danielle Stevenson, Phoebe Ly, Abdi Garniwan, and Thomas Haensel. A special thanks to Benjamin Maki, Macon Abernathy, and Dr. Wen Zhuang for the friendship during the period in the Dirty Lab.

To the very sweet family, Raul, Mary, and sons for the hospitality during the period in Riverside. To Mauro and Karyn for the hospitality and solicitousness. A special thank for Assunta Maria (Sunnie) and Rosedith (Rosita) for the friendship, companionship, affection, and hospitality during the period in Riverside, CA.

To friends that I met in Piracicaba, Isabela Silva, Douglas Viana, Samuel de Paula, Aline Martíni, Matheus Barreto, Gustavo Valani, Ana Luisa, Karina Marques, Arnaldo Souza, Caroline Jardim, Mariane Chiapini, Marcos Siqueira (Tucano), and Beatriz Motta.

To the friends from Espírito Santo who always helped me in the fieldwork at Doce River estuary, Luiz Gomes Lucas Vescovi, and Fabrício Gabriel.

To the old friends from Ceará, Danilo Marques, Diego Ricarte, Gustavo Galeazzi, Gabriel Castro, Daniel Pontes, Gislaine Albuquerque, Juliana Vieira, and Adriana Guirado.

And to all those, who directly or indirectly, contributed to the accomplishment of this thesis.

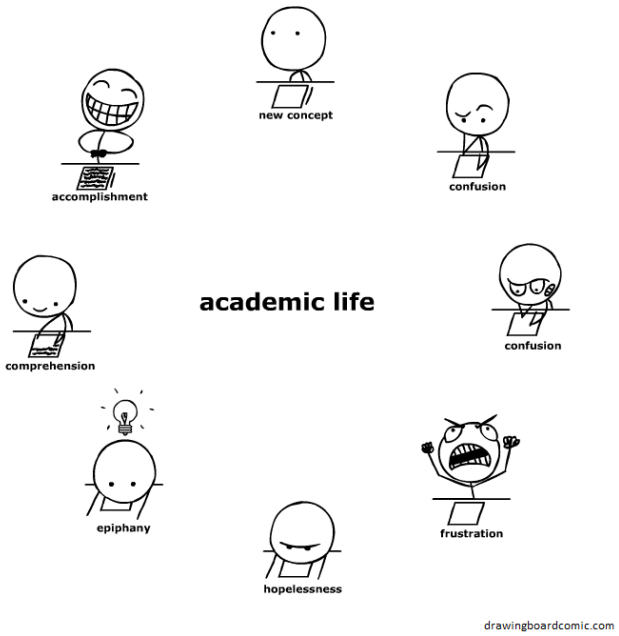
accomplishment
new concept
confusion
comprehension
academic life
confusion
epiphany
hopelessness
frustration
drawingboardcomic.com

RESUMO 11

ABSTRACT 13

1. GENERAL INTRODUCTION 15

REFERENCES 17

2. CHANGES IN SOIL IRON BIOGEOCHEMISTRY IN RESPONSE TO EXTENSIVE MANGROVE MORTALITY ... 27

ABSTRACT 27

2.1. INTRODUCTION 28

2.2. MATERIAL AND METHODS 30

2.2.1. STUDIED SITES AND SOIL SAMPLING 30

2.2.2. DETERMINATION OF SOIL ORGANIC CARBON AND SOIL CARBON STOCKS 32

2.2.3. FE SEQUENTIAL EXTRACTIONS 32

2.2.4. STATISTICAL ANALYSES 33

2.3. RESULTS 34

2.3.1. PHYSICOCHEMICAL CONDITIONS 34

2.3.2. SOIL CARBON STOCKS 35

2.3.3. FE SEQUENTIAL EXTRACTION AND DEGREE OF FE PYRITIZATION 35

2.4. DISCUSSION 38

2.4.1. BIOGEOCHEMICAL CHANGES UPON MAGROVE MORTALITY 38

2.4.2. ENVIRONMENTAL CONSEQUENCES 42

2.5. CONCLUSIONS 44

REFERENCES 45

3. THE SAMARCO MINE TAILING DISASTER: A POSSIBLE TIME-BOMB FOR HEAVY METALS CONTAMINATION? 58

ABSTRACT 58

3.1. INTRODUCTION 59

3.2. MATERIALS AND METHODS 60

3.3. RESULTS 62

3.3.1. ANALYSIS OF TAILINGS 62

3.3.2 SOIL PROPERTIES AND COMPOSITION 67

3.3.3 TOTAL CONTENTS AND METAL PARTITIONING IN SOILS 68

3.4. DISCUSSION 70

3.5. CONCLUSIONS 75

ACKNOWLEDGEMENTS 76

REFERENCES 76

SUPPLEMENTARY MATERIAL 83

4. ROLE OF FE DYNAMIC IN RELEASE OF METALS AT RIO DOCE ESTUARY: UNFOLDING OF A MINING DISASTER 89

ABSTRACT 89

ACKNOWLEDGMENTS 99

REFERENCES 100

SUPPLAMENTARY MATERIAL 107

5. MANGANESE: THE OVERLOOKED CONTAMINANT IN THE WORLD LARGEST MINE TAILINGS DAM COLLAPSE 109

ABSTRACT 109

5.1. INTRODUCTION 110

5.2. MATERIAL AND METHODS 112

5.2.1. SITE DESCRIPTION 112

5.2.2. SAMPLE COLLECTION 113

5.2.3. TOTAL CONTENTS AND SEQUENTIAL EXTRACTION OF FE AND MN 114

5.2.4. X-RAY ABSORPTION SPECTROSCOPY 115

5.2.5. DIFFUSE REFLECTANCE SPECTROSCOPY 116

5.2.6. FISH COLLECTION AND ANALYSES OF METAL CONTENTS IN TISSUES 117

5.2.7. CONTAMINATION FACTOR DETERMINATION 117

5.2.8. STATISTICAL ANALYSES 118

5.3. RESULTS 118

5.3.1. PHYSICOCHEMICAL CONDITIONS, FE AND MN TOTAL CONTENTS AND FRACTIONATING 118

5.3.2. SPECTRAL REFLECTANCE CHARACTERISTICS 122

5.3.3. XANES AND EXAFS CHARACTERIZATION 123

5.3.4. MN IN WATER AND IN FISH TISSUES 126

5.4. DISCUSSION 128

5.4.1. MINING TAILING DISASTER AND ITS IMPACTS ON MN GEOCHEMISTRY 128

5.4.2. ENVIRONMENTAL CONSEQUENCES 132

5.5. CONCLUSIONS 136

ACKNOWLEDGMENTS 137

REFERENCES 138

SUPPLEMENTARY MATERIAL 151

REFERENCES (SUPPLEMENTARY MATERIAL) 153

6. FROM SINKS TO SOURCES: THE ROLE OF FE OXYHYDROXIDE TRANSFORMATIONS ON PHOSPHORUS DYNAMICS IN ESTUARINE SOILS 155

ABSTRACT 155

6.1. INTRODUCTION 156

6.2. MATERIAL AND METHODS 158

6.2.1. SITE DESCRIPTION, SAMPLING, AND IN-SITU MEASUREMENTS 158

6.2.2. CHEMICAL AND MINERALOGICAL ANALYSES OF THE SOIL AND WATER SAMPLES 160

6.2.3. THE FREUNDLICH AND LANGMUIR ADSORPTION ISOTHERMS 161

6.2.4. STATISTICAL ANALYSES 162

6.3. RESULTS 162

6.3.1. IRON FRACTIONATING AND TOTAL CONTENTS OF IRON AND PHOSPHORUS 162
6.3.2. FE-RICH MINE TAILINGS MINERALOGICAL CHARACTERISTICS 164
6.3.3. SORPTION ISOTHERMS 165
6.3.4. DISSOLVED P CONTENTS IN ESTUARY WATER 166
6.4. DISCUSSION 167
6.4.1. THE PHOSPHORUS IN THE RIO DOCE ESTUARY: CONTENTS AND SOURCES 167
6.4.2. CHANGES IN P AVAILABILITY OVER TIME 171
6.4.3. RISKS OF EUTROPHICATION IN THE ESTUARINE SOILS OF RIO DOCE 174
6.5. CONCLUSIONS 176
ACKNOWLEDGMENTS 177
REFERENCES 177
SUPPLEMENTARY MATERIAL 191
7. IRON-RICH TAILINGS UNDER A REDOX ACTIVE ENVIRONMENT: MINERALOGICAL CHANGES AND POTENTIAL ENVIRONMENTAL CONSEQUENCES 193
ABSTRACT 193
7.1. INTRODUCTION 194
7.2. MATERIALS AND METHODS 196
7.2.1. STUDY SITE AND SAMPLING 196
7.2.2. X-RAY DIFFRACTION AND CALCULATING OF MEAN CRYSTAL SIZE (MCS) 198
7.2.3. ATTENUATED TOTAL REFLECTANCE FOURIER TRANSFORM INFRARED (ATR-FTIR) 198
7.2.4. SCANNING ELECTRON MICROSCOPY – SEM ANALYSIS 198
7.2.5. FE SEQUENTIAL CHEMICAL EXTRACTION 199
7.3. RESULTS 199
7.3.1. PHYSICOCHEMICAL CONDITIONS 199
7.3.2. X-RAY DIFFRACTION AND MEAN CRYSTAL SIZE RESULTS (MCS) 200
7.3.3. ATR-FTIR RESULTS 202
7.3.4. SEM-EDS RESULTS FROM TAILINGS AND SAMPLES FROM THE DOCE RIVER ESTUARY 204
7.3.5. SEQUENTIAL EXTRACTION OF FE 205
7.4. DISCUSSION 207
7.4.1. THE PHYSICOCHEMICAL CHANGES 207
7.4.3. POTENTIAL ENVIRONMENTAL IMPLICATIONS 210
7.5. CONCLUSIONS 211
ACKNOWLEDGMENTS 212
REFERENCES 212
8. FROM MUD TO SOILS: EARLY PEDOGENESIS OF ANTHROPOGENIC SOILS PRODUCED BY THE WORLD LARGEST MINING DISASTER 223
ABSTRACT 223
8.1. INTRODUCTION 223
8.2. MATERIALS AND METHODS 225

8.2.1. SITE DESCRIPTION 225
8.2.2. FIELD WORK: SAMPLING, SOIL DESCRIPTION, AND IN SITU MEASUREMENTS 226
8.2.3. PHYSICAL, CHEMICAL, AND MINERALOGICAL ANALYSIS OF SOIL AND TAILING SAMPLES 229
8.3. RESULTS 229
8.3.1. MINE TAILINGS 229
8.3.2. ANTHROPOGENIC SOIL 232
8.4. DISCUSSION 236
8.5. CONCLUSIONS 244
ACKNOWLEDGMENTS 244
REFERENCES 245
9. FINAL CONSIDERATIONS 253

CONTENTS

RESUMO

Geoquímica do ferro em solos estuarinos tropicais afetados por desastres antrópicos e naturais

Ferro (Fe) é um dos elementos mais abundantes e dinâmicos da Terra. Está presente em rochas, minerais, solos, oceanos e é um elemento essencial para praticamente todos os seres vivos em ecossistemas terrestres. Devido à sua dinâmica no ambiente, o Fe desperta o interesse de diversas áreas da ciência. Para a ciência do solo, a importância desse elemento está principalmente relacionada à sua capacidade de interagir com vários elementos químicos. Nesse sentido, o ciclo biogeoquímico do Fe está diretamente associado aos ciclos de outros elementos, como carbono (C), fósforo (F), enxofre (S) e metais pesados. Em solos estuarinos, a geoquímica do Fe é marcada por um equilíbrio dinâmico regido pelas oscilações redox dos solos nesses ambientes. No entanto, distúrbios antrópicos ou naturais podem afetar o comportamento geoquímico de Fe e, consequentemente, o destino de outros elementos (e.g., C, P, S e metais). Nesse sentido, este estudo teve como objetivos: (i) estudar a geoquímica do Fe em solos estuarinos tropicais afetados por impactos antrópicos e naturais; e (ii) avaliar o controle da geoquímica do Fe sobre a dinâmica de outros elementos, como metais traço, P, S e C. Para isso, dois estuários tropicais, afetados por desastres antrópicos (i.e., afetados por deposição de rejeitos de Fe) e naturais (morte maciça de mangue) foram avaliados. Observamos uma mudança significativa nas condições físico-químicas dos solos após uma enorme mortalidade da floresta de mangue. Os solos dos manguezais mortos mudaram de um ambiente predominantemente anóxico para um ambiente subóxico. Essa mudança resultou em uma redução de 50% nos teores de Fe do solo. As perdas de Fe foram principalmente associadas às frações pirita e oxihidróxidos de Fe de baixa cristalinidade. Além disso, estimamos uma perda de 170 toneladas de Fe dos 500 hectares de florestas de mangue mortas. Além disso, o processo de piritização foi profundamente comprometido e, portanto, a capacidade das florestas de mangue de fornecer serviços ecossistêmicos, como retenção de poluentes (ou seja, metais) e sequestro de carbono. Em outro cenário, o estuário do Rio Doce recebeu cerca de 60 milhões de m^3 de rejeitos ricos em Fe após o rompimento da barragem de Fundão. O comportamento biogeoquímico do Fe controlou o destino dos metais, P, e a pedogênese dos solos estuarinos após este evento, reconhecido como o maior desastre de mineração do mundo. Os rejeitos, principalmente compostos por oxihidróxidos de Fe de alta cristalinidade (e.g., goethita e hematita), foram transportados por 600 km direção ao estuário. Ao longo deste caminho, os rejeitos atuaram como um transportador de contaminantes (e.g., metais) e grandes quantidades de P. Após a chegada dos rejeitos, observou-se aumento expressivo dos teores de P e metais nos solos estuarinos. Esses poluentes foram predominantemente associados aos oxihidróxidos de Fe. Com o passar do tempo, a deposição de rejeitos favoreceu o estabelecimento e o crescimento de plantas que promoveram aporte de C no solo e drásticas mudanças físico-químicas. Essas mudanças resultaram em um ambiente de redução favorável à redução do Fe microbiano e um aumento das formas de Fe de baixa cristalinidade (e.g., ferrihidrita e lepidocrocita). Essas condições levaram à dissolução redutiva dos oxihidróxidos de Fe, perdas de Fe e aumento da biodisponibilidade de metais. Dentre os metais estudados, o manganês (Mn) apresentou as maiores perdas no solo e aumento de 880% na água estuarina. O aumento da biodisponibilidade de Mn levou a um aumento dos níveis de Mn no fígado e músculos dos peixes comumente consumidos pela população local. A dinâmica de Fe recém-estabelecida desencadeou liberações maciças de Mn e altos riscos de contaminação. Nesse

contexto, um comportamento semelhante foi observado para P. As mudanças associadas à redução dissimilatória do Fe levaram a um aumento do P prontamente disponível nos solos estuarinos e na água. Além disso, nossos resultados indicam que os oxihidróxidos de Fe atuam como uma fonte contínua de P dissolvido para o ecossistema, e que os rejeitos, ricos em Fe, depositados no ecossistema estuarino podem estar ligados a um potencial processo de eutrofização. No entanto, dentro de quatro anos após o desastre, o crescimento da vegetação sobre os rejeitos depositados desencadeou a formação de um solo no estuário. diferentes processos pedogenéticos foram descritos e evidenciados (e.g., melanização, bioturbação, incipiente paludização e gleização). O Technossolo recém-formado mostrou evidências de potencialmente fornecer serviços ecossistêmicos, como sequestro de carbono e ciclagem de nutrientes, que antes não eram fornecidos no estuário. Em resposta às mudanças biogeoquímicas, observamos uma perda maciça de Fe dos solos estuarinos, que pode representar uma importante fonte de Fe do estuário para as águas do oceano. A entrada de Fe nos oceanos (i.e., a fertilização dos oceanos com Fe) está diretamente associada à produtividade marinha e ao fornecimento de serviços, como o sequestro de carbono. Assim, este estudo traz uma nova abordagem de como os impactos antrópicos ou naturais podem alterar a dinâmica do Fe em ecossistemas costeiros e como isso afeta os ciclos de outros elementos importantes tanto para o estuário quanto para os ambientes adjacentes.

Palavras-chave: Mudanças climáticas, Manguezais, Desastre de Mariana, Metais, Eutrofização, Pedogênese

ABSTRACT

Iron geochemistry in tropical estuarine soils affected by anthropic and natural disasters

Iron (Fe) is one of the most abundant and dynamic elements on Earth. It is present in rocks, minerals, soils, oceans, and is an essential element for virtually all living beings on terrestrial ecosystems. Due to its dynamics in the environment, Fe arouses the interest of several science fields. For soil science, the importance of this element is mostly related with its ability to interact with various chemical elements. In this sense, the Fe biogeochemical cycle is directly associated with cycles of other elements such as carbon (C), phosphorus (F), sulfur (S), and heavy metals. In estuarine soils, Fe geochemistry is marked by a dynamic equilibrium ruled by the redox oscillations active in these environments. However, anthropic or natural disturbances may affect the Fe geochemical behavior and consequently the fate of other associated elements (e.g., C, P, S, and metals). In this sense, this study had as objectives: (i) to study the Fe geochemistry in tropical estuarine soils affected by both anthropic and natural impacts and (ii) to assess the control of Fe geochemistry over the dynamic of other elements, such as trace metals, P, S, and C. To achieve these objectives, two tropical estuaries, affected by anthropic (i.e., affected by iron tailing deposition) and natural (massive mangrove dieback) disasters were evaluated. We observed a significant change in physicochemical conditions of soils after a massive mangrove forest mortality. The soils from dead mangroves changed from a chiefly anoxic environment to a suboxic environment. This change resulted in a decrease by 50% in the soils Fe contents. The Fe losses were mostly associated with the pyrite and low crystallinity Fe oxyhydroxides fractions. In addition, we estimated a loss of 170 tons of Fe from the 500 hectares of dead mangrove forests. Ultimately, the pyritization process was deeply compromised and therefor the capacity of mangrove forests to provide ecosystem services such as pollutant (i.e., metals) retention and carbon sequestration. In another scenario, the Rio Doce estuary received about 60 million m^3 of Fe-rich tailings after Fundão dam rupture. the Fe biogeochemical behavior controlled the fate of metals, P, and the pedogenesis of estuarine soils after this event recognized as the world's largest mining disaster. The tailings, mostly composed of high crystallinity Fe oxyhydroxides (e.g., goethite and hematite), were transported 600 km downstream towards the estuary. Throughout this path, the tailings acted as a carrier of contaminants (e.g., metals) and large amounts of P. An expressive increase of P and metals contents in the estuarine soils were observed after the arrival of the tailings. These pollutants were predominantly associated with Fe oxyhydroxides. Over time, the tailings' deposition favored the establishment and growth of plants which promoted a soil C input and drastic physicochemical changes. These changes resulted in a reducing environment favorable to microbial Fe reduction and an increase of low crystallinity Fe forms (e.g., ferrihydrite and lepidocrocite). These conditions led to the reductive dissolution of Fe oxyhydroxides, Fe losses, and an increased bioavailability of metals. Among the studied metals, manganese (Mn) showed the highest losses in the soil and an increase of 880% in the estuarine water. The increase in Mn bioavailability led to an increase of Mn levels in the liver and muscles of fish commonly consumed by the local population. The newly established Fe dynamic triggered massive Mn releases and high contamination risks. In this context, a similar behavior was observed for P. The changes associated with the dissimilatory Fe reduction led to an increase of readily available P in the estuarine soils and water. Moreover, our results indicate that Fe oxyhydroxides are a continuous source of dissolved P for the ecosystem, and that the Fe-rich tailings deposited in the estuarine ecosystem may be linked to a potential eutrophication

process. Nevertheless, within four years after the disaster, the vegetation growth on the deposited tailings triggered the soil formation in the estuary. different pedogenetic processes were described and evidenced (e.g., melanization, bioturbation, incipient paludization, and gleization). The newly formed Technosol showed evidences of potentially providing ecosystem services such as carbon sequestration and nutrient cycling that were previously unprovided in the estuary. In response to the biogeochemical changes, we observed a massive Fe loss from the estuarine soils which may represent an important Fe source from the estuary to the ocean waters. The Fe input into oceans (i.e., Fe ocean fertilization) is directly associated with marine productivity and the providing of services such as carbon sequestration. Thus, this study brings a novel approach to how anthropic or natural impacts may alter Fe dynamics in coastal ecosystems and how this affects the cycles of other important elements both to the estuary and the adjacent environments.

Keywords: Climate change, Mangrove, Mariana’s disaster, Metals, Eutrophication, Pedogenesis

1. GENERAL INTRODUCTION

Iron (Fe) is one of the most abundant elements on earth (Schwertmann and Taylor, 1989). It is present in a great variety of natural materials such as rocks, minerals, soils, oceans and rivers (Faivre and Frankel, 2016) Iron is an essential element for almost all organisms living on Earth ecosystems (Sánchez et al., 2017; Selinus et al., 2013). Most Fe in nature is found as oxides and hydroxides minerals produced by the alteration of a pre-existing minerals, precipitation from natural solutions, or transported as residual mineral phases (Faivre and Frankel, 2016). A geochemical approach on Fe abundance and its applications range from its mineral formation, to the mining industry, high tech industry, medicine, art, global climate change (Cornell and Schwertmann, 2003; Faivre and Frankel, 2016). The different implications of Fe biogeochemistry arouse a great interest by different science fields (Bigham et al., 2002; Lam et al., 2008; Magro et al., 2018; Navrotsky et al., 2008; Sánchez et al., 2017; Selinus et al., 2013).

For soil scientists Fe stands out due to its participation in several important geochemical processes, such as isomorphic substitutions, redox processes, nutrient cycling, adsorption of contaminants, organic matter stabilization (Cornell and Schwertmann, 2003; Faivre and Frankel, 2016; Reddy and DeLaune, 2008; Schwertmann and Taylor, 1989). Fe dynamics in soils is mostly associated with its mineralogical characteristics, oxidation states (i.e., Fe^{3+} or Fe^{2+}), and interactions with various other biogeochemical cycles e.g., oxygen, phosphorus, carbon, manganese, nitrogen, and sulphur (Faivre and Frankel, 2016; Raiswell and Canfield, 2012; Reddy and DeLaune, 2008). Their small particle size (as small as 1 or 2 nanometers), large specific surface area (up to 600 $m^2\ g^{-1}$), and structural ordering, makes iron oxides one of the most reactive group of minerals in the terrestrial environments (Cornell and Schwertmann, 2003; Roden and Zachara, 1996).

From a pedogenetic point of view Fe plays a key role in wide a range of soil forming processes (e.g., *ferrolysis*, *gleization*, *laterization*, *brunification*, *rubification*, *ferritization*, and *pyritization*; Duball et al., 2020; Schaetzl and Thompson, 2015; Schwertmann, 1958). From an environmental point of view, Fe oxyhydroxides are known for their capacity to decrease the bioavailability of heavy metals in soils under oxidic environments (Gadepalle et al., 2007; Herbert, 1996; Li et al., 2019). Under oxic conditions, Fe oxyhydroxides may retain metals through adsorption complexes (Cornell and Schwertmann, 2003), forming mono- and bi-

nuclear complexes (Arai and Sparks, 2001; Stumm, 1995) which are stable and virtually irreversible leading to metals immobilization (Buerge-Weirich et al., 2002; Cui et al., 2020; Herbert, 1996; Randall et al., 1999). Additionally, Fe oxyhydroxides are also known to form strong surface complexes with phosphorus (P) limiting their availability in the soil environment (Arias et al., 2006; Yan et al., 2016). These Fe–P interactions play a key role on P retention and immobilization and, in most soils, limits the availability of P (Cui et al., 2011; Fink et al., 2016). In fact, Fe–P interactions are among the most important mechanisms regulating P fluxes from soils to other terrestrial reservoirs, such as oceans and lakes (Fink et al., 2016; Werner and Ami, 2014). The role of Fe oxyhydroxides in controlling the availability of metals and P in oxidic soil conditions is a consequence of their high stability in these environments (Fink et al., 2016; Inda Junior and Kämpf, 2005; Rieuwerts, 2007; Schaefer et al., 2008). Under oxidizing geochemical conditions and in the absence of complexing (e.g., organic compounds) Fe oxyhydroxides are highly insoluble (i.e. stable) in a wide pH range (4–10) (Benjamin et al., 1996; Cornell and Schwertmann, 2003; Hartley et al., 2004).

However, in redox-active soils and sediments, different reactions may alter Fe oxyhydroxides stability, and thus, their control over P and metals dynamics (Kraal et al., 2015; Miao et al., 2006). Under redox-active soil environments, due to constant flooding, high organic matter contents, oxygen depletion, and establishment of anaerobic conditions the microbial reduction of sulfate (MRS) and the microbial reduction of Fe (MRFe) are considered the main metabolic pathways responsible soil respiration (Ferreira et al., 2007; Kristensen et al., 2008).

The MRFe leads to the dissolution Fe oxyhydroxides and the subsequent release of the previously sorbed elements (e.g., phosphorus and/or metals) (Du Laing et al., 2009; Kraal et al., 2015; Pan et al., 2019; Zachara et al., 2001). In fact, several studies have reported the increase of P and metals availability in wetland soils and waters as a result of MRFe (Khan et al., 2019; Li et al., 2012; Murray and Hesterberg, 2006 Du Laing et al., 2009; Miao et al., 2006; Tack et al., 2006; Zhang et al., 2012).

On the other hand, both MRFe and MRS are poorly efficient pathways of soil organic matter decomposition. (Alongi, 2020; Hyun et al., 2017; Marchand, 2017). These less efficient metabolisms are recognized as a key piece on climate warming mitigation and for decreasing carbon concentrations from the atmosphere (Alongi, 2012; Brodersen et al., 2019; Mitsch et al., 2013). Moreover, the MRS and MRFe pathways may lead to pyrite formation; a highly

stable Fe sulfide formed under anoxic conditions and widely known for its capacity to immobilize metals (Huerta-Diaz and Morse, 1992; Lin and Morse, 1991; Machado et al., 2014; Nóbrega et al., 2013; Ye et al., 2010).

Thus, the environmental conditions will determine both the type and intensity of the active biogeochemical processes in wetland soils (Hedges, 1992; Megonigal and Neubauer, 2018). Several studies have reported changes in the biogeochemical processes as a result of anthropic and natural impacts (Ahmed et al., 2017; Bao et al., 2013; Chowdhury et al., 2017; Kauffman et al., 2018; Duke et al., 2007; Lovelock et al., 2017; Sippo et al., 2020; Ward et al., 2016). Among the main impacts are pollution (e.g., discharge of wastes), land-use change, deforestation, sea-level rise, extreme climatic events (heavy rainfall, windstorms, or tsunamis), changes in rainfall patterns, and severe droughts (Bao et al., 2013; Bindoff et al., 2019; Borges et al., 2009; Doney et al., 2012; Lacerda et al., 2008; Sandilyan and Kathiresan, 2014). These environmental impacts directly affect the well-functioning of diverse biogeochemical cycles (e.g., C, P, S, and heavy metals) which are closely associated with the Fe biogeochemical cycle (Cabrera et al., 1981; Jian et al., 2017; Nóbrega et al., 2014; Parsons et al., 2017)

Therefore, the biogeochemical behavior of Fe in wetlands plays a key role in the dynamics, cycle, and fate of different chemical elements (e.g., S, C, P, heavy metals) (Buesseler and Andrews, 2004; Falkowski, 2000; Jickells, 2005). In this sense, the objectives of the present work were: (i) to study the Fe geochemistry in tropical estuarine soils affected by both anthropic and natural impacts and (ii) to assess the control of Fe geochemistry over the dynamic of other elements, such as trace metals, P, S, and C. This study brings new insights regarding on the sensitivity and resilience of tropical estuarine ecosystems in the face of man-produced and natural impacts.

References

Ahmed, N., Cheung, W.W.L., Thompson, S., Glaser, M., 2017. Solutions to blue carbon emissions: Shrimp cultivation, mangrove deforestation and climate change in coastal Bangladesh. Mar. Policy 82, 68–75. https://doi.org/10.1016/j.marpol.2017.05.007

Alongi, D.M., 2020. Carbon Balance in Salt Marsh and Mangrove Ecosystems: A Global Synthesis. J. Mar. Sci. Eng. 8, 767. https://doi.org/10.3390/jmse8100767

Alongi, D.M., 2012. Carbon sequestration in mangrove forests. Carbon Manag. 3, 313–322. https://doi.org/10.4155/cmt.12.20

Arai, Y., Sparks, D.L., 2001. ATR–FTIR Spectroscopic Investigation on Phosphate Adsorption Mechanisms at the Ferrihydrite–Water Interface. J. Colloid Interface Sci. 241, 317–326. https://doi.org/10.1006/jcis.2001.7773

Arias, M., Da Silva-Carballal, J., García-Río, L., Mejuto, J., Núñez, A., 2006. Retention of phosphorus by iron and aluminum-oxides-coated quartz particles. J. Colloid Interface Sci. 295, 65–70. https://doi.org/10.1016/j.jcis.2005.08.001

Bao, H., Wu, Y., Unger, D., Du, J., Herbeck, L.S., Zhang, J., 2013. Impact of the conversion of mangroves into aquaculture ponds on the sedimentary organic matter composition in a tidal flat estuary (Hainan Island, China). Cont. Shelf Res. 57, 82–91. https://doi.org/10.1016/j.csr.2012.06.016

Benjamin, M.M., Sletten, R.S., Bailey, R.P., Bennett, T., 1996. Sorption and filtration of metals using iron-oxide-coated sand. Water Res. 30, 2609–2620. https://doi.org/10.1016/S0043-1354(96)00161-3

Bigham, J.M., Fitzpatrick, R.W., Schulze, D.G., 2002. Iron Oxides, in: Soil Mineralogy with Environmental Applications. Soil Science Society of America, Madison, Wisconsin, pp. 323–366. https://doi.org/10.2136/sssabookser7.c10

Bindoff, N.L., Cheung, W.W.L., Kairo, J.G., Arístegui, J., Guinder, V.A., Hallberg, R., Hilmi, N., Jiao, N., Karim, M.S., Levin, L., O'Donoghue, S., Cuicapusa, S.R.P., Rinkevich, B., Suga, T., Tagliabue, A., Williamson, P., 2019. Changing Ocean, Marine Ecosystems, and Dependent Communities, in: Pörtner, H.-O., Roberts, D.C., Masson-Delmotte, V., Zhai, P., Tignor, M., Poloczanska, E., Mintenbeck, K., Alegría, A., Nicolai, M., Okem, A., Petzold, J., Rama, B., Weyer, N.M. (Eds.), IPCC Special Report on the Ocean and Cryosphere in a Changing Climate. p. In press.

Borges, A.C., Sanders, C.J., Santos, H.L.R., Araripe, D.R., Machado, W., Patchineelam, S.R., 2009. Eutrophication history of Guanabara Bay (SE Brazil) recorded by phosphorus flux to sediments from a degraded mangrove area. Mar. Pollut. Bull. 58, 1750–1754. https://doi.org/10.1016/j.marpolbul.2009.07.025

Brodersen, K.E., Trevathan-Tackett, S.M., Nielsen, D.A., Connolly, R.M., Lovelock, C.E., Atwood, T.B., Macreadie, P.I., 2019. Oxygen consumption and sulfate reduction in vegetated coastal habitats: Effects of physical disturbance. Front. Mar. Sci. 6. https://doi.org/10.3389/fmars.2019.00014

Buerge-Weirich, D., Hari, R., Xue, H., Behra, P., Sigg, L., 2002. Adsorption of Cu, Cd, and Ni on goethite in the presence of natural groundwater ligands. Environ. Sci. Technol. 36, 328–336. https://doi.org/10.1021/es010892i

Buesseler, K.O., Andrews, J.E., 2004. The Effects of Iron Fertilization. Science (80-.). 304, 414–417.

Cabrera, F., de Arambarri, P., Madrid, L., Toga, C.G., 1981. Desorption of phosphate from iron oxides in relation to equilibrium pH and porosity. Geoderma 26, 203–216. https://doi.org/10.1016/0016-7061(81)90016-1

Chowdhury, R.R., Uchida, E., Chen, L., Osorio, V., Yoder, L., 2017. Anthropogenic drivers of mangrove loss: Geographic patterns and implications for livelihoods, Mangrove Ecosystems: A Global Biogeographic Perspective: Structure, Function, and Services. https://doi.org/10.1007/978-3-319-62206-4_9

Cornell, R.M., Schwertmann, U., 2003. The Iron Oxides: Structure, Reactions, Occurences and Uses, WILEY-VCH. https://doi.org/10.1002/3527602097.ch1

Cui, H.-J., Wang, M.K., Fu, M.-L., Ci, E., 2011. Enhancing phosphorus availability in phosphorus-fertilized zones by reducing phosphate adsorbed on ferrihydrite using rice straw-derived biochar. J. Soils Sediments 11, 1135–1141. https://doi.org/10.1007/s11368-011-0405-9

Cui, H., Zhang, X., Wu, Q., Zhang, S., Xu, L., Zhou, Jing, Zheng, X., Zhou, Jun, 2020. Hematite enhances the immobilization of copper, cadmium and phosphorus in soil amended with hydroxyapatite under flooded conditions. Sci. Total Environ. 708, 134590. https://doi.org/10.1016/j.scitotenv.2019.134590

Doney, S.C., Ruckelshaus, M., Emmett Duffy, J., Barry, J.P., Chan, F., English, C.A., Galindo, H.M., Grebmeier, J.M., Hollowed, A.B., Knowlton, N., Polovina, J., Rabalais, N.N., Sydeman, W.J., Talley, L.D., 2012. Climate Change Impacts on Marine Ecosystems. Ann. Rev. Mar. Sci. 4, 11–37. https://doi.org/10.1146/annurev-marine-041911-111611

Du Laing, G., Rinklebe, J., Vandecasteele, B., Meers, E., Tack, F.M.G., 2009. Trace metal behaviour in estuarine and riverine floodplain soils and sediments: A review. Sci. Total Environ. 407, 3972–3985. https://doi.org/10.1016/j.scitotenv.2008.07.025

Duball, C., Vaughan, K., Berkowitz, J.F., Rabenhorst, M.C., VanZomeren, C.M., 2020. Iron monosulfide identification: Field techniques to provide evidence of reducing conditions in soils. Soil Sci. Soc. Am. J. 84, 303–313. https://doi.org/10.1002/saj2.20044

Duke, N.C., Meynecke, J.-O., Dittmann, S., Ellison, A.M., Anger, K., Berger, U., Cannicci, S., Diele, K., Ewel, K.C., Field, C.D., Koedam, N., Lee, S.Y., Marchand, C., Nordhaus, I., Dahdouh-Guebas, F., 2007. A World Without Mangroves? Science (80-.). https://doi.org/10.1126/science.317.5834.41b

Faivre, D., Frankel, R.B., 2016. Iron Oxides: From Nature to Applications, 1st ed. Wiley-VCH, Weinheim, Germany.

Falkowski, P., 2000. The Global Carbon Cycle: A Test of Our Knowledge of Earth as a System. Science (80-.). 290, 291–296. https://doi.org/10.1126/science.290.5490.291

Ferreira, T.O., Vidal-Torrado, P., Otero, X.L., Macías, F., 2007. Are mangrove forest substrates sediments or soils? A case study in southeastern Brazil. CATENA 70, 79–91. https://doi.org/10.1016/j.catena.2006.07.006

Fink, J.R., Inda, A.V., Tiecher, T., Barrón, V., 2016. Iron oxides and organic matter on soil phosphorus availability. Cienc. e Agrotecnologia 40, 369–379. https://doi.org/10.1590/1413-70542016404023016

Gadepalle, V.P., Ouki, S.K., Van Herwijnen, R., Hutchings, T., 2007. Immobilization of heavy metals in soil using natural and waste materials for vegetation establishment on contaminated sites. Soil Sediment Contam. 16, 233–251. https://doi.org/10.1080/15320380601169441

Hartley, W., Edwards, R., Lepp, N.W., 2004. Arsenic and heavy metal mobility in iron oxide-amended contaminated soils as evaluated by short- and long-term leaching tests. Environ. Pollut. 131, 495–504. https://doi.org/10.1016/j.envpol.2004.02.017

Hedges, J.I., 1992. Global biogeochemical cycles: progress and problems. Mar. Chem. 39, 67–93. https://doi.org/10.1016/0304-4203(92)90096-S

Herbert, R.B., 1996. Metal retention by iron oxide precipitation from acidic ground water in Dalarna, Sweden. Appl. Geochemistry 11, 229–235. https://doi.org/10.1016/0883-2927(95)00070-4

Huerta-Diaz, M.A., Morse, J.W., 1992. Pyritization of trace metals in anoxic marine sediments. Geochim. Cosmochim. Acta 56, 2681–2702. https://doi.org/10.1016/0016-7037(92)90353-K

Hyun, J.-H., Kim, S.-H., Mok, J.-S., Cho, H., Lee, T., Vandieken, V., Thamdrup, B., 2017. Manganese and iron reduction dominate organic carbon oxidation in surface sediments of the deep Ulleung Basin, East Sea. Biogeosciences 14, 941–958. https://doi.org/10.5194/bg-14-941-2017

Inda Junior, A.V., Kämpf, N., 2005. Variabilidade de goethita e hematita via dissolução redutiva em solos de região tropical e subtropical. Rev. Bras. Ciência do Solo 29, 851–866. https://doi.org/10.1590/s0100-06832005000600003

Jian, L., Junyi, Y., Jingchun, L., Chongling, Y., Haoliang, L., Spencer, K.L., 2017. The effects of sulfur amendments on the geochemistry of sulfur, phosphorus and iron in the mangrove plant (Kandelia obovata (S. L.)) rhizosphere. Mar. Pollut. Bull. https://doi.org/10.1016/j.marpolbul.2016.10.070

Jickells, T.D., 2005. Global Iron Connections Between Desert Dust, Ocean Biogeochemistry, and Climate. Science (80-.). 308, 67–71. https://doi.org/10.1126/science.1105959

Kauffman, J.B., Bernardino, A.F., Ferreira, T.O., Bolton, N.W., Gomes, L.E. de O., Nobrega, G.N., 2018. Shrimp ponds lead to massive loss of soil carbon and greenhouse gas emissions in northeastern Brazilian mangroves. Ecol. Evol. 8, 5530–5540. https://doi.org/10.1002/ece3.4079

Khan, I., Fahad, S., Wu, L., Zhou, W., Xu, P., Sun, Z., Salam, A., Imran, M., Jiang, M., Kuzyakov, Y., Hu, R., 2019. Labile organic matter intensifies phosphorous mobilization in paddy soils by microbial iron (III) reduction. Geoderma 352, 185–196. https://doi.org/10.1016/j.geoderma.2019.06.011

Kraal, P., Burton, E.D., Rose, A.L., Kocar, B.D., Lockhart, R.S., Grice, K., Bush, R.T., Tan, E., Webb, S.M., 2015. Sedimentary iron–phosphorus cycling under contrasting redox conditions in a eutrophic estuary. Chem. Geol. 392, 19–31. https://doi.org/10.1016/j.chemgeo.2014.11.006

Kristensen, E., Bouillon, S., Dittmar, T., Marchand, C., 2008. Organic carbon dynamics in mangrove ecosystems: A review. Aquat. Bot. 89, 201–219. https://doi.org/10.1016/j.aquabot.2007.12.005

Lacerda, L.D., Molisani, M.M., Sena, D., Maia, L.P., 2008. Estimating the importance of natural and anthropogenic sources on N and P emission to estuaries along the Ceará State Coast NE Brazil. Environ. Monit. Assess. 141, 149–164. https://doi.org/10.1007/s10661-007-9884-y

Lam, U.T., Mammucari, R., Suzuki, K., Foster, N.R., 2008. Processing of iron oxide nanoparticles by supercritical fluids. Ind. Eng. Chem. Res. 47, 599–614. https://doi.org/10.1021/ie070494+

Li, Q., Wang, X., Kan, D., Bartlett, R., Pinay, G., Ding, Y., Ma, W., 2012. Enrichment of Phosphate on Ferrous Iron Phases during Bio-Reduction of Ferrihydrite. Int. J. Geosci. 03, 314–320. https://doi.org/10.4236/ijg.2012.32033

Li, X. cheng, Yang, Z. zhu, Zhang, C., Wei, J. jing, Zhang, H. qing, Li, Z. hao, Ma, C., Wang, M. sheng, Chen, J. qi, Hu, J. wei, 2019. Effects of different crystalline iron oxides on immobilization and bioavailability of Cd in contaminated sediment. Chem. Eng. J. 373, 307–317. https://doi.org/10.1016/j.cej.2019.05.015

Lin, S., Morse, J., 1991. Sulfate reduction and iron sulfide mineral formation in Gulf of Mexico anoxic sediments. Am. J. Sci. https://doi.org/10.2475/ajs.291.1.55

Lovelock, C.E., Feller, I.C., Reef, R., Hickey, S., Ball, M.C., 2017. Mangrove dieback during fluctuating sea levels. Sci. Rep. 7, 1680. https://doi.org/10.1038/s41598-017-01927-6

Machado, W., Borrelli, N.L., Ferreira, T.O., Marques, A.G.B., Osterrieth, M., Guizan, C., 2014. Trace metal pyritization variability in response to mangrove soil aerobic and anaerobic oxidation processes. Mar. Pollut. Bull. 79, 365–370. https://doi.org/10.1016/j.marpolbul.2013.11.016

Magro, M., Baratella, D., Bonaiuto, E., de A. Roger, J., Vianello, F., 2018. New Perspectives on Biomedical Applications of Iron Oxide Nanoparticles. Curr. Med. Chem. 25, 540–555. https://doi.org/10.2174/0929867324666170616102922

Marchand, C., 2017. Soil carbon stocks and burial rates along a mangrove forest chronosequence (French Guiana). For. Ecol. Manage. 384, 92–99. https://doi.org/10.1016/j.foreco.2016.10.030

Megonigal, J.P., Neubauer, S.C., 2018. Biogeochemistry of tidal freshwater wetlands, Coastal Wetlands: An Integrated Ecosystem Approach. https://doi.org/10.1016/B978-0-444-63893-9.00019-8

Miao, S., DeLaune, R.D., Jugsujinda, A., 2006. Influence of sediment redox conditions on release/solubility of metals and nutrients in a Louisiana Mississippi River deltaic plain freshwater lake. Sci. Total Environ. 371, 334–343. https://doi.org/10.1016/j.scitotenv.2006.07.027

Mitsch, W.J., Bernal, B., Nahlik, A.M., Mander, Ü., Zhang, L., Anderson, C.J., Jørgensen, S.E., Brix, H., 2013. Wetlands, carbon, and climate change. Landsc. Ecol. 28, 583–597. https://doi.org/10.1007/s10980-012-9758-8

Murray, G.C., Hesterberg, D., 2006. Iron and Phosphate Dissolution during Abiotic Reduction of Ferrihydrite-Boehmite Mixtures. Soil Sci. Soc. Am. J. 70, 1318–1327. https://doi.org/10.2136/sssaj2005.0292

Navrotsky, A., Mazeina, L., Majzlan, J., 2008. Size-Driven Structural and Thermodynamic Complexity in Iron Oxides. Science (80-.). 319, 1635–1638. https://doi.org/10.1126/science.1148614

Nóbrega, G.N., Ferreira, T.O., Romero, R.E., Marques, A.G.B., Otero, X.L., 2013. Iron and sulfur geochemistry in semi-arid mangrove soils (Ceará, Brazil) in relation to seasonal changes and shrimp farming effluents. Environ. Monit. Assess. 185, 7393–7407. https://doi.org/10.1007/s10661-013-3108-4

Nóbrega, G.N., Otero, X.L., Macías, F., Ferreira, T.O., 2014. Phosphorus geochemistry in a Brazilian semiarid mangrove soil affected by shrimp farm effluents. Environ. Monit. Assess. 186, 5749–5762. https://doi.org/10.1007/s10661-014-3817-3

Pan, F., Liu, H., Guo, Z., Li, Z., Wang, B., Cai, Y., Gao, A., 2019. Effects of tide and season changes on the iron-sulfur-phosphorus biogeochemistry in sediment porewater of a mangrove coast. J. Hydrol. 568, 686–702. https://doi.org/10.1016/j.jhydrol.2018.11.002

Parsons, C.T., Rezanezhad, F., O'Connell, D.W., Van Cappellen, P., 2017. Sediment phosphorus speciation and mobility under dynamic redox conditions. Biogeosciences 14, 3585–3602. https://doi.org/10.5194/bg-14-3585-2017

Raiswell, R., Canfield, D.E., 2012. The iron biogeochemical cycle past and present. Geochemical Perspect. 1, 1–232. https://doi.org/10.7185/geochempersp.1.1

Randall, S.R., Sherman, D.M., Ragnarsdottir, K. V., Collins, C.R., 1999. The mechanism of cadmium surface complexation on iron oxyhydroxide minerals. Geochim. Cosmochim. Acta 63, 2971–2987. https://doi.org/10.1016/S0016-7037(99)00263-X

Reddy, K.R., DeLaune, R.D., 2008. Biogeochemistry of wetlands: science and applications, 1st ed. CRC Press.

Rieuwerts, J.S., 2007. The mobility and bioavailability of trace metals in tropical soils: a review. Chem. Speciat. Bioavailab. 19, 75–85. https://doi.org/10.3184/095422907X211918

Roden, E.E., Zachara, J.M., 1996. Microbial Reduction of Crystalline Iron(III) Oxides: Influence of Oxide Surface Area and Potential for Cell Growth. Environ. Sci. Technol. 30, 1618–1628. https://doi.org/10.1021/es9506216

Sánchez, M., Sabio, L., Gálvez, N., Capdevila, M., Dominguez-Vera, J.M., 2017. Iron chemistry at the service of life. IUBMB Life 69, 382–388. https://doi.org/10.1002/iub.1602

Sandilyan, S., Kathiresan, K., 2014. Decline of mangroves – A threat of heavy metal poisoning in Asia. Ocean Coast. Manag. 102, 161–168. https://doi.org/10.1016/j.ocecoaman.2014.09.025

Schaefer, C.E.G.R., Fabris, J.D., Ker, J.C., 2008. Minerals in the clay fraction of Brazilian Latosols (Oxisols): a review. Clay Miner. 43, 137–154. https://doi.org/10.1180/claymin.2008.043.1.11

Schaetzl, R.J., Thompson, M.L., 2015. Soils: Genesis and Geomorphology, 2nd ed. Cambridge University Press, New York, NY.

Schwertmann, U., 1958. The Effect of Pedogenic Environments on Iron Oxide Minerals. Springer, New York, NY, pp. 171–200. https://doi.org/10.1007/978-1-4612-5046-3_5

Schwertmann, U., Taylor, R.M., 1989. Iron Oxides, in: Minerals in Soil Environments. pp. 379–438. https://doi.org/10.2136/sssabookser1.2ed.c8

Selinus, O., Alloway, B., Centeno, J.A., Finkelman, R.B., Fuge, R., Lindh, U., Smedley, P., 2013. Essentials of medical geology: Revised edition, Essentials of Medical Geology: Revised Edition. https://doi.org/10.1007/978-94-007-4375-5

Sippo, J.Z., Sanders, C.J., Santos, I.R., Jeffrey, L.C., Call, M., Harada, Y., Maguire, K., Brown, D., Conrad, S.R., Maher, D.T., 2020. Coastal carbon cycle changes following mangrove loss. Limnol. Oceanogr. lno.11476. https://doi.org/10.1002/lno.11476

Stumm, W., 1995. The Inner-Sphere Surface Complex, in: Aquatic Chemistry. Advances in Chemistry; American Chemical Society, Washington, DC, pp. 1–32. https://doi.org/10.1021/ba-1995-0244.ch001

Ward, R.D., Friess, D.A., Day, R.H., Mackenzie, R.A., 2016. Impacts of climate change on mangrove ecosystems: a region by region overview. Ecosyst. Heal. Sustain. 2, e01211. https://doi.org/10.1002/ehs2.1211

Werner, E., Ami, N., 2014. The phosphorus cycle. Aquat. Ecol. 6, 347–363. https://doi.org/10.1007/978-94-017-8944-8_20

Yan, J., Jiang, T., Yao, Y., Lu, S., Wang, Q., Wei, S., 2016. Preliminary investigation of phosphorus adsorption onto two types of iron oxide-organic matter complexes. J. Environ. Sci. (China) 42, 152–162. https://doi.org/10.1016/j.jes.2015.08.008

Ye, S., Laws, E.A., Wu, Q., Zhong, S., Ding, X., Zhao, G., Gong, S., 2010. Pyritization of trace metals in estuarine sediments and the controlling factors: A case in Jiaojiang Estuary of Zhejiang Province, China. Environ. Earth Sci. 61, 973–982. https://doi.org/10.1007/s12665-009-0416-7

Zachara, J.M., Fredrickson, J.K., Smith, S.C., Gassman, P.L., 2001. Solubilization of Fe(III) oxide-bound trace metals by a dissimilatory Fe(III) reducing bacterium. Geochim. Cosmochim. Acta 65, 75–93. https://doi.org/10.1016/S0016-7037(00)00500-7

2. CHANGES IN SOIL IRON BIOGEOCHEMISTRY IN RESPONSE TO EXTENSIVE MANGROVE MORTALITY

Abstract

Fe biogeochemistry is associated with important ecosystem services provided by mangrove forests, including carbon sequestration and the retention of potentially toxic elements. The biogeochemical processes controlling Fe fate in mangroves are naturally affected by the soil geochemical environment, which controls Fe dynamics. However, ongoing climate changes and the associated extreme weather events may drastically affect the biogeochemistry of this important micronutrient for both terrestrial and oceanic environments. Therefore, this study aimed to evaluate how massive mangrove mortality after an extreme weather event altered the Fe dynamics in mangrove soils. The results show a significant decrease in soil carbon stock in the dead mangrove forests (24.9 Kg m^{-2}), as compared with the undisturbed forests (37.0 Kg m^{-2}). In addition, we observed a substantial Fe loss (greater than 50% of soil Fe forms, i.e., 17,000 mg kg^{-1}) in the dead mangrove soils, which was associated with pyrite (9,000 mg kg^{-1}) and low crystallinity Fe oxyhydroxides (2,400 mg kg^{-1}). These impacts led to a decrease in the pyritization in soils, which resulted in a loss of 170 tons of Fe from 500 ha of dead mangrove forests within one year. Thus, the pyritization process may critically compromise a mangrove forests' ability to immobilize pollutants (e.g., metals) and sequester carbon in the long term, thereby altering their ability to provide these ecosystem services. Overall, our results revealed that the Fe biogeochemical cycle of mangrove forests is very sensitive to future climate change scenarios and increased extreme weather events.

Keywords: tropical mangroves, natural disaster, climate change, soil biogeochemistry.

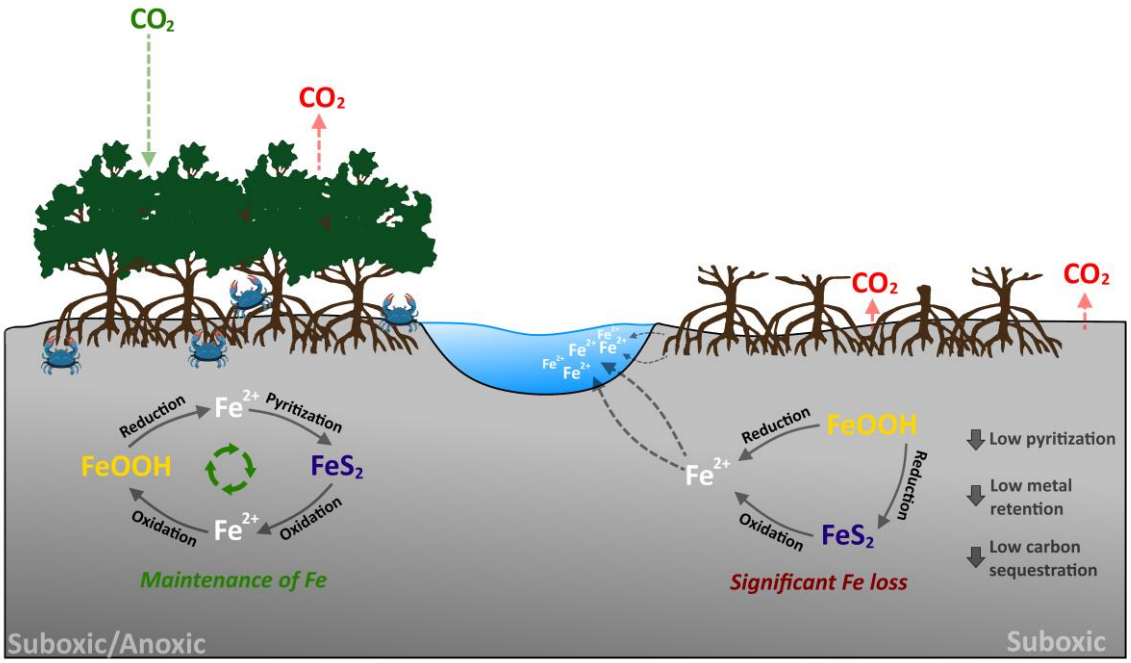

2.1. Introduction

In mangrove forests, Fe performs several vital roles as it is an essential nutrient for both plants (Alongi 2010) and marine plankton (Quéguiner 2013), and controls the cycle of crucial elements, including C, P, trace metals, and S (Sherman et al. 1998). The coupling of Fe and S cycles in estuarine soils directly affects the fate of potentially toxic elements (e.g., trace metals), which can be either immobilized in the soil or released into the environment (Huerta-Diaz and Morse 1990; Machado et al. 2008; Andrade et al. 2012; Nóbrega et al. 2013). The coupling of these elements occurs via microbial iron and sulfate reduction pathways, which are the most common pathways for soil organic matter decomposition in mangrove soils (Alongi et al. 2000; Kristensen et al. 2008; Nóbrega et al. 2013). Thus, the intensity of Fe and sulfate reduction are controlled by soil properties (e.g., redox potential, pH, tidal frequency, and organic matter content; Ferreira et al., 2010; Kristensen et al., 2008; Marchand et al., 2004; Nóbrega et al., 2016).

As Fe oxyhydroxides have a strong affinity for trace metals and P (Du Laing et al., 2009; Miao et al., 2006; Queiroz et al., 2018a; Queiroz et al., 2021), their reductive dissolution may release these adsorbed elements into the pore water, potentially triggering water eutrophication (Rozan et al. 2002; Reef et al. 2010) and contamination. Conversely, the sulfate reduction process may act as a sink for trace metals, as the produced sulfides (e.g., mackinawite, greigite, pyrite, and other metallic sulfides) decrease the bioavailability of trace metals (Lin and Morse 1991; Huerta-Diaz and Morse 1992; Liamleam and Annachhatre 2007; Ye et al. 2010; Nóbrega et al. 2013) via co-precipitation. Additionally, Fe oxyhydroxides favor soil organic matter stabilization by enhancing organo-mineral interactions (Sun et al. 2019; Kida and Fujitake 2020), causing C sequestration in mangrove soils, which influences the ability of these ecosystems to act as blue carbon sinks (Rovai et al., 2018; Kauffman et al., 2018a). Estuarine soils may also represent a potential Fe source to the ocean, which plays a key role in a wide range of organism (e.g., bacteria, algae, and phytoplankton) and ocean biogeochemical cycles (Breitbarth et al. 2010; Boyd and Ellwood 2010; Taylor and Konhauser 2011; Shaked and Lis 2012). Therefore, the regulation and maintenance of several ecosystem services provided by mangrove forests are largely dependent on the Fe biogeochemical cycle within mangrove soils (e.g., carbon sequestration, pollutant retention, and primary production; Blain et al., 2007; Lehtoranta et al., 2014; Twilley et al., 2019).

Although mangroves provide highly valuable ecosystem services (Int. approximately $47 trillion/year; Groot, 2021; Costanza et al., 2014), they are among the most threatened ecosystems worldwide (Friess et al. 2019). Mangrove forests are commonly affected by both natural and anthropogenic disturbances, such as hurricanes, deforestation, aquaculture, and climate change (Ahmed et al., 2017; Atwood et al., 2017; Bernardino et al., 2018; Kauffman et al., 2018b; Lovelock et al., 2011; Malik et al., 2015; Vo et al., 2012). Most of these disturbances reduce the ability of mangrove forests to provide a range of ecosystem services (e.g., biodiversity protection, supporting coastal food webs, and sequestering carbon and aquatic pollutants (Duke et al., 2007; Polidoro et al., 2010; Sippo et al., 2018).

Moreover, climate change has directly impacted mangroves, lowering plant productivity, reducing forest cover, and causing mass mortality as a result of extreme weather events (Dam Roy and Krishnan 2005; Aung et al. 2013; Kauffman et al. 2014; Andreetta et al. 2016; Duke et al. 2017; Gomes and Bernardino 2020; Gomes et al. 2021b). The loss of vegetation directly affects atmospheric CO_2 uptake and aboveground carbon sequestration (Alongi 2012; Murdiyarso et al. 2015; Akhand et al. 2017; Lovelock et al. 2017). However, it is unknown how vegetation losses affect basic soil biogeochemical processes (i.e., Fe and sulfate reduction) in mangrove soils and how these losses impact the ecosystem services provided by mangroves.

Therefore, this study aimed to evaluate how massive mangrove mortality alters the Fe biogeochemical dynamics of mangrove soils. We hypothesized that mangrove forest loss would significantly alter Fe biogeochemistry and the performance of ecosystem services by tropical mangrove forests.

2.2. Material and Methods

2.2.1. Studied sites and soil sampling

The Piraquê-Açú-Mirim estuary located in southeast Brazil has a Y-shaped morphology with 1746 ha of mangrove forests (Fig. 1) formed by the Piraquê-mirim (PM) and Piraquê-Açú (PA) rivers. The estuary is part of the eastern Brazil Marine Ecoregion, which has dry winters (April to September) and wet summers (October to March). Its climate is classified as a tropical wet and dry climate (Aw) according to the Köppen-Geiger climate classification (Alvares et al. 2013; Bernardino et al. 2015). The area is located within a Marine Protected Area, with nearly 1,600 ha of pristine mangrove forests (Bissoli and Bernardino 2018; Hadlich et al. 2018). This estuary experienced a severe drought after the 2015 El Niño (Gomes and Bernardino 2020), and massive mangrove mortality occurred in association with a severe hailstorm in June 2016, leading to a 24% (500 ha) loss of its forests (Servino et al. 2018).

In August 2017, 14 months after the extreme weather events, the soils at four different mangrove forests were sampled in both the PM and PA (Fig. 1). Specifically, the samples were taken from two non-impacted mangrove forests (natural or preserved mangroves) (N-PM and N-PA) and two impacted mangrove forests (I-PM and I-PA) (i.e., dead mangrove forests).

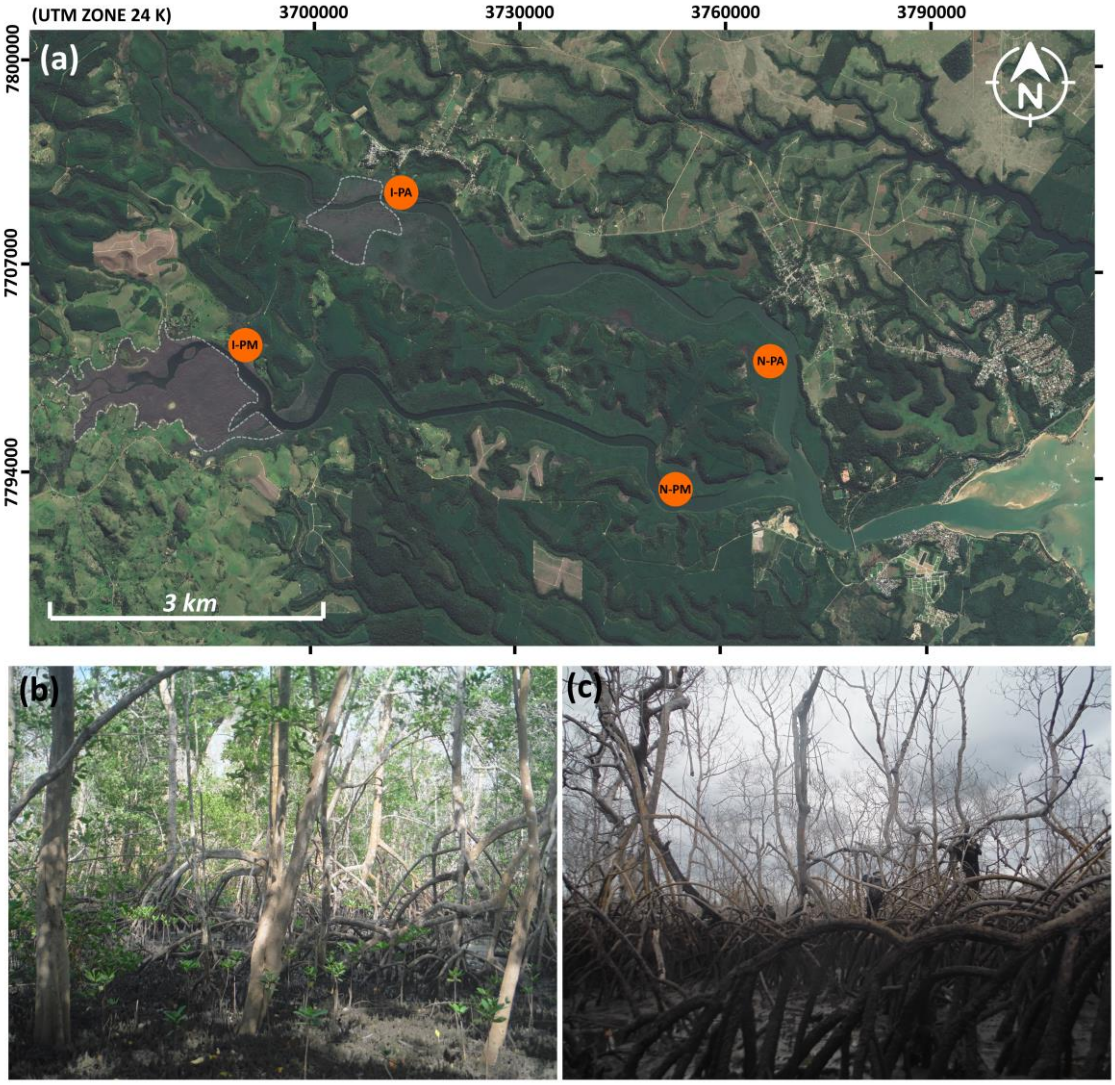

Fig. 1. (A) Sampled sites in the Piraquê-açú (PA) and Piraquê-mirim (PM) rivers on the Espírito Santo coast (Brazil). The dashed lines indicate the dead mangrove forests in both rivers. Photographs of the (B) non-impacted mangrove forest at the PA river and (C) the impacted mangrove forest at PM. The satellite images were obtained from Google Earth™.

Five cores of undisturbed soil samples were collected using a polyvinyl chloride tube (0.05 m diameter and 0.5 m length) coupled to a sampler for waterlogged soils. The redox potential (Eh) and pH values were measured in the field using platinum and glass electrodes, respectively. The final Eh readings were adjusted by adding a reference calomel electrode value of +244 mV. The pH measurements were performed with a calibrated glass electrode (standardized solutions of pH = 4.0 and 7.0).

Immediately after soil collection, all the samples were refrigerated at 4 °C. In the laboratory, soil cores were sectioned into five different depth intervals (0 – 5 cm, 5 – 10 cm, 10 – 15 cm, 15 – 30 cm, and 30 – 50 cm). Note that one of the undisturbed soil cores was used

to obtain the soil bulk density (ρ = mass of the soil solids/total soil volume) in order to calculate the soil carbon stocks (SCSs).

2.2.2. Determination of soil organic carbon and soil carbon stocks

In the laboratory, soil samples were acidified using 1 mol L^{-1} hydrochloric acid to remove carbonates (Howard et al. 2014). Subsequently, the soil samples were dried at 45 °C until a constant weight was achieved, and then weighed. The content of soil organic carbon (SOC) was determined using a Flash Elemental Analyzer coupled to a Thermo Fisher Delta V isotope ratio mass spectrometer (analytical precision, C = 0.1%). The SCS for each site was quantified to a depth of 50 cm using the ρ and SOC content (SCS = SOC × ρ × 50 cm; McKenzie et al., 2000).

2.2.3. Fe sequential extractions

Solid-phase Fe fractionation was performed using a sequential extraction procedure following the methods of Ferreira et al. (2007) and Otero et al. (2009), which allows the differentiation of six operationally defined fractions, as follows:

Exchangeable and soluble Fe (FeEX): extracted with 30 mL of a 1 mol L^{-1} magnesium chloride solution at a pH adjusted to 7. The samples were agitated for 30 min and then centrifuged at 10,000 rpm for 30 min.

Fe bound to carbonates (FeCA): extracted with 30 mL of 1 mol L^{-1} sodium acetate solution at a pH of 5. The samples were agitated for 5 h and then centrifuged at 10,000 rpm for 30 min.

Fe associated with ferrihydrite (FeFR): extracted with 30 mL of 0.04 mol L^{-1} hydroxylamine + acetic acid 25% (v/v) solution. The samples were agitated for 6 h at 30 °C and then centrifuged at 10,000 rpm for 30 min.

Fe associated with lepidocrocite (FeLP): extracted with 30 mL of 0.04 mol L^{-1} hydroxylamine + acetic acid 25% (v/v) solution. Samples were agitated for 6 h at 96 °C and then centrifuged at 10,000 rpm for 30 min.

Fe associated with crystalline Fe oxyhydroxides (goethite and hematite) (FeCR): extracted with 20 mL of 0.25 mol L^{-1} sodium citrate + 0.11 mol L^{-1} sodium bicarbonate solution

with 3 g of sodium dithionite. The samples were agitated for 30 min at 75 °C and centrifuged at 10,000 rpm for 30 min.

Fe associated with pyrite (FePY) was extracted with 10 mL of concentrated nitric acid. The samples were agitated for 2 h then washed with 15 mL of ultrapure water.

Before extracting the FePY, the samples were treated with 10 mol L^{-1} hydrofluoric acid for 16 h under agitation to eliminate sheet silicates. Then, concentrated sulfuric acid was added to eliminate the Fe associated with organic matter (for further details, see Huerta-Diaz and Morse, 1990).

Between each extraction procedure, the samples were washed with 20 mL of ultrapure water and then centrifuged to remove it. The Fe concentration in each extract was determined using inductively coupled plasma optical emission spectroscopy.

The degree of Fe pyritization (DOP) was quantified based on the content of each fraction. The DOP determines the percentage of reactive Fe (ΣFeEX → FeCR) incorporated into pyrite (FePY) (Berner, 1970), and was calculated as follows:

$$DOP = \left[\frac{FePY}{(Fe_{reactive} + FePY)}\right] \times 100.$$

In addition, the pseudo-total Fe content was calculated using the sum of all the Fe fractions (pseudo-total Fe = ΣFeEX + FeCA + FeFR + FeLP + FeCR + FePY).

2.2.4. Statistical analyses

A non-parametric Kruskal–Wallis test with a significance level of $p < 0.05$ was conducted to assess differences between the Eh, pH, Fe mean content, and SCS between the non-impacted and impacted mangrove forests (Reimann et al., 2008; XLSTAT version 2014.5.03). The soil variable correlations were determined using Spearman's correlation coefficients (*r*), as this method does not require a normal distribution. Meanwhile, the relationships between the soil variables and the studied mangroves were evaluated using a discriminant analysis with two components (Reimann et al. 2008).

2.3. Results

2.3.1. Physicochemical conditions

The soil Eh varied widely between the studied areas, ranging from −256 mV to +344 mV, while the pH ranged from 5.4 to 7.6 (Fig. 2). In addition, the Eh values were significantly different between the non-impacted and impacted mangrove forests (k= 29.89; $p < 0.001$; Fig. 2). In the non-impacted sites, the mean Eh values were +107 ± 31 mV in N-PM and −36 ± 56mV in N-PA (Fig. 2), whereas in the impacted forests, higher Eh values were recorded (mean: +212 ± 107 mV in I-PM and +46 ± 145 mV in I-PA; Fig 2).

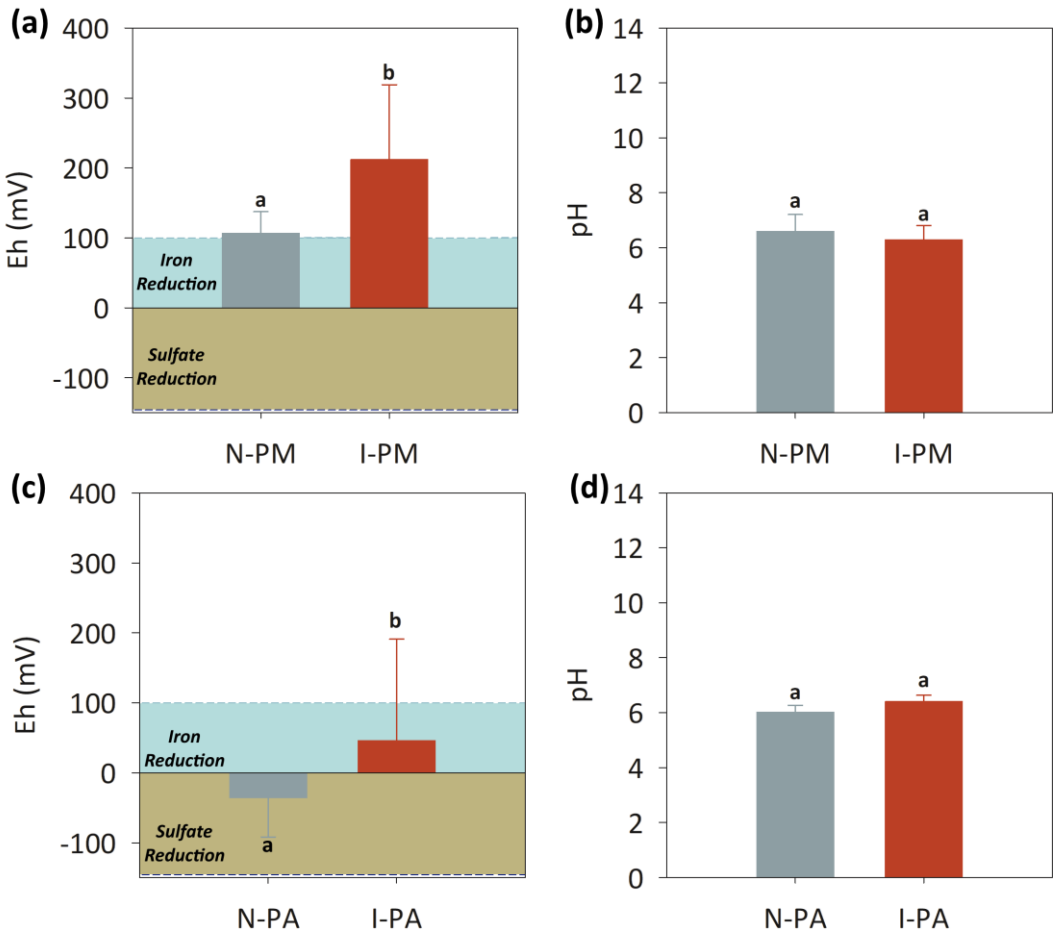

Fig. 2. (A) Redox potential (Eh) and (B) and pH values for Piraquê-mirim (PM) river, and (C) Eh and (D) pH values for Piraquê-açú (PA) river. The blue area represents the Eh interval indicative of Fe reduction (+100 to 0 mV), whereas the brown area represents the Eh interval indicative of sulfate reduction (0 to −200 mV), both at near neutral pH conditions (Søndergaard 2009). The different lowercase letters indicate a significant difference between the values determined by the Kruskal-Wallis test at a 5% probability level.

2.3.2. Soil carbon stocks

Mean SCS values were significantly higher (k= 16.487; p < 0.001) in the non-impacted mangrove forests (Fig. 3) than in the impacted forests. Specifically, in the non-impacted, the SCS values were 35.7 ± 5.2 Kg m^{-2} for N-PM and 38.3 ± 10.1 Kg m^{-2} for N-PA. Conversely, in the dead mangrove forests, the SCS values were 27.1 ± 5.5 Kg m^{-2} (I-PM) and 28.8 ± 1.7 Kg m^{-2} (I-PA; Fig. 3).

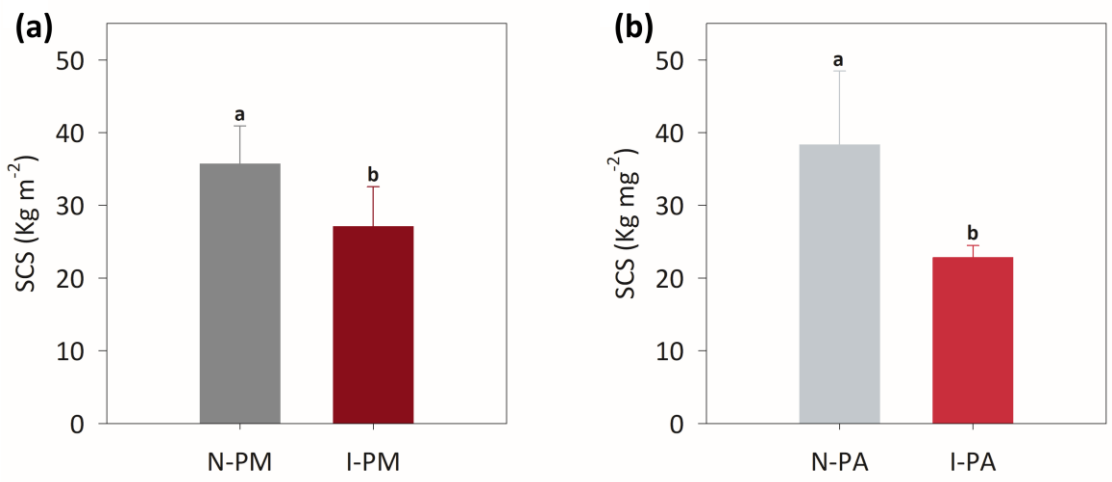

Fig. 3. Soil carbon stocks (SCSs) for the studied mangrove forests at the (A) Piraquê-mirim (PM) and (B) Piraquê-açú (PA) rivers. Bars labeled with the same lowercase letters indicate the absence of significant differences according to the Kruskal–Wallis test at a 5% probability level. N-PM: non-impacted site at PM river; I-PM: impacted site at PM river; N-PA: non-impacted site at PA river; I-PM: impacted site at PA river.

2.3.3. Fe sequential extraction and degree of Fe pyritization

The sequential extraction data revealed clear differences between the non-impacted and impacted (i.e., dead) mangrove forests (Fig. 4). Regardless of the estuary, in the impacted forests, the pseudo-total Fe content was approximately 50% lower (i.e., I-PM and I-PA; mean of pseudo-total Fe content, 17000 ± 6900 mg kg^{-1}; Fig. 4), as compared with the non-impacted areas (i.e., N-PM and N-PA; mean of pseudo-total Fe content: 34000 ± 8400 mg kg^{-1}; Fig. 4).

In the non-impacted areas, FePY was the predominant fraction (mean values for all depths, N-PM: 11,400 ± 2,650 mg kg^{-1} and N-PA: 22,650 ± 3,500 mg kg^{-1}). Further, the FePY contents in the non-impacted areas were, on average, 47% higher than those in the impacted areas (Fig. 4). The low-crystallinity Fe oxyhydroxide (FeFR + FeLP) fractions were the second dominant fractions and were also significantly higher (k= 11.57; p < 0.001) in the non-impacted areas (N-PM: 8600 ± 920 mg kg^{-1}, N-PA: 11,500 ± 2,120 mg kg^{-1}). The mean FeCR contents in

N-PM and N-PA were 5,250 ± 780 mg kg^{-1} and 4650 ± 1260 mg kg^{-1}, respectively (Fig. 4). In contrast, FeEX in the non-impacted areas contributed only 5% of the pseudo-total Fe (mean value for all depths: N-PM: 2,000 ± 720 mg kg^{-1} and N-PA: 1100 ± 140 mg kg^{-1}), and FeCA represented less than 1% of pseudo-total Fe (Fig. 4).

Similarly, in the impacted areas, FePY was the predominant fraction (mean value for all depths, I-PM: 7,100 ± 3,900 mg kg^{-1} and I-PA: 8,900 ± 7,500 mg kg^{-1}), followed by the low-crystallinity Fe oxyhydroxides (i.e., FeFR + FeLP; mean value for all depths, I-PM: 4,300 ± 2,400 mg kg^{-1} and I-PA: 6,200 ± 5,190 mg kg^{-1}) and high crystallinity Fe oxyhydroxides (i.e., FeCR; I-PM: 3,150 ± 1,500 mg kg^{-1} and I-PA: 6,200 ± 5,190 mg kg^{-1}). The FeEX and FeCA fractions in the impacted areas accounted for only a small fraction of the pseudo-total Fe, representing less than 1% (Fig. 4).

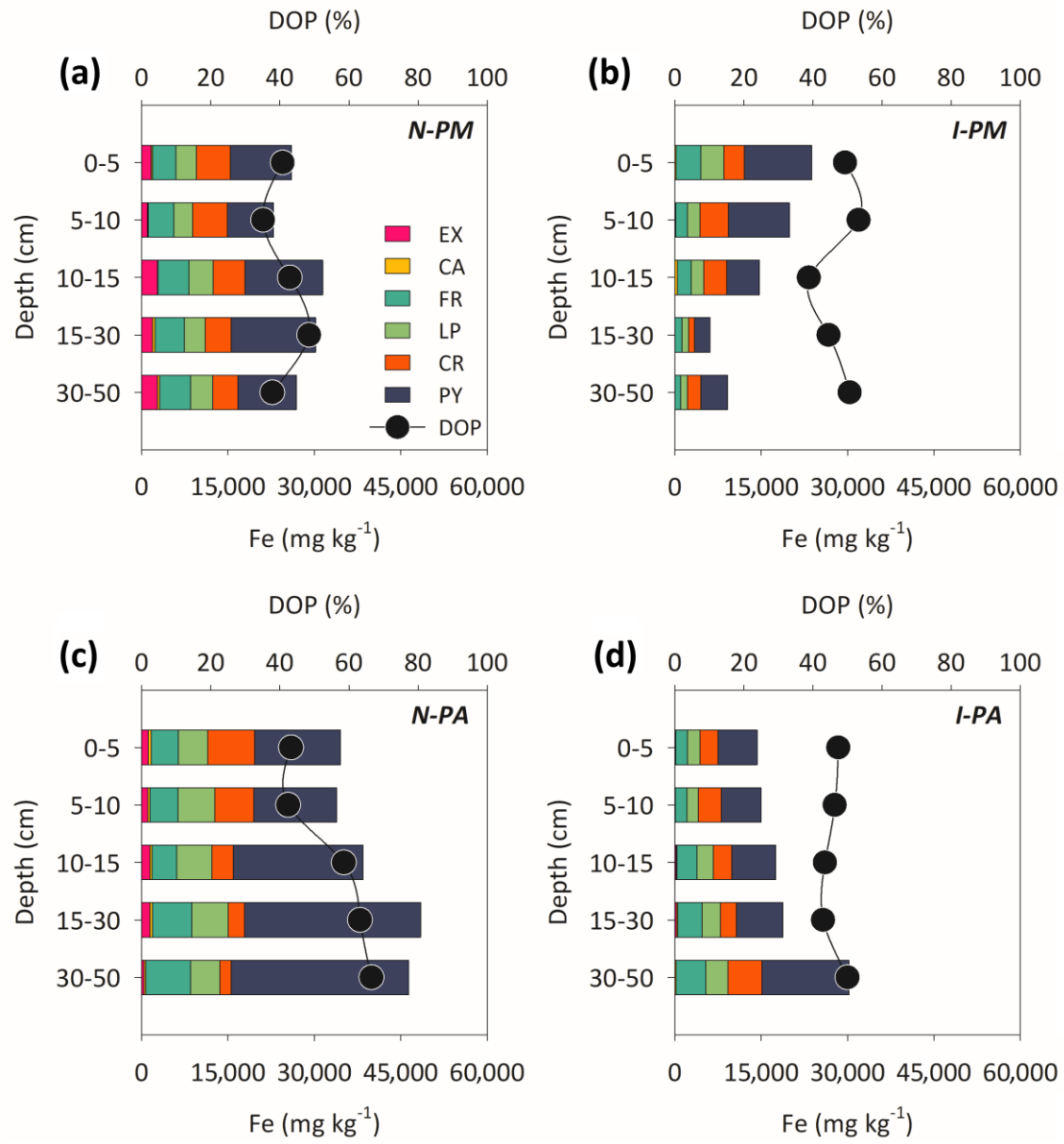

Fig. 4. Fe solid-phase fractionation and degree of Fe pyritization (DOP, %) for the (A) non-impacted mangrove forest at the Piraquê-mirim river (N-PM), (B) impacted site at the Piraquê-mirim river (I-PM), (C) non-impacted site at the Piraquê-açú river (I-PA), and (D) impacted site at the Piraquê-açú river (I-PA).

No significant differences were observed between the non-impacted and impacted forests regarding their DOP values. On average, the DOP values were 41% and 47% at N-PM and I-PA, respectively, and 55% and 46% at N-PA and I-PA, respectively (Fig. 4).

2.4. Discussion

2.4.1. Biogeochemical changes upon magrove mortality

The physicochemical results (Fig. 2) showed that the non-impacted mangroves were suboxic (+120 < Eh < +414 mV) to anoxic (Eh < 120 mV), whereas the dead mangrove forests were marked by a dominant suboxic environment (Essington 2015). Under this suboxic geochemical environment (Fig. 2), microbial Fe reduction is the main pathway for soil organic matter decomposition (Canfield et al. 1993; Reddy and DeLaune 2008). In this case, Fe-reducing bacteria use Fe oxyhydroxides as electron acceptors for soil organic matter decomposition, leading to the production of Fe^{2+} (Lovley 1991). Moreover, under suboxic conditions, pyrite and other reduced sulfur compounds may also act as electron donors for the reduction of Fe^{3+}, resulting in the anaerobic oxidation of pyrite (see Reactions 1 and 2; Moses et al., 1987; Moses and Herman, 1991; Reddy and DeLaune, 2008).

$$FeS_2 + 14Fe^{3+} + 8H_2O \rightarrow 15Fe^{2+} + 2SO_4^{2-} + 16H^+, \text{(Reaction 1)}$$

$$FeS + Fe^{3+} + 4H_2O \rightarrow 2Fe^{2+} + SO_4^{2-} + 4H^+, \text{(Reaction 2)}$$

$$Fe^{2+} + 3H_2O + {}^1/_2\, O_{2(aq)} \rightarrow 2FeOOH + H^+. \text{(Reaction 3)}$$

However, the Fe^{2+} resulting from either the Fe^{3+} microbial decomposition pathway or the anaerobic pyrite oxidation may have different fates (Cuadros et al. 2017). Specifically, it may be washed out of the estuary during ebb tides, resulting in Fe losses (Yu et al. 2007; Chaudry and Zwolsman 2008; Frohne et al. 2011), or it may be re-oxidized to Fe^{3+}, forming poorly crystalline Fe oxyhydroxides (Straub et al. 2001; Karimian et al. 2018), which will further feed both processes (i.e., Fe reduction and anaerobic pyrite oxidation; see Reaction 3; Rose and Waite, 2003; von Gunten and Schneider, 1991).

The coupling of these processes may have been responsible for approximately 50% of the Fe loss from the dead mangrove soils (Fig. 4). In particular, the mean values of pseudo-total Fe, FeEX, FeFR + FeLP, and pyrite in the dead forests were significantly lower than those in the non-impacted forests (Fig. 5). Moreover, the losses in the impacted mangrove forests may be enhanced by the runoff and erosion of smaller particles (e.g., clay, silt, and organic matter) during ebb tides, as dead trees cannot retain finer particles (Grellier et al. 2017; Arias-

Ortiz et al. 2020; Gomes et al. 2021b). Mangrove living roots have been reported to promote the trapping of fine particles, improving the structure and vertical accretion of mangrove soils (Cahoon and Lynch 1997). Thus, the absence of vegetation and living roots decreases soil structure and enhances soil erosion during ebb tides (Xiong et al. 2019). As Fe oxyhydroxides and pyrite are commonly found in soil fractions < 2 µm in size (Ding et al. 2014; Andrade et al. 2018), these mineral fractions can be easily washed out during this process.

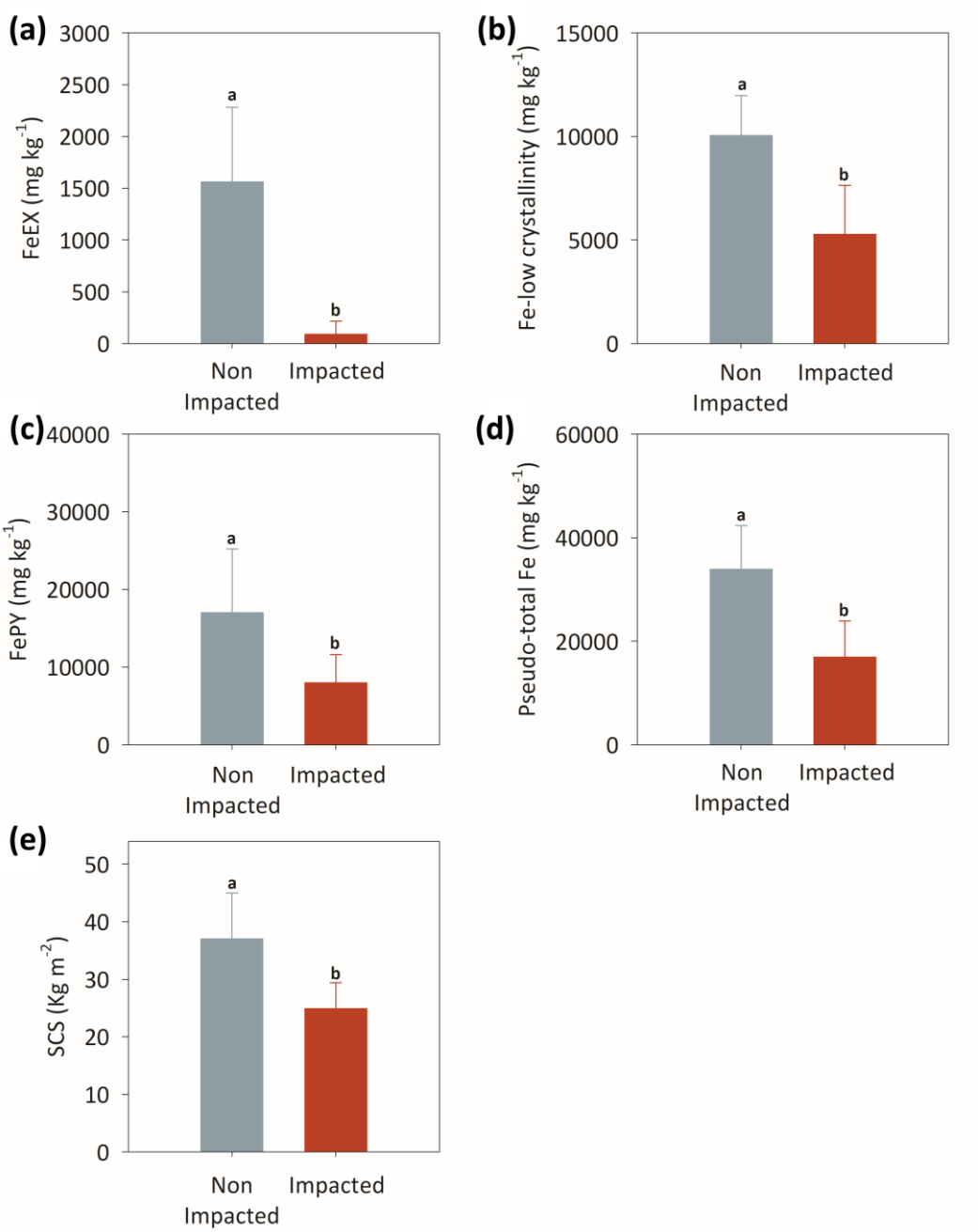

Fig. 5. (A) Mean contents of exchangeable Fe (FeEX), (B) low crystallinity Fe oxyhydroxides (FeFR + FeLP), (C) pyritic Fe (FePY), and (D) pseudo-total Fe in the non-impacted and impacted mangrove forest soils. (E) Mean soil carbon stocks (SCS; upper 50 cm) in the non-impacted

and impacted mangrove forests. The different lowercase letters indicate a significant difference between the variables as determined by the Kruskal-Wallis test at a 5% probability level.

The suboxic conditions observed in the impacted areas may also indicate the action of more energetic decomposition pathways (e.g., NO_3^-, MnO_2, and Fe reduction), which increase organic matter decomposition rates and lead to lower SCSs. These highly efficient respiration pathways, along with erosive processes, were most likely responsible for the sharp decline in the SCS contents in the impacted areas. As compared with the non-impacted areas, the SCS decreased by 33% in the dead mangroves (Fig. 5E). In the long term, dead mangrove forests cannot offset their CO_2 emissions from soil organic matter decomposition through photosynthesis (Castillo et al. 2017; Martinez and Ardón 2021). Thus, a constant decline in SCSs in impacted areas is expected over time.

Meanwhile, non-impacted mangrove soils showed a commonly reported biogeochemical equilibrium, in which Fe and sulfate reduction are coupled (Lin and Morse 1991; Nóbrega et al. 2013). Specifically, under suboxic/anoxic conditions, both microbial Fe and sulfate reduction are favored (Reddy and DeLaune 2008; Essington 2015). Under these physicochemical conditions, both acid-volatile sulfides and Fe sulfides (FeS and FeS_2) are the major end products (Minuzzi et al. 2007; Otero et al. 2017; Queiroz et al. 2018b), which explains the higher FePY fraction recorded in the non-impacted mangrove forest soils (i.e., N-PM and N-PA; Fig. 5C). In healthy mangrove forests, root exudates (i.e., labile dissolved organic carbon) stimulate sulfate-reducing bacteria and enhance pyritization (Alongi 2005; Kristensen and Alongi 2006). In addition, in pristine mangrove forests, soil fauna activity (e.g., crab burrowing) and root activity play key roles in Fe^{2+} oxidation, leading to Fe immobilization as low-crystallinity Fe oxyhydroxides (Kristensen and Alongi 2006; Araújo Júnior et al. 2012; Mokhtari et al. 2016).

Therefore, the higher content of Fe oxyhydroxides observed in the non-impacted mangroves (Fig. 4) under suboxic/anoxic conditions may increase sulfate reduction because Fe oxyhydroxides are consumed during the formation of pyrite (Jakobsen and Postma, 1999; Machado et al., 2004; Queiroz et al., 2018b). Various studies have reported that an increase in sulfate reduction promotes an increase in pyritization in wetland soils with abundant reactive Fe forms (Luther 2005; Machado et al. 2008; Keene et al. 2011; Julian et al. 2017). In this study, the significant positive correlation between the DOP and low-crystallinity Fe

oxyhydroxides (r = 0.733; p = 0.0198; Fig. 6) corroborates the positive effect of higher Fe availability, especially low-crystallinity Fe (Nealson and Myers 1992; Patrick and Jugsujinda 1992), on pyrite formation in the non-impacted mangrove forests. In contrast, the absence of the same correlation (r = −0.175; p = 0.6320; Fig. 6) in the dead mangroves corroborates the lack of these Fe immobilization mechanisms (i.e., pyritization and Fe^{2+} oxidation).

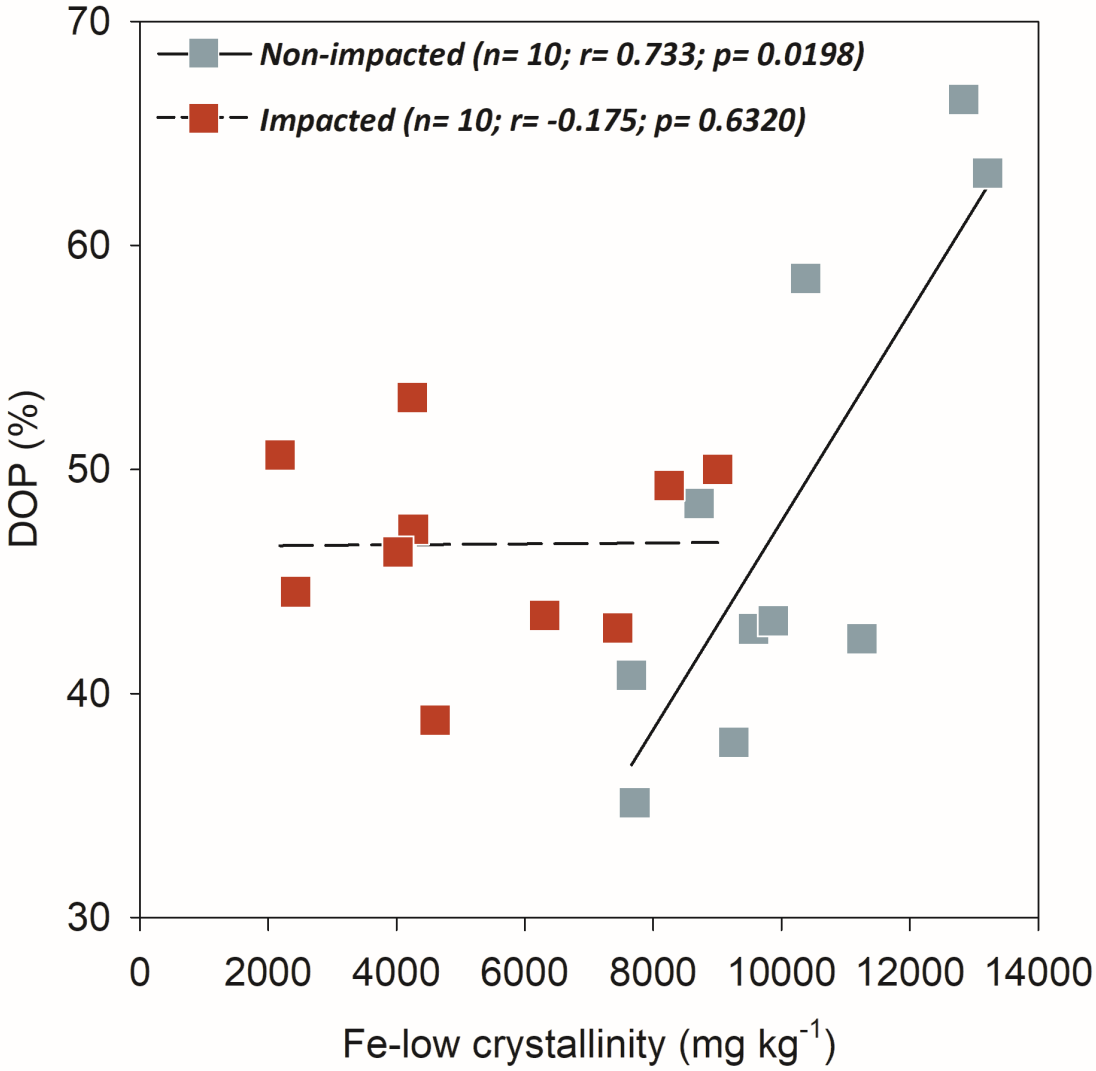

Fig. 6. Spearman correlations between the mean contents of the low crystallinity Fe oxyhydroxides (i.e., FR and LP) and the degree of Fe pyritization (DOP) at non-impacted (N-PM and N-PA) and impacted studied mangrove forests (I-PM and I-PA). PM: Piraquê-mirim; PA: Piraquê-açú.

2.4.2. Environmental consequences

Our data revealed that one year after the extreme events that resulted in the mangrove death, the forests exhibited drastically different Fe biogeochemistries (Fig. 7). These changes (i.e., losses of Fe oxyhydroxides, FePY, and SCS; Fig. 5) suggest an imminent decline in the ecosystem services provided by the impacted mangrove forests, especially regarding carbon sequestration and contaminant immobilization. As Fe oxyhydroxides contribute to soil organic matter stabilization (Dicen et al. 2019; Sun et al. 2019; Kida and Fujitake 2020), the lower Fe content in the dead mangrove soils (Fig. 7) may affect this stabilization mechanism. In addition, more oxidizing conditions (Fig. 2) increase the soil organic carbon decomposition rates (Aller 1994; Kristensen et al. 2008; Kim et al. 2021). In particular, our results indicated a significant decrease in the SCSs (Fig. 5E) of the impacted mangroves within one year, which is likely because of the increase in organic matter decomposition and soil erosion (Gomes et al. 2021a).

Moreover, the lower contents of reactive Fe and FePY in the impacted mangroves (Fig. 7) directly affect the ability of these mangrove forests to control the bioavailability of trace metals. Several studies have highlighted pyrite as one of the most important sinks for metals in mangrove forests (Huerta-Diaz and Morse 1992; Otero and Macias 2003; Machado et al. 2008; Ye et al. 2010; Nóbrega et al. 2013). Thus, with decreased pyritization, the dead mangrove forests acted as sources of metals for estuarine and oceanic waters. Further investigations regarding how mangrove mortality may affect trace metal availability could provide valuable information on this matter. Similarly, the significant Fe losses from the dead mangrove soils (50% of pseudo-total Fe; Fig. 5D) may represent an important source of Fe to the ocean.

Fe is an essential nutrient for a wide range of organisms in the ocean, and several studies have reported positive effects of ocean Fe fertilization on phytoplankton growth and carbon sequestration (Buesseler and Andrews 2004; Blain et al. 2007; Powell 2008; Quéguiner 2013). However, some studies have pointed out the risks of excessive Fe input from external sources to the ocean (Silver et al. 2010; Trick et al. 2010; Olesen et al. 2021), revealing that Fe enrichment in the ocean may stimulate the growth of the toxigenic diatom genus *Pseudonitzschia* and the production of the neurotoxin domoic acid, which impacts marine productivity. In this study, we estimated a potential loss of 170 tons of Fe/year by comparing

the sums of the pseudo-total Fe from the non-impacted areas (sum of pseudo-total Fe in N-PM and N-PA, 67,800 mg kg^{-1}) and impacted areas (sum of pseudo-total Fe in I-PM and I-PA, 33,950 mg kg^{-1}), and considering the areas with mangrove mortality (500 ha).

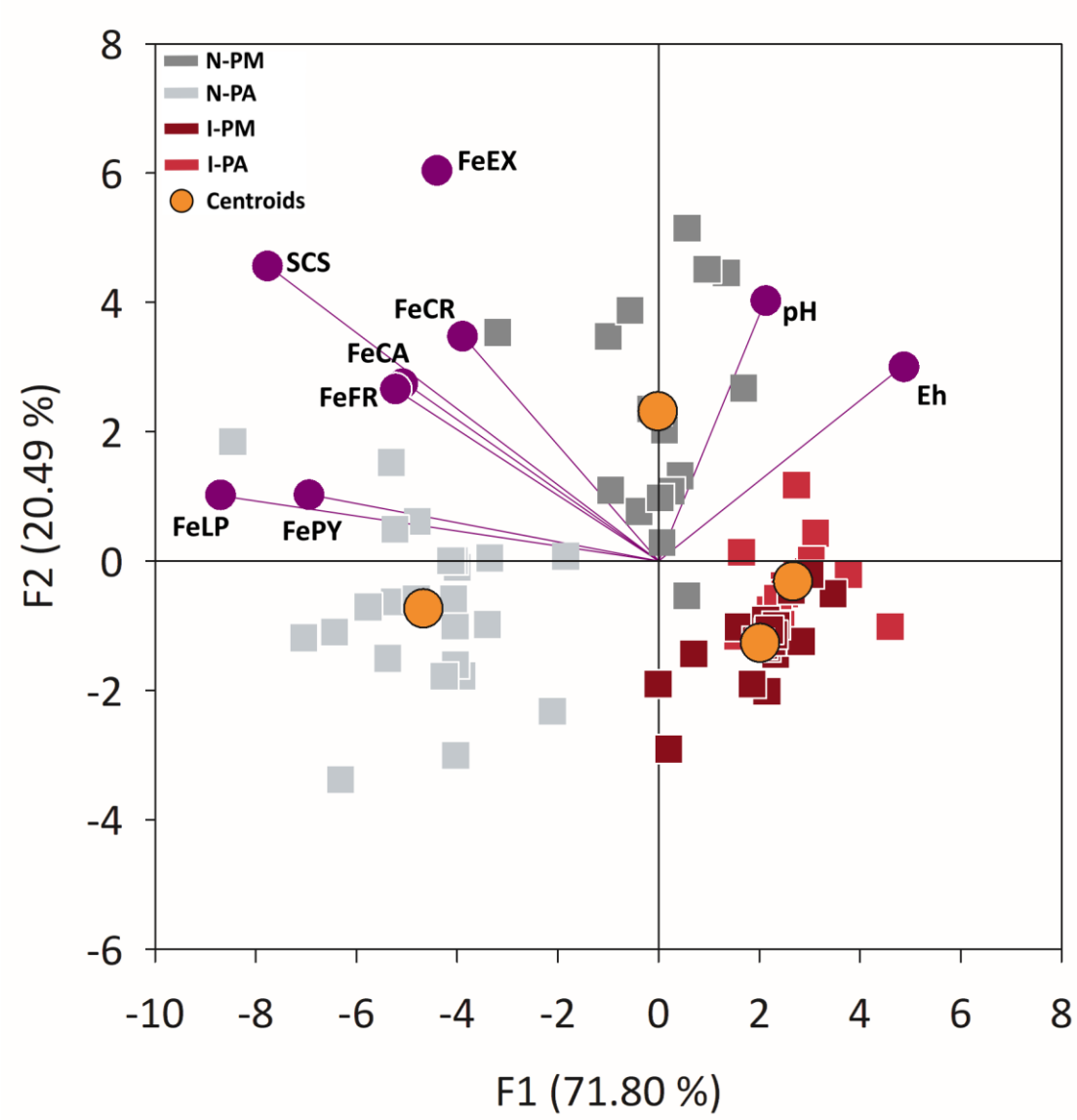

Fig. 7. Spearman correlations between the mean contents of the low crystallinity Fe oxyhydroxides (i.e., FR and LP) and the degree of Fe pyritization (DOP) at non-impacted (N-PM and N-PA) and impacted studied mangrove forests (I-PM and I-PA). PM: Piraquê-mirim; PA: Piraquê-açú.

The drastic shift in the Fe biogeochemical dynamics in the dead mangrove forests reveals that these tropical ecosystems are highly sensitive to climate change. Therefore, future research should focus on providing broad estimates of how climate change will affect soil biogeochemical processes, and consequently, the ecosystem services provided by

mangrove forests (e.g., freshwater and nutrient cycles). The results of this study also confirm the need for concern regarding the impacts of extreme weather events in mangrove forests worldwide, especially in the face of a future climate change scenario where extreme weather events are expected to effect more locations with higher frequencies (Gilman et al. 2008; Godoy and Lacerda 2015; Sippo et al. 2018).

2.5. Conclusions

The findings of this study revealed that mangrove mortality significantly altered the soil biogeochemical conditions and established a suboxic environment. The new geochemical conditions favored more energetic soil organic matter decomposition pathways, which led to a 33% decline in the SCSs. In the dead mangrove forests, microbial Fe reduction coupled with anoxic pyrite oxidation were the main pathways for soil organic matter decomposition. The coupling of these mechanisms led to a 50% loss of Fe (i.e., approximately 170 tons of Fe) from the dead mangrove forests within one year.

Our data suggest that the dynamics of other elements (e.g., S and C) are also affected by Fe biogeochemical changes. As a result, a decreased ability to provide carbon sequestration and immobilize potentially toxic elements (e.g., trace metals) is expected in the impacted mangrove forests.

This study shows that mangrove forests, which are widely known for their potential to mitigate climate change, are especially sensitive to climate change effects (e.g., hailstorms, droughts, and windstorms), which causes them to lose their capacity to provide key ecosystem services (e.g., immobilization of contaminants and carbon sequestration). Furthermore, dead mangrove forests may act as Fe, P, and metal sources to estuarine and oceanic waters. Therefore, the restoration of dead mangrove forests is pivotal for preserving soil biogeochemical cycles, which are strongly associated with the ecosystem services provided by these tropical forests.

Acknowledgements

This work was funded by Coordenação de Aperfeiçoamento de Pessoal de Nível Superior CAPES (Finance Code 001 and V. Asensio thanks grans n. 88887.136289/2017-00 CNPq-CAPES-PELD, subproject 441243/2016-9) and CNPq (grant numbers 301161/2017-8 and 305996/2018-5 to AFB and TOF, respectively). Also, we are grateful for the financial support

provided by the São Paulo Research Foundation (FAPESP; grant numbers 2018/04259-2; 2019/02855-0; 2019/14800-5; 2019/19987-6 and 2018/08408-2 to HMQ, ADF, DB, and TOF, respectively). Fundação Carlos Chagas Filho de Amparo à Pesquisa do Estado do Rio de Janeiro (GNN, JCNE Grant E-26/202.757/2019). This is a PELD-HCES contribution #016

References

Ahmed, N., Cheung, W.W.L., Thompson, S., Glaser, M., 2017. Solutions to blue carbon emissions: Shrimp cultivation, mangrove deforestation and climate change in coastal Bangladesh. Mar. Policy 82, 68–75. https://doi.org/10.1016/j.marpol.2017.05.007

Akhand, A., Mukhopadhyay, A., Chanda, A., Mukherjee, S., Das, A., Das, S., Hazra, S., Mitra, D., Choudhury, S.B., Rao, K.H., 2017. Potential CO2 Emission Due to Loss of Above Ground Biomass from the Indian Sundarban Mangroves During the Last Four Decades. J. Indian Soc. Remote Sens. 45, 147–154. https://doi.org/10.1007/s12524-016-0567-4

Aller, R.C., 1994. Bioturbation and remineralization of sedimentary organic matter: effects of redox oscillation. Chem. Geol. 114, 331–345. https://doi.org/10.1016/0009-2541(94)90062-0

Alongi, D.M., 2012. Carbon sequestration in mangrove forests. Carbon Manag. 3, 313–322. https://doi.org/10.4155/cmt.12.20

Alongi, D.M., 2005. Mangrove-microbe-soil relations, in: Interactions Between Macro- and Microorganisms in Marine Sediments. pp. 85–103. https://doi.org/10.1029/CE060p0085

Alongi, D.M., Tirendi, F., Clough, B.F., 2000. Below-ground decomposition of organic matter in forests of the mangroves Rhizophora stylosa and Avicennia marina along the arid coast of Western Australia. Aquat. Bot. https://doi.org/10.1016/S0304-3770(00)00110-8

Alongi, D.M., Tirendi, F., Dixon, P., Trott, L.A., Brunskill, G.J., 1999. Mineralization of Organic Matter in Intertidal Sediments of a Tropical Semi-enclosed Delta. Estuar. Coast. Shelf Sci. 48, 451–467. https://doi.org/http://dx.doi.org/10.1006/ecss.1998.0465

Alvares, C.A., Stape, J.L., Sentelhas, P.C., de Moraes Gonçalves, J.L., Sparovek, G., 2013. Köppen's climate classification map for Brazil. Meteorol. Zeitschrift 22, 711–728. https://doi.org/10.1127/0941-2948/2013/0507

Andrade, G.R.P., Cuadros, J., Partiti, C.S.M., Cohen, R., Vidal-Torrado, P., 2018. Sequential mineral transformation from kaolinite to Fe-illite in two Brazilian mangrove soils.

Geoderma 309, 84–99. https://doi.org/10.1016/j.geoderma.2017.08.042

Andrade, R.A., Sanders, C.J., Boaventura, G., Patchineelam, S.R., 2012. Pyritization of trace metals in mangrove sediments. Environ. Earth Sci. 67, 1757–1762. https://doi.org/10.1007/s12665-012-1620-4

Andreetta, A., Huertas, A.D., Lotti, M., Cerise, S., 2016. Land use changes affecting soil organic carbon storage along a mangrove swamp rice chronosequence in the Cacheu and Oio regions (northern Guinea-Bissau). Agric. Ecosyst. Environ. 216, 314–321. https://doi.org/10.1016/j.agee.2015.10.017

Araújo Júnior, J.M.C., Otero, X.L., Marques, a. G.B., Nóbrega, G.N., Silva, J.R.F., Ferreira, T.O., 2012. Selective geochemistry of iron in mangrove soils in a semiarid tropical climate: effects of the burrowing activity of the crabs Ucides cordatus and Uca maracoani. Geo-Marine Lett. 32, 289–300. https://doi.org/10.1007/s00367-011-0268-5

Arias-Ortiz, A., Masqué, P., Glass, L., Benson, L., Kennedy, H., Duarte, C.M., Garcia-Orellana, J., Benitez-Nelson, C.R., Humphries, M.S., Ratefinjanahary, I., Ravelonjatovo, J., Lovelock, C.E., 2020. Losses of Soil Organic Carbon with Deforestation in Mangroves of Madagascar. Ecosystems 1–19. https://doi.org/10.1007/s10021-020-00500-z

Atwood, T.B., Connolly, R.M., Almahasheer, H., Carnell, P.E., Duarte, C.M., Lewis, C.J.E., Irigoien, X., Kelleway, J.J., Lavery, P.S., Macreadie, P.I., Serrano, O., Sanders, C.J., Santos, I., Steven, A.D.L., Lovelock, C.E., 2017. Global patterns in mangrove soil carbon stocks and losses. Nat. Clim. Chang. 7, 523–528. https://doi.org/10.1038/nclimate3326

Aung, T.T., Mochida, Y., Than, M.M., 2013. Prediction of recovery pathways of cyclone-disturbed mangroves in the mega delta of Myanmar. For. Ecol. Manage. 293, 103–113. https://doi.org/10.1016/j.foreco.2012.12.034

Bernardino, A.F., Netto, S.A., Pagliosa, P.R., Barros, F., Christofoletti, R.A., Rosa Filho, J.S., Colling, A., Lana, P.C., 2015. Predicting ecological changes on benthic estuarine assemblages through decadal climate trends along Brazilian Marine Ecoregions. Estuar. Coast. Shelf Sci. 166, 74–82. https://doi.org/10.1016/j.ecss.2015.05.021

Bissoli, L.B., Bernardino, A.F., 2018. Benthic macrofaunal structure and secondary production in tropical estuaries on the Eastern Marine Ecoregion of Brazil. PeerJ 2018. https://doi.org/10.7717/peerj.4441

Blain, S., Quéguiner, B., Armand, L., Belviso, S., Bombled, B., Bopp, L., Bowie, A., Brunet, C., Brussaard, C., Carlotti, F., Christaki, U., Corbière, A., Durand, I., Ebersbach, F., Fuda, J.L., Garcia, N., Gerringa, L., Griffiths, B., Guigue, C., Guillerm, C., Jacquet, S., Jeandel, C., Laan, P., Lefèvre, D., Lo Monaco, C., Malits, A., Mosseri, J., Obernosterer, I., Park, Y.H., Picheral, M., Pondaven, P., Remenyi, T., Sandroni, V., Sarthou, G., Savoye, N., Scouarnec, L., Souhaut, M., Thuiller, D., Timmermans, K., Trull, T., Uitz, J., Van Beek, P., Veldhuis, M., Vincent, D., Viollier, E., Vong, L., Wagener, T., 2007. Effect of natural iron fertilization on carbon sequestration in the Southern Ocean. Nature 446, 1070–1074. https://doi.org/10.1038/nature05700

Boyd, P.W., Ellwood, M.J., 2010. The biogeochemical cycle of iron in the ocean. Nat. Geosci. 3, 675–682. https://doi.org/10.1038/ngeo964

Breitbarth, E., Achterberg, E.P., Ardelan, M. V., Baker, A.R., Bucciarelli, E., Chever, F., Croot, P.L., Duggen, S., Gledhill, M., Hassellöv, M., Hassler, C., Hoffmann, L.J., Hunter, K.A., Hutchins, D.A., Ingri, J., Jickells, T., Lohan, M.C., Nielsdóttir, M.C., Sarthou, G., Schoemann, V., Trapp, J.M., Turner, D.R., Ye, Y., 2010. Iron biogeochemistry across marine systems - progress from the past decade. Biogeosciences 7, 1075–1097. https://doi.org/10.5194/bg-7-1075-2010

Buesseler, K.O., Andrews, J.E., 2004. The Effects of Iron Fertilization. Science (80-.). 304, 414–417.

Cahoon, D., Lynch, J., 1997. Vertical accretion and shallow subsidence in a mangrove forest of southwestern Florida, U.S.A. Mangroves Salt Marshes 3, 173–186. https://doi.org/10.1023/A:1009904816246

Canfield, D.E., Thamdrup, B., Hansen, J.W., 1993. The anaerobic degradation of organic matter in Danish coastal sediments: Iron reduction, manganese reduction, and sulfate reduction. Geochim. Cosmochim. Acta 57, 3867–3883. https://doi.org/10.1016/0016-7037(93)90340-3

Castillo, J.A.A., Apan, A.A., Maraseni, T.N., Salmo, S.G., 2017. Soil greenhouse gas fluxes in tropical mangrove forests and in land uses on deforested mangrove lands. CATENA 159, 60–69. https://doi.org/10.1016/j.catena.2017.08.005

Chaudry, M.A., Zwolsman, J.J.G., 2008. Seasonal Dynamics of Dissolved Trace Metals in the Scheldt Estuary: Relationship with Redox Conditions and Phytoplankton Activity. Estuaries and Coasts 31, 430–443. https://doi.org/10.1007/s12237-007-9030-7

Dam Roy, S., Krishnan, P., 2005. Mangrove stands of Andamans vis-à-vis tsunami. Curr. Sci. 89, 1800–1804.

Dicen, G.P., Navarrete, I.A., Rallos, R. V., Salmo, S.G., Garcia, M.C.A., 2019. The role of reactive iron in long-term carbon sequestration in mangrove sediments. J. Soils Sediments 19, 501–510. https://doi.org/10.1007/s11368-018-2051-y

Ding, H., Yao, S., Chen, J., 2014. Authigenic pyrite formation and re-oxidation as an indicator of an unsteady-state redox sedimentary environment: Evidence from the intertidal mangrove sediments of Hainan Island, China. Cont. Shelf Res. 78, 85–99. https://doi.org/10.1016/j.csr.2014.02.011

Du Laing, G., Rinklebe, J., Vandecasteele, B., Meers, E., Tack, F.M.G., 2009. Trace metal behaviour in estuarine and riverine floodplain soils and sediments: A review. Sci. Total Environ. 407, 3972–3985. https://doi.org/10.1016/j.scitotenv.2008.07.025

Duke, N.C., Kovacs, J.M., Griffiths, A.D., Preece, L., Hill, D.J.E., van Oosterzee, P., Mackenzie, J., Morning, H.S., Burrows, D., 2017. Large-scale dieback of mangroves in Australia. Mar. Freshw. Res. 68, 1816. https://doi.org/10.1071/MF16322

Duke, N.C., Meynecke, J.-O., Dittmann, S., Ellison, A.M., Anger, K., Berger, U., Cannicci, S., Diele, K., Ewel, K.C., Field, C.D., Koedam, N., Lee, S.Y., Marchand, C., Nordhaus, I., Dahdouh-Guebas, F., 2007. A World Without Mangroves? Science (80-.). https://doi.org/10.1126/science.317.5834.41b

Essington, M.E., 2015. Soil and Water Chemistry: An Integrative Approach, Second Edition, 2nd ed. CRC Press, Boca Raton, FL.

Ferreira, T.O., Otero, X.L., de Souza Junior, V.S., Vidal-Torrado, P., Macías, F., Firme, L.P., 2010. Spatial patterns of soil attributes and components in a mangrove system in Southeast Brazil (São Paulo). J. Soils Sediments 10, 995–1006. https://doi.org/10.1007/s11368-010-0224-4

Ferreira, T.O., Otero, X.L., Vidal-Torrado, P., Macías, F., 2007. Redox Processes in Mangrove Soils under Rhizophora mangle in Relation to Different Environmental Conditions. Soil Sci. Soc. Am. J. 71, 484–491. https://doi.org/10.2136/sssaj2006.0078

Frohne, T., Rinklebe, J., Diaz-Bone, R.A., Du Laing, G., 2011. Controlled variation of redox conditions in a floodplain soil: Impact on metal mobilization and biomethylation of arsenic and antimony. Geoderma 160, 414–424. https://doi.org/10.1016/j.geoderma.2010.10.012

Gomes, L.E. de O., Bernardino, A.F., 2020. Drought effects on tropical estuarine benthic assemblages in Eastern Brazil. Sci. Total Environ. 703, 135490. https://doi.org/10.1016/j.scitotenv.2019.135490

Gomes, L.E. de O., Sanders, C.J., Nobrega, G.N., Vescovi, L.C., Queiroz, H.M., Kauffman, J.B., Ferreira, T.O., Bernardino, A.F., 2021a. Ecosystem carbon losses following a climate-induced mangrove mortality in Brazil. J. Environ. Manage.

Gomes, L.E. de O., Vescovi, L.C., Bernardino, A.F., 2021b. The collapse of mangrove litterfall production following a climate-related forest loss in Brazil. Mar. Pollut. Bull. 162, 111910. https://doi.org/10.1016/j.marpolbul.2020.111910

Grellier, S., Janeau, J.L., Dang Hoai, N., Nguyen Thi Kim, C., Le Thi Phuong, Q., Pham Thi Thu, T., Tran-Thi, N.T., Marchand, C., 2017. Changes in soil characteristics and C dynamics after mangrove clearing (Vietnam). Sci. Total Environ. 593–594, 654–663. https://doi.org/10.1016/j.scitotenv.2017.03.204

Hadlich, H.L., Venturini, N., Martins, C.C., Hatje, V., Tinelli, P., Gomes, L.E. de O., Bernardino, A.F., 2018. Multiple biogeochemical indicators of environmental quality in tropical estuaries reveal contrasting conservation opportunities. Ecol. Indic. 95, 21–31. https://doi.org/10.1016/j.ecolind.2018.07.027

Howard, J., Hoyt, S., Isensee, K., Telszewski, M., Pidgeon, E., Telszewski, M., 2014. Coastal blue carbon: methods for assessing carbon stocks and emissions factors in mangroves, tidal salt marshes, and seagrasses, Conservation International. Conservation International, Intergovernmental Oceanographic Commission of UNESCO, International Union for Conservation of Nature, Arlington, VA, USA, Arlington, VA, USA.

Huerta-Diaz, M.A., Morse, J.W., 1992. Pyritization of trace metals in anoxic marine sediments. Geochim. Cosmochim. Acta 56, 2681–2702. https://doi.org/10.1016/0016-7037(92)90353-K

Huerta-Diaz, M.A., Morse, J.W., 1990. A quantitative method for determination of trace metal concentrations in sedimentary pyrite. Mar. Chem. 29, 119–144. https://doi.org/10.1016/0304-4203(90)90009-2

Jakobsen, R., Postma, D., 1999. Redox zoning, rates of sulfate reduction and interactions with Fe-reduction and methanogenesis in a shallow sandy aquifer, Rømø, Denmark. Geochim. Cosmochim. Acta 63, 137–151. https://doi.org/10.1016/S0016-7037(98)00272-5

Julian, P., Chambers, R., Russell, T., 2017. Iron and Pyritization in Wetland Soils of the Florida Coastal Everglades. Estuaries and Coasts 40, 822–831. https://doi.org/10.1007/s12237-016-0180-3

Karimian, N., Johnston, S.G., Burton, E.D., 2018. Iron and sulfur cycling in acid sulfate soil wetlands under dynamic redox conditions: A review. Chemosphere 197, 803–816. https://doi.org/10.1016/j.chemosphere.2018.01.096

Kauffman, J.B., Bernardino, A.F., Ferreira, T.O., Bolton, N.W., Gomes, L.E. de O., Nobrega, G.N., 2018. Shrimp ponds lead to massive loss of soil carbon and greenhouse gas emissions in northeastern Brazilian mangroves. Ecol. Evol. 8, 5530–5540. https://doi.org/10.1002/ece3.4079

Kauffman, J.B., Heider, C., Norfolk, J., Payton, F., 2014. Carbon stocks of intact mangroves and carbon emissions arising from their conversion in the Dominican Republic. Ecol. Appl. 24, 518–527. https://doi.org/10.1890/13-0640.1

Keene, A.F., Johnston, S.G., Bush, R.T., Sullivan, L.A., Burton, E.D., McElnea, A.E., Ahern, C.R., Powell, B., 2011. Effects of hyper-enriched reactive Fe on sulfidisation in a tidally inundated acid sulfate soil wetland. Biogeochemistry 103, 263–279. https://doi.org/10.1007/s10533-010-9461-2

Kida, M., Fujitake, N., 2020. Organic Carbon Stabilization Mechanisms in Mangrove Soils: A Review. Forests 11, 981. https://doi.org/10.3390/f11090981

Kim, J., Lee, J., Yang, Y., Yun, J., Ding, W., Yuan, J., Khim, J.S., Kwon, B.O., Kang, H., 2021. Microbial decomposition of soil organic matter determined by edaphic characteristics of mangrove forests in East Asia. Sci. Total Environ. 763, 142972. https://doi.org/10.1016/j.scitotenv.2020.142972

Kristensen, E., Alongi, D.M., 2006. Control by fiddler crabs (Uca vocans) and plant roots (Avicennia marina) on carbon, iron, and sulfur biogeochemistry in mangrove sediment. Limnol. Oceanogr. 51, 1557–1571. https://doi.org/10.4319/lo.2006.51.4.1557

Kristensen, E., Bouillon, S., Dittmar, T., Marchand, C., 2008. Organic carbon dynamics in mangrove ecosystems: A review. Aquat. Bot. 89, 201–219. https://doi.org/10.1016/j.aquabot.2007.12.005

Lehtoranta, J., Ekholm, P., Vihervaara, P., Kortelainen, P., 2014. Coupled biogeochemical cycles and ecosystem services, Reports of the Finnish Environment Institute 21. Finnish Environment Institute, Helsinki.

Liamleam, W., Annachhatre, A.P., 2007. Electron donors for biological sulfate reduction. Biotechnol. Adv. 25, 452–463. https://doi.org/10.1016/j.biotechadv.2007.05.002

Lin, S., Morse, J., 1991. Sulfate reduction and iron sulfide mineral formation in Gulf of Mexico anoxic sediments. Am. J. Sci. https://doi.org/10.2475/ajs.291.1.55

Lovelock, C.E., Feller, I.C., Reef, R., Hickey, S., Ball, M.C., 2017a. Mangrove dieback during fluctuating sea levels. Sci. Rep. 7, 1680. https://doi.org/10.1038/s41598-017-01927-6

Lovelock, C.E., Fourqurean, J.W., Morris, J.T., 2017b. Modeled CO2 Emissions from Coastal Wetland Transitions to Other Land Uses: Tidal Marshes, Mangrove Forests, and Seagrass Beds. Front. Mar. Sci. 4, 1–11. https://doi.org/10.3389/fmars.2017.00143

Lovelock, C.E., Ruess, R.W., Feller, I.C., 2011. Co2 efflux from cleared mangrove peat. PLoS One 6, 1–4. https://doi.org/10.1371/journal.pone.0021279

Lovley, D.R., 1991. Dissimilatory Fe(III) and Mn(IV) Reduction. Microbiol. Rev. 55, 259–287.

Luther, G.W., 2005. Acid volatile sulfide—a comment. Mar. Chem. 97, 198–205. https://doi.org/10.1016/j.marchem.2005.08.001

Machado, W., Carvalho, M.F., Santelli, R.E., Maddock, J.E.L., 2004. Reactive sulfides relationship with metals in sediments from an eutrophicated estuary in Southeast Brazil. Mar. Pollut. Bull. 49, 89–92. https://doi.org/10.1016/j.marpolbul.2004.01.012

Machado, W., Santelli, R.E., Carvalho, M.F., Molisani, M.M., Barreto, R.C., Lacerda, L.D., 2008. Relation of Reactive Sulfides with Organic Carbon, Iron, and Manganese in Anaerobic Mangrove Sediments: Implications for Sediment Suitability to Trap Trace Metals. J. Coast. Res. 4, 25–32. https://doi.org/10.2112/06-0736.1

Malik, A., Fensholt, R., Mertz, O., 2015. Mangrove exploitation effects on biodiversity and ecosystem services. Biodivers. Conserv. 24, 3543–3557. https://doi.org/10.1007/s10531-015-1015-4

Marchand, C., Baltzer, F., Lallier-Vergès, E., Albéric, P., 2004. Pore-water chemistry in mangrove sediments: relationship with species composition and developmental stages (French Guiana). Mar. Geol. 208, 361–381. https://doi.org/10.1016/j.margeo.2004.04.015

McKenzie, N., Ryan, P., And, P.F., Wood, J., 2000. Sampling, measurement and analytical protocols for carbon estimation in soil, litter and coarse woody debris. Natl. carbon Account. Syst. Tech. Rep. No. 14.

Miao, S., DeLaune, R.D., Jugsujinda, A., 2006. Influence of sediment redox conditions on release/solubility of metals and nutrients in a Louisiana Mississippi River deltaic plain freshwater lake. Sci. Total Environ. 371, 334–343. https://doi.org/10.1016/j.scitotenv.2006.07.027

Mokhtari, M., Ghaffar, M.A., Usup, G., Cob, Z.C., 2016. Effects of fiddler crab burrows on sediment properties in the mangrove mudflats of sungai sepang, Malaysia. Biology (Basel). https://doi.org/10.3390/biology5010007

Moses, C.O., Herman, J.S., 1991. Pyrite oxidation at circumneutral pH. Geochim. Cosmochim. Acta 55, 471–482. https://doi.org/10.1016/0016-7037(91)90005-P

Moses, C.O., Kirk Nordstrom, D., Herman, J.S., Mills, A.L., 1987. Aqueous pyrite oxidation by dissolved oxygen and by ferric iron. Geochim. Cosmochim. Acta 51, 1561–1571. https://doi.org/10.1016/0016-7037(87)90337-1

Murdiyarso, D., Purbopuspito, J., Kauffman, J.B., Warren, M.W., Sasmito, S.D., Donato, D.C., Manuri, S., Krisnawati, H., Taberima, S., Kurnianto, S., 2015. The potential of Indonesian mangrove forests for global climate change mitigation. Nat. Clim. Chang. 5, 1089–1092. https://doi.org/10.1038/nclimate2734

Nealson, K.H., Myers, C.R., 1992. Microbial reduction of manganese and iron: New approaches to carbon cycling. Appl. Environ. Microbiol. 58, 439–443.

Nóbrega, G.N., Ferreira, T.O., Romero, R.E., Marques, A.G.B., Otero, X.L., 2013. Iron and sulfur geochemistry in semi-arid mangrove soils (Ceará, Brazil) in relation to seasonal changes and shrimp farming effluents. Environ. Monit. Assess. 185, 7393–7407. https://doi.org/10.1007/s10661-013-3108-4

Nóbrega, G.N., Ferreira, T.O., Siqueira Neto, M., Queiroz, H.M., Artur, A.G., Mendonça, E.D.S., Silva, E.D.O., Otero, X.L., 2016. Edaphic factors controlling summer (rainy season) greenhouse gas emissions (CO2 and CH4) from semiarid mangrove soils (NE-Brazil). Sci. Total Environ. 542, 685–693. https://doi.org/10.1016/j.scitotenv.2015.10.108

Olesen, A.J., Leithoff, A., Altenburger, A., Krock, B., Beszteri, B., Eggers, S.L., Lundholm, N., 2021. First Evidence of the Toxin Domoic Acid in Antarctic Diatom Species. Toxins (Basel). 13, 93. https://doi.org/10.3390/toxins13020093

Otero, X.L., Ferreira, T.O., Huerta-Díaz, M.A., Partiti, C.S.M., Souza, V., Vidal-Torrado, P., Macías, F., 2009. Geochemistry of iron and manganese in soils and sediments of a mangrove system, Island of Pai Matos (Cananeia — SP, Brazil). Geoderma 148, 318–335. https://doi.org/10.1016/j.geoderma.2008.10.016

Otero, X.L., Macias, F., 2003. Spatial variation in pyritization of trace metals in salt-marsh soils. Biogeochemistry 62, 59–86. https://doi.org/10.1023/A:1021115211165

Otero, X.L., Méndez, A., Nóbrega, G.N., Ferreira, T.O., Santiso-Taboada, M.J., Meléndez, W., Macías, F., 2017. High fragility of the soil organic C pools in mangrove forests. Mar. Pollut. Bull. 119, 460–464. https://doi.org/10.1016/j.marpolbul.2017.03.074

Patrick, W.H., Jugsujinda, A., 1992. Sequential Reduction and Oxidation of Inorganic Nitrogen, Manganese, and Iron in Flooded Soil. Soil Sci. Soc. Am. J. 56, 1071. https://doi.org/10.2136/sssaj1992.03615995005600040011x

Polidoro, B.A., Carpenter, K.E., Collins, L., Duke, N.C., Ellison, A.M., Ellison, J.C., Farnsworth, E.J., Fernando, E.S., Kathiresan, K., Koedam, N.E., Livingstone, S.R., Miyagi, T., Moore, G.E., Ngoc Nam, V., Ong, J.E., Primavera, J.H., Salmo, S.G., Sanciangco, J.C., Sukardjo, S., Wang, Y., Yong, J.W.H., 2010. The Loss of Species: Mangrove Extinction Risk and Geographic Areas of Global Concern. PLoS One 5, e10095. https://doi.org/10.1371/journal.pone.0010095

Powell, H., 2008. Will ocean iron fertilization work? Oceanus 46, 9–10.

Quéguiner, B., 2013. Iron fertilization and the structure of planktonic communities in high nutrient regions of the Southern Ocean. Deep. Res. Part II Top. Stud. Oceanogr. 90, 43–54. https://doi.org/10.1016/j.dsr2.2012.07.024

Queiroz, H.M., Ferreira, T.O., Barcellos, D., Nóbrega, G.N., Antelo, J., Otero, X.L., Bernardino, A.F., 2021. From sinks to sources: The role of Fe oxyhydroxide transformations on phosphorus dynamics in estuarine soils. J. Environ. Manage. 278, 111575. https://doi.org/10.1016/j.jenvman.2020.111575

Queiroz, H.M., Nóbrega, G.N., Ferreira, T.O., Almeida, L.S., Romero, T.B., Santaella, S.T., Bernardino, A.F., Otero, X.L., 2018a. The Samarco mine tailing disaster: A possible time-bomb for heavy metals contamination? Sci. Total Environ. 637–638, 498–506. https://doi.org/10.1016/j.scitotenv.2018.04.370

Queiroz, H.M., Nóbrega, G.N., Otero, X.L., Ferreira, T.O., 2018b. Are acid volatile sulfides (AVS) important trace metals sinks in semi-arid mangroves? Mar. Pollut. Bull. 126, 318–322. https://doi.org/10.1016/j.marpolbul.2017.11.020

Reddy, K.R., DeLaune, R.D., 2008. Biogeochemistry of wetlands: science and applications, 1st ed. CRC Press.

Reef, R., Feller, I.C., Lovelock, C.E., 2010. Nutrition of mangroves. Tree Physiol. 30, 1148–1160. https://doi.org/10.1093/treephys/tpq048

Reimann, C., Filzmoser, P., Garrett, R.G., Dutter, R., 2008. Statistical Data Analysis Explained, Statistical Data Analysis Explained: Applied Environmental Statistics with R. John Wiley & Sons, Ltd, Chichester, UK, UK. https://doi.org/10.1002/9780470987605

Rose, A.L., Waite, T.D., 2003. Predicting iron speciation in coastal waters from the kinetics of sunlight-mediated iron redox cycling. Aquat. Sci. 65, 375–383. https://doi.org/10.1007/s00027-003-0676-3

Rozan, T.F., Taillefert, M., Trouwborst, R.E., Glazer, B.T., Ma, S., Herszage, J., Valdes, L.M., Price, K.S., Luther, G.W., 2002. Iron-sulfur-phosphorus cycling in the sediments of a shallow coastal bay: Implications for sediment nutrient release and benthic macroalgal blooms. Limnol. Oceanogr. 47, 1346–1354. https://doi.org/10.4319/lo.2002.47.5.1346

Servino, R.N., Gomes, L.E. de O., Bernardino, A.F., 2018. Extreme weather impacts on tropical mangrove forests in the Eastern Brazil Marine Ecoregion. Sci. Total Environ. 628–629, 233–240. https://doi.org/10.1016/j.scitotenv.2018.02.068

Shaked, Y., Lis, H., 2012. Disassembling iron availability to phytoplankton. Front. Microbiol. 3, 1–26. https://doi.org/10.3389/fmicb.2012.00123

Sherman, R.E., Fahey, T.J., Howarth, R.W., 1998. Soil-plant interactions in a neotropical mangrove forest: Iron, phosphorus and sulfur dynamics. Oecologia. https://doi.org/10.1007/s004420050553

Silver, M.W., Bargu, S., Coale, S.L., Benitez-Nelson, C.R., Garcia, A.C., Roberts, K.J., Sekula-Wood, E., Bruland, K.W., Coale, K.H., 2010. Toxic diatoms and domoic acid in natural and iron enriched waters of the oceanic Pacific. Proc. Natl. Acad. Sci. U. S. A. 107, 20762–20767. https://doi.org/10.1073/pnas.1006968107

Sippo, J.Z., Lovelock, C.E., Santos, I.R., Sanders, C.J., Maher, D.T., 2018. Mangrove mortality in a changing climate: An overview. Estuar. Coast. Shelf Sci. 215, 241–249. https://doi.org/10.1016/j.ecss.2018.10.011

Sippo, J.Z., Maher, D.T., Schulz, K.G., Sanders, C.J., McMahon, A., Tucker, J., Santos, I.R., 2019. Carbon outwelling across the shelf following a massive mangrove dieback in Australia: Insights from radium isotopes. Geochim. Cosmochim. Acta 253, 142–158. https://doi.org/10.1016/j.gca.2019.03.003

Sippo, J.Z., Sanders, C.J., Santos, I.R., Jeffrey, L.C., Call, M., Harada, Y., Maguire, K., Brown, D., Conrad, S.R., Maher, D.T., 2020. Coastal carbon cycle changes following mangrove loss. Limnol. Oceanogr. lno.11476. https://doi.org/10.1002/lno.11476

Søndergaard, M., 2009. Redox Potential, in: Encyclopedia of Inland Waters. Elsevier, pp. 852–859. https://doi.org/10.1016/B978-012370626-3.00115-0

Straub, K.L., Benz, M., Schink, B., 2001. Iron metabolism in anoxic environments at near neutral pH. FEMS Microbiol. Ecol. 34, 181–186. https://doi.org/10.1016/S0168-6496(00)00088-X

Sun, H., Jiang, J., Cui, L., Feng, W., Wang, Y., Zhang, J., 2019. Soil organic carbon stabilization mechanisms in a subtropical mangrove and salt marsh ecosystems. Sci. Total Environ. 673, 502–510. https://doi.org/10.1016/j.scitotenv.2019.04.122

Taylor, K.G., Konhauser, K.O., 2011. In earth surface systems: A major player in chemical and biological processes. Elements 7, 83–88. https://doi.org/10.2113/gselements.7.2.83

Trick, C.G., Bill, B.D., Cochlan, W.P., Wells, M.L., Trainer, V.L., Pickell, L.D., 2010. Iron enrichment stimulates toxic diatom production in high-nitrate, low-chlorophyll areas. Proc. Natl. Acad. Sci. U. S. A. 107, 5887–5892. https://doi.org/10.1073/pnas.0910579107

Twilley, R.R., Rivera-Monroy, V.H., Rovai, A.S., Castañeda-Moya, E., Davis, S., 2019. Mangrove Biogeochemistry at Local to Global Scales Using Ecogeomorphic Approaches, in: Coastal Wetlands. https://doi.org/10.1016/b978-0-444-63893-9.00021-6

Vo, Q.T., Kuenzer, C., Vo, Q.M., Moder, F., Oppelt, N., 2012. Review of valuation methods for mangrove ecosystem services. Ecol. Indic. 23, 431–446. https://doi.org/10.1016/j.ecolind.2012.04.022

von Gunten, U., Schneider, W., 1991. Primary products of the oxygenation of iron(II) at an oxic-anoxic boundary: Nucleation, aggregation, and aging. J. Colloid Interface Sci. 145, 127–139. https://doi.org/10.1016/0021-9797(91)90106-I

Ward, R.D., Friess, D.A., Day, R.H., Mackenzie, R.A., 2016. Impacts of climate change on mangrove ecosystems: a region by region overview. Ecosyst. Heal. Sustain. 2, e01211. https://doi.org/10.1002/ehs2.1211

Xiong, Y., Ola, A., Phan, S.M., Wu, J., Lovelock, C.E., 2019. Soil Structure and Its Relationship to Shallow Soil Subsidence in Coastal Wetlands. Estuaries and Coasts 42, 2114–2123. https://doi.org/10.1007/s12237-019-00659-2

Ye, S., Laws, E.A., Wu, Q., Zhong, S., Ding, X., Zhao, G., Gong, S., 2010. Pyritization of trace metals in estuarine sediments and the controlling factors: A case in Jiaojiang Estuary of Zhejiang Province, China. Environ. Earth Sci. 61, 973–982. https://doi.org/10.1007/s12665-009-0416-7

Yu, K., Böhme, F., Rinklebe, J., Neue, H.-U., DeLaune, R.D., 2007. Major Biogeochemical Processes in Soils-A Microcosm Incubation from Reducing to Oxidizing Conditions. Soil Sci. Soc. Am. J. 71, 1406–1417. https://doi.org/10.2136/sssaj2006.0155

3. THE SAMARCO MINE TAILING DISASTER: A POSSIBLE TIME-BOMB FOR HEAVY METALS CONTAMINATION?

Abstract

In November 2015, the largest socio-environmental disaster in the history of Brazil occurred when approximately 50 million cubic meters of mine tailings were released into the Doce River (SE Brazil), during the greatest failure of a tailings dam worldwide. The mine tailings passed through the Doce River basin, reaching the ecologically important estuary 17 days later. On the arrival of the mine wastes to the coastal area, contamination levels in the estuarine soils were measured to determine the baseline level of contamination and to enable an environmental risk assessment. Soil and tailings samples were collected and analyzed to determine the redox potential (Eh), pH, grain size and mineralogical composition, total metal contents (Fe, Mn, Cr, Zn, Ni, Cu, Pb and Co) and organic matter content. The metals were fractionated to elucidate the mechanisms governing the trace metal dynamics. The mine tailings are mostly composed of Fe (mean values for Fe: 45,200 ± 2850; Mn: 433±110; Cr: 63.9 ± 15.1; Zn: 62.4 ± 28.4; Ni: 24.7 ± 10.4; Cu: 21.3 ± 4.6; Pb: 20.2 ± 4.6 and Co: 10.7 ± 4.8 mg kg^{-1}), consisting of Fe-oxyhydroxides (goethite, hematite); kaolinite and quartz. The metal contents of the estuarine soils, especially the surface layers, indicate trace metal enrichment caused by the tailings. However, the metal contents were below threshold levels reported in Brazilian environmental legislation. Despite the fact that only a small fraction (< 2%) of the metals identified are readily bioavailable (i.e., soluble and exchangeable fraction), trace metals associated with Fe oxyhydroxides contributed between 69.8 and 87.6 % of the total contents. Control of the trace metal dynamics by Fe oxyhydroxides can be ephemeral, especially in wetland soils in which the redox conditions oscillate widely. Indeed, the physicochemical conditions (Eh < 100 mV and circumneutral pH) of estuarine soils favor Fe reduction microbial pathways, which will probably increase the trace metal bioavailability and contamination risk.

Keywords: Iron oxides; Fe reduction; Estuarine soils; Doce River; Environmental impact.

Queiroz, H.M., Nóbrega, G.N., Ferreira, T.O., Almeida, L.S., Romero, T.B., Santaella, S.T., Bernardino, A.F., Otero, X.L., 2018. The Samarco mine tailing disaster: A possible time-bomb for heavy metals contamination? Sci. Total Environ. 637–638, 498–506. https://doi.org/10.1016/j.scitotenv.2018.04.370

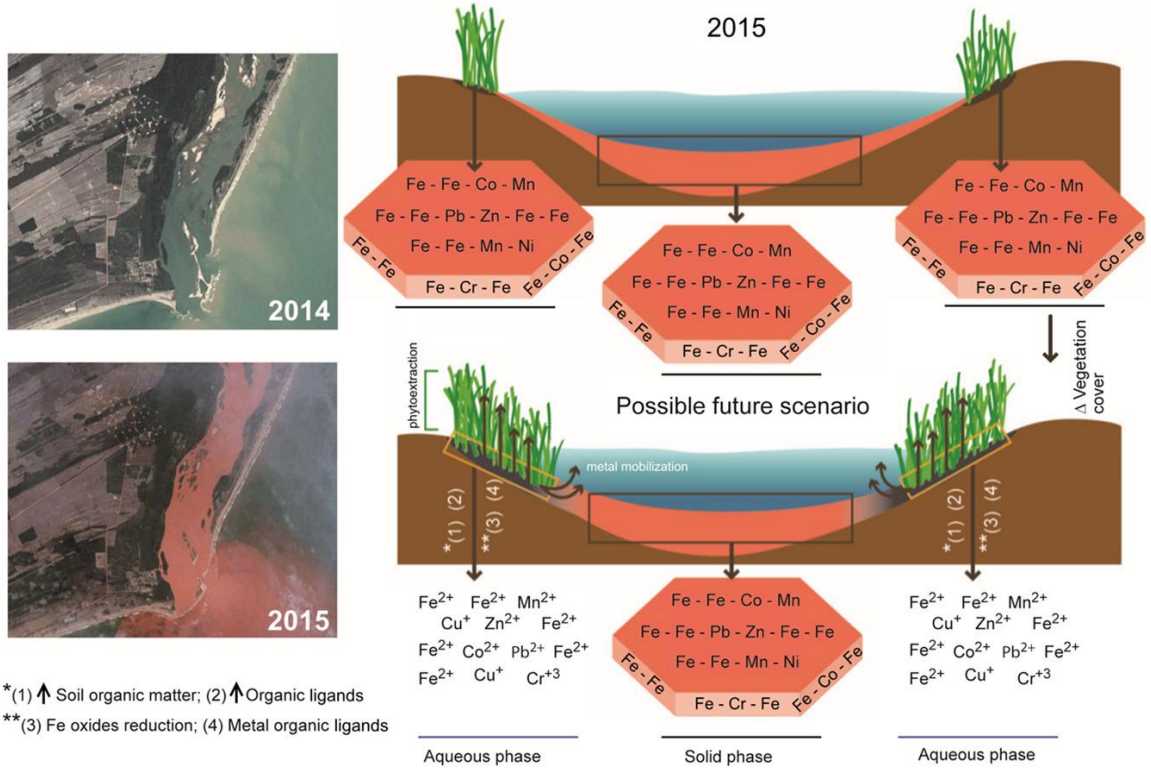

3.1. Introduction

In November 2015, the collapse of the Fundão dam (Samarco mining company) in Brazil led to the spillage of more than 50 million cubic meters of mine tailings into the Doce River (*Rio Doce*, in Portuguese). The tailings were then transported 600 km downriver to the *Regência* estuary (Espirito Santo state, SE Brazil; Marta-Almeida et al., 2016). The incident represents one of the largest failures of a tailings dam ever recorded (Hatje et al., 2017) and caused extensive ecological and cultural damage (Carmo et al., 2017). The event led to the death of 19 people and thousands of fishes and invertebrates and is considered the largest socio-environmental disaster in the history of Brazil (Escobar, 2015; Fonseca and Fonseca, 2016).

Multidisciplinary studies have been conducted using different approaches to identify the ecological magnitude of the collapse and to investigate the impacts on the quality of the inland soils (Guerra et al., 2017; Silva et al., 2017), on estuarine benthic assemblages (Gomes

et al., 2017), macrophyte growth (Bottino et al., 2017) and water quality (e.g. concentrations of dissolved metals and suspended solid material) along the river (Hatje et al., 2017). Although the baseline level of contamination was determined and early impact assessment of metal contamination on the Doce River basin was carried out (Gomes et al., 2017), the local drivers of trace metal bioavailability in the soils are not yet known. Knowledge of these drivers is crucial to understanding the environmental risks associated with the incident.

Estuarine wetland soils, which are very active ecological systems with a wide range of ecological functions and roles, are characterized as highly productive ecosystems (Barbier et al., 2011; Reed, 2005). Trace metal dynamics in these ecosystems are controlled by factors such as the frequency and duration of inundation, freshwater inputs, bioturbation and climatic variation, which control the redox potential (Eh), pH and organic matter content (OM) (Chapman and Wang, 2001; Ferreira et al., 2010; Laing et al., 2007; Machado et al., 2010). Because of the highly dynamic and variable characteristics of estuarine soils (Otero and Macias, 2002; Otero et al., 2017a, 2017b), sequential fractionation is a useful tool for environmental studies, providing valuable information about the association between elements and the solid phase and enabling assessment of the environmental impacts (Bacon and Davidson, 2008; Clark et al., 2000).

The objective of this study was to assess the contamination levels in the wetland soils affected by the tailing spillage in the Doce River estuary, thus providing baseline levels of contamination and identifying the drivers of the dynamics of the contaminants. This study also aims to contribute to assessing the potential effects that metal bioavailability may have on the impacted estuarine ecosystem.

3.2. Materials and methods

The study region is characterized by a humid tropical climate (Alvares et al., 2013), classified as Am according to the Köppen-Geiger Climate classification (Peel et al., 2007). There are two distinct seasons, a dry winter (April to September) and a wet summer (October to March); the mean annual temperature is 22 ºC and the maximum and minimum temperatures are 28-30 ºC and 15 ºC respectively (Albino et al., 2006; Bernardino et al., 2015).

Soil samples were collected at 4 different sites in the Doce River estuary (*Espírito Santo* state, SE Brazil), 7 days after the arrival of the contamination plume (Figure 1). A sampler for

flooded soils was used to collect soil samples (n=6) in PVC tubes, which were hermetically sealed and transported in a vertical position (at approximately 4 °C) to the laboratory. During the sampling procedure, the Eh values were determined using a platinum electrode, corrected by adding the value for the calomel reference electrode potential (+244 mV); the pH readings were obtained with a calibrated glass electrode (calibrated with pH = 4.0 and 7.0 standard solutions). In the laboratory, the soil cores were cut into 0-3, 3-5, 5-10 and 15-30 cm sections.

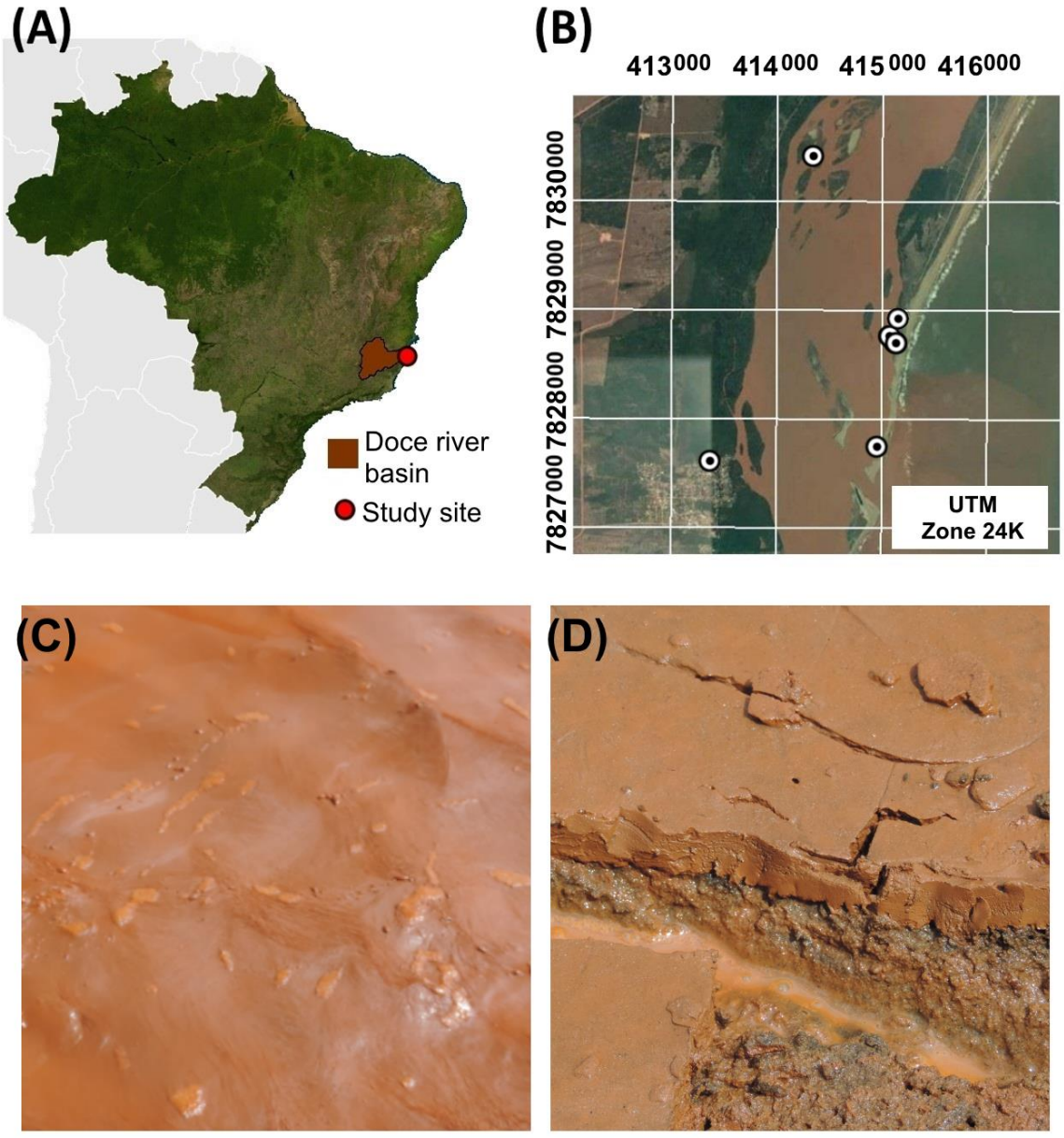

Figure 1. (A) Location of the Doce River basin and (B) the sites sampled. In detail: (C) the water in the Doce River after the tailings spillage and (D) deposition of the tailings along the coastal wetland soils.

Additional tailings samples were collected from the estuary (Figure 1D) and characterized according to their mineralogical composition by XRD analysis, by using Cu-Kα radiation, at 0.02° 2θ s^{-1} in the range of 3-60° 2θ as a non-oriented powder (Chen, 1977). Soil and tailings samples were analyzed for grain size composition and organic matter (OM) contents. The grain size composition was determined by sieving and was classified as follows: coarse sand (2000 to 200 µm), fine sand (200 to 50 µm), and mud (i.e., clay + silt; < 50 µm). The OM was determined by loss-on-ignition at 450º C (Goldin, 1987; Nóbrega et al., 2015).

The total metal contents of the soils and tailings were determined after microwave-assisted triacid digestion (HCl + HNO_3 + HF; USEPA, 1996). Additionally, fractionation of the solid phase Fe, Mn, Cr, Zn, Cu, Ni, Pb, and Co was performed by a combination of the methods proposed by Tessier et al. (1979), Huerta-Diaz and Morse (1990) and Fortín et al. (1993), to obtain six operationally distinct fractions: the exchangeable and soluble fraction (EX); the fraction bound to carbonates (CA); the fraction associated with ferrihydrite (FR); the fraction associated with lepidocrocite (LP); the fraction associated with crystalline Fe oxy-hydroxides (CR) and the fraction associated with pyrite (PY). For further details, see Araújo Júnior et al. (2016), Machado et al. (2014) and Nóbrega et al. (2013). The trace metal concentrations in each extract were determined by ICP-OES. The degree of Fe and trace metal (Me) pyritization (DOP and DTMP, respectively) were calculated by considering the sum of Fe_{EX} to Fe_{CR} and Me_{EX} to Me_{CR} as the reactive phase ($Fe_{REACTIVE} = \Sigma Fe_{EX} \rightarrow Fe_{CR}$; and $Me_{REACTIVE} = \Sigma Me_{EX} \rightarrow Me_{CR}$; Ferreira et al., 2010). The DOP and DTMP were calculated as follows:

$$DOP\ (\%) = Fe_{PY}/(Fe_{PY} + Fe_{REACTIVE}) \times 100$$

$$DTMP\ (\%) = Me_{PY}/(Me_{PY} + Me_{REACTIVE}) \times 100$$

3.3. Results

3.3.1. Analysis of tailings

The tailings deposited in the estuary are characterized by a predominance of fine particles (e.g., mud + fine sand: 73.6%), with redox conditions ranging from anoxic to sub-oxic and a circumneutral pH (Table 1).

Table 1. Particle-size distribution, chemical properties and organic matter contents of the deposited mine tailings

Variable	
Coarse sand (%)	26.5
Fine sand (%)	31.9
Mud (%)	41.7
pH	6.5 ± 1.0
Eh (mV)	76 ± 172
Organic matter (%)	9.4 ± 0.9

The XRD analysis indicates that tailings are mainly composed by hematite, goethite, kaolinite and quartz (Figure 2). The dominance of these minerals is associated with the characteristics of the mined ore (e.g. Itabirite rocks) (Silva et al., 2017). The tailings were characterized by the following metal contents (in decreasing order of content): mean Fe content, 45,200±2,850 mg kg^{-1}; mean Mn content, 433±110 mg kg^{-1}; mean Cr content, 63.9±15.1 mg kg^{-1}; mean Zn content: 62.4±28.4 mg kg^{-1}; mean Ni content: 24.7±10.4 mg kg^{-1}; mean Cu content: 21.3±5.5 mg kg^{-1}; mean Pb content: 20.2±4.6 mg kg^{-1}; and mean Co content: 10.7±4.8 mg kg^{-1} (Table 2).

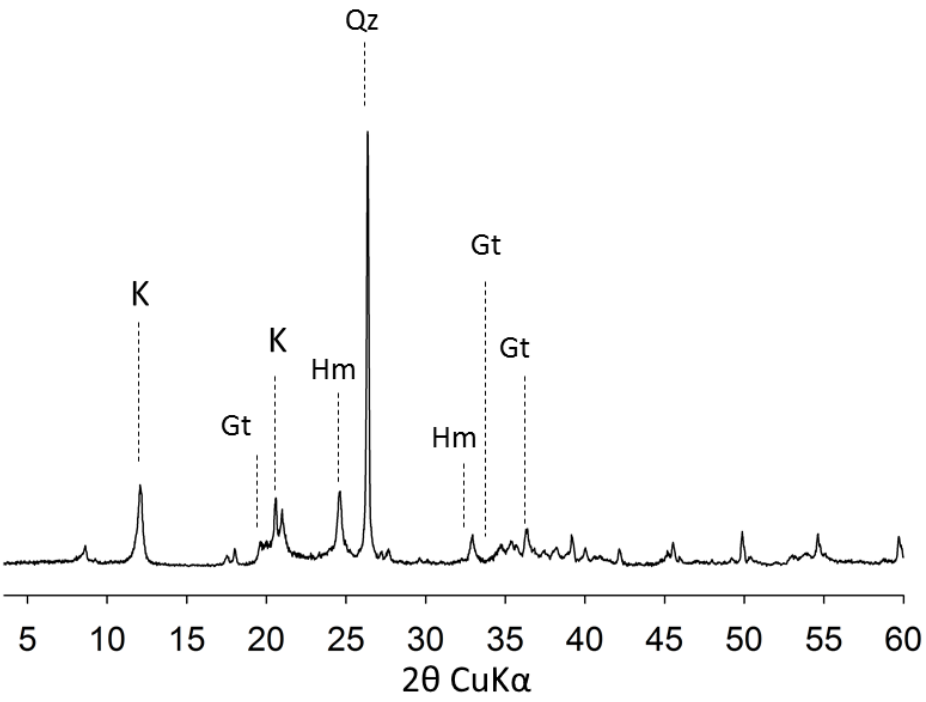

Figure 2. XRD analysis of the non-oriented sample of deposited tailings: K (kaolinite), il (illite), Gb (Gibbsite), Qr (Quartz), Gt (Goethita), Hm (Hematite)

The fractionation indicates that 89.4±2.3 % of the Fe content of the tailings was associated with crystalline oxides, followed by poorly crystalline Fe oxyhydroxides (percentage of the total content for Fe_{LP}: 5.6±0.1 and Fe_{FR}: 4.3±0.0 %). On the other hand, the Fe content associated with exchangeable and carbonates accounted for approximately 1.0±0.1 %, representing a small contribution to the total content.

Table 2. Total contents and fractionation of Fe, Mn, Cr, Zn, Ni, Cu, Pb and Co associated with the tailings.

	Fe	Mn	Cr	Zn	Ni	Cu	Pb	Co
	----------mg kg^{-1}----------							
Total								
	45,000±2,850	433±110	63.9±15.1	62.4±28.4	24.7±10.4	21.3±5.5	20.2±4.6	10.7±4.8
Fractions								
EX	11.2±5.6	1310±115	0.0±0.0	4.1±3.8	0.3±0.5	0.0±0.0	0.0±0.0	1.3±1.1
CA	800±530	44.0±33.0	0.0±0.0	2.9±1.7	0.8±0.7	1.0±0.4	0.0±0.0	2.0±0.9
FR	4,830±592	76.9±49.4	2.7±0.6	3.2±1.1	0.4±0.7	1.4±0.8	3.4±1.7	0.5±0.5
LP	6,330±1,230	76.9±27.5	4.5±0.9	4.8±1.3	0.3±0.3	1.1±0.6	6.4±1.4	1.0±0.4
CR	101,000±32,300	60.4±22.0	12±2.5	5.0±1.7	3.5±1.5	2.7±1.5	0.0±0.0	2.6±0.8
PY	5.6±5.6	0.0±0.0	0.5±0.8	0.0±0.1	0.3±0.1	0.9±0.4	1.9±2.1	0.2±0.2
DOP (%)	0.0	-		-	-	-	-	-
DTMP (%)	-	0.0	2.4	0.2	5.2	7.5	16.1	2.6

Exchangeable and soluble – EX; associated with carbonates – CA; associated with ferrihydrite – FR; associated with lepidocrocite – LP; associated with crystalline Fe oxy-hydroxides - CR; and associated with pyrite – PY; Degree of Fe pyritization – DOP; Degree of trace metal pyritization (DTMP).

The Ni, Cr, Co, Cu, and Zn contents were mainly associated with forms of crystalline Fe oxyhydroxides (percentage of the total content: Ni_{CR}, 67.0±13.8; Cr_{CR}, 60.9±2.7; Co_{CR}, 37.0±20.6; Cu_{CR}, 36.4±8.4; and Zn_{CR}, 25.7±9.5 %). Manganese mainly occurred as the soluble and exchangeable fraction (Mn_{EX}: 32.2±28.5 %) and associated with easily reducible Fe forms (Mn_{FR}: 21.0±15.2 and Mn_{LP}: 19.8±3.3 %), whereas Pb was mainly associated with easily reducible Fe oxyhydroxides (Pb_{LP}: 55.2±4.9 and Pb_{FR}: 29.2±11.8 %). The degree of trace metal pyritization (DTMP) was higher for Pb (Pb_{DTMP} = 15.6±14.3 %), Cu (Cu_{DTMP}: 14.9±10.5 %), Ni (Ni_{DTMP}: 6.0±2.3 %) Co (Co_{DTMP}: 2.2±2.0 %), and Cr (Cr_{DTMP} = 1.9±3.2 %), whereas the degree of Fe and Mn pyritization was zero (Table 2).

3.3.2 Soil properties and composition

Regarding the soil physicochemical conditions, the Eh values indicate anoxic conditions (Eh <100 mV; Otero et al., 2009), with values ranging from +6 to +134 mV (Figure 3A). On the other hand, pH values were circumneutral, with a small variation in depth (values ranging between 6.9±0.6 and 7.0±0.5; Figure 3B). The particle size indicated a predominantly sandy texture (mean values for all depths: coarse sand: 52.5±16.1%; fine sand: 25.2±15.5%; mud: 22.3±5.1%). However, higher contents of the finer fractions were observed in the surface soil layer (fine sand and mud, Figure 3C), resulting from deposition of the tailings. Furthermore, the OM varied greatly between the sampling sites, considered a characteristic feature of soils in sedimentary environments (Goñi et al., 2003), with values ranging between 2.7±2.3 and 6.3±3.5 % (Figure 3D).

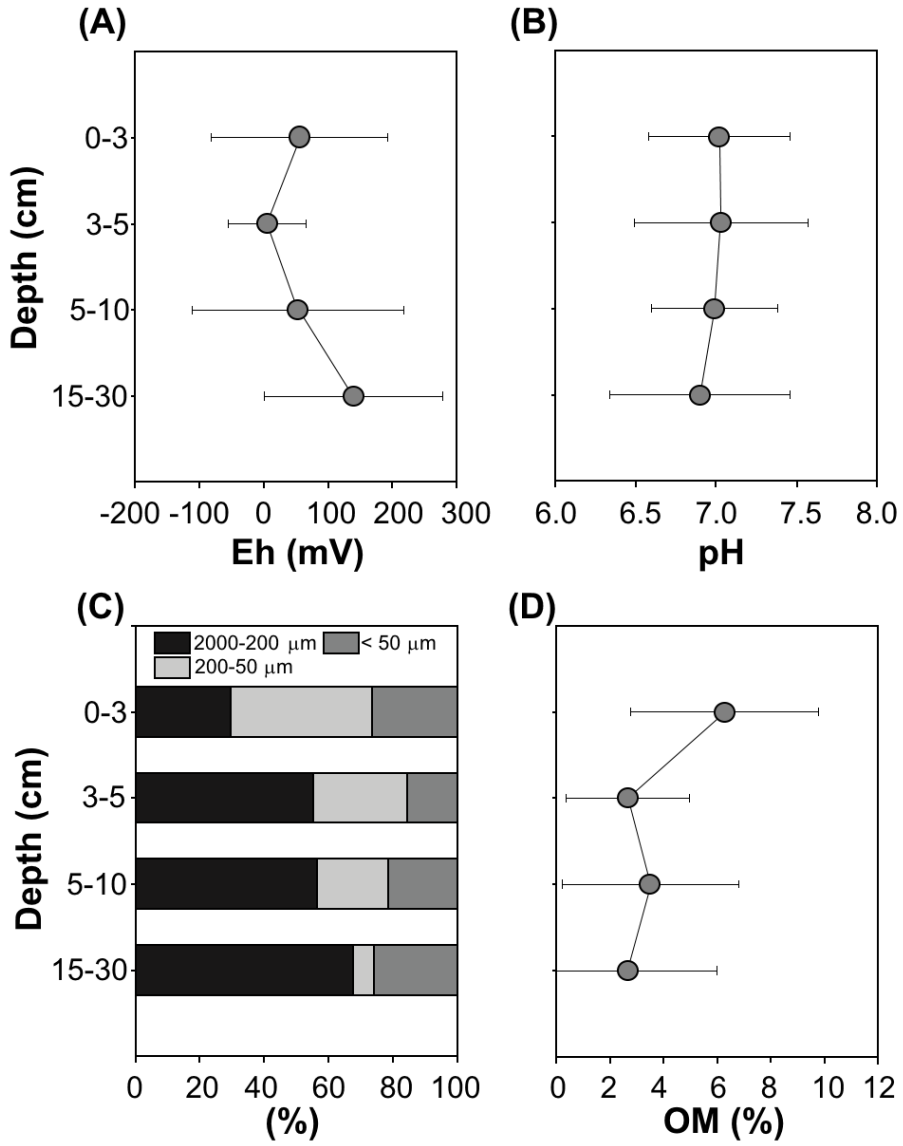

Figure 3. Characterization of estuarine soils: (A) Redox potential; (B) pH; (C) grain size composition; and (D) organic matter content

3.3.3 Total contents and metal partitioning in soils

Iron was found to be the most common metal in the soils (mean content 34,900±17,731.8 mg kg^{-1}), followed by Mn (mean content 586±500 mg kg^{-1}), Cr (content 51.3±32.4 mg kg^{-1}), Zn (content 49.3±34.4 mg kg^{-1}), Ni (content 20.4±15.1 mg kg^{-1}), Cu (content 17.9±13.7 mg kg^{-1}), Pb (content 16.1±11.8 mg kg^{-1}) and Co (content 9.9±6.3 mg kg^{-1}; Figure 4).

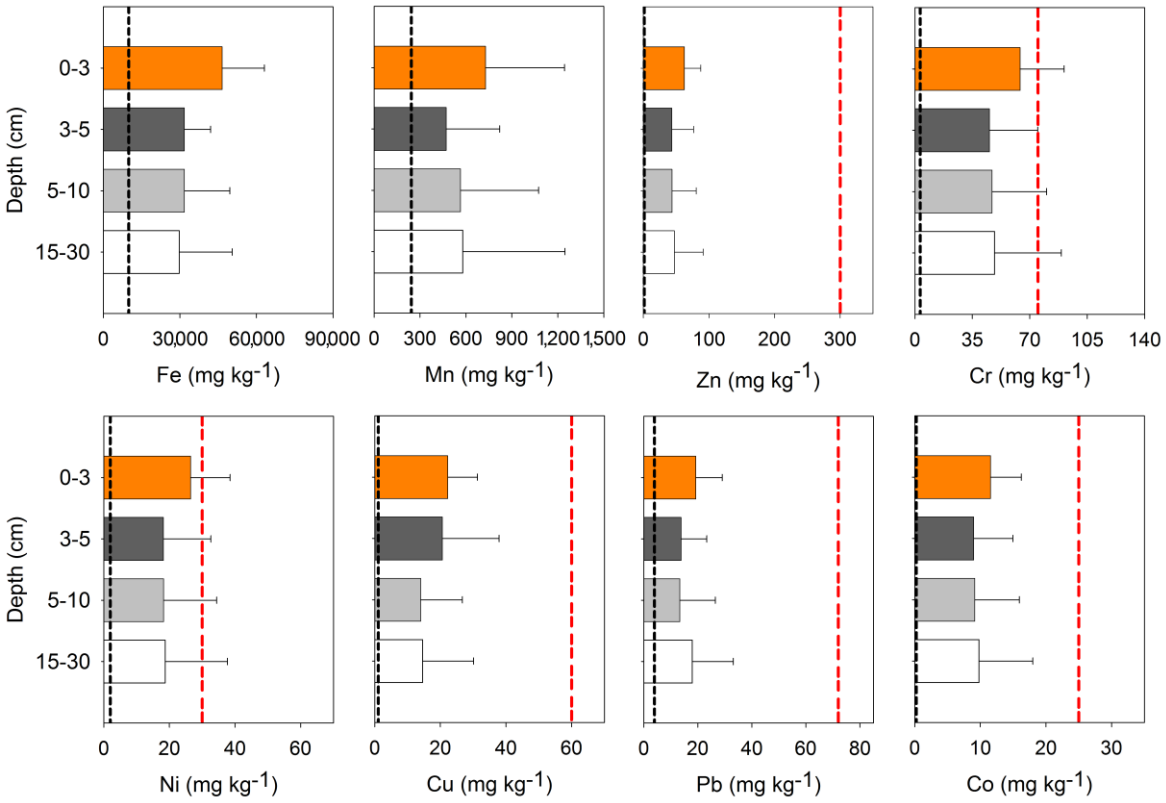

Figure 4. Total trace metal contents in the studied soils. The black dashed line represents the metal contents at the soil surface (0-2 cm), 2 days before the accident (Gomes et al., 2017). The red dashed line represents threshold values according to Brazilian legislation (CONAMA, 2009)

The tailings were not homogeneously deposited along the estuary, owing to the hydrodynamic conditions of each sampling site. Thus, the deposition was thicker at some sites than others (see supplementary table and figure). However, for all metals studied, the highest contents were generally recorded in the 0-3 cm layer, indicating the influence of the tailings (Figure 4).

The sequential extraction showed that the evaluated metals were mostly associated with Fe oxyhydroxides (FR + LP + CR; Figure 5). In fact, CR was the most important fraction for Fe (61,000±49,600 mg kg^{-1}), Cr (7.4±5.1 mg kg^{-1}), Zn (3.4±2.6 mg kg^{-1}), Ni (2.0±1.5 mg kg^{-1}), and Co (1.8±1.2 mg kg^{-1}), at all depths, whereas Mn (352±419 mg kg^{-1}) and Cu (1.8±1.9 mg kg^{-1}) were mainly associated with ferrihydrite and Pb (3.4±3.0 mg kg^{-1}) was mainly associated with lepidocrocite. Pyrite was a negligible fraction of all metals, representing less than 1%.

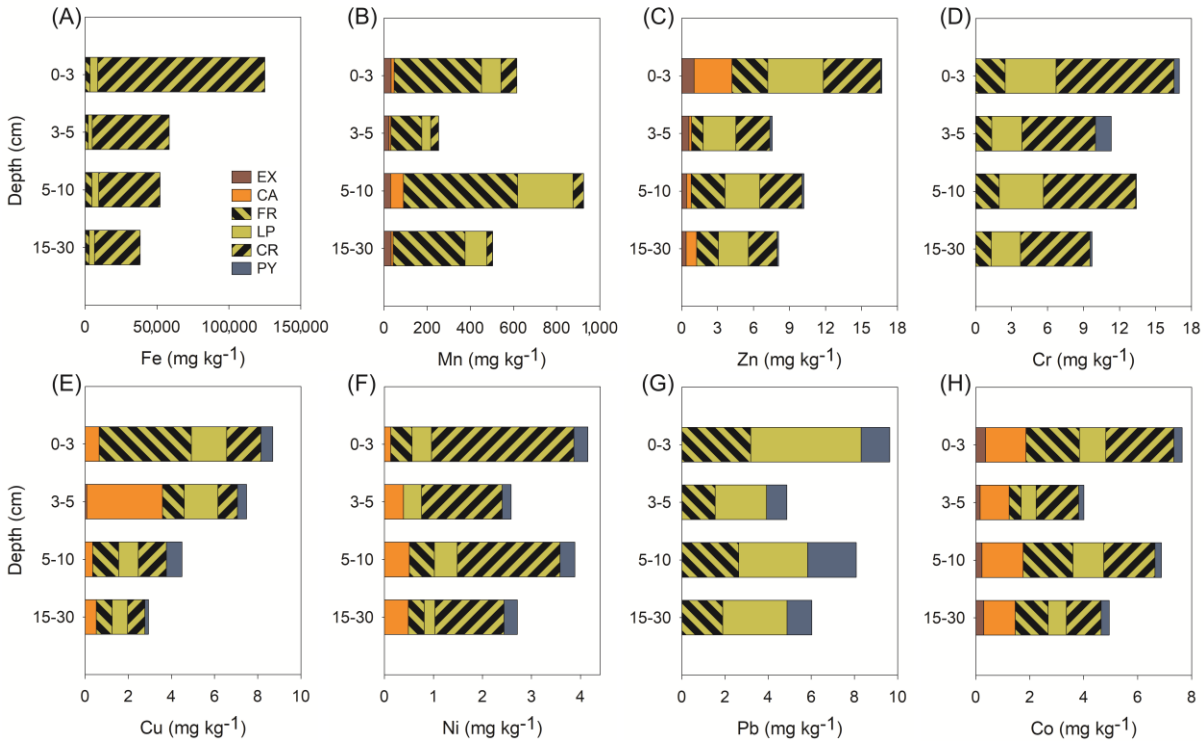

Figure 5. Solid-phase fractionation of the studied metals. Soluble and exchangeable fraction (EX), fraction bound to carbonates (CA), fraction associated with ferrihydrite-Fe and trace metals (FR); fraction associated with lepidocrocite and associated trace metals (LP); fraction associated with crystalline Fe oxides and associated trace metals (CR); and the fraction associated with pyrite (PY).

3.4. Discussion

The contents of all of the metals (except Ni and Cr) were below the threshold levels reported by Brazilian environmental law (CONAMA, 2009). However, despite being unevenly deposited, the tailings clearly affected the soil composition. Comparison of the mean metal contents recorded 2 days before the incident (Gomes et al., 2017) with those determined after the incident revealed that the latter values were at least 24 times higher (e.g. for Mn), and that the Zn and Cu contents were more than 200 times higher (Figure 4). In addition, the higher metal contents in the upper soil layers are consistent with the influence of the deposition of tailings on estuarine soil composition (e.g., mean Fe content in the 0-3 cm upper layer: 46,500±16,600 mg kg^{-1} compared to the deepest layer, 29,700±20,800 mg kg^{-1}; Figure 4). The highly significant correlation between Fe and the other metals considered supports the effects of tailings in trace metal deposition (Figure 6).

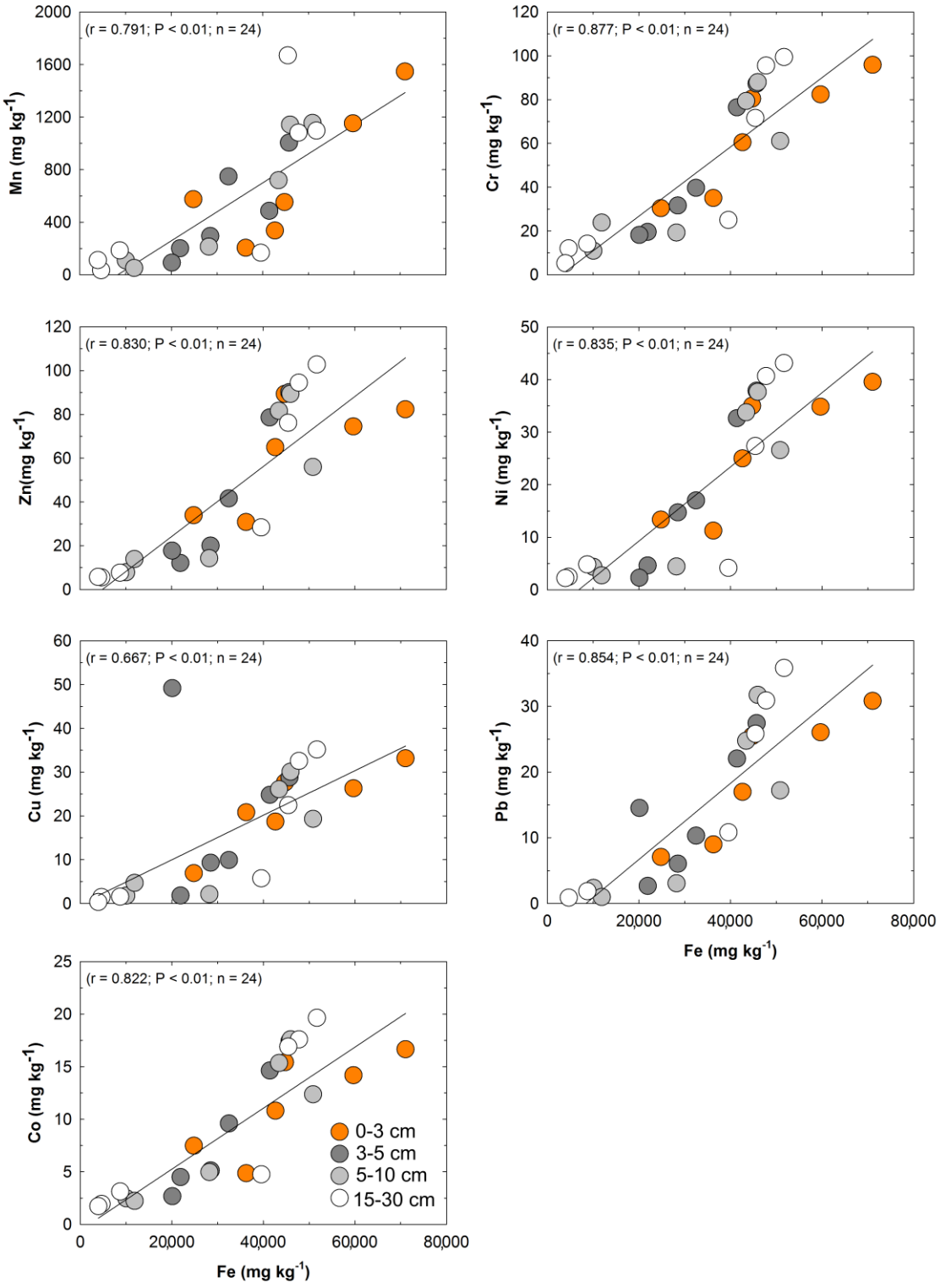

Figure 6. Correlation between total Fe and trace metal contents.

Considering the environmental conditions affecting the estuarine soil, which are different from those in dryland areas, the threshold values may not represent the real environmental risk. Thus, the reduction of Fe^{3+} (i.e. insoluble oxyhydroxides) to Fe^{2+} via the

microbial pathway (i.e. microbial reduction of iron: MRFe), through organic matter degradation processes inherent in coastal wetlands, has an important effect on metal bioavailability (Araújo Júnior et al., 2016; Bonneville et al., 2009, 2004; Lovley et al., 2004).

Iron oxyhydroxides are known to affect the bioavailability of trace metals and nutrients due to their high surface area and reactivity (Appelo and Postma, 2005; Rozan et al., 2002) and their ability to form complexes with metallic cations and anions (Zachara et al., 2001). However, redox fluctuations caused by flooding events in estuaries lead to sub-oxic conditions, which govern organic matter decomposition by MRFe (Lovley and Phillips, 1986; Zachara et al., 2001). Thus, the role of Fe oxyhydroxides in controlling trace metal bioavailability in the Doce River estuary may be transitory, as the Fe reduction leads to release of the associated trace metals and thus increasing their bioavailability (Zachara et al., 2001). Indeed, measurement of the physicochemical conditions in the studied soils indicated that the Fe oxyhydroxides may be solubilized and thus release the associated metals (Figure 7). Expansion of the riparian vegetation over the deposited mine tailings would increase the solubility of Fe oxyhydroxides via stimulation of MRFe activity by root exudates (Du Laing et al., 2009) or promoting the formation of organo-metallic complexes, which would increase trace metal bioavailability (Jones, 1998).

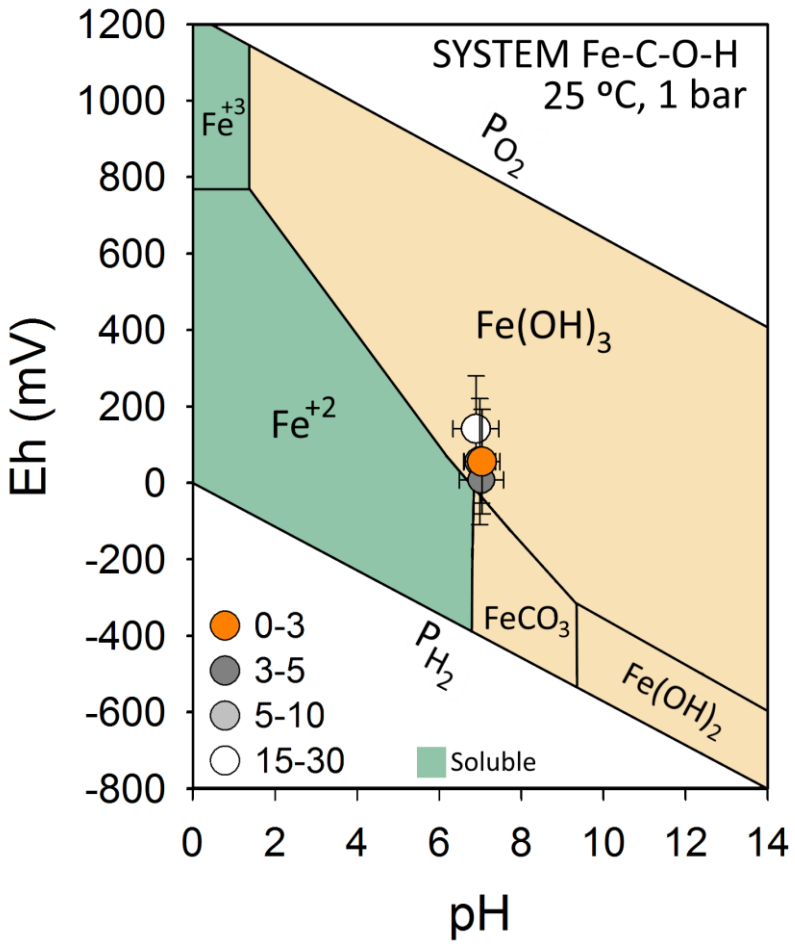

Figure 7. Eh-pH diagram (system Fe-C-O-H) for the studied soils (adapted from Brookins, 1988).

The environmental risk resulting from the reduction of the ferric iron could be minimized by the precipitation of trace metals as sulfides, e.g. pyrite (FeS_2), chalcocite (CuS_2) and sphalerite (ZnS) (Andrade et al., 2012; Cooper and Morse, 1998; Ferreira et al., 2007; Machado et al., 2014). However, the Doce River estuary has a minor tidal influence with typically low salinity levels (< 5 practical salinity units; Gomes et al., 2017). Thus, the low sulfate concentration limits pyrite formation (Canfield et al., 1993; Postma and Jakobsen, 1996), as indicated by the low Fe and metals degree of pyritization. Under more saline conditions, the formation of pyrite and sulfides may reduce the metal bioavailability, leading to the incorporation of soluble-bioavailable metals in more stable phases (Álvarez-Valero et al., 2009; Cooper et al., 1998; Otero et al., 2006) and reducing the associated environmental risks.

The conditions in the Doce River estuary contrast with those in most estuarine areas, as sulfate reduction is not favored. This increases the contamination risk of its biota if metals are released from Fe reduction. It is plausible to expect that Fe oxyhydroxides deposited on the estuarine soils in the Doce River may be solubilized (by MRFe and organic ligands), leading to a chronic trace metal contamination and potentially to the accumulation of trace metals in the biota (Figure 8). It is therefore likely that chronic impacts of tailings deposition in the estuary will last longer than expected, as the Fe redox cycle can trigger different biogeochemical processes.

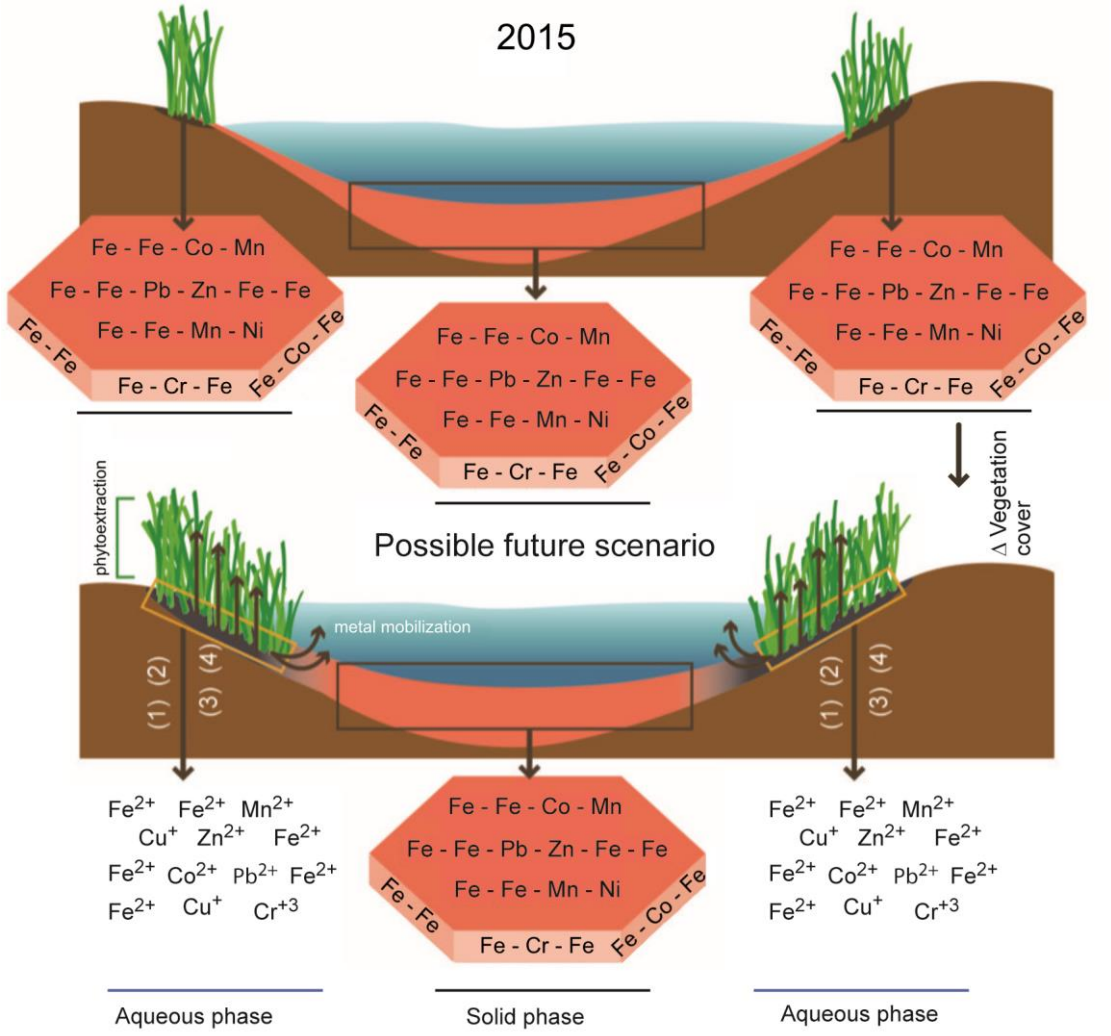

Figure 8. Schematic summary of processes involving trace metal mobilization in the Doce River estuary. The rupture of the Fundão dam (Samarco mining company) led to the formation of a red layer containing Fe-oxide (and associated metals) in the estuary Although the Fe-oxides were enriched in trace metals, the bioavailable contents of the trace metals were low. However, an increase in organic matter content in the soil by plant activity (1) may stimulate the reduction of Fe oxides (3) and the consequent release of trace metals to the water body (aqueous phase). Additionally, increasing vegetation cover may intensify the release of organic ligands (2), which may favour the incorporation of trace metals into the plant biomass (phytoextraction) and/or also their mobilization towards the water body (4).

3.5. Conclusions

The Samarco mine disaster involved the spillage of millions of tons of Fe-enriched tailings into the Doce River estuary. The dominant crystalline iron forms that settled in the estuarine wetland soils are closely associated with potentially toxic metals. Despite the accumulation of trace metals, the iron forms are mainly associated with less bioavailable

fractions (e.g., Fe-oxyhydroxides). However, transitory/cyclic anoxic conditions (common in estuarine soils and associated with plant or animal activity) may solubilize the Fe oxyhydroxides, thus releasing the associated metals and possibly leading to chronic contamination.

Acknowledgements

The authors are grateful for the financial support provided by the Coordenação de Aperfeiçoamento de Pessoal de Nível Superior (CAPES), São Paulo Research Foundation (FAPESP, grant number 2017/08101-1), National Council for Scientific and Technology Development (CNPq, process 308288/2014-9); Xunta de Galicia-Consellería de Educación e Ordeanción Universitaria de Galicia (Consolidation of competitive groups of investigation) and CRETUS strategic group (AGRUP2015/02). AFB and TOF were supported by FAPES grant N 77683544. The authors thank Esther Sierra for her contribution in elaborating the graphical abstract.

References

Albino, J., Girardi, G., Nascimento, K.A. do, 2006. Erosão e Progradação do Litoral do Espírito Santo, in: Muehe, D. (Ed.), Erosão E Progradação Do Litoral Do Brasil. Ministério do Meio Ambiente, Brasília, pp. 227–264.

Alvares, C.A., Stape, J.L., Sentelhas, P.C., de Moraes Gonçalves, J.L., Sparovek, G., 2013. Köppen's climate classification map for Brazil. Meteorol. Zeitschrift 22, 711–728. https://doi.org/10.1127/0941-2948/2013/0507

Álvarez-Valero, A.M., Sáez, R., Pérez-López, R., Delgado, J., Nieto, J.M., 2009. Evaluation of heavy metal bio-availability from Almagrera pyrite-rich tailings dam (Iberian Pyrite Belt, SW Spain) based on a sequential extraction procedure. J. Geochemical Explor. 102, 87–94. https://doi.org/10.1016/j.gexplo.2009.02.005

Andrade, R.A., Sanders, C.J., Boaventura, G., Patchineelam, S.R., 2012. Pyritization of trace metals in mangrove sediments. Environ. Earth Sci. 67, 1757–1762. https://doi.org/10.1007/s12665-012-1620-4

Appelo, C.A.J., Postma, D., 2005. Geochemistry, Groundwater and Pollution, 2nd ed. Taylor & Francis.

Araújo Júnior, J.M. de C., Ferreira, T.O., Suarez-Abelenda, M., Nóbrega, G.N., Albuquerque, A.G.B.M., Bezerra, A. de C., Otero, X.L., 2016. The role of bioturbation by Ucides cordatus crab in the fractionation and bioavailability of trace metals in tropical semiarid mangroves. Mar. Pollut. Bull. 111, 194–202. https://doi.org/10.1016/j.marpolbul.2016.07.011

Bacon, J.R., Davidson, C.M., 2008. Is there a future for sequential chemical extraction? Analyst 133, 25–46. https://doi.org/10.1039/B711896A

Barbier, E.B., Hacker, S.D., Kennedy, C., Koch, E.W., Stier, A.C., Silliman, B.R., 2011. The value of estuarine and coastal ecosystem services. Ecol. Monogr. 81, 169–193. https://doi.org/10.1890/10-1510.1

Bernardino, A.F., Netto, S.A., Pagliosa, P.R., Barros, F., Christofoletti, R.A., Rosa Filho, J.S., Colling, A., Lana, P.C., 2015. Predicting ecological changes on benthic estuarine assemblages through decadal climate trends along Brazilian Marine Ecoregions. Estuar. Coast. Shelf Sci. 166, 74–82. https://doi.org/10.1016/j.ecss.2015.05.021

Bonneville, S., Behrends, T., Van Cappellen, P., 2009. Solubility and dissimilatory reduction kinetics of iron(III) oxyhydroxides: A linear free energy relationship. Geochim. Cosmochim. Acta 73, 5273–5282. https://doi.org/10.1016/j.gca.2009.06.006

Bonneville, S., Van Cappellen, P., Behrends, T., 2004. Microbial reduction of iron(III) oxyhydroxides: Effects of mineral solubility and availability. Chem. Geol. 212, 255–268. https://doi.org/10.1016/j.chemgeo.2004.08.015

Bottino, F., Milan, J.A.M., Cunha-Santino, M.B., Bianchini, I., 2017. Influence of the residue from an iron mining dam in the growth of two macrophyte species. Chemosphere 186, 488–494. https://doi.org/10.1016/j.chemosphere.2017.08.030

Brookins, D.G., 1988. Eh-pH diagrams for geochemistry, 1st ed. Springer-Verlag Berlin Heidelberg. https://doi.org/10.1007/978-3-642-73093-1

Canfield, D.E., Thamdrup, B., Hansen, J.W., 1993. The anaerobic degradation of organic matter in Danish coastal sediments: Iron reduction, manganese reduction, and sulfate reduction. Geochim. Cosmochim. Acta 57, 3867–3883. https://doi.org/10.1016/0016-7037(93)90340-3

Carmo, F.F. do, Kamino, L.H.Y., Junior, R.T., Campos, I.C. de, Carmo, F.F. do, Silvino, G., Castro, K.J. da S.X. de, Mauro, M.L., Rodrigues, N.U.A., Miranda, M.P. de S., Pinto, C.E.F., 2017. Fundão tailings dam failures: The environment tragedy of the largest technological disaster of Brazilian mining in global context. Perspect. Ecol. Conserv. 15, 145–151. https://doi.org/10.1016/j.pecon.2017.06.002

Chapman, P.M., Wang, F., 2001. Assessing sediment contamination in estuaries. Environ. Toxicol. Chem. 20, 3–22. https://doi.org/10.1002/etc.5620200102

Chen, P.-Y., 1977. Table of key lines in X-ray powder diffraction patterns of minerals in clays and associated rocks. Department of Natural Resources, Indiana Geological Survey, Bloomington, Indiana.

Clark, M.W., Davies-Mcconchie, F., McConchie, D., Birch, G.F., 2000. Selective chemical extraction and grainsize normalisation for environmental assessment of anoxic sediments: Validation of an integrated procedure. Sci. Total Environ. 258, 149–170. https://doi.org/10.1016/S0048-9697(00)00532-5

Cooper, D.C., Morse, J.W., 1998. Biogeochemical Controls on Trace Metal Cycling in Anoxic Marine Sediments. Environ. Sci. Technol. 32, 327–330. https://doi.org/10.1021/es970387e

Cooper, D.C., Morse, J.W., Cooper, D.C., Morse, J.W., 1998. Biogeochemical Controls on Trace Metal Cycling in Anoxic Marine Sediments Biogeochemical Controls on Trace Metal Cycling in Anoxic Marine Sediments 32, 327–330. https://doi.org/10.1021/es970387e

Du Laing, G., Rinklebe, J., Vandecasteele, B., Meers, E., Tack, F.M.G., 2009. Trace metal behaviour in estuarine and riverine floodplain soils and sediments: A review. Sci. Total Environ. 407, 3972–3985. https://doi.org/10.1016/j.scitotenv.2008.07.025

Escobar, H., 2015. Mud tsunami wreaks ecological havoc in Brazil. Science (80-.). 350, 1138–1139. https://doi.org/10.1126/science.350.6265.1138

Ferreira, T.O., Otero, X.L., de Souza Junior, V.S., Vidal-Torrado, P., Macías, F., Firme, L.P., 2010. Spatial patterns of soil attributes and components in a mangrove system in Southeast Brazil (São Paulo). J. Soils Sediments 10, 995–1006. https://doi.org/10.1007/s11368-010-0224-4

Ferreira, T.O., Otero, X.L., Vidal-Torrado, P., Macías, F., 2007. Redox Processes in Mangrove Soils under in Relation to Different Environmental Conditions. Soil Sci. Soc. Am. J. 71, 484. https://doi.org/10.2136/sssaj2006.0078

Fonseca, P.G. da, Fonseca, I.G. da, 2016. Brazil's Greatest Environmental Catastrophe – Samarco's Fundão Tailings Dam –. Environ. Policy Law 46, 334–337. https://doi.org/10.3233/EPL-46505

Fortin, D., Leppard, G.G., Tessier, A., 1993. Characteristics of lacustrine diagenetic iron oxyhydroxides. Geochim. Cosmochim. Acta 57, 4391–4404. https://doi.org/10.1016/0016-7037(93)90490-N

Goldin, A., 1987. Reassessing the use of loss-on-ignition for estimating organic matter content in noncalcareous soils. Commun. Soil Sci. Plant Anal. 18, 1111–1116. https://doi.org/10.1080/00103628709367886

Gomes, L.E. de O., Correa, L.B., Sá, F., Neto, R.R., Bernardino, A.F., 2017. The impacts of the Samarco mine tailing spill on the Rio Doce estuary, Eastern Brazil. Mar. Pollut. Bull. 120, 28–36. https://doi.org/10.1016/j.marpolbul.2017.04.056

Goñi, M.A., Teixeira, M.J., Perkeya, D.W., 2003. Sources and distribution of organic matter in a river-dominated estuary (Winyah Bay, SC, USA). Estuar. Coast. Shelf Sci. 57, 1023–1048. https://doi.org/10.1016/S0272-7714(03)00008-8

Guerra, M.B.B., Teaney, B.T., Mount, B.J., Asunskis, D.J., Jordan, B.T., Barker, R.J., Santos, E.E., Schaefer, C.E.G.R., 2017. Post-catastrophe Analysis of the Fundão Tailings Dam Failure in the Doce River System, Southeast Brazil: Potentially Toxic Elements in Affected Soils. Water. Air. Soil Pollut. 228. https://doi.org/10.1007/s11270-017-3430-5

Hatje, V., Pedreira, R.M.A., De Rezende, C.E., Schettini, C.A.F., De Souza, G.C., Marin, D.C., Hackspacher, P.C., 2017. The environmental impacts of one of the largest tailing dam failures worldwide. Sci. Rep. 7, 1–13. https://doi.org/10.1038/s41598-017-11143-x

Huerta-Diaz, M.A., Morse, J.W., 1990. A quantitative method for determination of trace metal concentrations in sedimentary pyrite. Mar. Chem. 29, 119–144. https://doi.org/10.1016/0304-4203(90)90009-2

Jones, D.L., 1998. Organic acids in the rhizosphere - A critical review. Plant Soil 205, 25–44. https://doi.org/10.1023/A:1004356007312

Laing, G. Du, Vanthuyne, D., Tack, F.M.G., Verloo, M.G., 2007. Management Factors affecting metal mobility and bioavailability in the superficial intertidal sediment layer of the Scheldt estuary Factors affecting metal mobility and bioavailability in the superficial intertidal sediment layer of the Scheldt estuary. Aquat. Ecosyst. Health Manag. 10, 33–40. https://doi.org/10.1080/14634980701212969

Lovley, D.R., Holmes, D.E., Nevin, K.P., 2004. Dissimilatory Fe(III) and Mn(IV) reduction, Advances in Microbial Physiology. https://doi.org/10.1016/S0065-2911(04)49005-5

Lovley, D.R., Phillips, E.J.P., 1986. Organic-Matter Mineralization With Reduction of Ferric Iron in Anaerobic Sediments. Appl. Environ. Microbiol. 51, 683–689. https://doi.org/10.1080/01490458709385975

Machado, W., Borrelli, N.L., Ferreira, T.O., Marques, A.G.B., Osterrieth, M., Guizan, C., 2014. Trace metal pyritization variability in response to mangrove soil aerobic and anaerobic oxidation processes. Mar. Pollut. Bull. 79, 365–370. https://doi.org/10.1016/j.marpolbul.2013.11.016

Machado, W., Villar, L.S., Monteiro, F.F., Viana, L.C.A., Santelli, R.E., 2010. Relation of acid-volatile sulfides (AVS) with metals in sediments from eutrophicated estuaries: Is it limited by metal-to-AVS ratios? J. Soils Sediments 10, 1606–1610. https://doi.org/10.1007/s11368-010-0297-0

Marta-Almeida, M., Mendes, R., Amorim, F.N., Cirano, M., Dias, J.M., 2016. Fundão Dam collapse: Oceanic dispersion of River Doce after the greatest Brazilian environmental accident. Mar. Pollut. Bull. 112, 359–364. https://doi.org/10.1016/j.marpolbul.2016.07.039

Miranda, L.S., Marques, A.C., 2016. Hidden impacts of the Samarco mining waste dam collapse to Brazilian marine fauna – an example from the staurozoans (Cnidaria). Biota Neotrop. 16, 1–3. https://doi.org/10.1590/1676-0611

Nóbrega, G.N., Ferreira, T.O., Artur, A.G., de Mendonça, E.S., de O. Leão, R.A., Teixeira, A.S., Otero, X.L., 2015. Evaluation of methods for quantifying organic carbon in mangrove soils from semi-arid region. J. Soils Sediments 15, 282–291. https://doi.org/10.1007/s11368-014-1019-9

Nóbrega, G.N., Ferreira, T.O., Romero, R.E., Marques, A.G.B., Otero, X.L., 2013. Iron and sulfur geochemistry in semi-arid mangrove soils (Ceará, Brazil) in relation to seasonal changes and shrimp farming effluents. Environ. Monit. Assess. 185, 7393–7407. https://doi.org/10.1007/s10661-013-3108-4

Otero, X.L., Calvo De Anta, R.M., Macías, F., 2006. Sulphur partitioning in sediments and biodeposits below mussel rafts in the Ría de Arousa (Galicia, NW Spain). Mar. Environ. Res. 61, 305–325. https://doi.org/10.1016/j.marenvres.2005.10.006

Otero, X.L., Ferreira, T.O., Huerta-Díaz, M.A., Partiti, C.S.M., Souza, V., Vidal-Torrado, P., Macías, F., 2009. Geochemistry of iron and manganese in soils and sediments of a mangrove system, Island of Pai Matos (Cananeia - SP, Brazil). Geoderma 148, 318–335. https://doi.org/10.1016/j.geoderma.2008.10.016

Otero, X.L., Macias, F., 2002. Variation with depth and season in metal sulfides in salt marsh soils. Biogeochemistry 61, 247–268. https://doi.org/10.1023/A:1020230213864

Otero, X.L., Méndez, A., Nóbrega, G.N., Ferreira, T.O., Santiso-Taboada, M.J., Meléndez, W., Macías, F., 2017. High fragility of the soil organic C pools in mangrove forests. Mar. Pollut. Bull. 119, 460–464. https://doi.org/10.1016/j.marpolbul.2017.03.074

Peel, M.C., Finlayson, B.L., McMahon, T.A., 2007. Updated world map of the Köppen-Geiger climate classification. Hydrol. Earth Syst. Sci. Discuss. 4, 439–473. https://doi.org/10.5194/hessd-4-439-2007

Postma, D., Jakobsen, R., 1996. Redox zonation: Equilibrium constraints on the Fe(III)/SO4-reduction interface. Geochim. Cosmochim. Acta 60, 3169–3175. https://doi.org/10.1016/0016-7037(96)00156-1

Reed, D.J., 2005. Wetlands, in: Schwartz, M. (Ed.), Encyclopedia of Coastal Science. Springer Netherlands, Dordrecht, pp. 1077–1081. https://doi.org/10.1007/1-4020-3880-1_352

Rozan, T.F., Taillefert, M., Trouwborst, R.E., Glazer, B.T., Ma, S., Herszage, J., Valdes, L.M., Price, K.S., Luther III, G.W., 2002. Iron–sulfur–phosphorus cycling in the sediments of a shallow coastal bay: Implications for sediment nutrient release and benthic macroalgal blooms. Limnol. Ocean. 47, 1346–1354. https://doi.org/10.4319/lo.2002.47.5.1346

Silva, A.C., Cavalcante, L.C.D., Fabris, J.D., Júnior, R.F., Barral, U.M., Farnezi, M.M. de M., Viana, A.J.S., Ardisson, J.D., Fernandez-Outon, L.E., Lara, L.R.S., Stumpf, H.O., Barbosa, J.B.S., Silva, L.C. da, 2017. Características químicas, mineralógicas e físicas do material acumulado em terraços fluviais, originado do fluxo de lama proveniente do rompimento de barragem de rejeitos de mineração de ferro em Bento Rodrigues, Minas Gerais, Brasil. Rev. Espinhaço | UFVJM; Rev. Espinhaço #9.

Tessier, A., Campbell, P.G.C., Bisson, M., 1979. Sequential Extraction Procedure for the Speciation of Particulate Trace Metals. Anal. Chem. 51, 844–851. https://doi.org/10.1021/ac50043a017

USEPA, U.S.E.P.A., 1996. EPA Method 3050B (SW-846): Acid Digestion of Sediments, Sludges, and Soils 12.

Zachara, J.M., Fredrickson, J.K., Smith, S.C., Gassman, P.L., 2001. Solubilization of Fe(III) oxide-bound trace metals by a dissimilatory Fe(III) reducing bacterium. Geochim. Cosmochim. Acta 65, 75–93. https://doi.org/10.1016/S0016-7037(00)00500-7

Supplementary Material

Table S1- Total metal contents (mg kg^{-1}) in sampled sites at the Doce river estuary.

Site	Location	Depth (cm)	Co	Cr	Cu	Fe	Mn	Ni	Pb	Zn
			mg kg^{-1}							
1	415079.26 E 7828772.83 S	0-3	14	82	26	59696	1152	35	26	74
		3-5	4	20	2	21944	201	5	3	12
		5-10	5	19	2	28234	213	4	3	14
		15-30	8	40	10	22225	237	15	11	33
2	415112.14 E 7828756.19 S	0-3	15	80	28	44743	552	35	25	89
		3-5	17	87	29	45724	1004	38	27	90
		5-10	18	88	30	45967	1142	38	32	89
		15-30	18	100	34	50923	1148	42	34	101
3	415107.13 E 7828896.06 S	0-3	11	60	19	42646	336	25	17	65
		3-5	15	76	25	41437	486	33	22	79
		5-10	15	79	26	43454	719	34	25	82
		15-30	19	101	35	50939	1160	43	35	102
4	414962.39 E 7827762.19 S	0-3	17	96	33	71063	1547	40	31	82
		3-5	5	32	9	28522	295	15	6	20
		5-10	2	11	2	10093	109	4	2	8
		15-30	2	9	1	4334	72	2	1	6
5	414348.45 E 7830429.01 S	0-3	7	30	7	24824	574	13	7	34
		3-5	10	40	10	32511	748	17	10	42
		5-10	12	61	19	50883	1155	27	17	56
		15-30	17	72	22	45467	1669	27	26	76
6	413376.99 E 7827618.65 S	0-3	5	35	21	36275	205	11	9	31
		3-5	3	18	49	20130	92	2	15	18
		5-10	2	24	5	11906	51	3	1	14
		15-30	5	25	6	39584	167	4	11	28

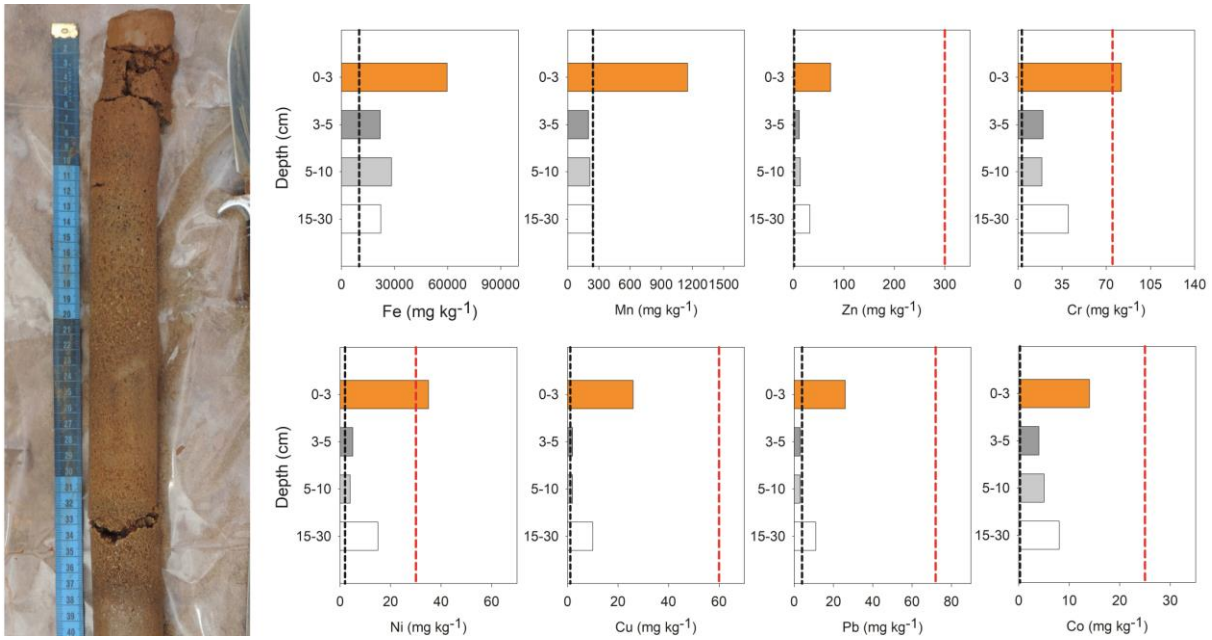

Fig. S1. Trace metals total contents for the site 1 sampled. At left, a soil profile. Black dashed line represents metal contents in soil surface (0-2 cm) 2 days before the accident (Gomes et al., 2017). Red dashed line represents prevention values according to Brazilian legislation (CONAMA, 2009)

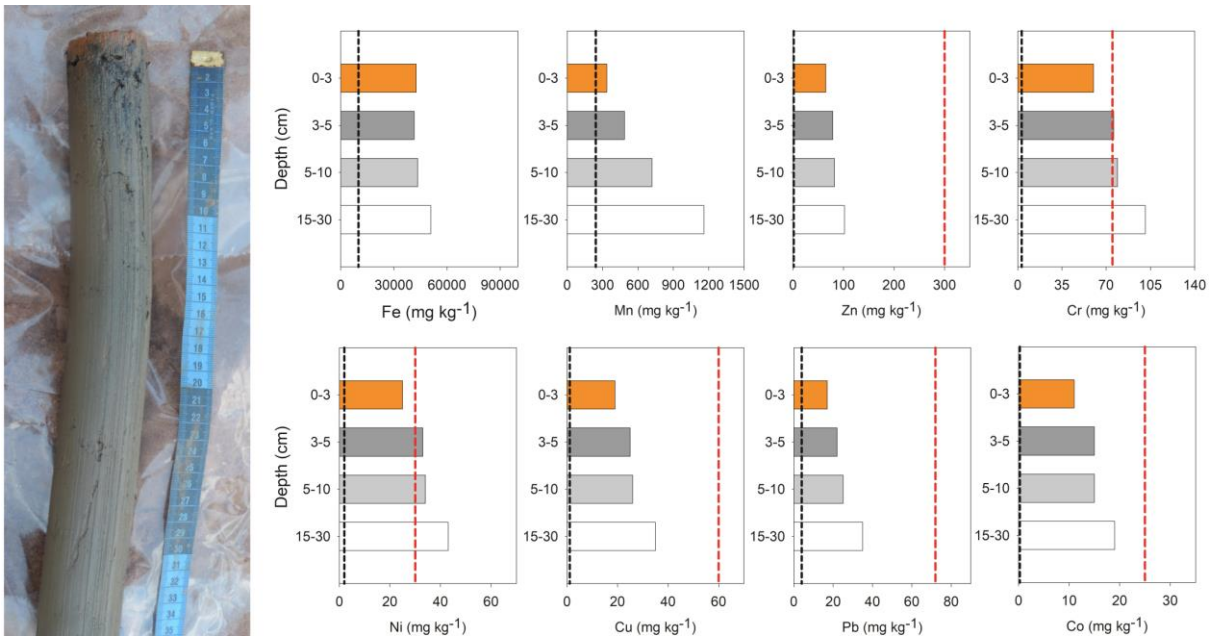

Fig. S2. Trace metals total contents for the site 2 sampled. At left, a soil profile. Black dashed line represents metal contents in soil surface (0-2 cm) 2 days before the accident (Gomes et al., 2017). Red dashed line represents prevention values according to Brazilian legislation (CONAMA, 2009)

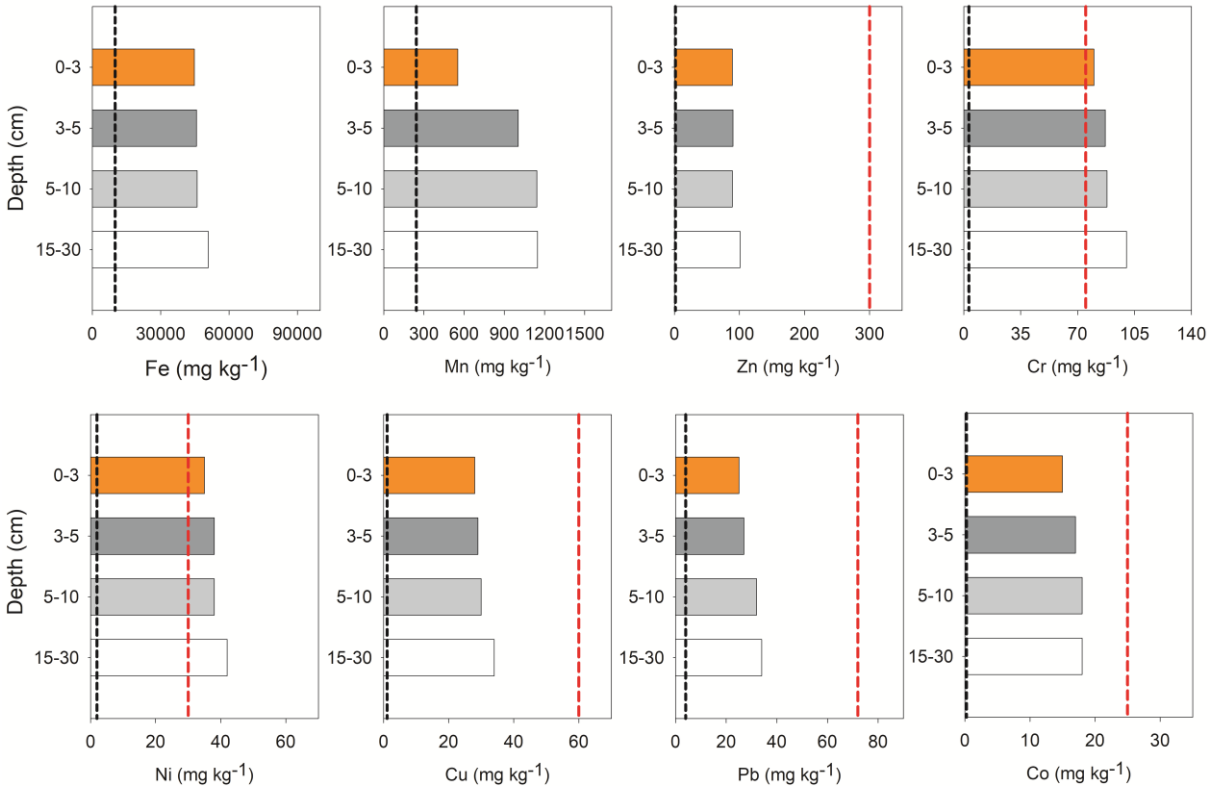

Fig. S3. Trace metals total contents for the site 3 sampled. Black dashed line represents metal contents in soil surface (0-2 cm) 2 days before the accident (Gomes et al., 2017). Red dashed line represents prevention values according to Brazilian legislation (CONAMA, 2009)

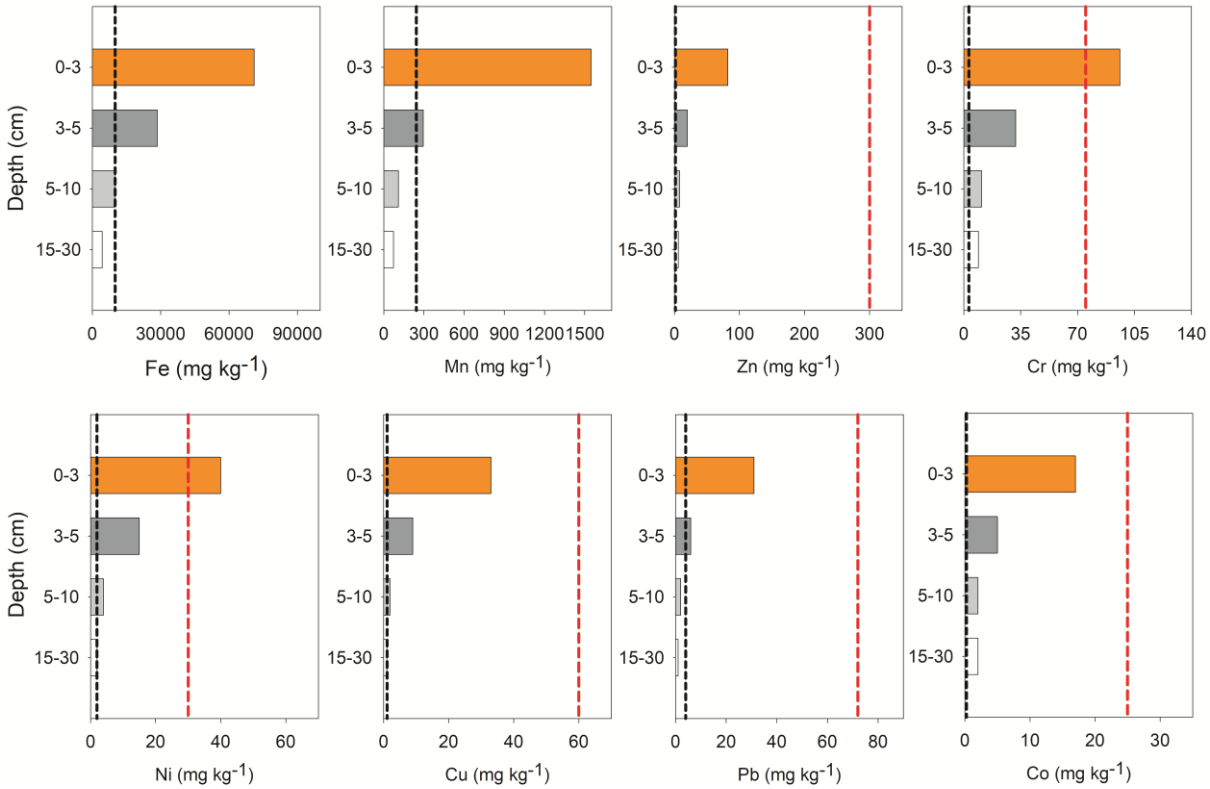

Fig. S4. Trace metals total contents for the site 4 sampled. Black dashed line represents metal contents in soil surface (0-2 cm) 2 days before the accident (Gomes et al., 2017). Red dashed line represents prevention values according to Brazilian legislation (CONAMA, 2009)

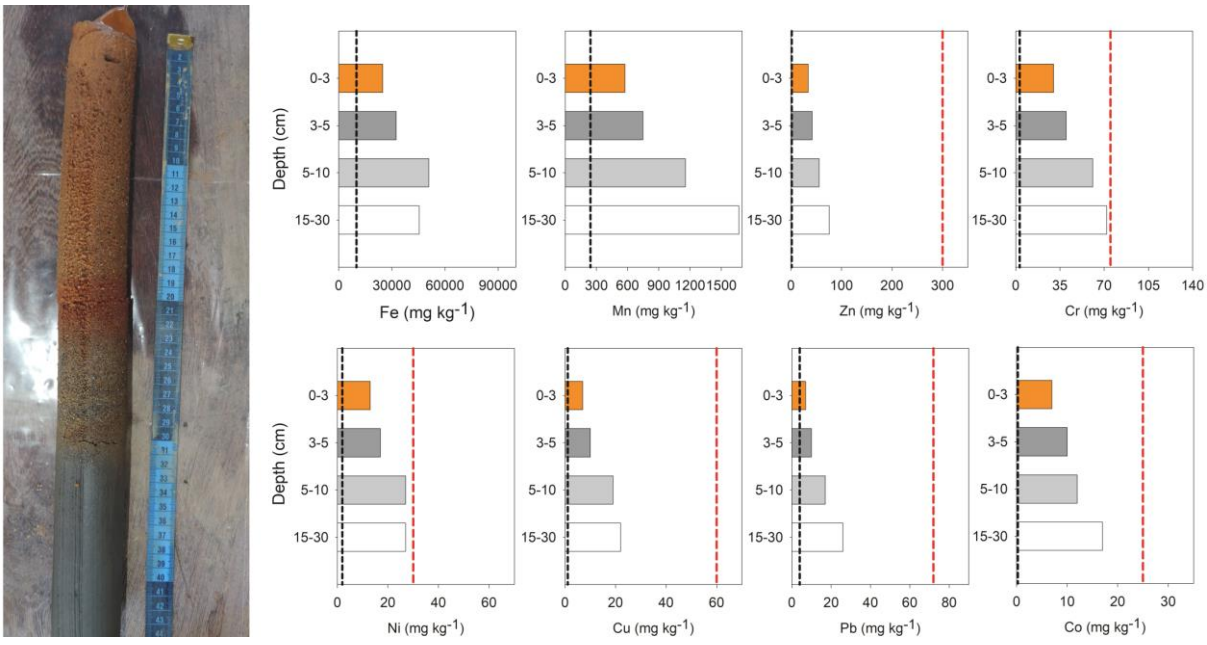

Fig. S5. Trace metals total contents for the site 5 sampled. At left, a soil profile. Black dashed line represents metal contents in soil surface (0-2 cm) 2 days before the accident (Gomes et al., 2017). Red dashed line represents prevention values according to Brazilian legislation (CONAMA, 2009)

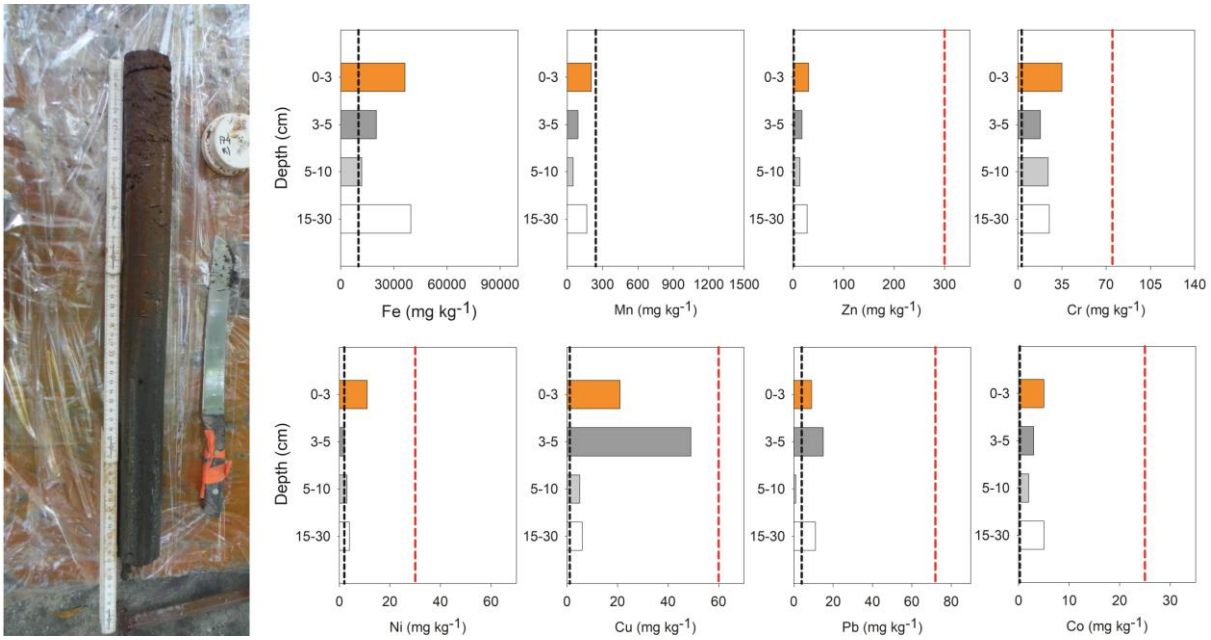

Fig. S6. Trace metals total contents for the site 6 sampled. At left, a soil profile. Black dashed line represents metal contents in soil surface (0-2 cm) 2 days before the accident (Gomes et al., 2017). Red dashed line represents prevention values according to Brazilian legislation (CONAMA, 2009)

4. ROLE OF FE DYNAMIC IN RELEASE OF METALS AT RIO DOCE ESTUARY: UNFOLDING OF A MINING DISASTER

Abstract

The role of Fe oxyhydroxides dynamic on metal bioavailability was studied in the Rio Doce estuary after the largest mining disaster in the world. Soon after the disaster in 2015, metals were associated with Fe oxyhydroxides under a redox-active estuarine environment. Our results indicate that organic matter inputs from plant colonization on deposited tailings over estuarine soils led to a reductive dissolution of Fe oxyhydroxides within two years. Soil pseudo-total Fe content decreased by 70% between 2015 and 2017, while the total metal contents (Cr, Cu, Ni, Pb, and Zn) decreased by 79% in the soil. The losses of Fe and metals coupled to changes in Fe oxides crystallinity reveal a future ephemeral control of Fe oxyhydroxides over metal immobilization. Our results suggest a potential chronic contamination at the estuary and points to an aggravating scenario for the following years due to the increasing dominance of poorly crystalline Fe oxyhydroxides.

Keywords: Samarco mining disaster, redox processes, trace metals, environmental contamination, Fe oxides

Queiroz, H.M., Ying, S.C., Bernardino, A.F., Barcellos, D., Gabriel, N.N., Otero, L., Ferreira, T.O., 2021. Role of Fe dynamic in release of metals at Rio Doce estuary : Unfolding of a mining disaster. Mar. Pollut. Bull. 166, 112267. https://doi.org/10.1016/j.marpolbul.2021.112267

Following the world's largest mining disaster in November 2015, the Doce River (i.e., *Rio Doce*) estuary was the final destination of approximately 50 million m^3 of Fe ore mine tailings released after the Fundão dam rupture in Mariana, Minas Gerais State, Brazil (Escobar, 2015; Marta-Almeida et al., 2016). The tailings travelled approximately 600 km towards the ocean killing 19 people and causing extensive ecological (Bernardino et al., 2019; Gabriel et al., 2020) and socioeconomic damages (Fernandes et al., 2016), reaching the estuary 16 days after the dam failure (Gomes et al., 2017; Queiroz et al., 2021). Since then, several multidisciplinary studies have been conducted in the estuarine region to assess the associated environmental, social, and economic damages (Fernandes et al., 2016; Gabriel et al., 2020).

Several studies have found an increase in metal contents in the estuarine soil and sediments soon after the arrival of the Fe-rich tailings (Bernardino et al., 2019; Gabriel et al., 2020; Gomes et al., 2017). Although the Fe-rich tailings were reported to be free of metals (Davila et al., 2020), their main constituent, Fe oxyhydroxides of varying crystallinity, are known for their high metal retention capacity (Cui et al., 2020; Kypritidou and Argyraki, 2020). Queiroz et al. (2018) found total contents of Ni and Cr in the Rio Doce estuarine soils to be significantly higher than the threshold levels for contaminated soil set under the Brazilian environmental laws (CONAMA, 2009). The authors also reported that 70–90% of the studied metals (Cr, Cu, Co, Mn, Ni, Pb, and Zn) were associated with Fe oxyhydroxides and anticipated a potential release of metals within the following years (Queiroz et al., 2018). Fe oxyhydroxides are prone to reductive dissolution under the geochemical environment normally found in estuarine soils (Canfield et al., 1993; Lovley et al., 2004; Nóbrega et al., 2013). Due to the frequent flooding and presence of organic matter, the O_2 concentration is usually low in estuarine soils and sediments, and microbial decomposition is mediated by anaerobic pathways by the reduction of NO_3^-, Mn^{4+}, Fe^{3+}, and SO_4^{2-} (Canfield et al., 1993; Holmboe et al., 2001; Kristensen et al., 2000). Thus, we hypothesized that upon the settlement of Fe-rich tailings in the estuarine environment, Fe oxyhydroxides may no longer control metal availability and become a source of these elements. Our objective was to evaluate the release of metals in the Rio Doce estuary within two years (2017) since the arrival of the tailings (in 2015) and to assess potential risks of contamination.

We sampled soils in two field campaigns at the Rio Doce estuary, which contrast with most estuarine areas due to low salinity resulting from high freshwater discharge (Bernardino et al., 2019; Oliveira and Quaresma, 2017). The samples were collected using PVC tubes

(previously washed with 10% HCl) attached to a soil auger. The first campaign was conducted in 2015, seven days after the deposition of mine tailings on the Rio Doce estuarine soils (Queiroz et al., 2018), and four sites were sampled (n = 21). The second campaign in 2017 was conducted in eight sites (n = 61), including the same sampled sites in 2015 and four more sites to achieve a more comprehensive representation of sites affected by the tailings (Fig. 1). After sampling, the PVC tubes were hermetically sealed, kept at 4 °C, and transported in an upright position to the laboratory. For the two field campaigns, samples were sectioned at different depth intervals in the laboratory: samples collected in 2015 were sectioned into 0–3, 3–5, 5–10, and 15–30 cm, whereas those from 2017 were sectioned into 0–3, 3–5, 5–10, 10–15, 15–20, 20–25, 25–30, and 30+ cm. Different depth intervals between the years were used to increase the resolution of the analysis over depth and to examine eventual changes throughout the soil profile. Soil redox potentials (Eh) and pH values were measured in the field using portable meters. The Eh values were obtained using a platinum electrode, and the final values were adjusted to a calomel reference electrode (adding +244 mV to the measured values). The pH values were recorded with a glass electrode previously calibrated with standard solutions (pH 4.0 and 7.0). The estuarine water salinity was measured in both campaigns using a portable refractometer (Model IPS-10T).

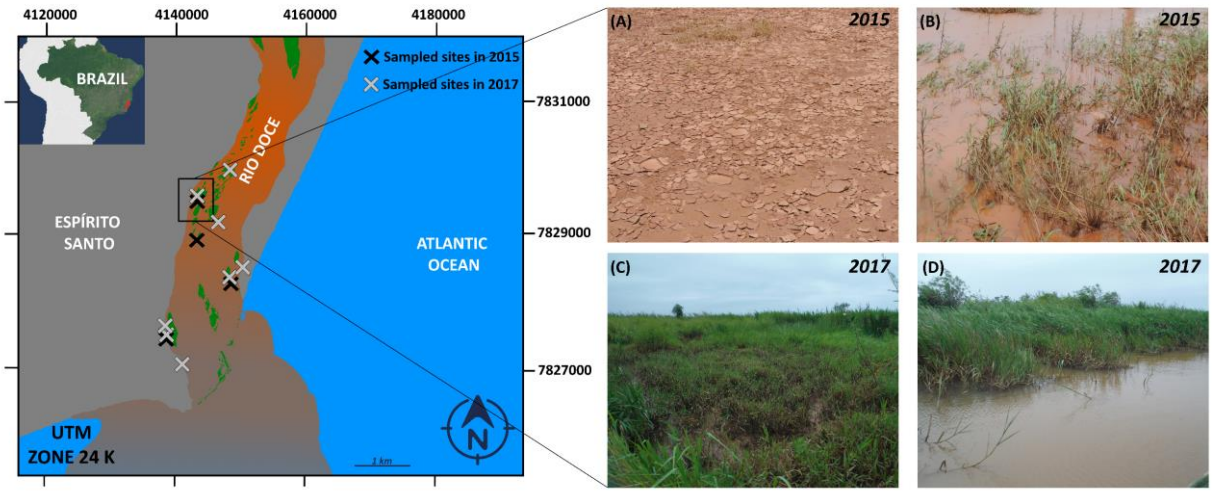

Fig. 1. Sampled sites in 2015 and 2017, at Rio Doce estuary, Regência, Espirito Santo, Brazil. In detail, images from the first field campaign (2015) seven days after the mine tailings arrival in one of the eight sampled sites (A and B), and at the same place two years later (2017), evidencing a profuse plant growth over the deposited mine tailings (C and D).

The total metal contents (Cr, Cu, Ni, Pb, and Zn) in soils were determined using inductively coupled plasma-optical emission spectrometry (Thermo Scientific, iCAP 6200) after triacid digestion (HF + HCl + HNO_3) (USEPA, 1996). Additionally, sequential Fe extraction was conducted using a combination of methods proposed by Ferreira et al. (2007a, 2007b). This combined method determines six operationally distinct fractions: exchangeable and soluble Fe (FeEX); Fe bound to carbonates (FeCA); Fe bound to poorly crystalline oxyhydroxides, i.e., ferrihydrite (FeFR) and lepidocrocite (FeLP); crystalline Fe oxyhydroxides (i.e., goethite and hematite, FeCR); and pyritic Fe (FePY). The sum of these fractions was used to determine the pseudo-total Fe. The contents of soil organic matter (SOM) were obtained via loss on ignition. Samples weighed after dried at 105 °C, then re-weighed after the heat at 450 °C for a period of 2 hours (Nóbrega et al., 2015).

A batch experiment was conducted to evaluate the susceptibility of the Fe oxyhydroxides present in the mine tailings to be dissolved under anoxic conditions and with an input of soil organic matter. The batch experiment was conducted in a glove-bag (with an atmosphere of 95% N_2:5% H_2:0% O_2) with field samples from the 0–3 cm depth collected in 2015, the depth most affected by tailing deposition (a total of 18 replicates). The experiment consisted of two treatments run over 45 days: in treatment I, 40 mL of 15 mM sodium chloride was added to 500 mg of the tailings in falcon tubes to obtain a comparable aqueous phase with respect to ionic strength in both treatments; in treatment II, 40 mL of 15 mM sodium acetate was added to 500 mg of tailings to enhance the carbon source in the system and stimulate further biogeochemical reactions. All tubes were previously sterilized, and solutions were prepared using ultrapure water (>18 MΩ·cm) previously deoxygenated. The incubation ran over 45 days in order to guarantee maximum exposure to anoxic conditions and reach the peak of Fe^{2+} formation (Bhattacharyya et al., 2018; Ginn et al., 2017). The tubes were shaken periodically and incubated. After 45 days, the aqueous Fe^{2+} was quantified using the ferrozine assay (see Barcellos et al., 2018; Thompson et al., 2006).

A non-parametric test to evaluate the significant differences between means was performed on the field samples (campaigns of 2015 and 2017) using pH, Eh, SOM, pseudo-total Fe, and total metals and on the batch samples using Fe^{2+} data. The non-parametric Kruskal-Wallis test was performed at the 5% significance level using the XLSTAT version 2014.5.03. Tests of correlations were performed between the pseudo-total Fe content and total metal content by calculating Spearman's correlation coefficient (*r*).

The batch experiment showed a two-fold increase in Fe^{2+} concentrations (k = 5.334; p = 0.02; Fig. 2) with the addition of OAc (0 to 15 mM), demonstrating a sharp increase in Fe oxyhydroxide dissolution within the mine tailings. The batch experiment validated the propensity of Fe oxyhydroxides from tailings to undergo dissimilatory Fe^{III} reduction upon the input of labile organic matter (see Khan et al., 2019).

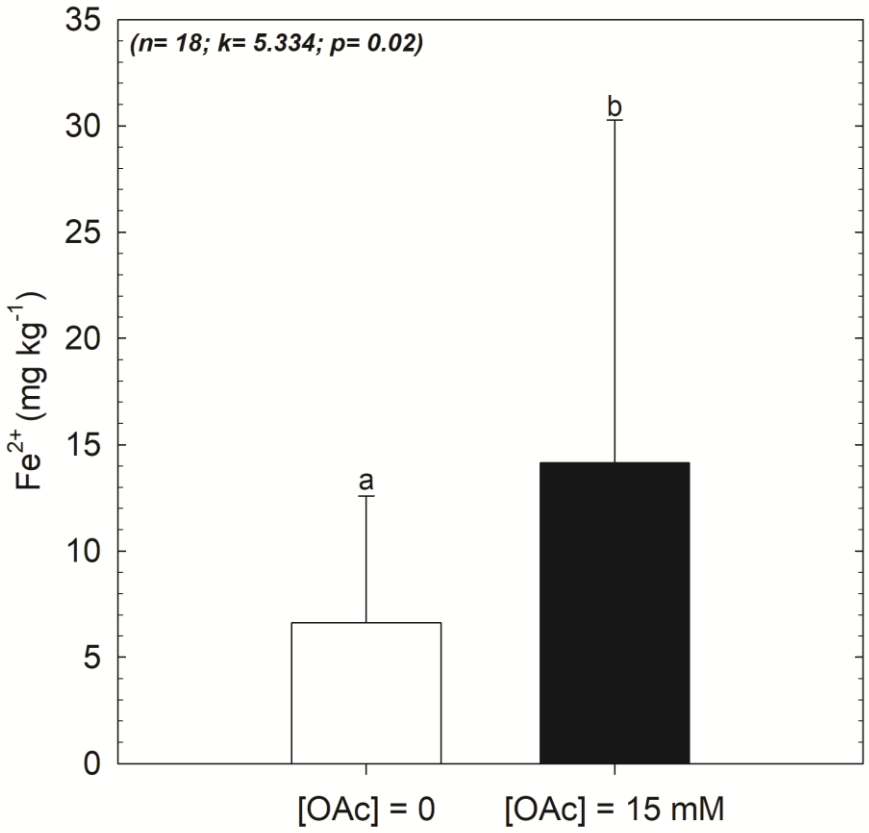

Fig. 2. Concentration of Fe^{2+} released after 45 days of the batch experiment using the surface soil from 2015 (i.e., 0–3 cm layer, most affected by the deposited mine tailings). [OAc] = concentration of sodium acetate. The different lowercase letters indicate a significant difference between the concentrations as determined by the Kruskal-Wallis test at the 5% probability level.

The batch experiment results also support the changes observed in the Fe fractionation between the 2015 and 2017 soil samples (Fig. 3). These data indicate an increase in the low-crystallinity Fe phases from 2015 to 2017 (FeFR: 2015 = 6 % and 2017 = 13 %; FeLP: 2015 = 8% and 2017 = 21%) and a decrease in the highly crystalline Fe oxyhydroxide phases (FeCR in 2015 = 85 % and 2017 = 65 %). The other fractions (i.e., EX, CA, and PY) represented approximately 1% of the soils collected during 2015 and 2017 (Fig. 3). Moreover, a significant decrease of approximately 50,000 mg kg^{-1} in the pseudo-total Fe contents (k = 6.5324; p = 0.010; Table S1)

was observed in the studied estuarine soils two years after arrival of the mine tailings (2015 = 71923 ± 67446 mg kg^{-1} and 2017 = 21466 ± 12086 mg kg^{-1}) with a higher decrease at the surface layer (i.e., 0–3 cm).

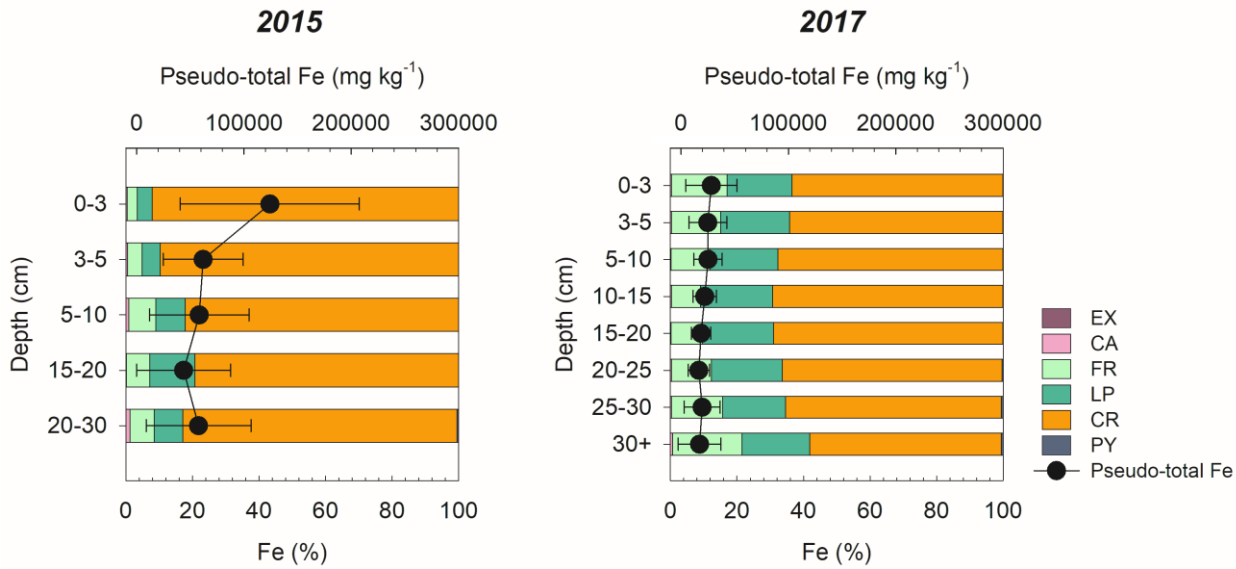

Fig. 3. Soil depth profiles showing the Fe fractionation and pseudo-total Fe changes at the Rio Doce estuarine soils from 2015 (n = 21) to 2017 (n = 61). Soluble and exchangeable Fe (EX), Fe bounded to carbonates (CA), Fe associated with ferrihydrite (FR); Fe associated with lepidocrocite (LP); Fe associated with crystalline Fe oxyhydroxides (CR); and Fe associated with pyrite (PY).

The changes in Fe oxyhydroxide crystallinity coupled with the decrease in the pseudo-total Fe content indicate a massive Fe reduction in the studied soils (Fig. 3), as demonstrated in the batch experiments (Fig. 2). The dissolutive reduction of Fe oxyhydroxides has been reported to occur within hours to weeks (Bonneville et al., 2004; Chen et al., 2019) in estuarine soils when Eh values remain below +100 mV (Søndergaard, 2009), and labile organic matter is present (Canfield et al., 1993). Our data showed marked changes in redox conditions between both years (Fig. 4). In 2015, the Eh and pH values measured in the field showed oxic conditions in the studied estuarine soils (Eh = +239 ± 113 mV; pH = 6.3 ± 1.1, Fig. 4), which would favor the stability of Fe oxyhydroxides (Reddy and DeLaune, 2008). However, in 2017, the near neutral pH values (6.4 ± 0.4; Fig. 4) were maintained at significantly lower Eh values (ranging between +174 and -197 mV; Fig. 4), indicating suboxic/anoxic conditions.

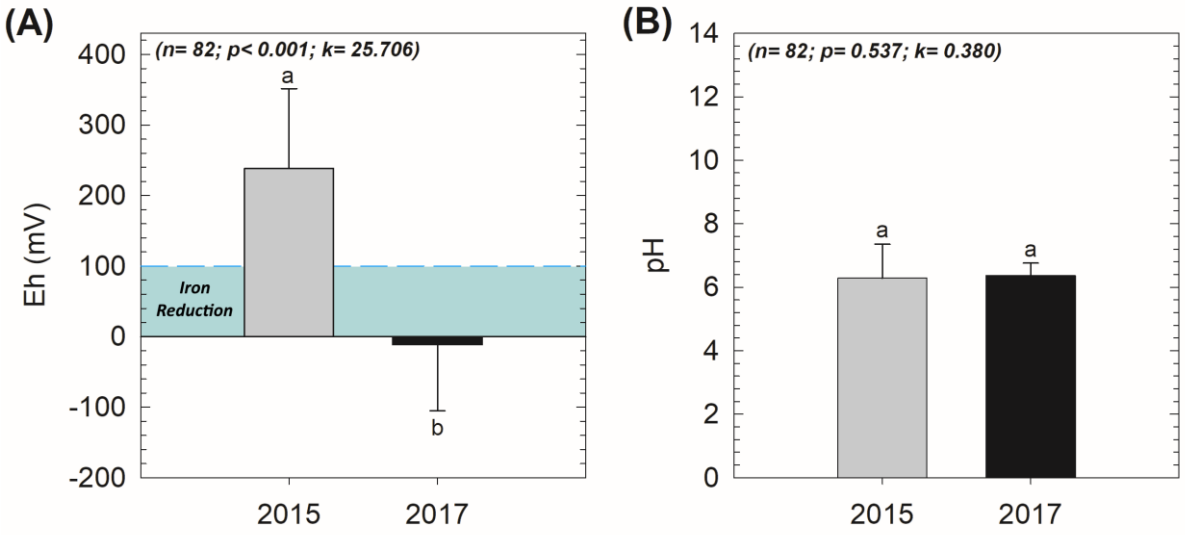

Fig. 4. Eh (A) and pH (B) values measured in the studied soils in 2015 (n = 21) and 2017 (n = 21). The shaded area indicates the Eh interval indicative of Fe reduction (+100–0 mV) at pH close to 7.0 (Søndergaard, 2009). The different lowercase letters indicate a significant difference between the concentrations as determined by the Kruskal-Wallis test at the 5% probability level.

The significantly lower Eh values in 2017 are related to the fast colonization of the deposited tailings by the estuarine plants (Fig. 1). Several studies have demonstrated the role of estuarine plants in promoting high inputs of organic matter in the soil, which when coupled with constant flooding and O_2 depletion enhance anaerobic processes inherent in estuarine regions (Anschutz et al., 2019; Mead et al., 2005; Ranjan et al., 2011; Vincent et al., 2017). Indeed, the soil organic matter (SOM) contents significantly increased from 2015 to 2017 (see Table S1) in response to fast plant colonization (Fig. 5). On average, the SOM contents in 2015 were 4.0 ± 3.4% whereas in 2017 were 14.8 ± 5.6%. This soil organic matter enrichment increased the anaerobic microbial activity and decreased the soil redox potential (Fig. 4). Moreover, estuarine plants are known to release organic acids with low molecular weights, which favor Fe reduction (Kristensen et al., 2008; Kristensen and Alongi, 2006; Luo et al., 2018).

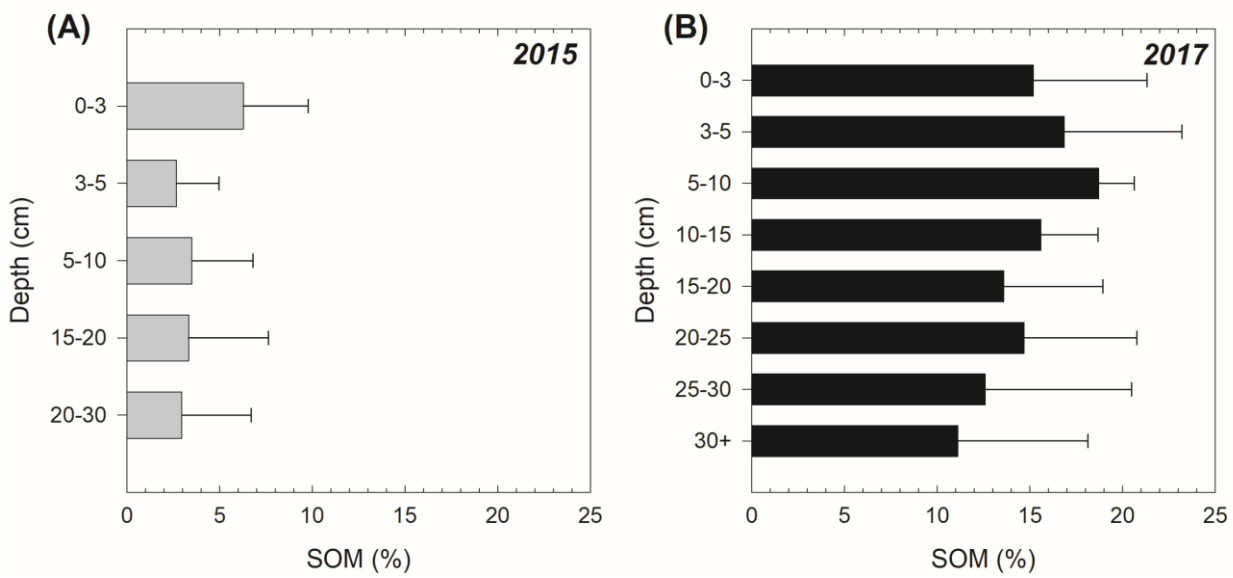

Fig. 5. The soil organic matter (SOM) contents in the studied soils in 2015 (A) and 2017 (B) obtained via loss on ignition. The results indicate an expressive in SOM over time in response to plant colonization.

The Fe losses under the anoxic/suboxic conditions observed in 2017 led to a decrease in the soil capacity to immobilize metals. Under oxic soil conditions, Fe oxyhydroxides decrease the bioavailability of metal contaminants because of their high surface area and reactivity (Buerge-Weirich et al., 2002; Herbert, 1996; Randall et al., 1999). Under oxic conditions, the retention of metals by Fe oxyhydroxides is rapid and virtually irreversible due to formation of stables complexes (Cornell and Schwertmann, 2003; Cui et al., 2020). For instance, goethite has a strong affinity for metals, and adsorption takes place over a wide pH range (3.0–8.5) forming monodentate surface hydroxy-complexes, followed by bi-nuclear internal complexes that are extremely stable (Rose and Bianchi-Mosquera, 1993; Trivedi and Axe, 2001). Poorly crystalline Fe oxyhydroxides (e.g., lepidocrocite and ferrihydrite) also have great potential for metal adsorption because of their characteristics (e.g., small size and high surface area) that enable high-affinity surface complexes at bi- and/or tri-dentate edge sharing sites (Manceau et al., 2000; Randall et al., 1999). However, in estuarine soils under anoxic/suboxic conditions and influenced by microbially mediated Fe^{III} reduction (Adhikari et al., 2017; Hyun et al., 2017), the resulting Fe solubilization directly limits the soil capacity to immobilize metals (Zhang et al., 2014, 2012). Additionally, along with the marked Fe losses, we observed a significant decrease in metal contents in the Rio Doce estuarine soils from 2015 to 2017 (Fig. 6; Table S1). The contents of Cr, Cu, Ni, Pb, and Zn decreased in the soil by 84%, 85%, 86%, 74%, and 67%, respectively, within two years (Fig. 6).

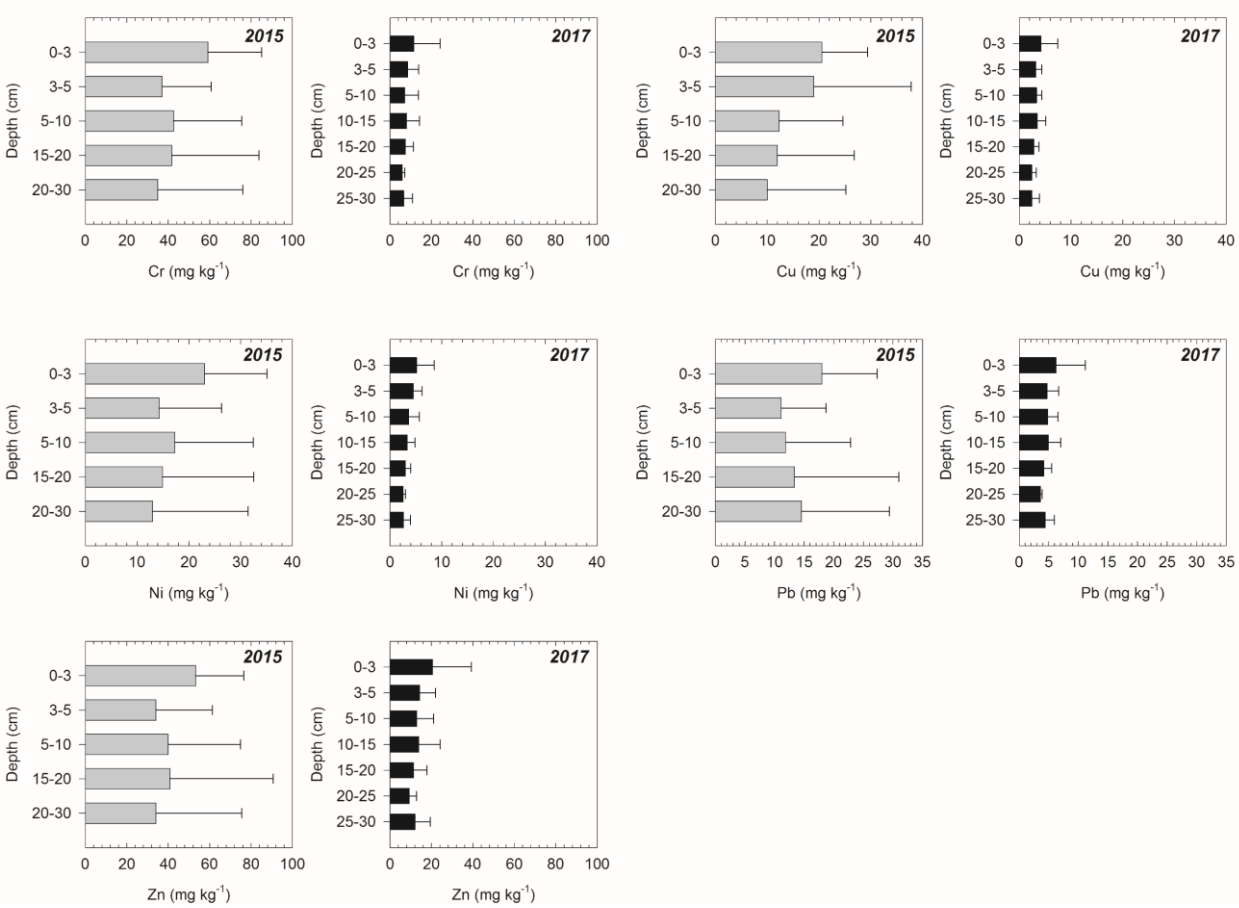

Fig. 6. Total metal contents (Cr, Cu, Ni, Pb, and Zn) in the Rio Doce estuarine soils in 2015 (n = 21) and 2017 (n= 61).

Furthermore, the correlations between pseudo-total Fe and metal contents showed a decrease in the *r*-value in 2017, indicating a lower capacity of Fe oxyhydroxides to retain metals (Table 1), despite the positive correlation. The increase of poorly crystalline Fe oxyhydroxides in 2017, reaching 34% of the pseudo-total Fe forms (Fig. 3), also represents a loss in the capacity of the studied soils to immobilize metals. Owing to their higher susceptibility to dissolution, poorly crystalline Fe oxyhydroxides are prone to a continued metal release upon their reduction (Larsen and Postma, 2001; Schwertmann, 1991).

Table 1 – Spearman's correlation coefficient (*r*) between pseudo-total Fe and total metal contents in both studied years.

Year	Variables	Cr	Cu	Ni	Pb	Zn
		Spearman's correlation coefficient (*r*)				
2015	Pseudo-total Fe	**0.6325**	**0.4805**	**0.6338**	**0.6104**	**0.5442**
2017	Pseudo-total Fe	0.2281	**0.4365**	**0.4486**	**0.5968**	**0.3303**
		p-values				
2015	Pseudo-total Fe	**0.0026**	**0.0287**	**0.0025**	**0.0039**	**0.0118**
2017	Pseudo-total Fe	0.0747	**0.0004**	**0.0003**	**0.0000**	**0.0090**

Values in bold indicate significant correlation a significance level alpha=0.05

The fate of released metals may be the estuarine water (Bryan and Langston, 1992), plants (Madejón et al., 2009), and/or animals (Vicente-Martorell et al., 2009). A recent study in the Rio Doce estuary (Gabriel et al., 2020) revealed high concentrations of metals (e.g., Cr, Cu, Zn) in both liver and muscle tissues of fish species often consumed by the local estuarine population. Another recent study reported the chronic effects of trace metals in the benthic assemblage at the Rio Doce estuary, 1.7 years after the disaster, as a result of exposure to metals present in the mine tailings (Bernardino et al., 2019).

Other mineral fractions that are more stable than Fe oxyhydroxides under the estuarine soil geochemical conditions (such as FeCA and FePY) could also have an important role in metal retention (Álvarez-Valero et al., 2009; Cooper and Morse, 1998; Otero et al., 2009). However, in 2017, these fractions represented only 0.6% of the pseudo-total Fe in the estuarine soils, further limiting their potential for metal retention. As reported by Queiroz et al. (2018), sulfate reduction is not favored in the Rio Doce estuary due to the low salinity and SO_4^{2-} concentration, which was corroborated by the low FePY content (Fig. 3). In fact, the recorded water salinity in both campaigns were very low, ranging from 1.30 ± 1.15 psu in 2015 to 0.14 ± 0.16 psu in 2017 (see Table S2) which is associated with the strong streamflow of freshwater of the Rio Doce (Oliveira and Quaresma, 2017). Moreover, sulfate reduction is not favored in Fe-rich environments, where the dissimilatory Fe^{III} reduction is the predominant anaerobic pathway (Chapelle and Lovley, 1992; Kumar et al., 2014). Carbonates (i.e., FeCA) could also be a stable fraction controlling the metal bioavailability (Sundaray et al., 2011). However, due to the high CO_2 partial pressure promoted by plant roots and the circumneutral pH, the presence and formation of carbonates is likely limited in the Rio Doce estuarine soils (Albuquerque et al., 2014; Du Laing et al., 2009).

Therefore, two years after the arrival of mine tailings, the geochemical conditions in the estuarine soils indicate a potential chronic metal contamination at the Rio Doce estuary as a result of the dissimilatory Fe^{III} reduction, which is both releasing metals and lowering the soil immobilization capacity. The increase in the poorly crystalline Fe oxyhydroxide phase leads to an ephemeral control of metal retention due to their higher susceptibility to dissolution in redox active environments (Liptzin and Silver, 2009; Zhang et al., 2012). Additionally, considering the huge amount of tailings deposited along the Rio Doce basin (Marta-Almeida et al., 2016), new events of Fe deposition are expected to occur in the Rio Doce estuary in the following years in response to seasonal floods, winds, and currents (Coimbra et al., 2019). These processes would further aggravate the chronic contamination scenario and ultimately compromise the estuary's health. Thus, we conclude that there is an imminent environmental risk in the following years for flora, fauna, and possibly humans as a result of the continuous metal release in response to redox change assigned by Fe dynamics.

Acknowledgments

This work was funded by grants to AFB and TOF from Fundação de Amparo do Espirito Santo (FAPES Rio Doce 77683544/2017), Coordenação de Aperfeiçoamento de Pessoal de Nível Superior CAPES - Finance Code 001 and CNPq (grant numbers, AFB: 301161/2017-8, TOF: 305996/2018-5). The authors are grateful for the financial support provided by the São Paulo Research Foundation (FAPESP, HMQ grants number 2018/04259-2 and 2019/17413-2; DB grant number 2019/02855-0; TOF grants number 2019/19987-6 and 2018/08408-2). Fundação Carlos Chagas Filho de Amparo à Pesquisa do Estado do Rio de Janeiro (GNN, JCNE Grant E-26/202.757/2019). Xunta de Galicia-Consellería de Educación e Ordeanción Universitaria de Galicia (consolidation of competitive groups of investigation: GRC GI 1574) and CRETUS strategic group (AGRUP2015/02). SCY was supported by the USDA NIFA Hatch Project CA-R-ENS-5151-H and Fulbright Award awarded by the J. William Fulbright Commission.

References

Adhikari, D., Zhao, Q., Das, K., Mejia, J., Huang, R., Wang, X., Poulson, S.R., Tang, Y., Roden, E.E., Yang, Y., 2017. Dynamics of ferrihydrite-bound organic carbon during microbial Fe reduction. Geochim. Cosmochim. Acta 212, 221–233. https://doi.org/10.1016/j.gca.2017.06.017

Albuquerque, A.G.B.M., Ferreira, T.O., Nóbrega, G.N., Romero, R.E., Júnior, V.S.S.S., Meireles, A.J.A.A., Otero, X.L., 2014. Soil genesis on hypersaline tidal flats (apicum ecosystem) in a tropical semi-arid estuary (Ceará, Brazil). Soil Res. 52, 140. https://doi.org/10.1071/SR13179

Álvarez-Valero, A.M., Sáez, R., Pérez-López, R., Delgado, J., Nieto, J.M., 2009. Evaluation of heavy metal bio-availability from Almagrera pyrite-rich tailings dam (Iberian Pyrite Belt, SW Spain) based on a sequential extraction procedure. J. Geochemical Explor. 102, 87–94. https://doi.org/10.1016/j.gexplo.2009.02.005

Anschutz, P., Bouchet, S., Abril, G., Bridou, R., Tessier, E., Amouroux, D., 2019. In vitro simulation of oscillatory redox conditions in intertidal sediments: N, Mn, Fe, and P coupling. Cont. Shelf Res. 177, 33–41. https://doi.org/10.1016/j.csr.2019.03.007

Barcellos, D., Cyle, K.T., Thompson, A., 2018. Faster redox fluctuations can lead to higher iron reduction rates in humid forest soils. Biogeochemistry 137, 367–378. https://doi.org/10.1007/s10533-018-0427-0

Bernardino, A.F., Pais, F.S., Oliveira, L.S., Gabriel, F.A., Ferreira, T.O., Queiroz, H.M., Mazzuco, A.C.A., 2019. Chronic trace metals effects of mine tailings on estuarine assemblages revealed by environmental DNA. PeerJ 7, e8042. https://doi.org/10.7717/peerj.8042

Bhattacharyya, A., Campbell, A.N., Tfaily, M.M., Lin, Y., Kukkadapu, R.K., Silver, W.L., Nico, P.S., Pett-Ridge, J., 2018. Redox Fluctuations Control the Coupled Cycling of Iron and Carbon in Tropical Forest Soils. Environ. Sci. Technol. 52, 14129–14139. https://doi.org/10.1021/acs.est.8b03408

Bonneville, S., Van Cappellen, P., Behrends, T., 2004. Microbial reduction of iron(III) oxyhydroxides: Effects of mineral solubility and availability. Chem. Geol. 212, 255–268. https://doi.org/10.1016/j.chemgeo.2004.08.015

Bryan, G.W., Langston, W.J., 1992. Bioavailability, accumulation and effects of heavy metals in sediments with special reference to United Kingdom estuaries: a review. Environ. Pollut. 76, 89–131. https://doi.org/10.1016/0269-7491(92)90099-V

Buerge-Weirich, D., Hari, R., Xue, H., Behra, P., Sigg, L., 2002. Adsorption of Cu, Cd, and Ni on goethite in the presence of natural groundwater ligands. Environ. Sci. Technol. 36, 328–336. https://doi.org/10.1021/es010892i

Canfield, D.E., Thamdrup, B., Hansen, J.W., 1993. The anaerobic degradation of organic matter in Danish coastal sediments: Iron reduction, manganese reduction, and sulfate reduction. Geochim. Cosmochim. Acta 57, 3867–3883. https://doi.org/10.1016/0016-7037(93)90340-3

Chapelle, F.H., Lovley, D.R., 1992. Competitive Exclusion of Sulfate Reduction by Fe(lll)-Reducing Bacteria: A Mechanism for Producing Discrete Zones of High-Iron Ground Water. Ground Water 30, 29–36. https://doi.org/10.1111/j.1745-6584.1992.tb00808.x

Chen, C., Barcellos, D., Richter, D.D., Schroeder, P.A., Thompson, A., 2019. Redoximorphic Bt horizons of the Calhoun CZO soils exhibit depth-dependent iron-oxide crystallinity. J. Soils Sediments. https://doi.org/10.1007/s11368-018-2068-2

Coimbra, K.T.O., Alcântara, E., de Souza Filho, C.R., 2019. An assessment of natural and manmade hazard effects on the underwater light field of the Doce River continental shelf. Sci. Total Environ. 685, 1087–1096. https://doi.org/10.1016/j.scitotenv.2019.06.127

CONAMA, 2009. Resolução Nº 420, de 28 de Dezembro de 2009, in: Brazilian National Environment Council (Ed.), Diário Oficial Da União. Ministério do Meio Ambiente, Brasília, pp. 81–84.

Cooper, D.C., Morse, J.W., 1998. Biogeochemical Controls on Trace Metal Cycling in Anoxic Marine Sediments. Environ. Sci. Technol. 32, 327–330. https://doi.org/10.1021/es970387e

Cornell, R.M., Schwertmann, U., 2003. The Iron Oxides: Structure, Reactions, Occurences and Uses, WILEY-VCH. https://doi.org/10.1002/3527602097.ch1

Cui, H., Zhang, X., Wu, Q., Zhang, S., Xu, L., Zhou, Jing, Zheng, X., Zhou, Jun, 2020. Hematite enhances the immobilization of copper, cadmium and phosphorus in soil amended with hydroxyapatite under flooded conditions. Sci. Total Environ. 708, 134590. https://doi.org/10.1016/j.scitotenv.2019.134590

Davila, R.B., Fontes, M.P.F., Pacheco, A.A., Ferreira, M. da S., 2020. Heavy metals in iron ore tailings and floodplain soils affected by the Samarco dam collapse in Brazil. Sci. Total Environ. 709, 136151. https://doi.org/10.1016/j.scitotenv.2019.136151

Du Laing, G., Rinklebe, J., Vandecasteele, B., Meers, E., Tack, F.M.G., 2009. Trace metal behaviour in estuarine and riverine floodplain soils and sediments: A review. Sci. Total Environ. 407, 3972–3985. https://doi.org/10.1016/j.scitotenv.2008.07.025

Escobar, H., 2015. Mud tsunami wreaks ecological havoc in Brazil. Science (80-.). 350, 1138–1139. https://doi.org/10.1126/science.350.6265.1138

Fernandes, G.W., Goulart, F.F., Ranieri, B.D., Coelho, M.S., Dales, K., Boesche, N., Bustamante, M., Carvalho, F.A., Carvalho, D.C., Dirzo, R., Fernandes, S., Galetti, P.M., Millan, V.E.G., Mielke, C., Ramirez, J.L., Neves, A., Rogass, C., Ribeiro, S.P., Scariot, A., Soares-Filho, B., 2016. Deep into the mud: ecological and socio-economic impacts of the dam breach in Mariana, Brazil. Nat. e Conserv. 14, 35–45. https://doi.org/10.1016/j.ncon.2016.10.003

Ferreira, T.O., Otero, X.L., Vidal-Torrado, P., Macías, F., 2007a. Redox Processes in Mangrove Soils under Rhizophora mangle in Relation to Different Environmental Conditions. Soil Sci. Soc. Am. J. 71, 484–491. https://doi.org/10.2136/sssaj2006.0078

Ferreira, T.O., Otero, X.L., Vidal-Torrado, P., Macías, F., 2007b. Effects of bioturbation by root and crab activity on iron and sulfur biogeochemistry in mangrove substrate. Geoderma 142, 36–46. https://doi.org/10.1016/j.geoderma.2007.07.010

Gabriel, F.Â., Hauser-Davis, R.A., Soares, L., Mazzuco, A.C.A., Rocha, R.C.C., Saint Pierre, T.D., Saggioro, E., Correia, F.V., Ferreira, T.O., Bernardino, A.F., 2020. Contamination and oxidative stress biomarkers in estuarine fish following a mine tailing disaster. PeerJ 8, e10266. https://doi.org/10.7717/peerj.10266

Ginn, B., Meile, C., Wilmoth, J., Tang, Y., Thompson, A., 2017. Rapid Iron Reduction Rates Are Stimulated by High-Amplitude Redox Fluctuations in a Tropical Forest Soil. Environ. Sci. Technol. 51, 3250–3259. https://doi.org/10.1021/acs.est.6b05709

Gomes, L.E. de O., Correa, L.B., Sá, F., Neto, R.R., Bernardino, A.F., 2017. The impacts of the Samarco mine tailing spill on the Rio Doce estuary, Eastern Brazil. Mar. Pollut. Bull. 120, 28–36. https://doi.org/10.1016/j.marpolbul.2017.04.056

Herbert, R.B., 1996. Metal retention by iron oxide precipitation from acidic ground water in Dalarna, Sweden. Appl. Geochemistry 11, 229–235. https://doi.org/10.1016/0883-2927(95)00070-4

Holmboe, N., Kristensen, E., Andersen, F., 2001. Anoxic decomposition in sediments from a tropical mangrove forest and the temperate wadden sea: Implications of N and P addition experiments. Estuar. Coast. Shelf Sci. https://doi.org/10.1006/ecss.2000.0794

Hyun, J.-H., Kim, S.-H., Mok, J.-S., Cho, H., Lee, T., Vandieken, V., Thamdrup, B., 2017. Manganese and iron reduction dominate organic carbon oxidation in surface sediments of the deep Ulleung Basin, East Sea. Biogeosciences 14, 941–958. https://doi.org/10.5194/bg-14-941-2017

Khan, I., Fahad, S., Wu, L., Zhou, W., Xu, P., Sun, Z., Salam, A., Imran, M., Jiang, M., Kuzyakov, Y., Hu, R., 2019. Labile organic matter intensifies phosphorous mobilization in paddy soils by microbial iron (III) reduction. Geoderma 352, 185–196. https://doi.org/10.1016/j.geoderma.2019.06.011

Kristensen, E., Alongi, D.M., 2006. Control by fiddler crabs (Uca vocans) and plant roots (Avicennia marina) on carbon, iron, and sulfur biogeochemistry in mangrove sediment. Limnol. Oceanogr. 51, 1557–1571. https://doi.org/10.4319/lo.2006.51.4.1557

Kristensen, E., Andersen, F., Holmboe, N., Holmer, M., Thongtham, N., 2000. Carbon and nitrogen mineralization in sediments of the Bangrong mangrove area, Phuket, Thailand. Aquat. Microb. Ecol. 22, 199–213. https://doi.org/10.3354/ame022199

Kristensen, E., Bouillon, S., Dittmar, T., Marchand, C., 2008. Organic carbon dynamics in mangrove ecosystems: A review. Aquat. Bot. 89, 201–219. https://doi.org/10.1016/j.aquabot.2007.12.005

Kumar, N., Omoregie, E.O., Rose, J., Masion, A., Lloyd, J.R., Diels, L., Bastiaens, L., 2014. Inhibition of sulfate reducing bacteria in aquifer sediment by iron nanoparticles. Water Res. 51, 64–72. https://doi.org/10.1016/j.watres.2013.09.042

Kypritidou, Z., Argyraki, A., 2020. Geochemical interactions in the trace element–soil–clay system of treated contaminated soils by Fe-rich clays. Environ. Geochem. Health 1. https://doi.org/10.1007/s10653-020-00542-1

Larsen, O., Postma, D., 2001. Kinetics of reductive bulk dissolution of lepidocrocite, ferrihydrite, and goethite. Geochim. Cosmochim. Acta 65, 1367–1379. https://doi.org/10.1016/S0016-7037(00)00623-2

Liptzin, D., Silver, W.L., 2009. Effects of carbon additions on iron reduction and phosphorus availability in a humid tropical forest soil. Soil Biol. Biochem. 41, 1696–1702. https://doi.org/10.1016/j.soilbio.2009.05.013

Lovley, D.R., Holmes, D.E., Nevin, K.P., 2004. Dissimilatory Fe(III) and Mn(IV) Reduction, in: Advances in Microbial Physiology. pp. 219–286. https://doi.org/10.1016/S0065-2911(04)49005-5

Luo, M., Liu, Y., Huang, J., Xiao, L., Zhu, W., Duan, X., Tong, C., 2018. Rhizosphere processes induce changes in dissimilatory iron reduction in a tidal marsh soil: a rhizobox study. Plant Soil 433, 83–100. https://doi.org/10.1007/s11104-018-3827-y

Madejón, P., Burgos, P., Murillo, J.M., Cabrera, F., Madejón, E., 2009. Bioavailability and accumulation of trace elements in soils and plants of a highly contaminated estuary (Domingo Rubio tidal channel, SW Spain). Environ. Geochem. Health 31, 629–642. https://doi.org/10.1007/s10653-008-9221-6

Marta-Almeida, M., Mendes, R., Amorim, F.N., Cirano, M., Dias, J.M., 2016. Fundão Dam collapse: Oceanic dispersion of River Doce after the greatest Brazilian environmental accident. Mar. Pollut. Bull. 112, 359–364. https://doi.org/10.1016/j.marpolbul.2016.07.039

Mead, R., Xu, Y., Chong, J., Jaffé, R., 2005. Sediment and soil organic matter source assessment as revealed by the molecular distribution and carbon isotopic composition of n-alkanes. Org. Geochem. 36, 363–370. https://doi.org/10.1016/j.orggeochem.2004.10.003

Nóbrega, G.N., Ferreira, T.O., Artur, A.G., de Mendonça, E.S., de O. Leão, R.A., Teixeira, A.S., Otero, X.L., 2015. Evaluation of methods for quantifying organic carbon in mangrove soils from semi-arid region. J. Soils Sediments 15, 282–291. https://doi.org/10.1007/s11368-014-1019-9

Nóbrega, G.N.N., Ferreira, T.O.O., Romero, R.E.E., Marques, A.G.B.G.B., Otero, X.L.L., 2013. Iron and sulfur geochemistry in semi-arid mangrove soils (Ceará, Brazil) in relation to seasonal changes and shrimp farming effluents. Environ. Monit. Assess. 185, 7393–7407. https://doi.org/10.1007/s10661-013-3108-4

Oliveira, K.S.S., Quaresma, V. da S., 2017. Temporal variability in the suspended sediment load and streamflow of the Doce River. J. South Am. Earth Sci. 78, 101–115. https://doi.org/10.1016/j.jsames.2017.06.009

Otero, X.L., Ferreira, T.O., Huerta-Díaz, M.A., Partiti, C.S.M., Souza, V., Vidal-Torrado, P., Macías, F., 2009. Geochemistry of iron and manganese in soils and sediments of a mangrove system, Island of Pai Matos (Cananeia — SP, Brazil). Geoderma 148, 318–335. https://doi.org/10.1016/j.geoderma.2008.10.016

Queiroz, H.M., Ferreira, T.O., Barcellos, D., Nóbrega, G.N., Antelo, J., Otero, X.L., Bernardino, A.F., 2021. From sinks to sources: The role of Fe oxyhydroxide transformations on phosphorus dynamics in estuarine soils. J. Environ. Manage. 278, 111575. https://doi.org/10.1016/j.jenvman.2020.111575

Queiroz, H.M., Nóbrega, G.N., Ferreira, T.O., Almeida, L.S., Romero, T.B., Santaella, S.T., Bernardino, A.F., Otero, X.L., 2018. The Samarco mine tailing disaster: A possible time-bomb for heavy metals contamination? Sci. Total Environ. 637–638, 498–506. https://doi.org/10.1016/j.scitotenv.2018.04.370

Randall, S.R., Sherman, D.M., Ragnarsdottir, K. V., Collins, C.R., 1999. The mechanism of cadmium surface complexation on iron oxyhydroxide minerals. Geochim. Cosmochim. Acta 63, 2971–2987. https://doi.org/10.1016/S0016-7037(99)00263-X

Ranjan, R.K., Routh, J., Ramanathan, A.L., Klump, J.V., 2011. Elemental and stable isotope records of organic matter input and its fate in the Pichavaram mangrove-estuarine sediments (Tamil Nadu, India). Mar. Chem. 126, 163–172. https://doi.org/10.1016/j.marchem.2011.05.005

Reddy, K.R., DeLaune, R.D., 2008. Biogeochemistry of wetlands: science and applications, 1st ed. CRC Press.

Rose, A.W., Bianchi-Mosquera, G.C., 1993. Adsorption of Cu, Pb, Zn, Co, Ni, and Ag on goethite and hematite; a control on metal mobilization from red beds into stratiform copper deposits. Econ. Geol. 88, 1226–1236. https://doi.org/10.2113/gsecongeo.88.5.1226

Schwertmann, U., 1991. Solubility and dissolution of iron oxides. Plant Soil. https://doi.org/10.1007/BF00011851

Søndergaard, M., 2009. Redox Potential, in: Encyclopedia of Inland Waters. Elsevier, pp. 852–859. https://doi.org/10.1016/B978-012370626-3.00115-0

Sundaray, S.K., Nayak, B.B., Lin, S., Bhatta, D., 2011. Geochemical speciation and risk assessment of heavy metals in the river estuarine sediments-A case study: Mahanadi basin, India. J. Hazard. Mater. 186, 1837–1846. https://doi.org/10.1016/j.jhazmat.2010.12.081

Thompson, A., Chadwick, O.A., Rancourt, D.G., Chorover, J., 2006. Iron-oxide crystallinity increases during soil redox oscillations. Geochim. Cosmochim. Acta. https://doi.org/10.1016/j.gca.2005.12.005

Trivedi, P., Axe, L., 2001. Ni and Zn Sorption to Amorphous versus Crystalline Iron Oxides: Macroscopic Studies. J. Colloid Interface Sci. 244, 221–229. https://doi.org/10.1006/jcis.2001.7970

USEPA, U.S.E.P.A., 1996. EPA Method 3050B (SW-846): Acid Digestion of Sediments, Sludges, and Soils 12.

Vicente-Martorell, J.J., Galindo-Riaño, M.D., García-Vargas, M., Granado-Castro, M.D., 2009. Bioavailability of heavy metals monitoring water, sediments and fish species from a polluted estuary. J. Hazard. Mater. 162, 823–836. https://doi.org/10.1016/j.jhazmat.2008.05.106

Vincent, S.G.T., Reshmi, R.R., Hassan, S.J., Nair, K.D., Varma, A., 2017. Predominant terminal electron accepting processes during organic matter degradation: Spatio-temporal changes in Ashtamudi estuary, Kerala, India. Estuar. Coast. Shelf Sci. 198, 508–517. https://doi.org/10.1016/j.ecss.2017.05.013

Zhang, C., Ge, Y., Yao, H., Chen, X., Hu, M., 2012. Iron oxidation-reduction and its impacts on cadmium bioavailability in paddy soils: A review. Front. Environ. Sci. Eng. China 6, 509–517. https://doi.org/10.1007/s11783-012-0394-y

Zhang, C., Yu, Z. gang, Zeng, G. ming, Jiang, M., Yang, Z. zhu, Cui, F., Zhu, M. ying, Shen, L. qing, Hu, L., 2014. Effects of sediment geochemical properties on heavy metal bioavailability. Environ. Int. 73, 270–281. https://doi.org/10.1016/j.envint.2014.08.010

Supplamentary Material

Table S1 – Means and Kruskal-Wallis non-parametric test summary for Eh and pH values, soil organic matter (SOM), Fe^{2+} contents, Total Fe, total contents of Cr, Cu, Mn, Ni, Pb, and Zn.

Variable	2015	2017	*p-value*	*K* (Observed value)
	Average ± SD			
Eh (mV)	239 ± 113	-11 ± 94	**< 0.0001**	25.7061
pH	6.3 ± 1.1	6.4 ± 0.4	0.5376	0.3801
SOM (%)	4.0 ± 3.4	14.8 ± 5.6	**< 0.0001**	29.8137
Total Fe (mg kg^{-1})	71923 ± 67446	21466 ± 12086	**0.0106**	6.5324
Cr (mg kg^{-1})	44 ± 30	7 ± 4	**< 0.0001**	37.6779
Cu (mg kg^{-1})	16 ± 13	2 ± 2	**< 0.0001**	15.2654
Mn (mg kg^{-1})	547 ± 498	145 ± 95	**< 0.0001**	17.4677
Ni (mg kg^{-1})	17 ± 14	2 ± 2	**< 0.0001**	31.7582
Pb (mg kg^{-1})	14 ± 10	4 ± 2	**0.0002**	13.7974
Zn (mg kg^{-1})	41 ± 30	14 ± 7	**0.0002**	13.5178
	[OAc] = 0	[OAc] = 15 mM		
Fe^{2+} (mg kg^{-1})	6.6 ± 6.0	14.1 ± 16.1	**0.0209**	5.3343

SD: standard deviation; *K* = Kruskal-Wallis test where *K* values above of K-critical (3.8415) indicate significant differences among the years at the 5% probability level. Bold *p-values* indicate significant differences at level alpha=0.05. [OAc] = acetate concentration.

Table S2 – Average (± SD) salinity values of estuarine water in sampling campaigns of 2015 and 2017.

Year	**Salinity (PSU)**
2015	1.30 ± 1.15
2017	0.14 ± 0.16

Table S3 – Detection limits and quality assurance and quality control used in the ICP-OES for total content and iron fractionating analyses.

Quality assurance	**Fe**	**Cr**	**Cu**	**Mn**	**Ni**	**Pb**	**Zn**
Detection limit (ppm)	0.01	0.01	0.01	0.01	0.01	0.01	0.01
Measured value	9.026	0.961	1.012	9.769	0.991	0.992	0.999
Certified value (NIST-1643f)	10.0	1.0	1.0	10.0	1.0	1.0	1.0
Recovery (%)	90.3	96.1	101.2	97.7	99.1	99.2	99.9

NIST-1643F: Certified standard reference material for trace elements in water used on Mn and Fe determinations from extracts of total contents and iron fractionating analyses.

5. MANGANESE: THE OVERLOOKED CONTAMINANT IN THE WORLD LARGEST MINE TAILINGS DAM COLLAPSE

Abstract

Manganese (Mn) is an abundant element in terrestrial and coastal ecosystems and an essential micronutrient in the metabolic processes of plants and animals. Mn is generally not considered a potentially toxic element due to its low content in both soil and water. However, in coastal ecosystems, the Mn dynamic (commonly associated with the Fe cycle) is mostly controlled by redox processes. Here, we assessed the potential contamination of the Rio Doce estuary (SE Brazil) by Mn after the world's largest mine tailings dam collapse, potentially resulting in chronic exposure to local wildlife and humans. Estuarine soils, water, and fish were collected and analyzed seven days after the arrival of the tailings in 2015 and again two years after the dam collapse in 2017. Using a suite of solid-phase analyses including X-ray absorption spectroscopy and sequential extractions, our results indicated that a large quantity of MnII arrived in the estuary in 2015 bound to Fe oxyhydroxides. Over time, dissolved Mn and Fe were released from soils when FeIII oxyhydroxides underwent reductive dissolution. Due to seasonal redox oscillations, both Fe and Mn were then re-oxidized to FeIII, MnIII, and MnIV and re-precipitated as poorly crystalline Fe oxyhydroxides and poorly crystalline Mn oxides. In 2017, redox conditions (Eh: -47 ± 83 mV; pH: 6.7 ± 0.5) favorable to both Fe and Mn reduction led to an increase (~880%) of dissolved Mn (average for 2015: 66 ± 130 μg L^{-1}; 2017: 582 ± 626 μg L^{-1}) in water and a decrease (~75%, 2015: 547 ± 498 mg kg^{-1}; 2017: 135 ± 80 mg kg^{-1}) in the total Mn content in soils. The crystalline Fe oxyhydroxides content significantly decreased while the fraction of poorly ordered Fe oxides increased in the soils limiting the role of Fe in Mn retention. The high concentration of dissolved Mn found within the estuary two years after the arrival of mine tailings indicates a possible chronic contamination scenario, which is supported by the high levels of Mn in two species of fish living in the estuary. Our work suggests a high risk to estuarine biota and human health due to the rapid Fe and Mn biogeochemical dynamic within the impacted estuary.

Keywords: estuarine soils, manganese contamination, iron oxides, redox processes, toxicity

Queiroz, H.M., Ying, S.C., Abernathy, M., Barcellos, D., Gabriel, F.A., Otero, X.L., Nóbrega, G.N., Bernardino, A.F., Ferreira, T.O., 2021. Manganese: The overlooked contaminant in the world largest mine tailings dam collapse. Environ. Int. 146, 106284. https://doi.org/10.1016/j.envint.2020.106284

5.1. Introduction

Manganese (Mn) is a widely distributed element in terrestrial and coastal ecosystems but usually occurs as trace amounts in most organisms (Levy and Nassetta, 2003; Pinsino et al., 2012). It is found in rocks (e.g., Mn content in Basalt: 1300 mg kg^{-1}; Gneiss: 600 mg kg^{-1}; Limestone: 550 mg kg^{-1}; Graham et al., 1988), associated with different primary soil minerals (Mn content in amphiboles: 400-7000 mg kg^{-1}; olivines: 100-6500 mg kg^{-1}; pyroxenes: 600-8000 mg kg^{-1}; Graham et al., 1988), and dissolved in natural waters (e.g., dissolved Mn in oceanic water ranges from 0.2 to 5.0 nmol kg^{-1}; Graham et al., 1988), exhibiting unique redox dynamics (as Mn^{II}, Mn^{III}, and Mn^{IV}) with Mn^{IV} being the most abundant form found in minerals (Burdige, 1993; Fischel et al., 2015).

For all living organisms, Mn is required in small amounts playing important roles in the maintenance of different biological functions and life (Arndt et al., 2014; Baly, 1989; Pinsino et al., 2012). For instance, in plants, Mn plays a key role in enzymatic activities and cell division (Broadley et al., 2012), while in humans and animals Mn acts as a protein transporter, is involved in neurological functions, and can also affect enzymatic activities (Fitsanakis et al., 2010). The required trace amounts of Mn considered beneficial to life are variable. In plants, such as soybean and corn, the critical quantity of Mn to reach toxic levels is 200 mg Mn kg^{-1} leaf dry weight (El-Jaoual and Cox, 1998). For humans, the World Health Organization, (WHO, 2011) set adequate intake levels for Mn at 2–3 mg day^{-1}.

The many physiological roles of Mn have often masked the perception of its potential toxicity, hence studies are rare that focus on the severe toxic effects produced by this element in different environments such as water, soil, and air (Finkelstein and Jerrett, 2007; Huang et al., 2016; Li et al., 2007). Thus, Mn often remains unnoticed as a contaminant due to its role as a micronutrient for plants and animals and to its ubiquity in the environment (Pinsino et al., 2012; Sigel and Sigel, 2000). However, consumption of high Mn concentrations may cause severe adverse health effects such as a neurodegenerative disorder (Levy and Nassetta, 2003; Sandilyan and Kathiresan, 2014; Singh et al., 2010), cardiovascular toxicity (Jiang and Zheng, 2005), and liver damage (O'Neal and Zheng, 2015). In marine coastal ecosystems such as estuaries, few studies reported Mn as a potentially toxic element since the concentrations are generally low in these ecosystems (Hadlich et al., 2018; McKinley et al., 2019). However, recent studies worldwide, motivated by increasingly large inputs of Mn from human activities,

such as mining activity, mining waste, and urban waste, have reported Mn as a potential contaminant for several aquatic species and, thus, its toxicity (Gabriel et al., 2020a; Harford et al., 2015; McKinley et al., 2019; Squadrone et al., 2016; Summer et al., 2019).

The risks associated with Mn are dynamic within estuaries since its bioavailability is driven by oscillating redox and acid-base conditions, leading to many possible fates (e.g., precipitation, adsorption, solubilization) and interactions with other mineral phases (carbonates, oxides, sulfates, and sulfides) (Du Laing et al., 2009b; Namgung et al., 2020; Otero et al., 2009; Thamdrup et al., 1994). Previous studies reported the precipitation of Mn with carbonates under anoxic conditions (Rhodochrosite; Lee et al., 2011; Zachara et al., 1991); at the same time, manganese sulfides (MnS), despite the restricted range of geochemical conditions favorable for their formation and stability, have also been reported under anoxic conditions (Lee et al., 2011; Stumm and Morgan, 1996). The oscillating redox conditions common in estuarine soils may also lead to Mn interactions with Fe oxyhydroxides (Mn associated with Fe; Burdige, 1993; Thamdrup et al., 1994) and formation of Mn oxides (e.g., birnessite; (Postma, 1985; Jacobsite; Burdige, 1993) during oxidizing periods. Thus, the Mn biogeochemical cycle is widely reported as closely associated with the Fe biogeochemical cycle (Burdige, 1993; Lewis and Landing, 1991; Slobodian and Badoz, 2019; Van Cappellen et al., 1998). In fact, these elements are involved in a wide spectrum of biogeochemical pathways such as mineral dissolution, microbial processes, flux-control of trace metals, the formation of a wide array of highly reactive solid phases (Fe and Mn oxy-hydroxides), and the biogeochemical cycles of other major elements (e.g. carbon, sulfur, and phosphorus; Borch et al., 2010; Duckworth et al., 2009). Therefore, coupled studies of Fe-Mn are crucial to advancing our understanding of a wide range of elemental cycles coupled with mechanisms that contribute to environmental contamination, particularly by manganese.

In 2015, a large-scale mine tailings dam disaster occurred in Brazil releasing 43 million m^3 of Fe-rich tailings into the Rio Doce, one of the country's largest river basins. The tailings were transported approximately 600 km downstream and reached the estuary and the ocean 16 d after the dam collapse (Gomes et al., 2017; Queiroz et al., 2021). The disaster represents one of the largest failures of a tailings dam ever recorded and the largest environmental disaster in Brazil's mining history (Carmo et al., 2017), also killing 19 people and causing extensive ecological (e.g., soil and water pollution; Bernardino et al., 2019; Gabriel et al., 2020b; Queiroz et al., 2018), economic, social and cultural damages (Fernandes et al., 2016).

In addition to the high content of Fe, previous studies have reported the presence of trace metals (e.g, Cu, Cr, Ni, and Zn) in the estuarine soils following the mine tailing contamination (Gomes et al., 2017; Queiroz et al., 2018). These metals arrived in the Rio Doce estuary associated with mine tailings, which are predominantly composed of Fe oxyhydroxides that have strong affinity with metals (Gabriel et al., 2020a; Queiroz et al., 2018). Among the reported elements, Mn does not have a threshold for soil quality according to Brazilian legislation for contaminated soil (CONAMA, 2009), but may pose different risks to the estuarine environment due to its naturally high affinity to Fe and its fast dynamics in redox active environments (Andreji and Stráňai, 2007; Gabriel et al., 2020b; Kennish, 2002; McKinley et al., 2019).

It is not surprising that Mn has not yet been reported as a contaminant in the Rio Doce estuary since Mn contamination in estuarine ecosystems is often overlooked (McKinley et al., 2019; Pinsino et al., 2012). We hypothesize that due to the redox environment in the Rio Doce estuarine soils, the Fe oxyhydroxides will act as sources of Mn leading to a potential risk of Mn contamination. Accordingly, the objective of this study was to evaluate the potential risk of Mn contamination in the Rio Doce estuary two years after the tailings arrival. We assessed the geochemical mechanisms controlling Mn bioavailability coupled to Fe dynamics in a redox active environment with Fe enrichment, to serve as a basis for public policies in coastal wetlands with potential risk of Mn contamination. Thus, the Rio Doce estuary offers a unique framework to evaluate the role of Fe oxyhydroxides controlling the Mn cycle and the environmental health in estuarine ecosystems.

5.2. Material and Methods

5.2.1. Site description

The Rio Doce estuary (19°37’51.45”S, 39°48’54.62”W) is located in SE-Brazil with a humid tropical climate classified as *Am*, according to the Köppen-Geiger climate classification system, presenting two distinct seasons including dry winters (from April to September) and wet summers (from October to March; Alvares et al., 2013; Bernardino et al., 2015). *Eleocharis acutangular*, *Typha domingensis*, and *Hibiscus tiliaceus* are the dominant local plant species. The Rio Doce basin is within the Brazilian Iron Quadrangle, a region rich in rocks such as

itabirites with highly concentrated ores of Fe, Mn, and Al and where mining activity (e.g., iron, gold, bauxite, and manganese) is of great economic importance (ANA, 2020; Rodrigues et al., 2014; Silva et al., 2017). In 2015, the Rio Doce estuary was the final destination of the Fe-rich mine tailings that were dumped into the river basin after the Mariana mining dam collapse (Gomes et al., 2017).

5.2.2. Sample collection

The estuarine soils were sampled in 2 periods: (i) in 2015, seven days after the arrival of the tailings to the estuary (for more details see Queiroz et al., 2018); and (ii) two years after the dam collapse, in 2017, to evaluate possible temporal variations. Samplings were performed during the same season in both campaigns (i.e., the wet season). Soil cores were collected using PVC tubes attached to a flooded soil sampler at four different sites in 2015. In 2017, cores were collected from eight sites, including the four sites sampled in 2015, to achieve a more comprehensive representation of sites affected by tailings deposition (Fig. 1). Additionally, a mine tailings sample collected inside the dam at the site of rupture located at Bento Rodrigues City, Minas Gerais, was donated by the Brazilian National Mining Agency (Agência Nacional de Mineração – ANM) and analyzed to determine the total Mn contents.

After sampling, cores were hermetically sealed and transported upright to the laboratory. In the laboratory, cores were sectioned at different depths depending on the year they were collected. In 2015 the samples were sectioned into 0–3, 3–5, 5–10, and 15–30 cm sections, totaling 21 samples (n = 21); whereas the samples collected in 2017 were sectioned into 0–3, 3–5, 5–10, 10–15, 15–20, 20–25, 25–30, and 30–35 cm intervals (total of 60 samples), to obtain a higher resolution of changes along the soil profiles.

Redox potential (Eh) and pH values of soils were determined in the field using portable meters and an electrode system using samples collected with a semi-open cylindrical soil auger. The pH meter was calibrated at pH 4.0 and 7.0 with standard solutions and the Eh meter measurements used a calomel reference electrode (+244 mV S.H.E.).

Water samples were collected in both years (n=10 and n=20 for the years 2015 and 2017, respectively), filtered (pore size 0.45 µm), and acidified with 0.45 mol L^{-1} HCl (trace metal grade) for the determination of dissolved Mn concentration. Water samples were collected from boreholes made with PVC tubes during soil core collection representing the pore water

from the saturated soil zone that naturally drains towards the river. The total Mn content in all water samples was determined using ICP-OES (Thermo Scientific – iCAP 6200).

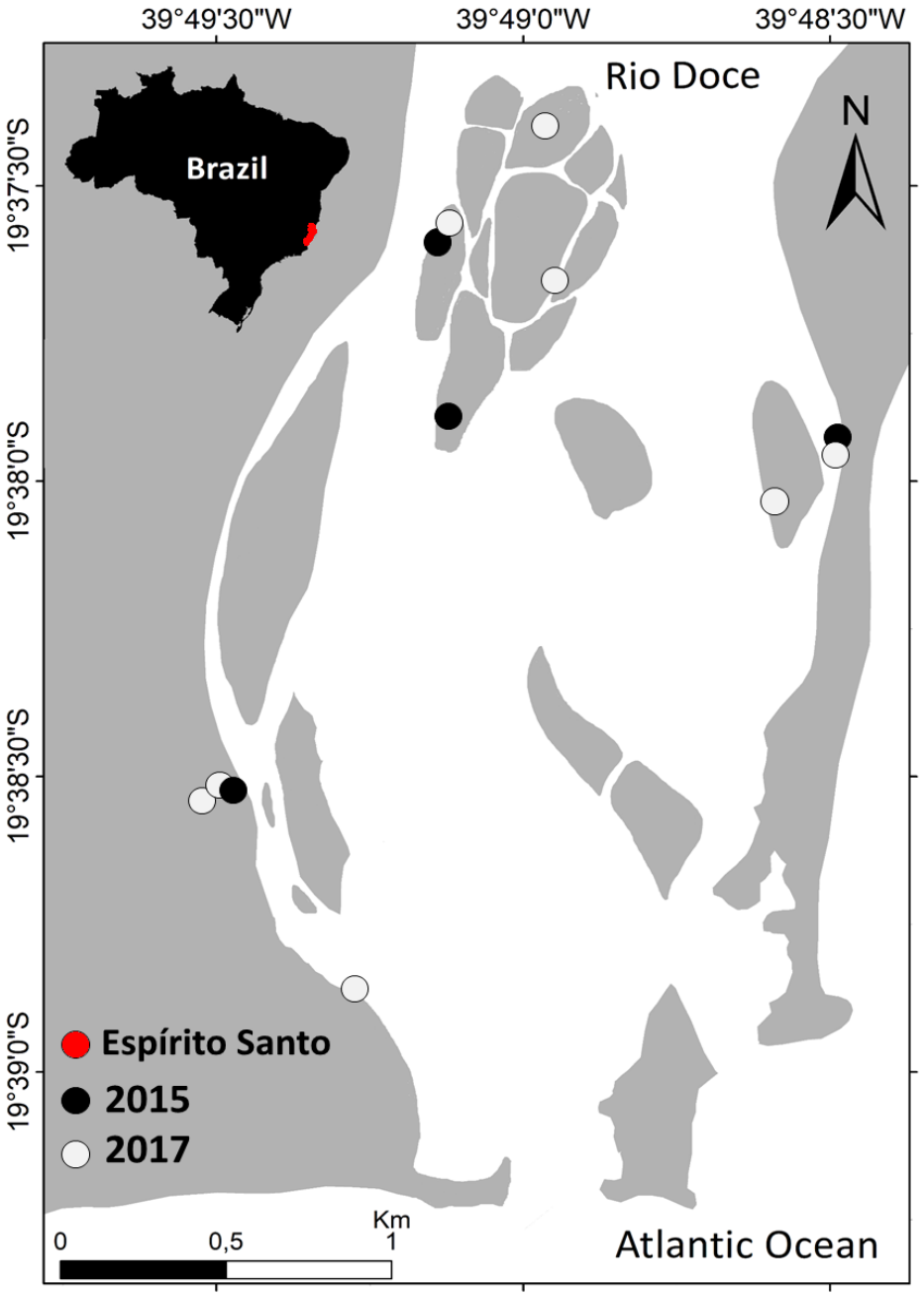

Fig. 1. Location of soil sampling sites in 2015 and 2017 in the Rio Doce Estuary, Regência, Espírito Santo, Brazil.

5.2.3. Total contents and Sequential Extraction of Fe and Mn

The total contents of Fe were obtained from estuarine soil samples and total Mn contents were obtained from both estuarine soil and mine tailings from inside the dam. The

total contents were determined using ICP-OES (Thermo Scientific iCAP 6200) after tri-acid digestion in a microwave ($HF+HCl+HNO_3$; USEPA, 1996).

Sequential extraction of Fe and Mn was performed on soil samples using a combination of methods proposed by Tessier et al. (1979), Huerta-Diaz and Morse (1990), and Fortin et al. (1993) to determine 6 operationally distinct fractions:

1. Exchangeable and soluble Fe and Mn (EX): extracted with 30 mL of 1 mol L^{-1} $MgCl_2$ solution at pH 7.0 at 4 °C, agitated continuously for 30 min.
2. Fe and Mn bound to carbonates (CA): obtained with 30 mL of 1 mol L^{-1} NaOAc at pH 5.0, agitated for 5 h.
3. Fe and Mn bound to ferrihydrite (FR): extracted with 30 mL of 0.04 mol L^{-1} hydroxylamine + acetic acid (25% v/v) solution by shaking for 6 h at 30 °C.
4. Fe and Mn bound to lepidocrocite (LP): extracted with 30 mL of 0.04 mol L^{-1} hydroxylamine + acetic acid (25% v/v) solution by shaking for 6 h at 96 °C.
5. Fe and Mn bound to crystalline Fe oxyhydroxides (mainly goethite; CR): extracted with 20 mL of 0.25 mol L^{-1} sodium citrate + 0.11 mol L^{-1} sodium bicarbonate with 3 g sodium dithionite, agitated for 30 minutes at 75 °C.
6. Fe and Mn associated with pyrite (PY): extracted with concentrated HNO_3 (2 h agitation) previously treated with 10 mol L^{-1} HF for silicates removal.

5.2.4. X-ray Absorption Spectroscopy

X-ray absorption spectra from the five most representative estuarine soil samples were obtained using beamline 7-3 at the Stanford Synchrotron Radiation Lightsource. Spectra were collected at the Mn K-edge using a Si (220) crystal set with orientation ϕ=90°, with the beam detuned by 50% at 7500 eV. Soil samples had been previously dried in a 95% N_2: 5% H_2 atmosphere before being ground using a mortar and pestle. Samples were packed into aluminum sample holders and sealed with 0.5 mil Kapton tape prior to XAS analysis under ambient conditions. For each sample, two replicate scans were obtained, and beam damage was avoided by moving fresh sample into the beam path. An in-line Mn foil was used as a reference for all scans.

Calibration, normalization, and merging of replicate scans was performed using the Demeter package (version 9.26) (Ravel and Newville, 2005) with Larch running as a backend

(Newville, 2013) on Windows 10. The average Mn oxidation number (AMON) of the Mn in each sample was obtained through linear combination fitting analysis of the Mn X-ray absorption near-edge structure (XANES) spectra and was performed in Athena (Ravel and Newville, 2005) using the Combo method of Manceau et al. (2012). In all cases, reference spectra from 12 pure-valent Mn species were used to perform unconstrained linear fits. Any reference yielding a negative loading was progressively removed on a per-sample basis and re-added to the reference list before fitting the next sample.

The fraction of Mn^{II}, Mn^{III}, and Mn^{IV} and AMON were calculated from the fits according to Manceau et al. (2012). A paired-sample t-test was used to assess the difference between the means of the AMON data corresponding to soil samples. For the assessment of the relative fraction of Mn distributed between adsorbed Mn^{II} and Mn oxide phases, linear combination fitting of EXAFS was used. For this technique, three Mn^{II} standards, 6 $Mn^{III,IV}$ oxides, and 2 Mn oxides containing Mn^{II} were used to fit the spectra. EXAFS references were a mixture of spectra collected in-house and those obtained by Santelli et al. (2011). The fractional weights for all oxide phases were combined and compared to the combined weight of the Mn^{II} standards prior to comparison of means through a paired-sample t-test. Fits were conducted between K=3 and K=11. XANES and EXAFS data from the standards used in all linear combination fitting, as well as the XANES linear combination fittings and data are available in the SI.

5.2.5. Diffuse reflectance spectroscopy

Diffuse reflectance spectroscopy (DRS) was used for the mineralogical characterization of soil samples. DRS spectra were measured from 300 to 800 nm at 1 nm increments with a 110 mm integrating sphere using a Varian Cary 5 Spectrophotometer. The results were transformed using the Kubelka Munk function to calculate the second derivative. Spectra from surface soil samples (0–3 cm, from 2015 and 2017) and subsurface samples (30–40 cm, depth with lower tailings deposition influence) from 2017 were obtained to compare the estuarine soil composition after tailings deposition as well as mineralogical changes over time.

5.2.6. Fish collection and analyses of metal contents in tissues

To assess the risk of Mn contamination to local wildlife, two fish species were collected in 2017 using a bottom Otter Trawl, at random locations in proximity to the soil sampling sites (Fig. 1). *Cathorops spixii* (Agassiz, 1829) (Madamango sea catfish; n= 15) and *Genidens genidens* (Valenciennes, 1839) (Guri sea catfish; n=18) are estuarine species which spend their entire life cycle associated with bottom sediment. In addition, these species have been used previously as bioindicators of pollution and are an important food resources for the local population (Azevedo et al., 2009; Pinheiro and Joyeux, 2007).

After collection, fish were immediately frozen until dissection in the laboratory. Fish liver and axial muscle tissues were dissected and stored at −80 °C until quantification of total metal contents. The total contents of Mn and Fe were determined using approximately 100 mg of dried sample (muscle or liver) weighed in sterile polypropylene tubes, followed by the addition of 1.0 mL of double-distilled HNO_3. The blanks containing only 1.0 mL of double-distilled HNO_3 were prepared in triplicate. The DORM-4 (Dogfish muscle – National Research Council, Canada) Certified Reference Material (CRM) was used for quality control. The samples, blanks, and CRM were left in contact with HNO_3 for approximately 12 hours overnight then heated for digestions the following morning on a digester block for 4 hours at approximately 100 °C. The closed tubes were monitored hourly with manual pressure relief when necessary. After heating, the samples, CRM, and blanks were left to cool until room temperature and made up to appropriate volumes with ultra-pure water (resistivity > 18.2 MΩ). The Mn and Fe quantification were performed by ICP-MS using an ICP-MS ELAN DRC II (Perkin-Elmer Sciex, Norwalk, CT, USA). ^{103}Rh was used as the internal standard at 20 µg L^{-1}.

5.2.7. Contamination factor determination

The contamination factor (Cf) was used to evaluate the Mn contamination at Rio Doce estuary, using as a background value the total Mn contents in the soils 11 d before the tailings arrival reported by Gomes et al., (2017). The Cf is a ratio between the content of an element in a soil sample and the background content of the same element at the studied site (Hakanson, 1980), following the equation Cf = Cs / Cb,

where Cs is the soil content of Mn in 2017 and Cb is the Mn background value. According to Hakanson (1980), the following interpretations are suggested for the Cf value: Cf < 1, low; 1 to < 3, moderate; 3 to < 6, considerable; and > 6, high contamination.

5.2.8. Statistical analyses

The Fe and Mn total contents in soil and water samples were assessed with a non-parametric Kruskal–Wallis ($p < 0.05$) test to assess differences between 2015 and 2017, whereas the Fe and Mn contents in fish muscles and livers were analyzed with a non-parametric Friedman test at the 5% significance level with multiple pairwise comparisons (Reimann et al., 2008; XLSTAT version 2014.5.03). Non-parametric statistical tests are appropriate for non-normal distributions and rely on fewer assumptions, which make them more robust for environmental data (Reimann et al., 2008). The correlations between the total of Fe and Mn in soil were determined by calculating Spearman's correlation coefficients (r) as this method does not assume a normal distribution.

5.3. Results

5.3.1. Physicochemical conditions, Fe and Mn total contents and fractionating

The Eh and pH values in 2015 were on average +218 ± 116 mV and 6.2 ± 1.3, respectively. In 2017, the pH remained close to neutral (average 6.7 ± 0.5) but the Eh values decreased considerably with a mean of -47 ± 83 mV (Fig. 2).

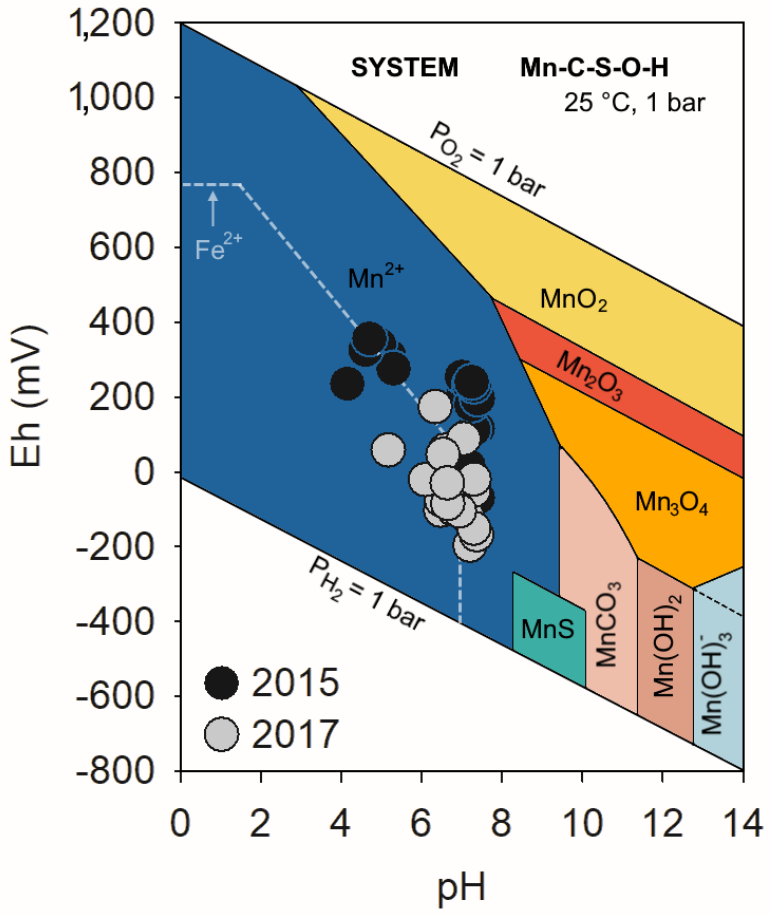

Fig. 2. Eh-pH diagram (system Mn-C-S-O-H) with the data for the studied soils in both years. The gray dashed line indicates the Fe^{2+} stability field on the system Fe-C-O-H. The Eh-pH diagram was adapted from Brookins (1988).

The total Mn content in mine tailings from inside the Fundão Dam was on average 644 ± 241 mg kg^{-1} whereas in the estuarine soil, in 2015, higher total Fe (47,133 ± 16,538 mg kg^{-1}) and Mn (704 ± 529 mg kg^{-1}) contents were measured in the surface soil layers (0–3 cm), the soil layer most affected by tailings deposition (Fig. 3). Two years later, the mean total Fe and Mn concentrations decreased by 75% and 74% respectively across all soil depths. In 2017, the highest Fe and Mn contents were still found in the upper 0–3 cm (11,997 ± 8,239 mg kg^{-1} and 186 ± 120 mg kg^{-1} respectively), followed by a decrease of both elements with soil depth (depths > 3 cm; Fig. 3). The contamination factor (Cf) using the Mn content in the 0-3 soil layer just after the tailing arrival (in 2015) was 3.2 indicating considerable contamination levels, whereas in 2017 the Cf decreased to 0.84 indicating low contamination.

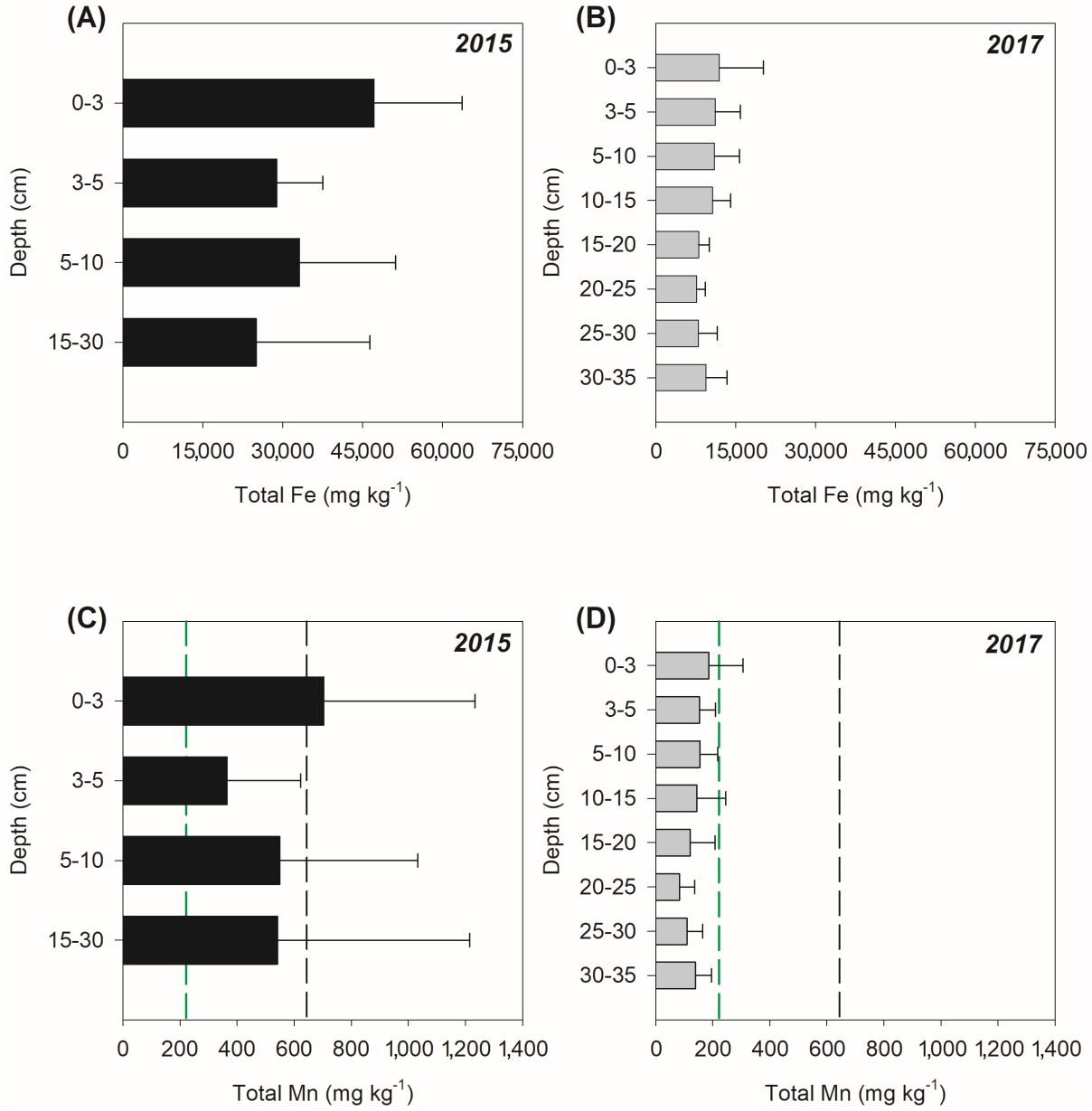

Fig. 3. Total Fe and Mn contents of Rio Doce estuarine soils collected in 2015 and 2017. The black dashed line indicates the contents of the total Mn in tailings from inside the Fundão dam. The green dashed line indicates the Mn contents in Rio Doce estuarine soil, prior to mine tailings arrival according to Gomes et al., (2017).

Solid-phase Fe and Mn fractionation of soils collected in 2015 (Fig. 4) shows Fe mostly held in crystalline Fe oxyhydroxides representing 88% of total Fe (on average: 64,154 ± 45,104 mg kg^{-1}), whereas poorly crystalline Fe oxyhydroxides represented only 11% (i.e., average: LP: 4,632 ± 3,635 mg kg^{-1} equivalent to 6%; and FR: 3,645 ± 3,573 mg kg^{-1} equivalent to 5%; Fig. 4). The sum of EX, CA, and PY fractions were approximately 1% of the total Fe.

In contrast, Mn was mainly associated (78%) with poorly crystalline Fe oxyhydroxides (FR: 286 ± 352 mg kg^{-1}; LP: 134 ± 171 mg kg^{-1}) and to a lesser degree (9%) with the crystalline

(CR) fraction (46 ± 27 mg kg^{-1}). Soluble and exchangeable (EX) fractions represented 9% (50 ± 78 mg kg^{-1}) and Mn associated with carbonates (CA: 25 ± 37 mg kg^{-1}) and pyrite (PY: 25 ± 37 mg kg^{-1}) represented about 5%.

In 2017, Fe showed a contrasting distribution to that of 2015, with a marked decrease in CR (14,326 ± 2,507 mg kg^{-1}; equivalent to 65%) followed by a significant increase in LP (4,493 ± 732 mg kg^{-1}; equivalent to 20%), and FR (3,042 ± 1,051 mg kg^{-1}; equivalent to 20%). On average, the crystalline Fe oxyhydroxide contents decreased 49,828 mg kg^{-1} when compared to 2015 (Fig. 4). The other fractions (i.e., EX, CA, and PY) remained close to 1% of the sum of all Fe fractions. Similar to 2015, in 2017 Mn was mostly associated with poorly crystalline Fe oxyhydroxides (FR: 241 ± 67 mg kg^{-1}; equivalent to 65%; LP: 68 ± 10 mg kg^{-1}; equivalent to 18%) and to a lesser extent (11%) associated with crystalline Fe oxyhydroxide phases (CR: 39 ± 8 mg kg^{-1}; Fig. 4). In contrast, the soluble and exchangeable Mn fraction decreased considerably (EX: 9 ± 4 mg kg^{-1}; equivalent to 2% of total Mn) and Mn associated with carbonates and pyrite represented the less important Mn fractions found in the solid-phase in that year (14 ± 3 mg $kg^{-1}$and 0.4 ± 0.1 mg kg^{-1} , respectively; representing about 4% of Mn).

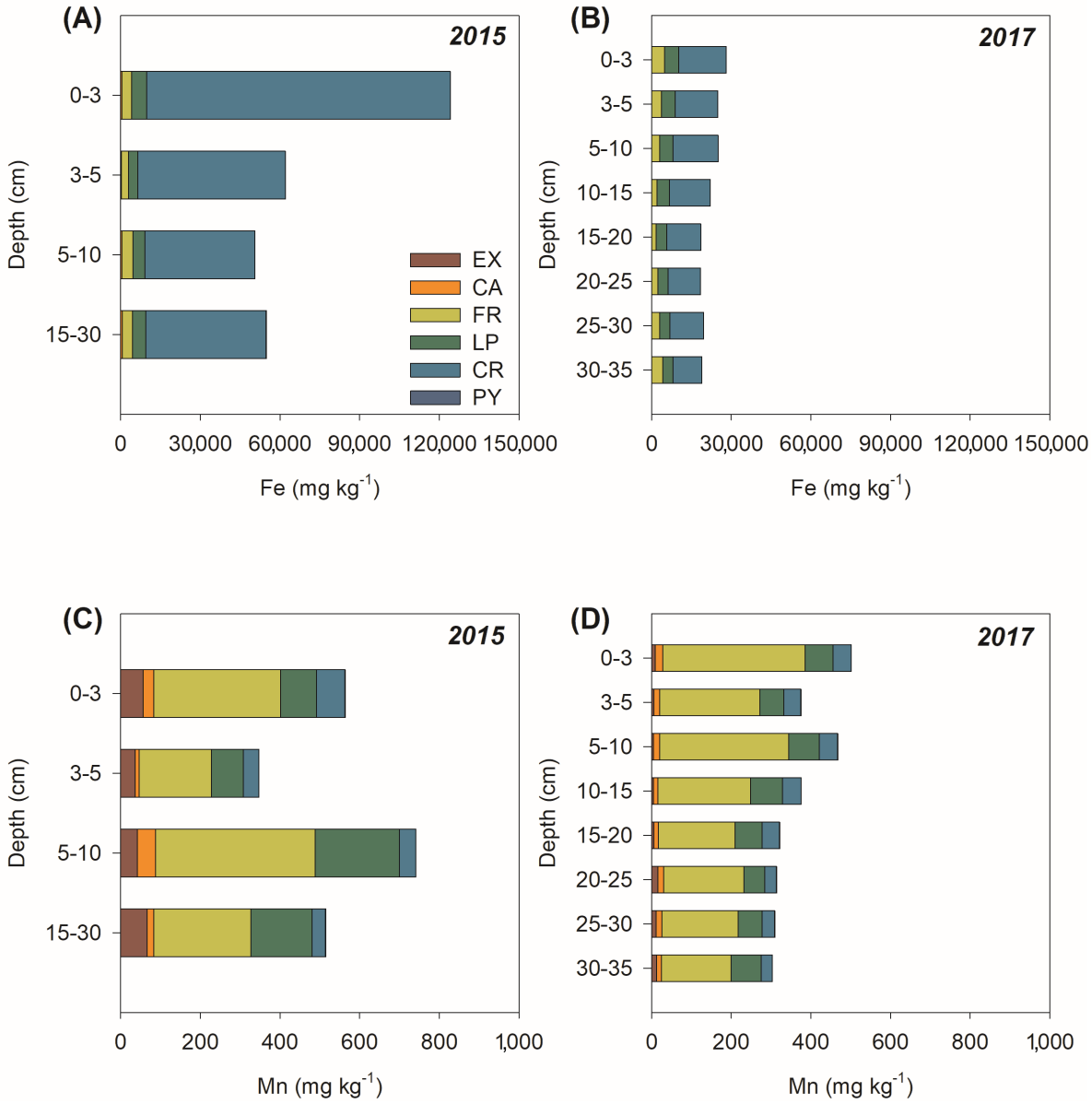

Fig. 4. Fe and Mn solid-phase fractionation from Rio Doce estuarine soils in 2015 and 2017. EX: Soluble and exchangeable Fe and Mn; CA: Fe and Mn associated with carbonates; FR: Fe and Mn associated with ferrihydrite; LP: Fe and Mn associated with lepidocrocite; CR: Fe and Mn associated with crystalline oxides; PY: Fe and Mn associated with pyrite.

5.3.2. Spectral reflectance characteristics

The DRS spectra corroborated the solid-phase fractionation and indicated a greater presence of both high- and low- crystallinity Fe oxyhydroxides in the surface soil layers (i.e., 0–3 cm) in both years. Deeper soil layers (30–35 cm) were less influenced by mine tailings with much smaller quantities of Fe oxyhydroxides (Fig. 5) as seen by the lower intensity of bands of iron oxides (Ji et al., 2002). It is noteworthy that band intensities changed over time, with a

lower intensity of bands in 2017 corroborating a loss in Fe oxides (Figures 3 and 4). In fact, the shift in the intensity of bands between 485 and 490 nm indicates a decrease of both lepidocrocite and goethite (absorption band at 488 nm) with time. The same patterns are observed for the absorption bands of ferrihydrite (seen between 484 and 499 nm; Scheinost, 1998) and hematite (absorption band shown at 533–588 nm; Hu et al., 2016). The Fe fractionation analyses (Fig. 4) can aid in distinguishing the relative contributions of the different iron forms to the DSR bands (Scheinost et al., 2001; Schwertmann and Taylor, 1989).

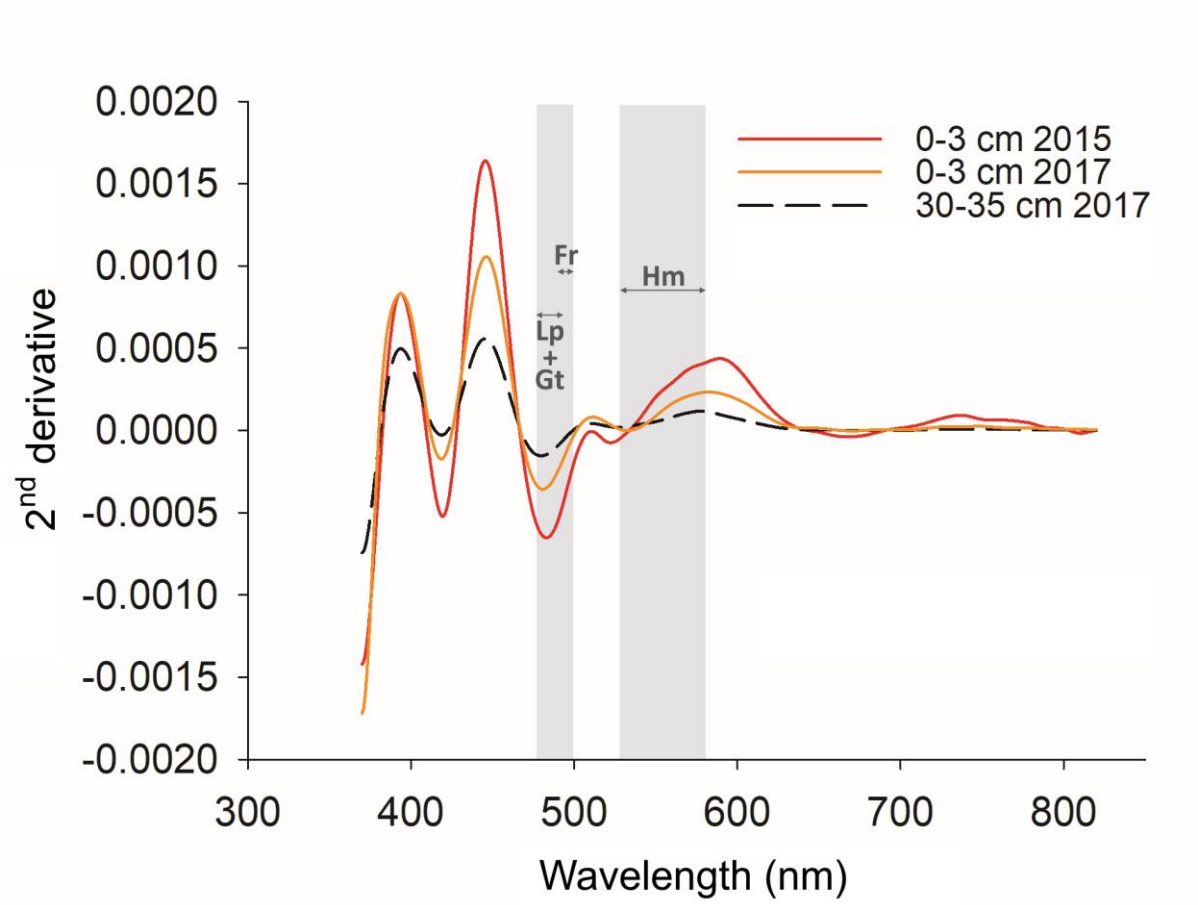

Fig. 5. Second-derivative spectra of surface (0–3 cm depth from 2015 and 2017) and sub-superficial soil samples (30–40 cm depth from 2017). Range of crystal field band position for lepidocrocite (Lp) and goethite (Gt) (488 nm), ferrihydrite (Fr; 484-499 nm), and hematite (Hm; 533-588 nm).

5.3.3. XANES and EXAFS Characterization

While Mn fractionation and acid digestions can quantify the total and relative mass of Mn in samples, X-ray absorption analyses including XANES and EXAFS provide Mn oxidation state and coordination information. Mn K-edge XANES showed that more than half of the Mn

in the soil solid phase was reduced (52 %; Table 1) in the soil surface samples (0–3 cm) from 2015 which represents the readily exchangeable or adsorbed Mn fractions (Tebo et al., 2004), while the abundance of Mn^{III} and Mn^{IV} were 32 % and 16 %, respectively (Table 1).

Table 1 – The relative abundance of solid-phase Mn^{II}, Mn^{III}, and Mn^{IV} within soil samples collected from multiple depths in 2017 and from the 0-3 cm depth in 2015 as determined by Mn K-edge XANES.

Sample	Mn K-edge XANES			AMON
	Mn^{II}	Mn^{III}	Mn^{IV}	
	rel. abundance (%)*			
2015 (0–3 cm)	52	32	16	2.626
2017 (0–3 cm) – R1	34	33	33	2.992
2017 (0–3 cm) – R2	36	48	15	2.789
2017 (30–35 cm) – R1	55	24	21	2.668
2017 (30–35 cm) – R2	77	17	6	2.290

AMON = Average Mn oxidation number; R1: Replicate 1; R2: Replicate 2. *Relative abundances determined using linear combination fitting.

In 2017, Mn EXAFS analysis shows that surface soil samples (0–3 cm) had a higher concentration of Mn^{III} and Mn^{IV} than soils from 2015, where these oxidized forms of Mn were present as phyllo- and tectomanganates (Fig. 6). In contrast, the corresponding subsurface (i.e., 30–35 cm) soils showed greater concentrations of the Mn^{II} (Table 1).

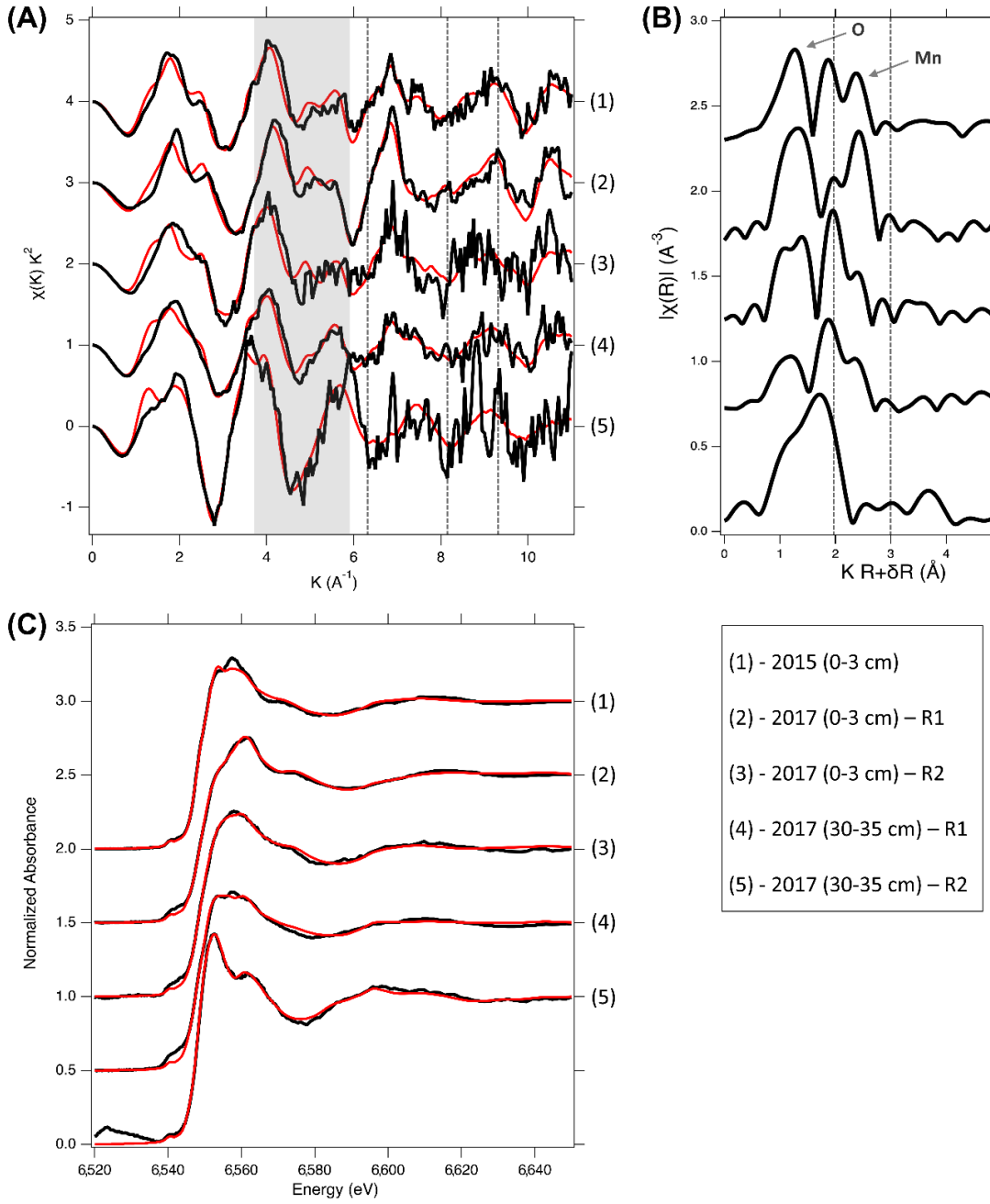

Fig. 6. Mn K-edge EXAFS of soil samples from 2015 and 2017 collected at two depths (0–3 cm and 30–35 cm). (A) Shaded area highlights the characteristic "staircase" feature of the EXAFS indicative of phyllomanganate presence; the vertical dashed lines mark the shoulder feature at 6.5 $Å^{-1}$ and the antinodes at 8.2 and 9 $Å^{-1}$. (B) Pseudo-radial structure functions of the Mn EXAFS; vertical lines mark features at 2 Å, 3 Å and 5 Å; the arrows point to the nearest Mn-O and Mn-Mn shells. (C) A comparison of the Mn XANES from 2017 soil samples with the soil surface sample from 2015. Data is shown in black, model generated from linear combination fitting is shown in red.

Mn K-edge EXAFS of the surface soil samples from 2017 displayed the characteristic phyllomanganate (e.g. birnessite; δ-MnO_2) "staircase" feature between 4 and 6 $Å^{-1}$ (Fig. 6). Extensive corner-sharing cation octahedra dispersed in the interlayer region (i.e. Mn^{II}, Mn^{III},

Zn, Ni) give rise to the shoulder development along the rising edge of the antinode at 6.4 $Å^{-1}$ (Fig. 5); the corresponding peak at ~3 $Å$ is also indicative of the presence of Mn^{III} or Mn^{IV} (Manceau et al., 2002; Marcus et al., 2004; Toner et al., 2006). In addition, the absence of a defined antinode at 8.1 $Å^{-1}$ in any of the samples suggests the presence of tectomanganates, such as pyrolusite (MnO_2), as well as Mn^{III}-rich octahedral sheets in the phyllosilicate minerals present in the 0–3 cm soil layer soil from 2017 (Marcus et al., 2004; Webb, 2005; Zhu et al., 2010).

5.3.4. Mn in water and in fish tissues

The mean total dissolved Mn concentration in water samples collected in 2015 was 66 ± 130 µg L^{-1}, whereas in 2017 the average concentration increased 9-fold to 582 ± 626 µg L^{-1} (Fig. 7). The 2017 concentrations are 5 times higher than the threshold outlined by the Brazilian water quality guidelines for brackish waters (100 µg L^{-1} for inorganic constituents in brackish waters without chronic toxic effects on organisms; CONAMA, 2005). In comparison, the concentration of dissolved Mn in 2017 was higher than the threshold for chronic contamination in marine water according to the National Oceanic and Atmospheric Administration, USA (100 µg L^{-1}; NOAA, 2008).

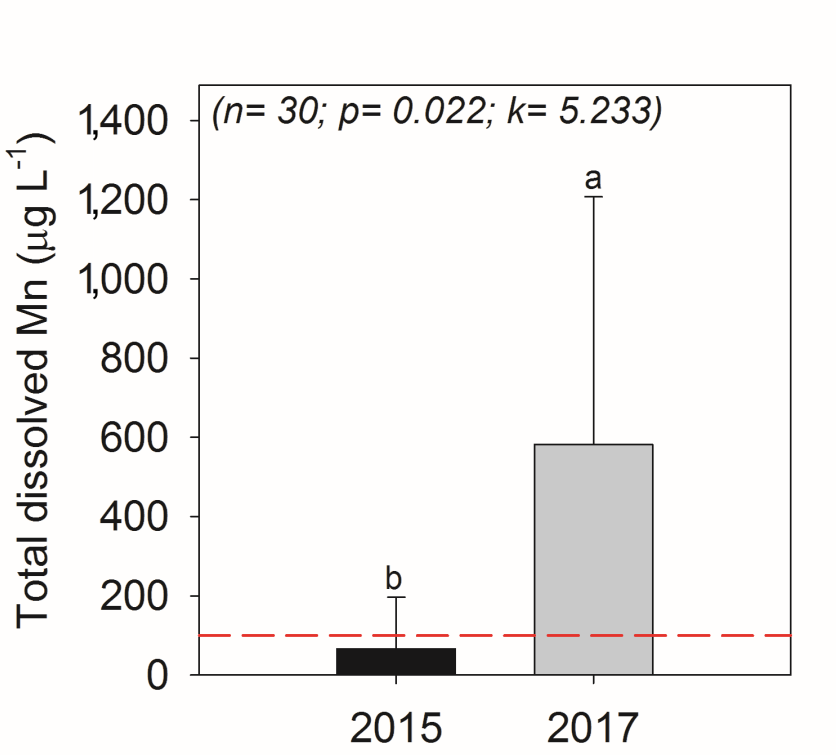

Fig. 7. Total concentration of dissolved Mn in the Rio Doce estuary water sampled in 2015 and 2017. The red dashed line indicates the threshold according to the Brazilian water quality guidelines for brackish water (100 µg L^{-1}; CONAMA, 2005). The different lowercase letters indicate a significant difference between the variables as determined by the Kruskal-Wallis test at the 5% probability level.

The Fe and Mn contents in fish liver and muscle tissues were significantly different, but did not differ between species (Fig. 8). Higher concentrations of Fe and Mn were observed in the liver than in the muscle (Fig. 8). The mean Fe content in the liver was 830.1 ± 638.0 mg kg^{-1} and 1,541.4 ± 1,725 mg kg^{-1} respectively in *Cathoropus spixii* and *Genidens genidens,* whereas the mean Mn contents were 3.2 ± 1.7 mg kg^{-1} and 2.1 ± 1.9 mg kg^{-1}. In the muscle, Fe and Mn concentrations in *Cathoropus spixii* were 26.8 ± 26.4 mg kg^{-1} and 1.0 ± 1.0 mg kg^{-1}, respectively; whereas in *Genidens genidens* mean Fe and Mn contents in muscles were 17.4 ± 11.4 mg kg^{-1} and 0.5 ± 0.2 mg kg^{-1}, respectively (Fig. 8). There is no contamination threshold for either Mn or Fe for both studied fish species.

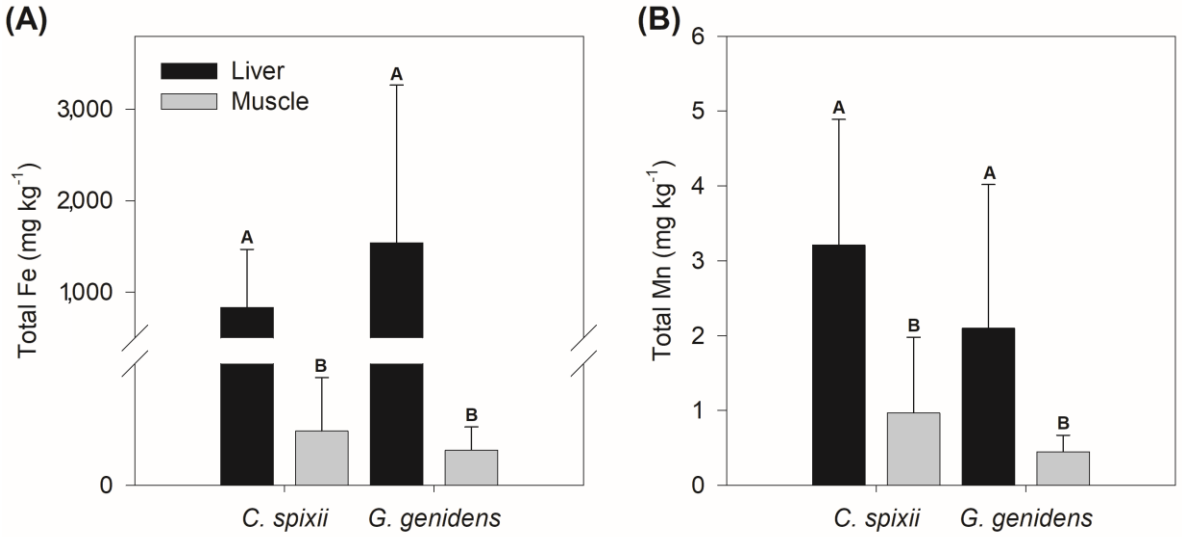

Fig. 8. Total contents of Fe (A) and Mn (B) in the liver and muscle of *Cathoropus spixii* and *Genidens genidens* from Rio Doce. Labelled bars with uppercase letters (A and B) indicate groups between which statistical differences among species or tissues exist at the 5% probability level using the non-parametric Friedman test.

5.4. Discussion

5.4.1. Mining tailing disaster and its impacts on Mn geochemistry

In 2015, because of the Fundão dam rupture, Fe-rich tailings were dumped into the Rio Doce basin and traveled 688 km downriver toward the estuary (Gomes et al., 2017). The tailings were made mostly of crystalline Fe oxyhydroxides which have high metal retention capacity (Cornell and Schwertmann, 2003; Queiroz et al., 2018). Therefore, we hypothesized the tailings may have acted as a Mn sink until its ultimate deposition in the estuary. In addition to the high content of Mn (644 ± 241 mg kg^{-1}) in the original tailings from inside the dam (Fig. 3), agricultural activities and pollution from large cities and villages along the basin may have acted as additional Mn sources to the mine tailings transported in the Rio Doce river on its way to the estuary (Queiroz et al., 2021). In the past, studies prior to the Mariana disaster also reported Mn contents ranging from 660 to 2,280 mg kg^{-1} in mine tailings from Samarco's dams located in the same mining complex as Fundão dam (Pereira et al., 2008). Indeed, the Mn contents in the surface soil layers (0–3 cm) from 2015 (704 ± 529 mg kg^{-1}), were on average 3-fold higher than Mn contents 11 d before the disaster (222 ± 13 mg kg^{-1}) reported by Gomes et al., (2017) indicating the tailings deposition effects. In this sense, the Cf calculated (3.2) indicates a Mn enrichment in the soil soon after the disaster and considerable contamination.

Moreover, the significant positive correlation between Fe and Mn (Fig. 9) in samples collected from 2015 support the arrival of Mn to the estuary in association with the Fe-rich mine-tailings (i.e., adsorbed to Fe oxyhydroxides).

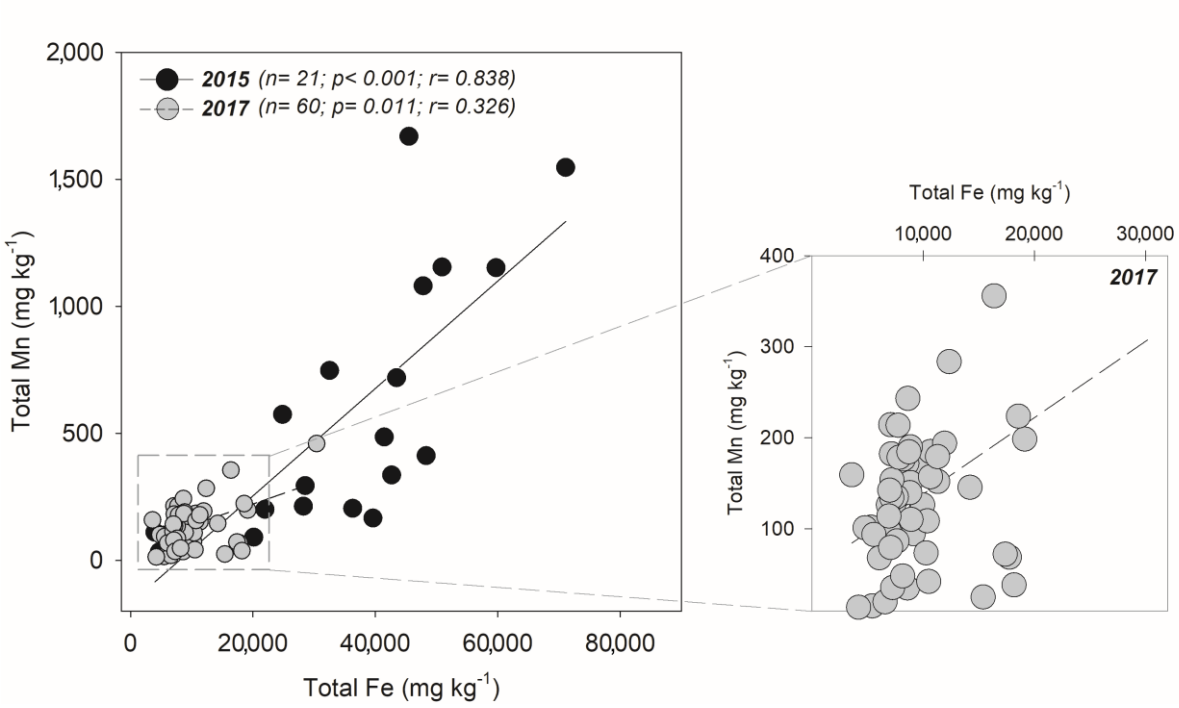

Fig. 9. Spearman correlations between total Fe and Total Mn in 2015 and 2017. The right panel shows in detail the spearman correlation between total Fe and total Mn content from 2017 highlighting the loss of correlation with time.

The interaction of Mn with Fe oxyhydroxides in soils has been widely reported due to the energetic favorability of Mn forming mono- and bi-nuclear inner-sphere complexes through reacting with excess structural OH^- groups on the Fe oxyhydroxide surface (Ugwu and Igbokwe, 2019; Zhu et al., 2020). In general, Fe oxyhydroxides uptake the Mn^{II} forming virtually irreversible complexes (Coughlin and Stone, 1995; Namgung et al., 2020). Indeed, the EXAFS results showed higher abundance of Mn^{II} in the 0–3 cm depth range from 2015 (Table 1), as well as in the Fe fractionation, which indicates that Mn was mostly associated with Fe oxyhydroxides (FR: 53%; LP: 25%; and CR: 9%). In addition, circumneutral pH and Eh values above +100 mV recorded in 2015 (Fig. 2) indicate suboxic conditions that are favorable to Fe oxyhydroxide formation (Reddy and DeLaune, 2008).

Once the Fe-rich tailings arrived and were deposited on the soils of the Rio Doce estuary, the tailings were then exposed to redox oscillating conditions caused by tidal flooding and plant activity (Bianchi, 2007; Du Laing et al., 2009a). By 2017, a sharp decrease in Eh (-46

± 83 mV, on average) was observed compared to measurements in 2015 (+218 ± 116 mV, on average) indicating increasingly anoxic conditions (Fig. 2) (Reddy and DeLaune, 2008; Søndergaard, 2009). The marked decrease in Eh over time is likely due to estuarine plants (i.e., *Eleocharis acutangula*, *Typha domingensis*, and *Hibiscus tiliaceus*) that serve as direct inputs of organic matter (e.g. via dead leaves and roots) while also efficiently trapping particulate organic matter (OM) that is transported downstream. These plants contributing OM inputs coupled with tidal flooding stimulate anaerobic OM degradation and Fe^{III} reduction (Badarudeen et al., 1996; Kristensen et al., 1995; Marín-Muñiz et al., 2014). Additionally, the plant growth enhances the maintenance of settled tailings since plant stems reduce the turbulence kinetics that could lead to physical tailings removal (Jay et al., 2007; Mudd et al., 2010).

Thus, Fe oxyhydroxides from the tailings were subjected to a biogeochemical environment highly favorable towards Fe^{III} reduction to Fe^{II} and its subsequent solubilization (Cummings et al., 2000; Xia et al., 2019). In estuaries, the fate of solubilized Fe^{II} following dissimilatory Fe reduction may vary, for instance as precipitation of poorly crystalline Fe oxyhydroxide, uptake by plants, or removal from the estuary into the ocean (Canfield et al., 2005; Johnston et al., 2011; Richard et al., 2020). The significant decrease in total Fe in soils collected in 2017 (r <0.001; Fig. 10), mainly at the soil surface, which was the soil layer most affected by tailings deposition, clearly corroborates a massive loss of total Fe through reduction (i.e., reductive dissolution). Additionally, the total Fe loss reflected the significant loss of the CR Fe fraction (Fig. 4) which was also supported by a clear decrease in the goethite and hematite bands of the DRS spectra likely due to their dissolution (Canfield et al., 1993; Lovley et al., 2004).

The total Mn content in the soil from 2017 also showed a significant decrease (p-value <0.001; about 75%) when compared to 2015 data (Fig. 10). Furthermore, the solid-phase fractionation showed that Mn associated with both high and low crystallinity Fe oxyhydroxides decreased on average 25% in 2017 (Fig. 4). Likely, the decrease of soil Mn contents was associated with its release as Mn^{II} in response to Fe oxyhydroxides dissolution. In fact, the association of Mn with high and low crystallinity Fe oxyhydroxides was clearly shown by the Mn K-edge XANES data (Table 1).

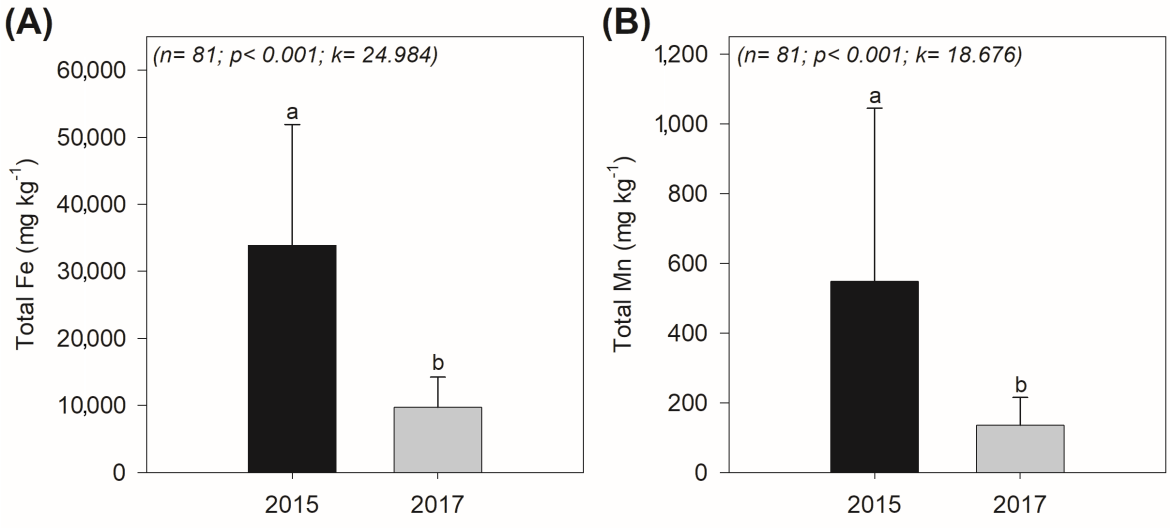

Fig. 10. Mean Fe (A) and Mn (B) total soil contents from 2015 and 2017. The different lowercase letters indicate significant differences among the variables using the Kruskal-Wallis test at the 5% probability level.

Following release and diffusion out of soils, dissolved Mn^{II} had a number of possible fates: 1) be transported further downstream and washed out from the estuary (particularly during the rainy season); 2) be retained on Fe oxyhydroxides; or 3) undergo oxidation followed by precipitation as Mn oxides (Chaudry and Zwolsman, 2008; Otero et al., 2009; Sundby et al., 2003). XANES analysis of soil samples from 2017 (Table 1) shows that a high proportion of Mn had been oxidized (i.e., Mn^{III} and Mn^{IV}) in the soil surface layers (i.e. 0–3 cm) corresponding to EXAFS spectra with characteristics attributable to phyllo- and tectomanganates (i.e., Mn oxides; Fig. 5). According to Oldham et al. (2019) Mn^{II} can be quickly oxidized to Mn oxides in estuarine surface soils because O_2 diffusion in the surface layers is more rapid than at depth.

It is likely during the first two years (2015 to 2017) after the arrival of the tailings that the prevailing conditions in the estuarine soils favored the release of Mn^{II} through reduction of Fe oxyhydroxides, with subsequent transformation of Mn^{II} into poorly crystalline Mn oxides due to redox fluctuations (Fig. 2). Previous studies reported that both dissolved Mn and Fe may re-oxidize or co-precipitate with a variety of different soil minerals (e.g. oxides, carbonates, sulfides) (Du Laing et al., 2009b; Otero et al., 2009). However, by 2017, the redox potential observed in Rio Doce estuarine soils indicated geochemical conditions (i.e., Eh and pH) had become favorable for anaerobic processes including both Fe and Mn dissimilatory reduction (Fig. 2) (Canfield et al., 1993; Lovley et al., 2004). It is widely known that anaerobic microorganisms through microbial reduction of both Fe and Mn may use Mn^{III}, Mn^{IV}, and Fe^{III}

present on minerals as electron acceptors for anaerobic respiration under anoxic conditions (Otero et al., 2009; Patrick and Jugsujinda, 1992). Thus, our results indicate that Mn released during 2017 onwards might have occurred through reduction of both Fe oxyhydroxides and poorly crystalline Mn oxides (Lovley et al., 2004; Postma and Appelo, 2000).

Therefore, an increase in dissolved Mn concentrations is expected given that Mn^{II} is generally more stable against abiotic oxidation by O_2 than Fe^{II}, which can be rapidly oxidized under Eh conditions above +100 mV and circumneutral pH (Burdige, 1993; Frohne et al., 2011). Although Mn oxides have been formed due to O_2 diffusion in surface layers, the Mn oxides required very strong oxic conditions (approximately +900 to +1000 mV at pH 5) to reach stability against reductive processes (Frohne et al., 2011). In our study, the highest Eh value measured in 2017 was +174 mV. The Fe^{II} oxidation, however, occurred rapidly according to the Eh measured in samples from 2017, leading to the formation of poorly crystalline Fe oxyhydroxides such as ferrihydrite and lepidocrocite (Frohne et al., 2011; Yu et al., 2007), both of which increased in 2017 representing 40% of Fe minerals (Fig. 4). Contrarily long-term the contents of FeCR will mostly decrease since its formation is very low in environments with redox oscillations (Winkler et al., 2018). It should be noted, however, that poorly crystalline Fe minerals (i.e., FeLP and FeFR) phases are more susceptible to reduction within redox-oscillating environments (Nealson and Myers, 1992; Patrick and Jugsujinda, 1992; Reddy and DeLaune, 2008).

Thus, results showing the significant loss of Fe in the tailings-affected estuarine soils and the higher susceptibility of poorly crystallinity Fe oxyhydroxides to undergo reductive dissolution under transitory/cyclic anoxic conditions both point toward a decreasing capacity of poorly crystalline Fe minerals to control future Mn retention. The decrease in the significance of the Spearman correlation coefficient between total Fe and Mn in 2017 reinforces a less marked capacity of Fe oxyhydroxides in Mn retention (Fig. 9).

5.4.2. Environmental Consequences

Metals can be absorbed into fish tissues through direct contact (i.e. through gills, skin or ingestion) such as with metals dissolved in the water column and associated with bottom sediments (Olsson et al., 1998; Weber et al., 2013). While the Cf in 2017 indicates low contamination levels of Mn in the soil at the studied site, high concentrations of Mn and other

trace metals in the Rio Doce estuary suggested a high ecological risk for marine life (Bernardino et al., 2019; Gabriel et al., 2020a). Thus, the high contents of Mn in fish livers is indicative of chronic or acute exposure given the liver's role in storage, redistribution, and metabolism of contaminants (Al-Yousuf et al., 2000). For these reasons, metal concentrations in the liver are useful indicators of bioaccumulation and are a bioindicator of Mn exposure in the Rio Doce estuary (Azevedo et al., 2009; Hauser-Davis et al., 2014). In fact, a recent study in the Rio Doce estuary indicated bioaccumulation of metals, including Mn, in tissues of *Cathoropus spixii* and *Genidens genidens* resulting in physiological effects due to chronic exposure to metal contaminants (Gabriel et al., 2020b).

The presence of Mn in fish muscle tissue poses a high risk to human health for the local community because the fish muscles are consumed by humans (Gabriel et al., 2020b; Gusso-Choueri et al., 2018). According to Gusso-Choueri et al. (2018), the consumption of metal-contaminated fish is one of the main routes of exposure for riverside communities. In most cases, the health risk is aggravated for those who depend on fish from the estuary to meet their daily dietary needs, which is the case for many people living near the Rio Doce estuary (Gabriel et al., 2020a).

According to the World Health Organization (WHO, 2011), food consumption is the primary route of exposure to Mn for humans, with the average concentration of Mn in staple protein sources such as beef, poultry, and fish ranging from 0.10-3.99 mg kg^{-1}. Estimates for adequate daily consumption of Mn varies from 2-3 mg day^{-1} for adults (WHO, 2011). Therefore, according to the average Mn content found in fish muscles and the adequate daily consumption of Mn, the daily threshold consumption of *C. spixii* and *G. genidens* for an adult would be 2.5 kg and 5 kg, respectively, which may pose a real risk to the local population over the long-term due to presence of other sources of Mn exposure, such as drinking water, dust, fruit, vegetables, and dairy (Jolly et al., 2013; O'Neal and Zheng, 2015).

High concentrations of dissolved Mn measured in 2017 resulting from reducing conditions in the estuary is likely to have caused Mn accumulation in the tissues of the studied fishes (Arndt et al., 2014; Gabriel et al., 2020b; Pinsino et al., 2012). Our results from fish muscle and liver analyses show that Mn content in local fish species selected for this study are higher than Mn concentrations measured in other economically important fish species collected from areas that have also reported high concentrations of dissolved Mn (Table 2).

Our findings suggest that fish living in the Rio Doce estuary may pose a chronic health risk for humans due to the elevated levels of tissue-bound Mn.

Table 2 – Mean values of Fe and Mn in liver and muscle for *Cathoropus spixii* and *Genidens genidens* collected 2017 from the Rio Doce estuary and for different commercial fish species worldwide.

Species	Total Fe		Total Mn		Reference
	Liver	Muscle	Liver	Muscle	
	mg kg^{-1}				
Cathoropus spixii	*830 ± 638*	*26.75 ± 26.35*	*3.2 ± 1.78*	*1.0 ± 1.0*	*This study*
Genidens genidens	*1,541 ± 1,725*	*17.36 ± 11.4*	*2.1 ± 1.9*	*0.5 ± 0.2*	*This study*
Silurus triostegus	35.3 ± 6.6	n.d	n.d	n.d	Karadede et al. (2004)
Lethrinus lentjan	n.d	n.d	1.4 ± 0.2	0.1 ± 0.0	Al-Yousuf et al. (2000)
Genidens barbus	181 ± 100	3.87 ± 0.82	n.d	n.d	Avigliano et al. (2019)
Chiloscyllium plagiosum	n.d	n.d	0.2 ± 0.1	0.1 ± 0.0	Cornish et al. (2007)
Mullus barbatus	161.00 ± 25.30	29.20 ± 7.96	0.9 ± 0.2	0.4 ± 0.1	Tepe et al. (2008)
Merlangius merlangus	49.90 ± 7.16	21.90 ± 3.26	1.6 ± 0.2	0.4 ± 0.0	Tepe et al. (2008)
Silurus glanis	54.48 ± 17.59	10.17 ± 4.66	1.1 ± 1.4	0.5 ± 0.3	Andreji and Stráňai, (2007)

n.d: not determined

It is likely that the continued release of Mn from the estuarine soils will lead to Mn accumulation in other species of fish (Rather et al., 2019), crabs (Zhang et al., 2019), plants (Intawongse and Dean, 2006), and oysters (Silva et al., 2003), all of which are likely important food sources for the local population. The risks of Mn within the food chain are often overlooked in estuarine ecosystems because information on the toxic effect of Mn in aquatic organisms from these ecosystems is poorly studied despite recent studies that have suggested Mn induces oxidative stress, damage to tissues, inflammation and neurodegeneration in fish

and crabs (Barrio-Parra et al., 2018; Vieira et al., 2012). Thus, this unnoticed toxicity of Mn increases the risk of bioaccumulation for the local population.

Moreover, a constant uptake of Mn trough food with high Mn concentrations a long-term may expose to local population to adverse human health effects promoted by high Mn accumulation as neurodegenerative disorder (Levy and Nassetta, 2003), cardiovascular toxicities (Jiang and Zheng, 2005), and liver damage (O'Neal and Zheng, 2015). In this sense, additional in vitro bio accessibility tests may be beneficial to provide toxicological issues that were not reported so far (Luo et al., 2012).

The continued downstream transport of the mine tailings accumulated along the Rio Doce basin will serve as a long-term source of Mn and other trace metals, and potentially maintain the continued bioaccumulation risks of Mn into the estuary. Therefore, chronic Mn contamination is expected to persist along with other trace metals, as a result of biogeochemical soil conditions that favor seasonal Fe and Mn oxide reduction, and the absence of other mineral fractions that can retain and immobilize Mn (except for poorly crystallinity Fe oxyhydroxides which exert ephemeral control; Fig. 11).

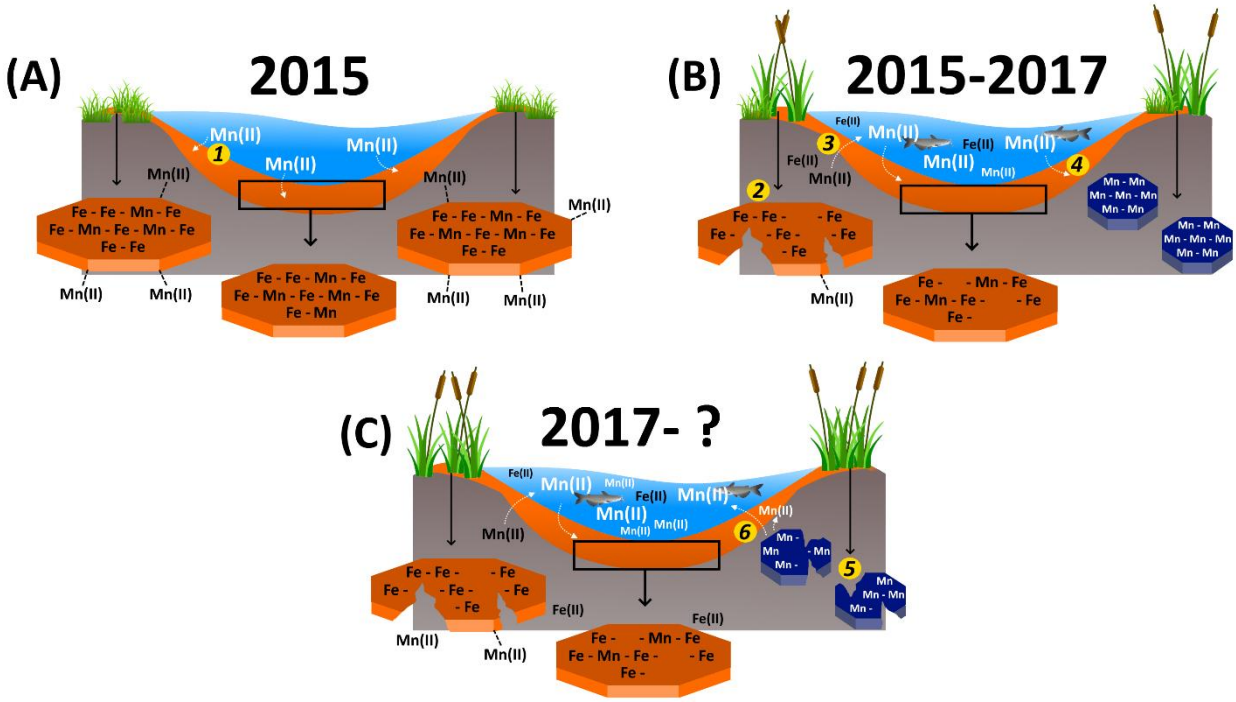

Fig. 11. Schematic summary of the sequence of processes (order provided in yellow circles) leading to Fe and Mn mobilization in the Doce River estuary. The deposited mine tailings in 2015 from the Fundão dam rupture (Samarco mining company) led to an Fe oxyhydroxide and Mn enrichment in the estuary. Initially, Mn that arrived was predominantly immobilized on Fe oxyhydroxides (1). Between 2015 to 2017, plant growth promoted organic matter input to estuarine soils which stimulated the reduction of Fe oxyhydroxides (2) and subsequent release of dissolved Fe and Mn to estuarine waters, exposing fish and other wildlife to high concentrations of the metals (3). Redox oscillations caused by seasonal changes in precipitation and water levels, tidal flooding, plant activity, and fauna, has favored precipitation of poorly crystalline Fe oxyhydroxides and poorly crystalline Mn oxides (4). Mn oxides are easily reducible (5) which can contribute to an increase of Mn in estuarine water (6). Poorly crystalline Fe oxyhydroxides are also susceptible to reduction limiting their role in Mn retention in the future.

5.5. Conclusions

The Fe-rich mine tailings deposited from the Samarco disaster in the Rio Doce estuarine soils largely increased Mn concentrations in soil, water, and fish. The Fe minerals exert a temporary control on Mn bioavailability because crystalline Fe oxyhydroxides are gradually solubilized and replaced by poorly crystalline Fe oxides which can be easily reduced. Although the Mn released from Fe minerals may be reoxidized into poorly crystalline Mn oxides over time, the redox conditions in the Rio Doce estuary are highly conducive to reductive dissolution of Mn^{III} and Mn^{IV} containing poorly crystalline oxides, such as

phyllomanganate and tectomanganates, which then ultimately leads to the continued increase in dissolved Mn.

Although Mn is considered an important micronutrient for all flora and fauna, the concentration of Mn found in the pore waters of the impacted estuary drastically exceeds the concentrations necessary for biological function leading to chronic Mn exposure. In this study, we found elevated Mn concentrations in liver and muscle tissues of multiple fish species that are regularly consumed by the local population. This discovery demonstrates that Mn sourced from the mine tailings can ultimately be impacting human health through long-term ecosystem contamination. Moreover, other animals and plants that are also consumed by the local population may accumulate Mn, worsening the risk to human health in the area.

Acknowledgments

This work was funded by grants to AFB and TOF from Fundação de Amparo do Espirito Santo (FAPES/CNPq/CAPES Rio Doce 77683544/2017), Coordenação de Aperfeiçoamento de Pessoal de Nível Superior CAPES - Finance Code 001 and CNPq (grant numbers, AFB: 301161/2017-8, TOF: 305996/2018-5; GNN: 409593/2018-4). The authors are grateful for the financial support provided by São Paulo Research Foundation (FAPESP, HMQ grant number 2018/04259-2 and 2019/17413-2; DB grant number 2019/02855-0; TOF grant numbers 2019/19987-6 and 2018/08408-2). Xunta de Galicia-Consellería de Educación e Ordeanción Universitaria de Galicia (Consolidation of competitive groups of investigation; GRC GI 1574) and CRETUS strategic group (AGRUP2015/02). Fundação Carlos Chagas Filho de Amparo à Pesquisa do Estado do Rio de Janeiro (GNN, JCNE Grant E-26/202.757/2019). Use of the Stanford Synchrotron Radiation Lightsource, SLAC National Accelerator Laboratory, is supported by the U.S. Department of Energy, Office of Science, Office of Basic Energy Sciences under Contract No. DE-AC02-76SF00515. The SSRL Structural Molecular Biology Program is supported by the DOE Office of Biological and Environmental Research, and by the National Institutes of Health, National Institute of General Medical Sciences (P41GM103393). MJA was supported by a fellowship from the National Institute of Health T32 Training Grant (T32 ES018827) and SCY was supported by USDA NIFA Hatch Project CA-R-ENS-5151-H and Fulbright Award awarded by the J. William Fulbright Commission.

References

Al-Yousuf, M.., El-Shahawi, M.., Al-Ghais, S.., 2000. Trace metals in liver, skin and muscle of Lethrinus lentjan fish species in relation to body length and sex. Sci. Total Environ. 256, 87–94. https://doi.org/10.1016/S0048-9697(99)00363-0

Alvares, C.A., Stape, J.L., Sentelhas, P.C., de Moraes Gonçalves, J.L., Sparovek, G., 2013. Köppen's climate classification map for Brazil. Meteorol. Zeitschrift 22, 711–728. https://doi.org/10.1127/0941-2948/2013/0507

ANA, A.N. de Á., 2020. Rio Doce - Sala de Situação [WWW Document]. Sala Situação da Agência Nac. Águas. URL https://www.ana.gov.br/sala-de-situacao/rio-doce/rio-doce-saiba-mais# (accessed 7.3.20).

Andreji, J., Stráňai, I., 2007. A contamination of tissues from fish originated from the lower part of Nitra river with some metals (Fe, Mn, Zn, Pb, Cu, Co, Ni, Cr, Cd). Slovak J. Anim. Sci. 40, 146–156.

Arndt, A., Borella, M.I., Espósito, B.P., 2014. Toxicity of manganese metallodrugs toward Danio rerio. Chemosphere 96, 46–50. https://doi.org/10.1016/j.chemosphere.2013.07.014

Avigliano, E., Maichak de Carvalho, B., Invernizzi, R., Olmedo, M., Jasan, R., Volpedo, A. V., 2019. Arsenic, selenium, and metals in a commercial and vulnerable fish from southwestern Atlantic estuaries: distribution in water and tissues and public health risk assessment. Environ. Sci. Pollut. Res. 26, 7994–8006. https://doi.org/10.1007/s11356-019-04258-3

Azevedo, J.S., Fernandez, W.S., Farias, L.A., Fávaro, D.T.I., Braga, E.S., 2009. Use of Cathorops spixii as bioindicator of pollution of trace metals in the Santos Bay, Brazil. Ecotoxicology 18, 577–586. https://doi.org/10.1007/s10646-009-0315-4

Badarudeen, A., Damodaran, K.T., Sajan, K., Padmalal, D., 1996. Texture and geochemistry of the sediments of a tropical mangrove ecosystem, southwest coast of India. Environ. Geol. 27, 164–169. https://doi.org/10.1007/BF00770428

Baly, D.L., 1989. Manganese in Metabolism and Enzyme Function. J. Nutr. https://doi.org/10.1093/jn/119.2.327

Barrio-Parra, F., Elío, J., De Miguel, E., García-González, J.E., Izquierdo, M., Álvarez, R., 2018. Environmental risk assessment of cobalt and manganese from industrial sources in an estuarine system. Environ. Geochem. Health 40, 737–748. https://doi.org/10.1007/s10653-017-0020-9

Bernardino, A.F., Netto, S.A., Pagliosa, P.R., Barros, F., Christofoletti, R.A., Rosa Filho, J.S., Colling, A., Lana, P.C., 2015. Predicting ecological changes on benthic estuarine assemblages through decadal climate trends along Brazilian Marine Ecoregions. Estuar. Coast. Shelf Sci. 166, 74–82. https://doi.org/10.1016/j.ecss.2015.05.021

Bernardino, A.F., Pais, F.S., Oliveira, L.S., Gabriel, F.A., Ferreira, T.O., Queiroz, H.M., Mazzuco, A.C.A., 2019. Chronic trace metals effects of mine tailings on estuarine assemblages revealed by environmental DNA. PeerJ 7, e8042. https://doi.org/10.7717/peerj.8042

Bianchi, T.S., 2007. Biogeochemistry of Estuaries, Eos, Transactions American Geophysical Union. Oxford University Press, Oxford; New York. https://doi.org/10.1029/2007EO520011

Borch, T., Kretzschmar, R., Skappler, A., Van Cappellen, P., Ginder-Vogel, M., Voegelin, A., Campbell, K., 2010. Biogeochemical redox processes and their impact on contaminant dynamics. Environ. Sci. Technol. 44, 15–23. https://doi.org/10.1021/es9026248

Broadley, M., Brown, P., Cakmak, I., Rengel, Z., Zhao, F., 2012. Function of Nutrients, in: Marschner's Mineral Nutrition of Higher Plants. Elsevier, pp. 191–248. https://doi.org/10.1016/B978-0-12-384905-2.00007-8

Brookins, D.G., 1988. Eh-pH diagrams for geochemistry, 1st ed. Springer-Verlag Berlin Heidelberg. https://doi.org/10.1007/978-3-642-73093-1

Burdige, D.J., 1993. The biogeochemistry of manganese and iron reduction in marine sediments. Earth-Science Rev. 35, 249–284. https://doi.org/10.1016/0012-8252(93)90040-E

Canfield, D.E., Erik Kristensen, Bo Thamdrup, 2005. The Iron and Manganese Cycles, in: Aquatic Geomicrobiology. pp. 269–312. https://doi.org/10.1016/S0065-2881(05)48008-6

Canfield, D.E., Thamdrup, B., Hansen, J.W., 1993. The anaerobic degradation of organic matter in Danish coastal sediments: Iron reduction, manganese reduction, and sulfate reduction. Geochim. Cosmochim. Acta 57, 3867–3883. https://doi.org/10.1016/0016-7037(93)90340-3

Carmo, Flávio Fonseca do, Kamino, L.H.Y., Junior, R.T., Campos, I.C. de, Carmo, Felipe Fonseca do, Silvino, G., Castro, K.J. da S.X. de, Mauro, M.L., Rodrigues, N.U.A., Miranda, M.P. de S., Pinto, C.E.F., 2017. Fundão tailings dam failures: the environment tragedy of the largest technological disaster of Brazilian mining in global context. Perspect. Ecol. Conserv. 15, 145–151. https://doi.org/10.1016/j.pecon.2017.06.002

Chaudry, M.A., Zwolsman, J.J.G., 2008. Seasonal Dynamics of Dissolved Trace Metals in the Scheldt Estuary: Relationship with Redox Conditions and Phytoplankton Activity. Estuaries and Coasts 31, 430–443. https://doi.org/10.1007/s12237-007-9030-7

CONAMA, 2009. Resolução Nº 420, de 28 de Dezembro de 2009, in: Brazilian National Environment Council (Ed.), Diário Oficial Da União. Ministério do Meio Ambiente, Brasília, pp. 81–84.

CONAMA, 2005. Brazilian water quality guidelines. Resolution n. 357 - 2005.

Cornell, R.M., Schwertmann, U., 2003. The Iron Oxides: Structure, Reactions, Occurences and Uses, WILEY-VCH. https://doi.org/10.1002/3527602097.ch1

Cornish, A.S., Ng, W.C., Ho, V.C.M., Wong, H.L., Lam, J.C.W., Lam, P.K.S., Leung, K.M.Y., 2007. Trace metals and organochlorines in the bamboo shark Chiloscyllium plagiosum from the southern waters of Hong Kong, China. Sci. Total Environ. 376, 335–345. https://doi.org/10.1016/j.scitotenv.2007.01.070

Coughlin, B.R., Stone, A.T., 1995. Nonreversible Adsorption of Divalent Metal Ions (MnII, CoII, NiII, CuII, and PbII) onto Goethite: Effects of Acidification, FeII Addition, and Picolinic Acid Addition. Environ. Sci. Technol. 29, 2445–2455. https://doi.org/10.1021/es00009a042

Cummings, D.E., March, A.W., Bostick, B., Spring, S., Caccavo, F., Fendorf, S., Rosenzweig, R F, Rosenzweig, R. Frank, 2000. Evidence for microbial Fe(III) reduction in anoxic, mining-impacted lake sediments (Lake Coeur d'Alene, Idaho). Appl. Environ. Microbiol. 66, 154–62.

Du Laing, G., Meers, E., Dewispelaere, M., Rinklebe, J., Vandecasteele, B., Verloo, M.G., Tack, F.M.G., 2009a. Effect of Water Table Level on Metal Mobility at Different Depths in Wetland Soils of the Scheldt Estuary (Belgium). Water. Air. Soil Pollut. 202, 353–367. https://doi.org/10.1007/s11270-009-9982-2

Du Laing, G., Rinklebe, J., Vandecasteele, B., Meers, E., Tack, F.M.G., 2009b. Trace metal behaviour in estuarine and riverine floodplain soils and sediments: A review. Sci. Total Environ. 407, 3972–3985. https://doi.org/10.1016/j.scitotenv.2008.07.025

Duckworth, O.W., Bargar, J.R., Sposito, G., 2009. Coupled biogeochemical cycling of iron and manganese as mediated by microbial siderophores. BioMetals 22, 605–613. https://doi.org/10.1007/s10534-009-9220-9

El-Jaoual, T., Cox, D.A., 1998. Manganese toxicity in plants. J. Plant Nutr. 21, 353–386. https://doi.org/10.1080/01904169809365409

Fernandes, G.W., Goulart, F.F., Ranieri, B.D., Coelho, M.S., Dales, K., Boesche, N., Bustamante, M., Carvalho, F.A., Carvalho, D.C., Dirzo, R., Fernandes, S., Galetti, P.M., Millan, V.E.G., Mielke, C., Ramirez, J.L., Neves, A., Rogass, C., Ribeiro, S.P., Scariot, A., Soares-Filho, B., 2016. Deep into the mud: ecological and socio-economic impacts of the dam breach in Mariana, Brazil. Nat. e Conserv. 14, 35–45. https://doi.org/10.1016/j.ncon.2016.10.003

Finkelstein, M.M., Jerrett, M., 2007. A study of the relationships between Parkinson's disease and markers of traffic-derived and environmental manganese air pollution in two Canadian cities. Environ. Res. 104, 420–432. https://doi.org/10.1016/j.envres.2007.03.002

Fischel, J.S., Fischel, M.H., Sparks, D.L., 2015. Advances in Understanding Reactivity of Manganese Oxides with Arsenic and Chromium in Environmental Systems, in: ACS Symposium Series. Oxford University Press, Washington, DC, pp. 1–27. https://doi.org/10.1021/bk-2015-1197.ch001

Fitsanakis, V.A., Zhang, N., Garcia, S., Aschner, M., 2010. Manganese (Mn) and Iron (Fe): Interdependency of Transport and Regulation. Neurotox. Res. 18, 124–131. https://doi.org/10.1007/s12640-009-9130-1

Fortin, D., Leppard, G.G., Tessier, A., 1993. Characteristics of lacustrine diagenetic iron oxyhydroxides. Geochim. Cosmochim. Acta 57, 4391–4404. https://doi.org/10.1016/0016-7037(93)90490-N

Frohne, T., Rinklebe, J., Diaz-Bone, R.A., Du Laing, G., 2011. Controlled variation of redox conditions in a floodplain soil: Impact on metal mobilization and biomethylation of arsenic and antimony. Geoderma 160, 414–424. https://doi.org/10.1016/j.geoderma.2010.10.012

Gabriel, F.A., Silva, A.G., Queiroz, H.M., Ferreira, T.O., Hauser-Davis, R.A., Bernardino, A.F., 2020a. Ecological Risks of Metal and Metalloid Contamination in the Rio Doce Estuary. Integr. Environ. Assess. Manag. 16, 655–660. https://doi.org/10.1002/ieam.4250

Gabriel, F.A., Hauser-Davis, R.A., Soares, L., Mazzuco, A.C.A., Rocha, R.C.C., Saint Pierre, T.D., Saggioro, E., Correia, F.V., Ferreira, T.O., Bernardino, A.F., 2020b. Contamination and oxidative stress biomarkers in estuarine fish following a mine tailing disaster. PeerJ 8, e10266. https://doi.org/10.7717/peerj.10266

Gomes, L.E. de O., Correa, L.B., Sá, F., Neto, R.R., Bernardino, A.F., 2017. The impacts of the Samarco mine tailing spill on the Rio Doce estuary, Eastern Brazil. Mar. Pollut. Bull. 120, 28–36. https://doi.org/10.1016/j.marpolbul.2017.04.056

Graham, R.D., Hannam, R.J., Uren, N.C., 1988. Manganese in Soils and Plants, Manganese in Soils and Plants. Springer Netherlands, Dordrecht. https://doi.org/10.1007/978-94-009-2817-6

Gusso-Choueri, P.K., Araújo, G.S. de, Cruz, A.C.F., Stremel, T.R. de O., Campos, S.X. de, Abessa, D.M. de S., Oliveira Ribeiro, C.A. de, Choueri, R.B., 2018. Metals and arsenic in fish from a Ramsar site under past and present human pressures: Consumption risk factors to the local population. Sci. Total Environ. 628–629, 621–630. https://doi.org/10.1016/j.scitotenv.2018.02.005

Hadlich, H.L., Venturini, N., Martins, C.C., Hatje, V., Tinelli, P., Gomes, L.E. de O., Bernardino, A.F., 2018. Multiple biogeochemical indicators of environmental quality in tropical estuaries reveal contrasting conservation opportunities. Ecol. Indic. 95, 21–31. https://doi.org/10.1016/j.ecolind.2018.07.027

Hakanson, L., 1980. An ecological risk index for aquatic pollution control.a sedimentological approach. Water Res. https://doi.org/10.1016/0043-1354(80)90143-8

Harford, A.J., Mooney, T.J., Trenfield, M.A., van Dam, R.A., 2015. Manganese toxicity to tropical freshwater species in low hardness water. Environ. Toxicol. Chem. 34, 2856–2863. https://doi.org/10.1002/etc.3135

Hauser-Davis, R.A., Bastos, F.F., Tuton, B., Chávez Rocha, R., Pierre, T. Saint, Ziolli, R.L., Arruda, M.A.Z., 2014. Bile and liver metallothionein behavior in copper-exposed fish. J. Trace Elem. Med. Biol. 28, 70–74. https://doi.org/10.1016/j.jtemb.2013.09.003

Hu, P., Jiang, Z., Liu, Q., Heslop, D., Roberts, A.P., Torrent, J., Barrón, V., 2016. Estimating the concentration of aluminum-substituted hematite and goethite using diffuse reflectance spectrometry and rock magnetism: Feasibility and limitations. J. Geophys. Res. Solid Earth 121, 4180–4194. https://doi.org/10.1002/2015JB012635

Huang, Z., Tang, Y., Zhang, K., Chen, Y., Wang, Y., Kong, L., You, T., Gu, Z., 2016. Environmental risk assessment of manganese and its associated heavy metals in a stream impacted by manganese mining in South China. Hum. Ecol. Risk Assess. An Int. J. 22, 1341–1358. https://doi.org/10.1080/10807039.2016.1169915

Huerta-Diaz, M.A., Morse, J.W., 1990. A quantitative method for determination of trace metal concentrations in sedimentary pyrite. Mar. Chem. 29, 119–144. https://doi.org/10.1016/0304-4203(90)90009-2

Intawongse, M., Dean, J.R., 2006. Uptake of heavy metals by vegetable plants grown on contaminated soil and their bioavailability in the human gastrointestinal tract. Food Addit. Contam. 23, 36–48. https://doi.org/10.1080/02652030500387554

Jay, D.A., Orton, P.M., Chisholm, T., Wilson, D.J., Fain, A.M.V., 2007. Particle trapping in stratified estuaries: Consequences of mass conservation. Estuaries and Coasts 30, 1095–1105. https://doi.org/10.1007/BF02841399

Ji, J., Balsam, W., Chen, J.U., Liu, L., 2002. Rapid and Quantitative Measurement of Hematite and Goethite in the Chinese Loess-paleosol Sequence by Diffuse Reflectance Spectroscopy. Clays Clay Miner. 50, 208–216. https://doi.org/10.1346/000986002760832801

Jiang, Y., Zheng, W., 2005. Cardiovascular Toxicities Upon Manganese Exposure. Cardiovasc. Toxicol. 5, 345–354. https://doi.org/10.1385/CT:5:4:345

Johnston, S.G., Keene, A.F., Bush, R.T., Burton, E.D., Sullivan, L.A., Isaacson, L., McElnea, A.E., Ahern, C.R., Smith, C.D., Powell, B., 2011. Iron geochemical zonation in a tidally inundated acid sulfate soil wetland. Chem. Geol. 280, 257–270. https://doi.org/10.1016/j.chemgeo.2010.11.014

Jolly, Y.N., Islam, A., Akbar, S., 2013. Transfer of metals from soil to vegetables and possible health risk assessment. Springerplus 2, 385. https://doi.org/10.1186/2193-1801-2-385

Karadede, H., Oymak, S.A., Ünlü, E., 2004. Heavy metals in mullet, Liza abu, and catfish, Silurus triostegus, from the Atatürk Dam Lake (Euphrates), Turkey. Environ. Int. 30, 183–188. https://doi.org/10.1016/S0160-4120(03)00169-7

Kennish, M.J., 2002. Environmental threats and environmental future of estuaries. Environ. Conserv. 29, 78–107. https://doi.org/10.1017/S0376892902000061

Kristensen, E., Ahmed, S.I., Devol, A.H., 1995. Aerobic and anaerobic decomposition of organic matter in marine sediment: Which is fastest? Limnol. Oceanogr. 40, 1430–1437. https://doi.org/10.4319/lo.1995.40.8.1430

Lee, J.-H., Kennedy, D.W., Dohnalkova, A., Moore, D.A., Nachimuthu, P., Reed, S.B., Fredrickson, J.K., 2011. Manganese sulfide formation via concomitant microbial manganese oxide and thiosulfate reduction. Environ. Microbiol. 13, 3275–3288. https://doi.org/10.1111/j.1462-2920.2011.02587.x

Levy, B.S., Nassetta, W.J., 2003. Neurologic Effects of Manganese in Humans: A Review. Int. J. Occup. Environ. Health 9, 153–163. https://doi.org/10.1179/oeh.2003.9.2.153

Lewis, B.L., Landing, W.M., 1991. The biogeochemistry of manganese and iron in the Black Sea. Deep Sea Res. Part A. Oceanogr. Res. Pap. 38, S773–S803. https://doi.org/10.1016/S0198-0149(10)80009-3

Li, M.S., Luo, Y.P., Su, Z.Y., 2007. Heavy metal concentrations in soils and plant accumulation in a restored manganese mineland in Guangxi, South China. Environ. Pollut. 147, 168–175. https://doi.org/10.1016/j.envpol.2006.08.006

Lovley, D.R., Holmes, D.E., Nevin, K.P., 2004. Dissimilatory Fe(III) and Mn(IV) Reduction, in: Advances in Microbial Physiology. pp. 219–286. https://doi.org/10.1016/S0065-2911(04)49005-5

Luo, X.S., Ding, J., Xu, B., Wang, Y.J., Li, H.B., Yu, S., 2012. Incorporating bioaccessibility into human health risk assessments of heavy metals in urban park soils. Sci. Total Environ. 424, 88–96. https://doi.org/10.1016/j.scitotenv.2012.02.053

Manceau, A., Marcus, M.A., Grangeon, S., 2012. Determination of Mn valence states in mixed-valent manganates by XANES spectroscopy. Am. Mineral. 97, 816–827. https://doi.org/10.2138/am.2012.3903

Manceau, A., Marcus, M.A., Tamura, N., 2002. Quantitative Speciation of Heavy Metals in Soils and Sediments by Synchrotron X-ray Techniques. Rev. Mineral. Geochemistry 49, 341–428. https://doi.org/10.2138/gsrmg.49.1.341

Marcus, M.A., Manceau, A., Kersten, M., 2004. Mn, Fe, Zn and As speciation in a fast-growing ferromanganese marine nodule. Geochim. Cosmochim. Acta 68, 3125–3136. https://doi.org/10.1016/j.gca.2004.01.015

Marín-Muñiz, J.L., Hernández, M.E., Moreno-Casasola, P., 2014. Comparing soil carbon sequestration in coastal freshwater wetlands with various geomorphic features and plant communities in Veracruz, Mexico. Plant Soil 378, 189–203. https://doi.org/10.1007/s11104-013-2011-7

McKinley, K., McLellan, I., Gagné, F., Quinn, B., 2019. The toxicity of potentially toxic elements (Cu, Fe, Mn, Zn and Ni) to the cnidarian Hydra attenuata at environmentally relevant concentrations. Sci. Total Environ. 665, 848–854. https://doi.org/10.1016/j.scitotenv.2019.02.193

Mudd, S.M., D'Alpaos, A., Morris, J.T., 2010. How does vegetation affect sedimentation on tidal marshes? Investigating particle capture and hydrodynamic controls on biologically mediated sedimentation. J. Geophys. Res. Earth Surf. 115, 1–14. https://doi.org/10.1029/2009JF001566

Namgung, S., Guo, B., Sasaki, K., Lee, S.S., Lee, G., 2020. Macroscopic and microscopic behaviors of Mn(II) (ad)sorption to goethite with the effects of dissolved carbonates under anoxic conditions. Geochim. Cosmochim. Acta 277, 300–319. https://doi.org/10.1016/j.gca.2020.03.036

Nealson, K.H., Myers, C.R., 1992. Microbial reduction of manganese and iron: New approaches to carbon cycling. Appl. Environ. Microbiol. 58, 439–443.

Newville, M., 2013. Larch: An Analysis Package for XAFS and Related Spectroscopies. J. Phys. Conf. Ser. 430, 012007. https://doi.org/10.1088/1742-6596/430/1/012007

NOAA, 2008. Screening Quick Reference Tables. National Oceanic and Atmospheric Administration, Seattle, WA.

O'Neal, S.L., Zheng, W., 2015. Manganese Toxicity Upon Overexposure: a Decade in Review. Curr. Environ. Heal. Reports 2, 315–328. https://doi.org/10.1007/s40572-015-0056-x

Oldham, V.E., Siebecker, M.G., Jones, M.R., Mucci, A., Tebo, B.M., Luther, G.W., 2019. The Speciation and Mobility of Mn and Fe in Estuarine Sediments. Aquat. Geochemistry 25, 3–26. https://doi.org/10.1007/s10498-019-09351-0

Olsson, P.-E., Kling, P., Hogstrand, C., 1998. Mechanisms of heavy metal accumulation and toxicity in fish, in: Metal Metabolism in Aquatic Environments. https://doi.org/10.1007/978-1-4757-2761-6_10

Otero, X.L., Ferreira, T.O., Huerta-Díaz, M.A., Partiti, C.S.M., Souza, V., Vidal-Torrado, P., Macías, F., 2009. Geochemistry of iron and manganese in soils and sediments of a mangrove system, Island of Pai Matos (Cananeia — SP, Brazil). Geoderma 148, 318–335. https://doi.org/10.1016/j.geoderma.2008.10.016

Patrick, W.H., Jugsujinda, A., 1992. Sequential Reduction and Oxidation of Inorganic Nitrogen, Manganese, and Iron in Flooded Soil. Soil Sci. Soc. Am. J. 56, 1071. https://doi.org/10.2136/sssaj1992.03615995005600040011x

Pereira, A.A., Van Hattum, B., Brouwer, A., Van Bodegom, P.M., Rezende, C.E., Salomons, W., 2008. Effects of iron-ore mining and processing on metal bioavailability in a tropical coastal lagoon. J. Soils Sediments 8, 239–252. https://doi.org/10.1007/s11368-008-0017-1

Pinheiro, H.T., Joyeux, J.-C., 2007. Pescarias multi-específicas na região da foz do Rio Doce, ES, Brasil: características, problemas e opções para um futuro sustentável. Brazilian J. Aquat. Sci. Technol. 11, 15. https://doi.org/10.14210/bjast.v11n2.p15-23

Pinsino, A., Matranga, V., Roccheri, M.C., 2012. Manganese: A New Emerging Contaminant in the Environment, in: Environmental Contamination. InTech. https://doi.org/10.5772/31438

Postma, D., 1985. Concentration of Mn and separation from Fe in sediments—I. Kinetics and stoichiometry of the reaction between birnessite and dissolved Fe(II) at 10°C. Geochim. Cosmochim. Acta 49, 1023–1033. https://doi.org/10.1016/0016-7037(85)90316-3

Postma, D., Appelo, C.A.J., 2000. Reduction of Mn-oxides by ferrous iron in a flow system: column experiment and reactive transport modeling. Geochim. Cosmochim. Acta 64, 1237–1247. https://doi.org/10.1016/S0016-7037(99)00356-7

Queiroz, H.M., Ferreira, T.O., Barcellos, D., Nóbrega, G.N., Antelo, J., Otero, X.L., Bernardino, A.F., 2021. From sinks to sources: The role of Fe oxyhydroxide transformations on phosphorus dynamics in estuarine soils. J. Environ. Manage. 278, 111575. https://doi.org/10.1016/j.jenvman.2020.111575

Queiroz, H.M., Nóbrega, G.N., Ferreira, T.O., Almeida, L.S., Romero, T.B., Santaella, S.T., Bernardino, A.F., Otero, X.L., 2018. The Samarco mine tailing disaster: A possible time-bomb for heavy metals contamination? Sci. Total Environ. 637–638, 498–506. https://doi.org/10.1016/j.scitotenv.2018.04.370

Rather, M.Y., Tilwani, Y.M., Dey, A., 2019. Assessment of heavy metal contamination in two edible fish species Carassius carassius and Triplophysa kashmirensis of Dal Lake, Srinagar, Kashmir, India. Environ. Monit. Assess. 191. https://doi.org/10.1007/s10661-019-7382-7

Ravel, B., Newville, M., 2005. ATHENA , ARTEMIS , HEPHAESTUS : data analysis for X-ray absorption spectroscopy using IFEFFIT. J. Synchrotron Radiat. 12, 537–541. https://doi.org/10.1107/S0909049505012719

Reddy, K.R., DeLaune, R.D., 2008. Biogeochemistry of wetlands: science and applications, 1st ed. CRC Press.

Reimann, C., Filzmoser, P., Garrett, R.G., Dutter, R., 2008. Statistical Data Analysis Explained, Statistical Data Analysis Explained: Applied Environmental Statistics with R. John Wiley & Sons, Ltd, Chichester, UK, UK. https://doi.org/10.1002/9780470987605

Richard, E. da C., Estrada, G.C.D., Bechtold, J., Aguiar Duarte, H., Maioli, B.G., Freitas, A.H.A., Warner, K.E., Figueiredo, L.H.M., 2020. Water and Sediment Quality in the Coastal Zone Around the Mouth of Doce River After the Fundão Tailings Dam Failure. Integr. Environ. Assess. Manag. 16, 643–654. https://doi.org/10.1002/ieam.4309

Rodrigues, A.S. de L., Malafaia, G., Costa, A.T., Nalini Júnior, H.A., 2014. Iron ore mining promotes iron enrichment in sediments of the Gualaxo do Norte River basin, Minas Gerais State, Brazil. Environ. Earth Sci. 71, 4177–4186. https://doi.org/10.1007/s12665-013-2808-y

Sandilyan, S., Kathiresan, K., 2014. Decline of mangroves – A threat of heavy metal poisoning in Asia. Ocean Coast. Manag. 102, 161–168. https://doi.org/10.1016/j.ocecoaman.2014.09.025

Santelli, C.M., Webb, S.M., Dohnalkova, A.C., Hansel, C.M., 2011. Diversity of Mn oxides produced by Mn(II)-oxidizing fungi. Geochim. Cosmochim. Acta 75, 2762–2776. https://doi.org/10.1016/j.gca.2011.02.022

Scheinost, A.C., 1998. Use and Limitations of Second-Derivative Diffuse Reflectance Spectroscopy in the Visible to Near-Infrared Range to Identify and Quantify Fe Oxide Minerals in Soils. Clays Clay Miner. 46, 528–536. https://doi.org/10.1346/CCMN.1998.0460506

Scheinost, A.C., Stanjek, H., Schulze, D.G., Gasser, U., Sparks, D.L., 2001. Structural environment and oxidation state of Mn in goethite-groutite solid-solutions. Am. Mineral. 86, 139–146. https://doi.org/10.2138/am-2001-0115

Schwertmann, U., Taylor, R.M., 1989. Iron Oxides, in: Minerals in Soil Environments. pp. 379–438. https://doi.org/10.2136/sssabookser1.2ed.c8

Sigel, A., Sigel, H., 2000. Manganese and Its Role in Biological Processes, in: Metal Ions in Biological Systems. CRC Press, New York, NY, pp. 2969–2969. https://doi.org/10.1021/jm000216b

Silva, A.C., Cavalcante, L.C.D., Fabris, J.D., Júnior, R.F., Barral, U.M., Farnezi, M.M. de M., Viana, A.J.S., Ardisson, J.D., Fernandez-Outon, L.E., Lara, L.R.S., Stumpf, H.O., Barbosa, J.B.S., Silva, L.C. da, 2017. Características químicas, mineralógicas e físicas do material acumulado em terraços fluviais, originado do fluxo de lama proveniente do rompimento de barragem de rejeitos de mineração de ferro em Bento Rodrigues, Minas Gerais, Brasil. Rev. Espinhaço | UFVJM; Rev. Espinhaço #9.

Silva, C.A.R., Rainbow, P.S., Smith, B.D., 2003. Biomonitoring of trace metal contamination in mangrove-lined Brazilian coastal systems using the oyster Crassostrea rhizophorae: Comparative study of regions affected by oil, salt pond and shrimp farming activities. Hydrobiologia 501, 199–206. https://doi.org/10.1023/A:1026242417427

Singh, N., Singh, A., Das, D., Mohan, M.L., 2010. Redox Control of Prion and Disease Pathogenesis. Antioxid. Redox Signal. 12, 1271–1294. https://doi.org/10.1089/ars.2009.2628

Slobodian, L., Badoz, L., 2019. Tangled roots and changing tides: mangrove governance for conservation and sustainable use, 1st ed. WWF Germany, Berlin, Germany and IUCN, Gland, Switzerland, Berlin, Germany; Gland, Switzerland.

Søndergaard, M., 2009. Redox Potential, in: Encyclopedia of Inland Waters. Elsevier, pp. 852–859. https://doi.org/10.1016/B978-012370626-3.00115-0

Squadrone, S., Brizio, P., Stella, C., Prearo, M., Pastorino, P., Serracca, L., Ercolini, C., Abete, M.C., 2016. Presence of trace metals in aquaculture marine ecosystems of the northwestern Mediterranean Sea (Italy). Environ. Pollut. 215, 77–83. https://doi.org/10.1016/j.envpol.2016.04.096

Stumm, W., Morgan, J.J., 1996. Aquatic Chemistry: Chemical Equilibria and Rates in Natural Waters, 3rd ed. John Wiley & Sons, Inc., Danvers.

Summer, K., Reichelt-Brushett, A., Howe, P., 2019. Toxicity of manganese to various life stages of selected marine cnidarian species. Ecotoxicol. Environ. Saf. 167, 83–94. https://doi.org/10.1016/j.ecoenv.2018.09.116

Sundby, B., Vale, C., Caetano, M., Luther III, G.W., 2003. Redox Chemistry in the Root Zone of a Salt Marsh Sediment in the Tagus Estuary, Portugal. Aquat. Geochemistry 9, 257–271. https://doi.org/10.1023/B:AQUA.0000022957.42522.9a

Tebo, B.M., Bargar, J.R., Clement, B.G., Dick, G.J., Murray, K.J., Parker, D., Verity, R., Webb, S.M., 2004. Biogenic manganese oxides: Properties and mechanisms of formation. Annu. Rev. Earth Planet. Sci. 32, 287–328. https://doi.org/10.1146/annurev.earth.32.101802.120213

Tepe, Y., Türkmen, M., Türkmen, A., 2008. Assessment of heavy metals in two commercial fish species of four Turkish seas. Environ. Monit. Assess. 146, 277–284. https://doi.org/10.1007/s10661-007-0079-3

Tessier, A., Campbell, P.G.C., Bisson, M., 1979. Sequential extraction procedure for the speciation of particulate trace metals. Anal. Chem. 51, 844–851. https://doi.org/10.1021/ac50043a017

Thamdrup, B., Fossing, H., Jørgensen, B.B., 1994. Manganese, iron and sulfur cycling in a coastal marine sediment, Aarhus bay, Denmark. Geochim. Cosmochim. Acta 58, 5115–5129. https://doi.org/10.1016/0016-7037(94)90298-4

Toner, B., Manceau, A., Webb, S.M., Sposito, G., 2006. Zinc sorption to biogenic hexagonal-birnessite particles within a hydrated bacterial biofilm. Geochim. Cosmochim. Acta 70, 27–43. https://doi.org/10.1016/j.gca.2005.08.029

Ugwu, I.M., Igbokwe, O.A., 2019. Sorption of Heavy Metals on Clay Minerals and Oxides: A Review, in: Advanced Sorption Process Applications. IntechOpen, pp. 1–23. https://doi.org/10.5772/intechopen.80989

USEPA, 1996. Method 3052, Microwave assisted acid digestion of siliceous and organically based matrices. Usepa 1–20. https://doi.org/10.1017/CBO9781107415324.004

Van Cappellen, P., Viollier, E., Roychoudhruy, A., Clark, L., Ingall, E., Lowe, K., Dichristina, T., 1998. Biogeochemical cycles of manganese and iron at the oxic-anoxic transoition of a stratified marine basin. Env Sci Technol 32, 2931–2939.

Vieira, M.C., Torronteras, R., Córdoba, F., Canalejo, A., 2012. Acute toxicity of manganese in goldfish Carassius auratus is associated with oxidative stress and organ specific antioxidant responses. Ecotoxicol. Environ. Saf. 78, 212–217. https://doi.org/10.1016/j.ecoenv.2011.11.015

Webb, S.M., 2005. Structural characterization of biogenic Mn oxides produced in seawater by the marine bacillus sp. strain SG-1. Am. Mineral. 90, 1342–1357. https://doi.org/10.2138/am.2005.1669

Weber, P., Behr, E.R., Knorr, C.D.L., Vendruscolo, D.S., Flores, E.M.M., Dressler, V.L., Baldisserotto, B., 2013. Metals in the water, sediment, and tissues of two fish species from different trophic levels in a subtropical Brazilian river. Microchem. J. 106, 61–66. https://doi.org/10.1016/j.microc.2012.05.004

WHO, 2011. Manganese in Drinking-water. Manganese Drink. Backgr. Doc. Dev. WHO Guidel. Drink. water Qual.

Winkler, P., Kaiser, K., Thompson, A., Kalbitz, K., Fiedler, S., Jahn, R., 2018. Contrasting evolution of iron phase composition in soils exposed to redox fluctuations. Geochim. Cosmochim. Acta. https://doi.org/10.1016/j.gca.2018.05.019

Xia, D., Yi, X., Lu, Y., Huang, W., Xie, Y., Ye, H., Dang, Z., Tao, X., Li, L., Lu, G., 2019. Dissimilatory iron and sulfate reduction by native microbial communities using lactate and citrate as carbon sources and electron donors. Ecotoxicol. Environ. Saf. 174, 524–531. https://doi.org/10.1016/j.ecoenv.2019.03.005

Yu, K., Böhme, F., Rinklebe, J., Neue, H.-U., DeLaune, R.D., 2007. Major Biogeochemical Processes in Soils-A Microcosm Incubation from Reducing to Oxidizing Conditions. Soil Sci. Soc. Am. J. 71, 1406–1417. https://doi.org/10.2136/sssaj2006.0155

Zachara, J.M., Cowan, C.E., Resch, C.T., 1991. Sorption of divalent metals on calcite. Geochim. Cosmochim. Acta 55, 1549–1562. https://doi.org/10.1016/0016-7037(91)90127-Q

Zhang, Z., Fang, Z., Li, J., Sui, T., Lin, L., Xu, X., 2019. Copper, zinc, manganese, cadmium and chromium in crabs from the mangrove wetlands in Qi'ao Island, South China: Levels, bioaccumulation and dietary exposure. Watershed Ecol. Environ. 1, 26–32. https://doi.org/10.1016/j.wsee.2019.09.001

Zhu, M., Ginder-Vogel, M., Parikh, S.J., Feng, X.-H., Sparks, D.L., 2010. Cation Effects on the Layer Structure of Biogenic Mn-Oxides. Environ. Sci. Technol. 44, 4465–4471. https://doi.org/10.1021/es1009955

Zhu, S., Zhang, P., Liang, Y., Wang, M., Xiong, J., Tan, W., 2020. Effects of aluminum substitution on the surface charge of colloidal goethite particles: experiments and MUSIC modeling. Environ. Sci. Pollut. Res. https://doi.org/10.1007/s11356-020-07793-6

Supplementary material

Calibration, normalization and merging of replicate scans was done using the Demeter package (Ravel and Newville, 2005), version 9.26 with Larch running as a backend (Newville, 2013), and using a PC running Windows 10. The average Mn valence (AMV) of the Mn in each sample was obtained through linear combination fitting analysis of the Mn X-ray absorption near edge structure (XANES) spectra was done in Athena (Ravel and Newville, 2005) using the Combo method of Manceau et al. (2012). In all cases, the 17 reference spectra from Manceau et al. (2012) with the addition of two Mn^{II} standards (Mn-Oxalate and $MnCl_2$) from the XAS standards repository in Demeter: (https://github.com/bruceravel/demeter/tree/master/lib/Demeter/share/standards/data) were used to perform unconstrained linear fits. Any reference yielding a negative loading was progressively removed on a per-sample basis and re-added to the reference list before fitting the next sample.

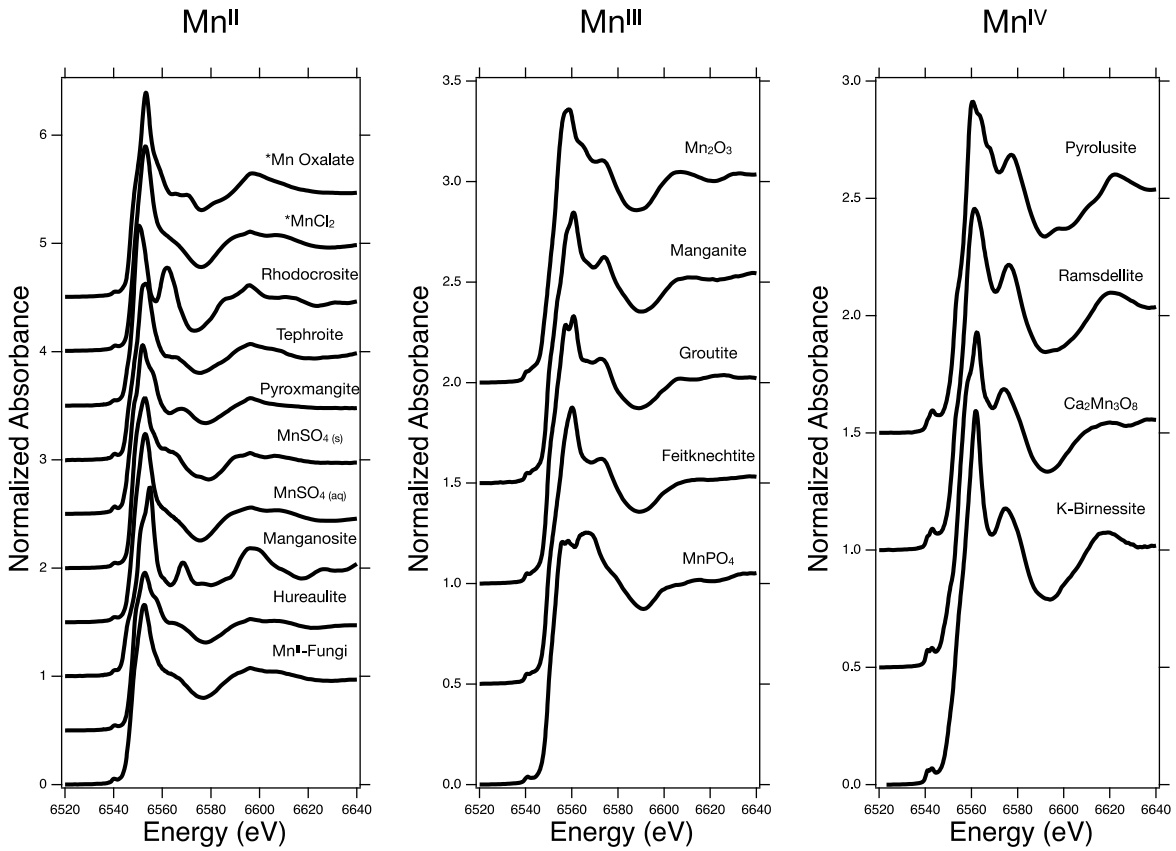

Fig. S1. Manganese standards used in the linear combination fitting analysis of the Mn K-edge XANES. Standards obtained from Manceau et al. (2012) and from the Demeter XAS standard repository. * designates standards obtained from the Demeter XAS repository.

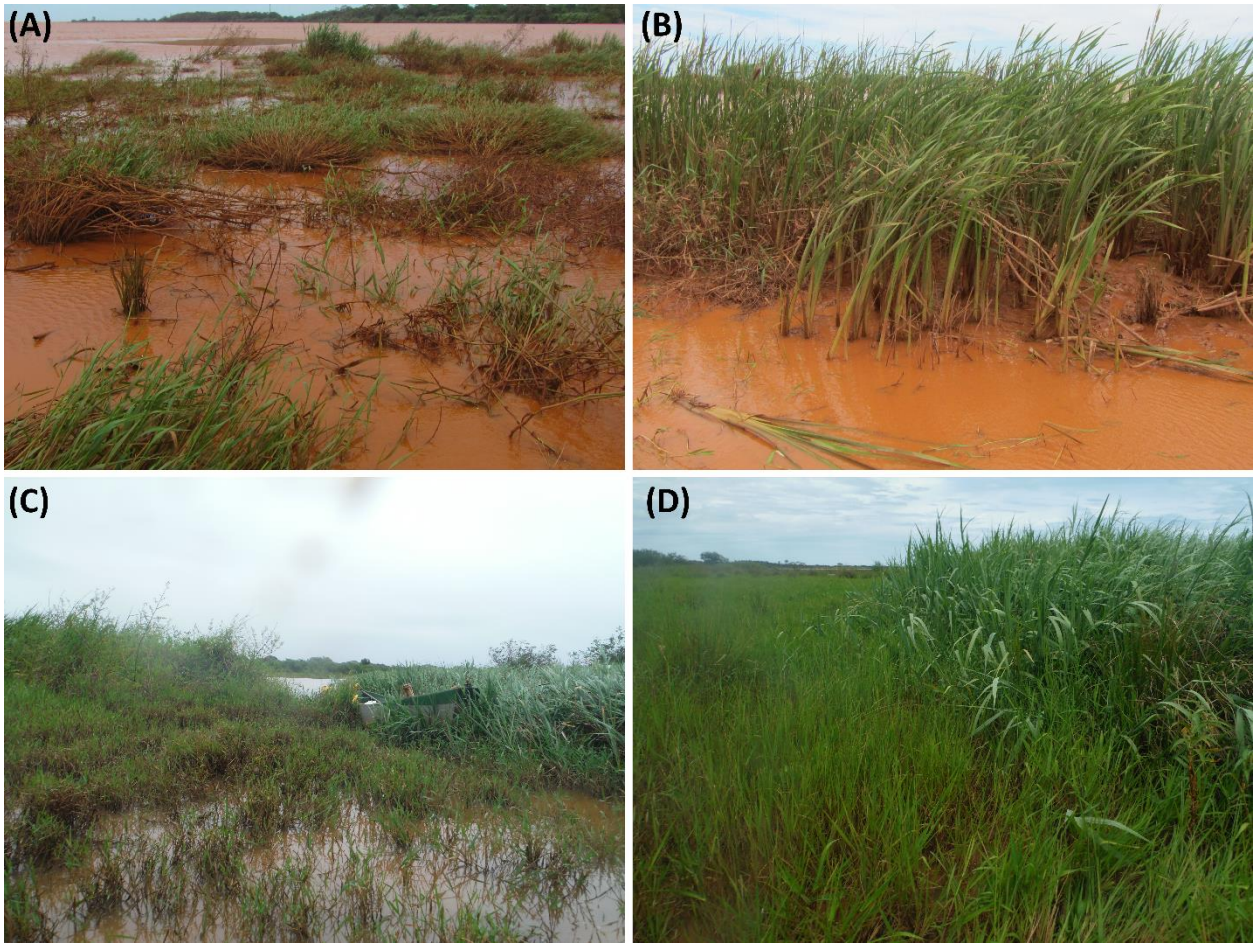

Fig. S2. An overview of Rio Doce estuary in 2015 (A and B) showing the predominant vegetations in the Rio Doce estuary: *Typha domingensis* (A; courtesy of Xosé L. Otero), and *Eleocharis acutangula* (C; courtesy of Hermano M. Queiroz). In 2017 (C and D) an overview of the same areas showing the expansion of the surface occupied by macrophytes.

Fig. S3. Location of soil sampling sites affected by tailings deposition in 2015 and 2017 in the Rio Doce Estuary, Regência, Espírito Santo, Brazil highlighting the permanent islands using satellite images from 2014, 2015, and 2017.

Table S1 – Description of solid-phase fractionation analysis of iron and manganese according to Tessier et al. (1979), Huerta-Diaz and Morse (1990), and Fortin et al. (1993).

Fraction	Abbreviation	Chemical Extractor/Procedure
Exchangeable and solube	EX	Extracted with a 1 mol L^{-1} $MgCl_2$ solution at pH adjusted to 7
Fe and Mn associated with carbonates	CA	Extracted with a 1 mol L^{-1} NaOAc (sodium acetate) solution at pH 5
Fe and Mn associated with ferrihydrite and lepidocrocite, i.e, low crystallinity Fe phases	LC	Extracted with a 0.04 mol L^{-1} hydroxylamine + acetic acid 25 % (v/v) solution at 30 °C (ferrihydrite) and 96 °C (lepidocrocite)
Fe and Mn associated with hematite and goethite, i.e, high crystallinity Fe phases	CR	Extracted with a 0.25 mol L^{-1} sodium citrate + 0.11 mol L^{-1} sodium bicarbonate solution and 3 g of sodium dithionite at 75 °C
Fe and Mn associated to pyrite	PY	Extracted with concentrated HNO_3. Before extraction the samples were subjected to treatment with 10 mol L^{-1} HF to remove phyllosilicates Fe, and concentrated H_2SO_4 was then added to remove Fe associated with organic matter

Table S2 – Detection limits and quality assurance and quality control used in the ICP-OES for total content and iron fractionating analyses.

Quality assurance	Fe	Mn
Detection limit	0.01	0.01
Measured value	9.026	9.769
Certified value (NIST-1643f)	10	10
Recovery (%)	90.3	97.7

NIST-1643F: Certified standard reference material for trace elements in water used on Mn and Fe determinations from extracts of total contents and iron fractionating analyses.

References (Supplementary material)

Fortín, D., Leppard, G.G., Tessier, A., 1993. Chactestis of lacustrine diagnetic iron oxyhydrodes 57, 4391–4404.

Huerta-Diaz, M.A., Morse, J.W., 1990. A quantitative method for determination of trace metal concentrations in sedimentary pyrite. Mar. Chem. 29, 119–144. https://doi.org/10.1016/0304-4203(90)90009-2

Manceau, A., Marcus, M.A., Grangeon, S., 2012. Determination of Mn valence states in mixed-valent manganates by XANES spectroscopy. Am. Mineral. 97, 816–827. https://doi.org/10.2138/am.2012.3903

Newville, M., 2013. Larch: An Analysis Package for XAFS and Related Spectroscopies. J. Phys. Conf. Ser. 430, 012007. https://doi.org/10.1088/1742-6596/430/1/012007

Ravel, B., Newville, M., 2005. ATHENA , ARTEMIS , HEPHAESTUS : data analysis for X-ray absorption spectroscopy using IFEFFIT. J. Synchrotron Radiat. 12, 537–541. https://doi.org/10.1107/S0909049505012719

Tessier, A., Campbell, P.G.C., Bisson, M., 1979. Sequential extraction procedure for the speciation of particulate trace metals. Anal. Chem. 51, 844–851. https://doi.org/10.1021/ac50043a017

6. FROM SINKS TO SOURCES: THE ROLE OF FE OXYHYDROXIDE TRANSFORMATIONS ON PHOSPHORUS DYNAMICS IN ESTUARINE SOILS

Abstract

The availability of phosphorus (P) in estuarine ecosystems is ultimately controlled by the nature of interactions between dissolved P and the soil components (e.g., soil minerals), especially iron (Fe) oxyhydroxides. P retention on Fe oxyhydroxides and its subsequent availability depends on mineral crystallinity and susceptibility to dissolution. However, in estuarine soils, geochemical conditions (e.g., redox oscillation and high soil organic matter content) may alter the fate of P and decrease the environmental quality of estuarine waters. The large input of Fe-rich tailings into the Rio Doce Estuary in Brazil in 2015 after a rupture of a Fe ore tailings dam (i.e., "Mariana mine disaster") offers a unique framework to evaluate the Fe oxyhydroxides role in P availability in estuarine soils, their potential effects on the cycling of P and eutrophication. We observed a significant correlation between Fe minerals and the P content in the estuary soils, suggesting that P enrichment was promoted by the deposited Fe-rich tailings. Adsorption isotherm curves indicated that mine tailings had a strong affinity for P due to presence of crystalline Fe oxyhydroxides in the tailings. Significant losses of Fe (62%) and P (56%) from the estuarine soil was observed two years after the initial impact and in response to redox conditions oscillations. Additionally, the content of high crystallinity Fe oxyhydroxides decreased significantly, whereas that of low crystallinity Fe oxyhydroxides showed an increase over time. These changes were associated with the dissimilatory Fe reduction, which led an increase in the concentrations of readily available P (2015: 2.30 ± 0.41 $mg \cdot kg^{-1}$; 2017: 3.83 ± 1.82 $mg \cdot kg^{-1}$; $p < 0.001$) in the studied soils. Moreover, in 2017, the dissolved P content exceeded the recommended environmental safety limits by five times. Our results indicate that Fe oxyhydroxides are a continuous source of dissolved P for the ecosystem, and Fe-rich tailings deposited in the estuarine ecosystem may be linked to a potential eutrophication.

Keywords: Fe oxides, crystallinity, eutrophication, pollution, redox processes, Samarco

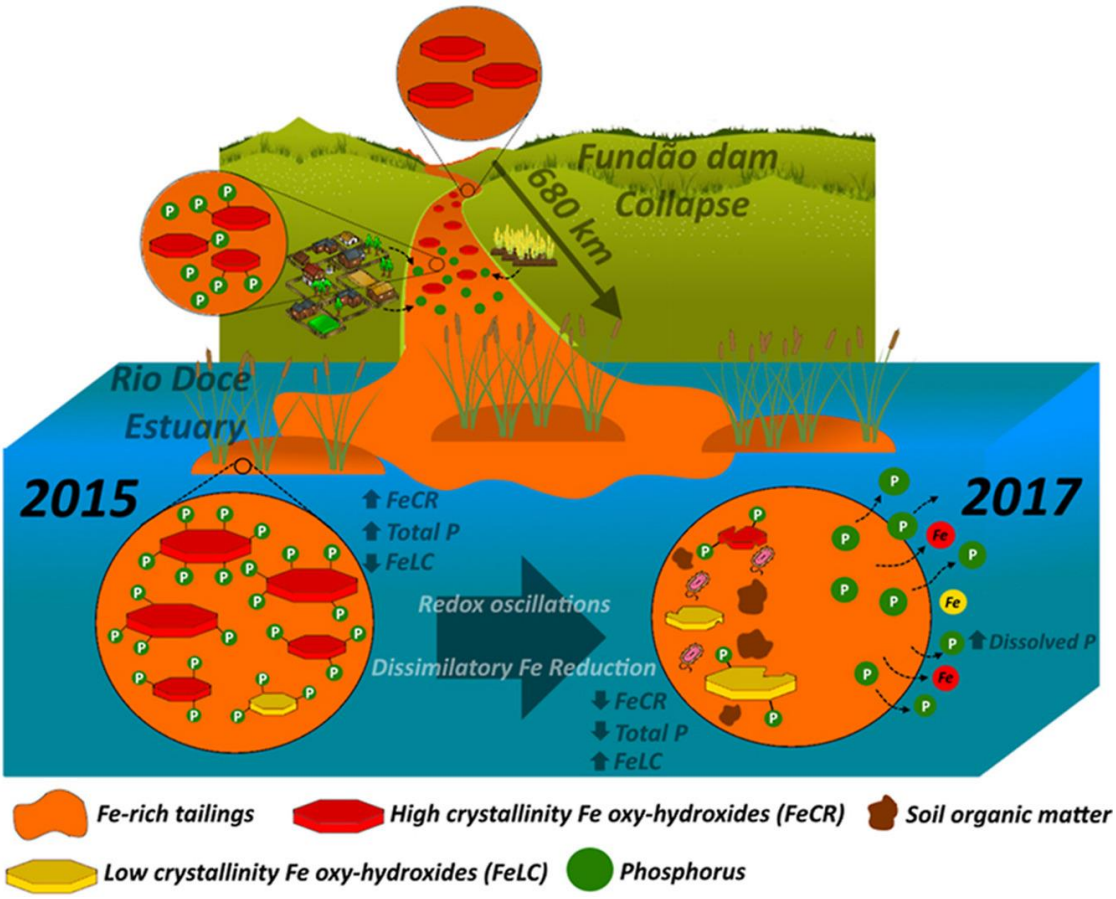

Queiroz, H.M., Ferreira, T.O., Barcellos, D., Nóbrega, G.N., Antelo, J., Otero, X.L., Bernardino, A.F., 2021. From sinks to sources: The role of Fe oxyhydroxide transformations on phosphorus dynamics in estuarine soils. J. Environ. Manage. 278, 111575. https://doi.org/10.1016/j.jenvman.2020.111575

6.1. Introduction

Phosphorus (P) is considered a limiting nutrient for all living organisms in terrestrial, marine, and coastal ecosystems (Elser et al., 2007; Vitousek et al., 2010). Considered an essential nutrient for plants, animals, and microorganisms, P modulates primary productivity in many terrestrial ecosystems (Ceulemans et al., 2017; Reinhard et al., 2017). The most abundant terrestrial P reservoirs are crustal rocks, soils and shallow marine sediments (0.27–1.3 Tmol P), the deep sea (2,810 Tmol P), and P mines (323–645 Tmol P) (Ruttenberg, 2001). Therefore, the P cycle involves living and non-living processes and various biogeochemical routes, including mineral formation (Paytan and McLaughlin, 2007), weathering (Filippelli and Delaney, 1994), mining (Ruttenberg, 2001) and microbial activity (Richardson and Simpson, 2011).

In soils, P availability is especially controlled by interactions with soil organic matter and different soil minerals (Holtan et al., 1988; Otero et al., 2018). Among these minerals, iron (Fe) oxyhydroxides are known to form especially strong surface complexes with P, limiting its availability to the environment (Arias et al., 2006; Cornell and Schwertmann, 2003). These Fe–P interactions are crucial for P retention and immobilization in most soils and thus limit the availability of P for virtually all terrestrial ecosystems (Cui et al., 2011; Fink et al., 2016). In fact, Fe–P interactions are among the most important mechanisms regulating P fluxes from soils to other reservoirs, such as oceans and lakes (Fink et al., 2016; Werner and Ami, 2014).

The P adsorption–desorption on Fe oxyhydroxides depends on the latter's crystallinity, specific surface area, isomorphic substitution, concentration of hydroxyl (OH) groups on the surface of the Fe minerals, and type of ligands (Cornell and Schwertmann, 2003; Fink et al., 2016). Among the different Fe oxides, goethite is known to be more efficient for P adsorption than hematite due to a higher concentration of OH groups and specific types of ligands called inner-sphere complexes (Antelo et al., 2005; Torrent et al., 1992). Moreover, the overall soil biogeochemical conditions can govern P availability by controlling parameters such as pH, redox potential, microbial activity, and organic matter decomposition (Antelo et al., 2005; Charana Walpola, 2012; Parsons et al., 2017).

In estuarine soils, for instance, redox processes may overrule the control of Fe on P availability because anaerobic pathways of organic matter decomposition (e.g., when NO_3^-, Mn(IV), Fe(III), and SO_4^{2-} serve as the electron acceptors) predominate in these redox oscillating environments (Jiménez-Cárceles and Álvarez-Rogel, 2008; Nóbrega et al., 2014). Thus, since Fe oxyhydroxides are redox-sensitive minerals (Larsen and Postma, 2001; Zachara et al., 2001), their strong control over P availability in estuarine ecosystems as well as the P biogeochemical cycle may be drastically affected. In fact, this process is largely overlooked in estuarine ecosystems, and only a few researchers have studied this aspect (Ekholm and Lehtoranta, 2012).

Although large inputs of bioavailable P are known to decrease the environmental quality of coastal ecosystems such as estuarine environments (Barcellos et al., 2019; Schendel et al., 2004; Wang et al., 2011), P is still considered a limiting element for primary production in these ecosystems (Elser et al., 2007; Kraal et al., 2015). In this sense, understanding the Fe–C–P coupling in estuarine soils is of key importance not only to assess and interpret P

availability (Cui et al., 2011; Liptzin and Silver, 2009; Otero et al., 2015), but also to predict and control the risk of coastal water eutrophication (Coelho et al., 2004; Kraal et al., 2015).

Here, we report a detailed study of the biogeochemical processes controlling P dynamics in estuarine soils that received a large input of mine tailings enriched in Fe oxyhydroxides (Queiroz et al., 2018) released after the world's largest mining disaster to date, the Mariana mine disaster in Brazil (Escobar, 2015). This disaster occurred in November 2015 after the rupture of a Fe ore tailings dam from Samarco Company, killing 19 people and destroying many villages, natural reserves and dumped into the Doce River (i.e., *Rio Doce*) approximately 50 million m^3 of Fe-enriched mine tailings (Escobar, 2015; Gabriel et al., 2020). A huge wave of a Fe-enriched material traveled hundreds of kilometers downstream reaching the estuary 16 d after the failure (Lima et al., 2020; Queiroz et al., 2018). Thus, the Samarco Dam failure offers a unique framework to study the coupled biogeochemical dynamics of Fe and P in an estuarine environment marked by soils under redox oscillating conditions. The study site also offers an important opportunity to evaluate the changes in the composition of Fe oxyhydroxides over time and their effects on the cycling of P in coastal ecosystems.

Accordingly, we hypothesized that (i) the Fe tailings may have acted as a P carrier to the Rio Doce Estuary and (ii) the active redox environment in these estuarine soils would affect the ability of Fe oxides to control P bioavailability. Thus, the objective of this study was to evaluate the role of Fe oxyhydroxides on the dynamic and bioavailability of P in a Fe-rich estuarine soil and to assess the potential environmental implications, especially with regard to a eutrophication risk using the Rio Doce estuary as a framework due to impacts of the inadvertent Fe-rich mine tailings disposal after Mariana's disaster.

6.2. Material and Methods

6.2.1. Site description, sampling, and in-situ measurements

The Rio Doce is a major river in southeastern Brazil. Its basin covers an area of 84,000 km^2, and it supplies water to approximately 3 million people (Medeiros et al., 2012; Pires et al., 2017). The basin has been modified by several decades of human activities, such as waste discharge, industrial activity, agriculture, and aquaculture in over 300 municipal districts located within its borders (Marques and Barbosa, 2001; Medeiros et al., 2012; Santolin et al.,

2015). In November 2015, a large amount of Fe-enriched mine tailings mostly composed by highly crystalline Fe oxyhydroxides (e.g., hematite and goethite) were dumped into Rio Doce Basin after the Fundão Dam collapse, reaching the Rio Doce Estuary in the Eastern Marine Ecoregion of Brazil (19°38'–19°45'S and 39°45'–39°55'W) (Gomes et al., 2017; Queiroz et al., 2018) and, ultimately, the ocean, where they dispersed over hundreds of kilometers (Marta-Almeida et al., 2016).

For the present study, soil samples were collected from the estuary during two field campaigns, the first in 2015 (a few days after initial mine tailings arrival) and the second in 2017. Both samplings were performed at the same sites (Fig. 1). The soils were sampled using polyvinyl chloride tubes attached to a sampler used for flooded soils (Howard et al., 2014; LaForce et al., 2000; Otero et al., 2009). The soil sampling was performed in areas close to the dominant vegetation (i.e., *Eleocharis acutangula*, *Typha domingensis*, and *Hibiscus tiliaceus)* to avoid vegetation bias and better assess the estuarine conditions. In addition, mine tailings samples from inside the Fundão Dam located in Bento Rodrigues City, Minas Gerais, were donated by the National Mining Agency and also analyzed.

After soil collection, the samples were hermetically sealed, maintained at a temperature of approximately 4°C in order to avoid extra microbial activities and chemical shifts, and transported in the vertical position to the laboratory (Barcellos et al., 2019; Howard et al., 2014; LaForce et al., 2000; Nóbrega et al., 2014). Thereafter, they were sectioned to depths of 0–3, 3–5, 5–10, and 15–30 cm, representing the depths most affected by tailings deposition. Soil redox potentials (Eh) were measured during sample collection using a Pt electrode, with the Eh values adjusted to a calomel reference electrode by adding +244 mV. Soil pH values were recorded with a glass electrode, previously calibrated with standard solutions of pH 4.0 and 7.0.

Water samples were also collected (2015: n = 10; 2017: n = 20) from the river channel close to the soil sampling sites. The water samples were collected in amber glass bottles, filtered (pore size = 3 µm), and acidified for quantification of total dissolved P.

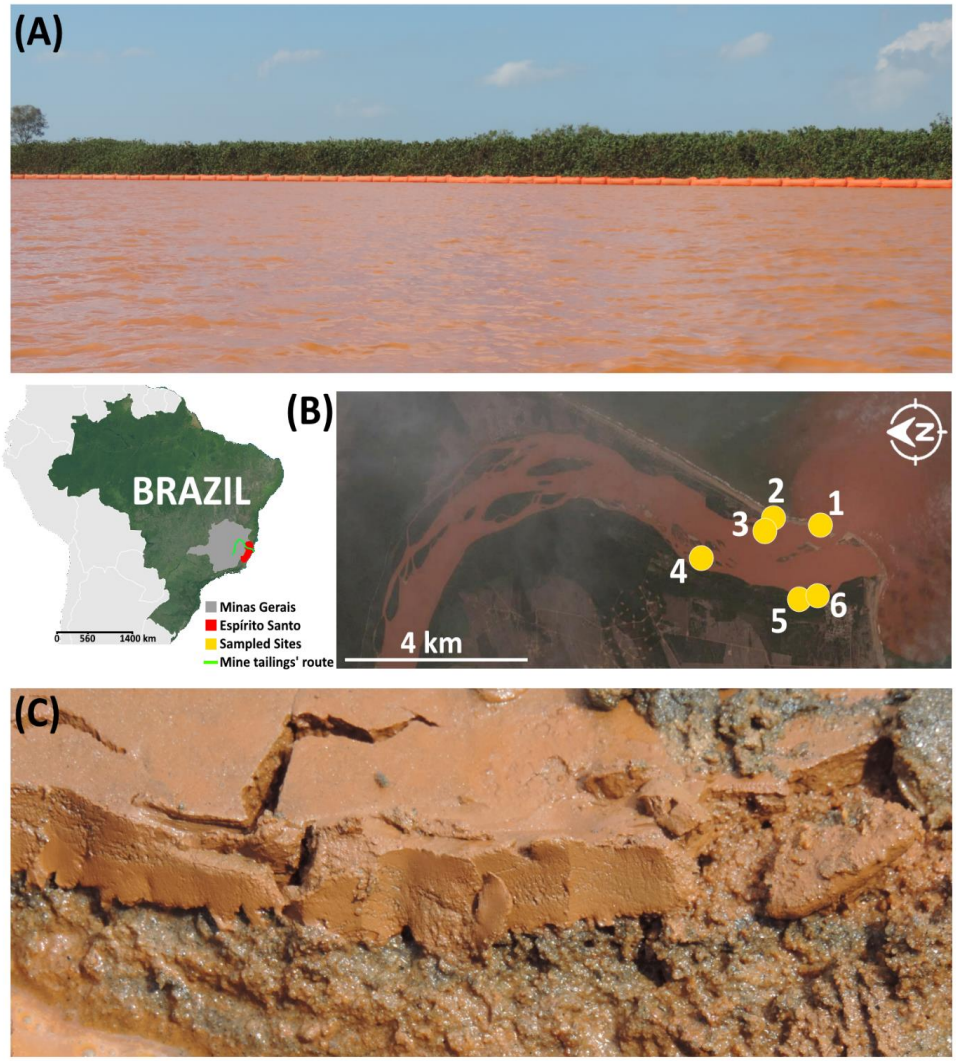

Fig. 1. (A) The Rio Doce Estuary soon after the arrival of the Fe mine tailings (November 2015). Note the red color of the water due to the fine particles of Fe oxyhydroxides in suspension, (B) locations of the soil sampling sites at the Rio Doce Estuary (Regência, Espírito Santo State, southeast Brazil), and (C) a close-up of the deposited Fe-rich mine tailings on the surface of the estuarine soil in November 2015, highlighting its fine composition and reddish color in comparison with the original estuarine soil.

6.2.2. Chemical and mineralogical analyses of the soil and water samples

The total P contents in the soil samples and mine tailings from Fundão Dam were determined by inductively coupled plasma-optical emission spectrometry (ICP-OES, iCAP 6200, Thermo Scientific) after a triacid (HF + HCl + HNO_3) digestion (USEPA, 1996). The dissolved P concentrations in the water samples were quantified via ICP-OES. To determine

the P bioavailability in the estuary soils, the exchangeable P content (Exch-P) was also determined after extraction with a 0.34 mol·L^{-1} NaCl solution (Paludan and Morris, 1999).

To assess the different forms of Fe (Fe oxyhydroxides and other Fe fractions) in the soil samples, Fe fractionation was performed using a combination of methods proposed by Tessier et al. (1979), Huerta-Diaz and Morse (1990), and Fortin et al. (1993). As a result, the following five operationally distinct fractions were assessed (for further details, see Table S1 and Queiroz et al., 2018): (i) exchangeable Fe (EX), (ii) Fe associated with carbonates (CA), (iii) Fe associated with ferrihydrite and lepidocrocite (i.e., low crystallinity Fe phases (LC)), (iv) Fe associated with hematite and goethite (i.e., high crystallinity Fe phases (CR)), and (v) Fe associated with pyrite (PY). The pseudo-total Fe was calculated using the sum of these five fractions (pseudo-total Fe = ∑EX + CA + LC + CR + PY).

A mineralogical characterization of the estuarine soils was performed using X-ray diffraction (XRD) with Cu Kα radiation at 0.02° 2θ s^{-1} in the range of 3–60° 2θ after treatment using NaClO to remove organic matter. The XRD analysis was carried out using soil samples from the superficial soil layers collected in 2015 and 2017 to evaluate the changes in the Fe oxyhydroxides over time. The analysis was performed in the clay fraction after a preconcentration step to remove kaolinite and gibbsite with 5 mol·L^{-1} NaOH and to concentrate the oxides (Kämpf and Schwertmann, 1982). The samples were washed with 0.5 mol·L^{-1} HCl to avoid sodalite peaks (Singh and Gilkes, 1991).

6.2.3. The Freundlich and Langmuir adsorption isotherms

To evaluate the P adsorption in the mine tailings and assess the maximum adsorbing capacity, two isotherm experiments were carried out using the mine tailings samples collected in 2015 as the adsorbent. Suspensions were prepared with a 0.01 M NaCl solution as an inert electrolyte at a solid/solution ratio of 2 g·L^{-1}. The total P concentration in the suspensions ranged between 0.1 and 10 mg·L^{-1}. The pH values of the suspensions were then adjusted to either pH 4.0 or 7.0 by the addition of either 0.1 or 1.0 mol·L^{-1} HNO_3 or NaOH solutions, respectively. During the 24 h equilibration period, the suspensions were continuously shaken, and the pH was periodically measured and readjusted if necessary. The suspensions were then centrifuged and filtered through 0.45 μm filters. The P concentrations in the solution were determined following the molybdenum blue method (Murphy and Riley, 1962), and the

concentrations of adsorbed P were determined by the difference between the total added amount and the final amount remaining in solution. The isotherm results were computed with the Freundlich and Langmuir isotherm models and nonlinear least squares regression (Boeykens et al., 2017; Xue et al., 2018).

6.2.4. Statistical analyses

The total P, pseudo-total Fe, Exch-P, and dissolved P in water were subjected to the non-parametric Kruskal–Wallis test to assess differences between 2015 and 2017 at the 5% significance level (software XLSTAT version 2014.5.03) (Reimann et al., 2008). The non-parametric test was selected because it depends on fewer assumptions and is more robust for environmental analysis (Reimann et al., 2008). Additionally, the collected data did not show a normal distribution, which favors the use of non-parametric statistics. Spearman correlations were also calculated to compute interactions between the variables, and the *r* and *p* values were reported.

6.3. Results

6.3.1. Iron fractionating and total contents of iron and phosphorus

The surface soil samples from 2015, which represent the soil layer most affected by the deposition of the mine tailings, showed the highest pseudo-total Fe content (depth = 0–3 cm; total Fe = 129,000 ± 88,000 mg·kg^{-1}; Fig. 2a). Similarly, the highest total P content was recorded in the surface soils (depth = 0–3 cm) from 2015 (soon after the mine tailings arrival; 430 ± 200 mg·kg^{-1}; Fig. 2c, and exchangeable P = 3.04 ± 0.35 mg·kg^{-1}; Fig. 3e). On the other hand, the total P content of the original mine tailings from inside the Fundão Dam was, on average, 1.5 times lower (mean = 288 ± 67 mg·kg^{-1}; Fig. 2c) than that of the mine tailings deposited on the estuary soil. In 2017, the total Fe contents decreased significantly (average 26,726 ± 14,849 mg·kg^{-1}; k = 5.400; p = 0.0201; Fig. 2b and Table S2) as well the total P contents (average: 136 ± 78 mg·kg^{-1}; k = 4.4611; p = 0.0347; Fig. 2d)

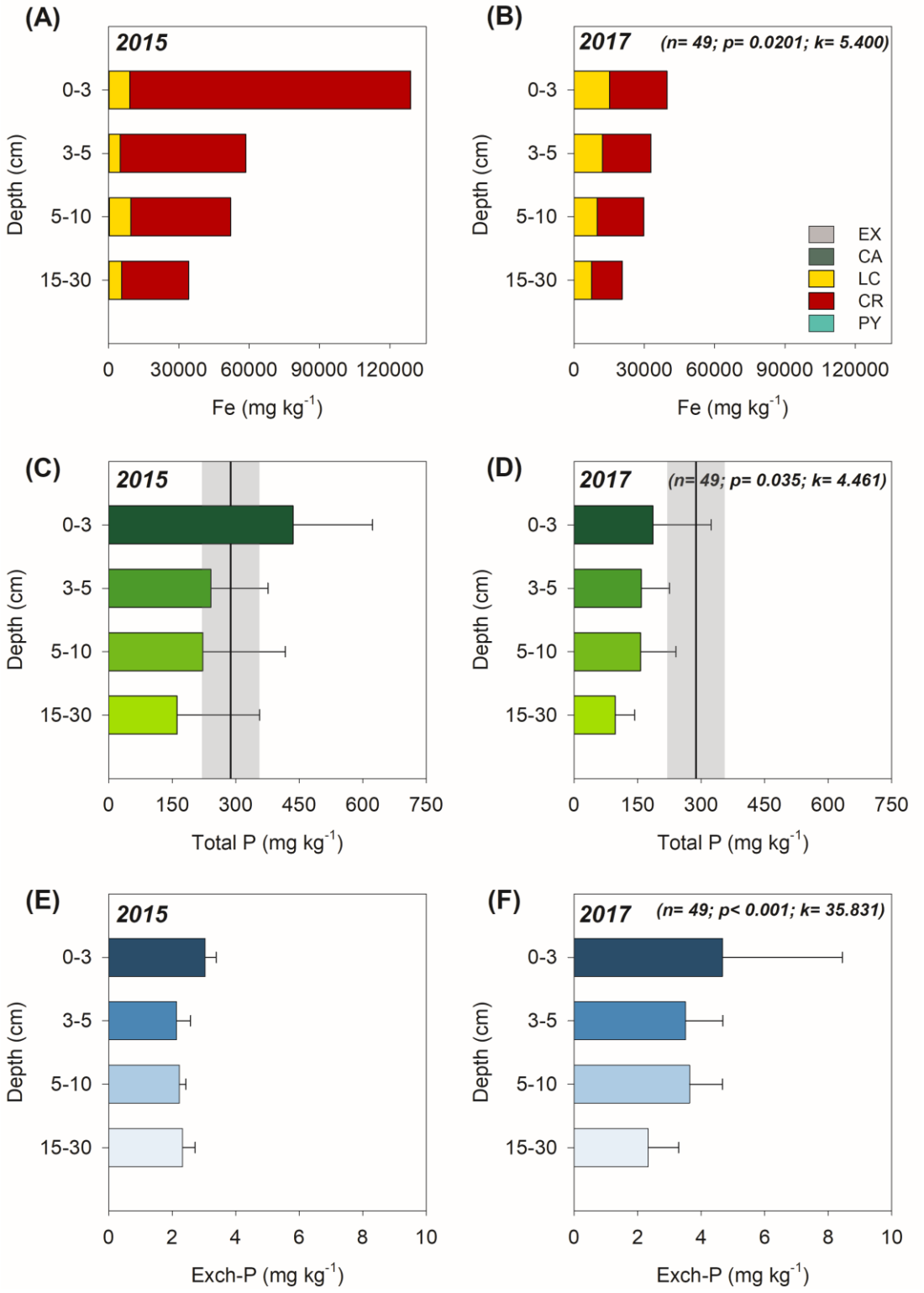

Fig. 2. Fe fractionations (A and B), total P (C and D), and Exch-P (E and F) for the soil samples collected in 2015 and 2017 (mean values, with error bars indicating a ±1 standard deviation (SD). The black solid line indicates the mean total P content (±SD; shaded area) of tailings from inside the Fundão Dam. The Kruskal–Wallis test at the 5% probability level was carried out to evaluate statistical differences between 2015 and 2017. *k* values above the critical *k* (3.84) indicate statistical differences.

The Fe solid-phase fractionation from 2015 indicates that most of the Fe present in the estuarine soils impacted by the mine tailings was associated with high crystallinity oxides such as hematite and goethite (FeCR = 89.3%), followed by low crystallinity oxides (FeLC = 10.3%), while the remaining Fe fractions (FeEX, FeCA, and FePY) represented less than 1% of the pseudo-total Fe (Fig. 2). In 2017, the Fe associated with FeCR decreased by 25% (FeCR in 2017: 63.5%; Fig. 2), followed by a significant increase by 26 % in Fe associated with FeLC whereas the Fe associated with FeEX, FeCA and FePY remained representing less than 1% of the pseudo-total Fe.

6.3.2. Fe-rich mine tailings mineralogical characteristics

The XRD results (Fig. 3) from the clay samples concentrated in Fe oxides from superficial soil layer (depth = 0–3 cm) collected in 2015 and 2017, which represents the deposited mine tailings on the estuarine soil indicate the prevalence of Fe oxyhydroxides of high crystallinity, such as goethite (d-spacing values = 4.18 and 21.33° 2θ) and hematite (d-spacing values = 3.67 and 24.37° 2θ), especially in 2015.

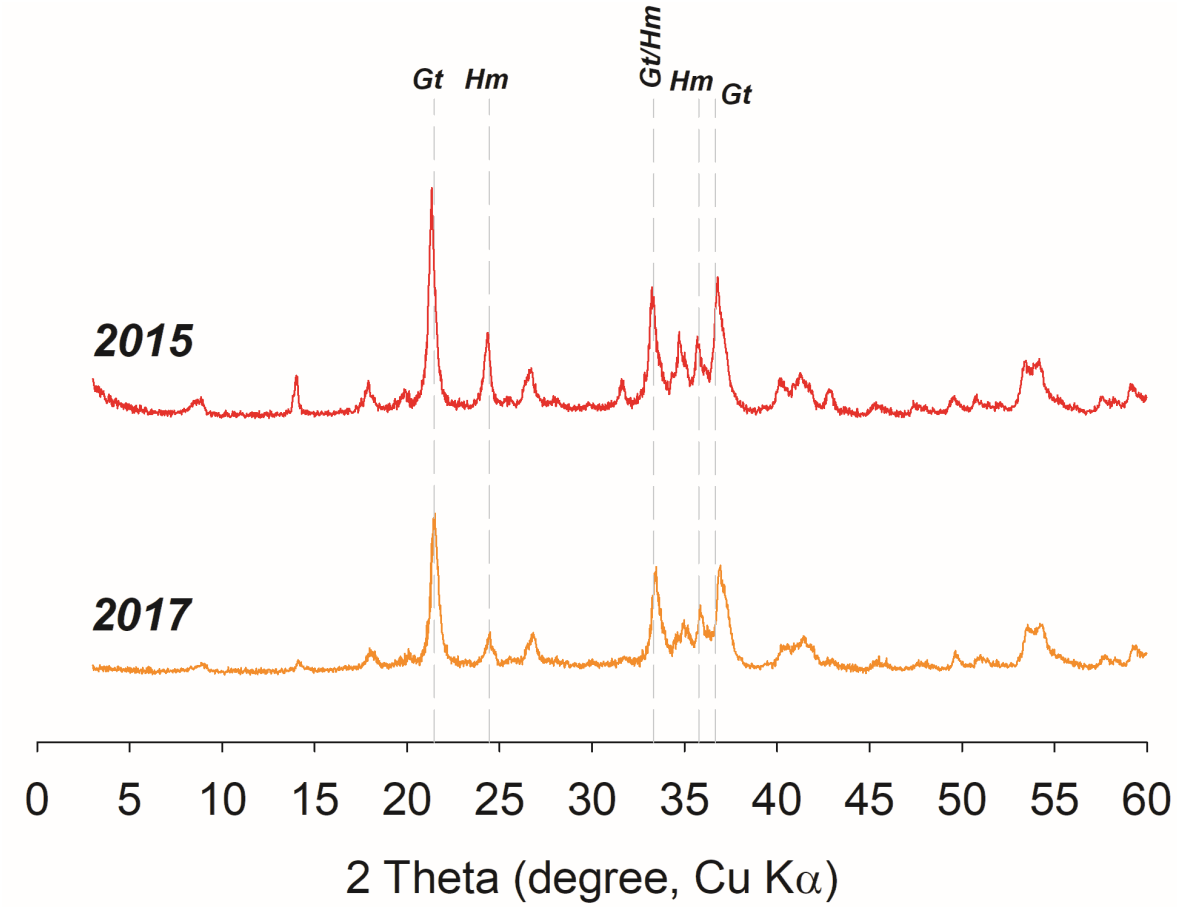

Fig. 3. Results of the XRD analysis of clay samples concentrated in Fe oxides from superficial soil (depth = 0–3 cm) collected in 2015 and 2017, representing the deposited mine tailings on the estuary soil. Gt (Goethite); Hm (Hematite).

6.3.3. Sorption isotherms

The Langmuir and Freundlich isotherms were performed for mine tailings samples collected in 2015 and Fig. 4 shows the effects of pH on P adsorption. The Langmuir and Freundlich isotherms curves showed similar characteristics, indicating an initial and higher P adsorption by the mine tailings at P concentration < 2.0 $mg \cdot L^{-1}$ and lower adsorption at P concentration > 2.0 $mg \cdot L^{-1}$ so that the plateau of slopes indicates no difference between the P concentrations of 4.0 and 10.0 $mg \cdot L^{-1}$.

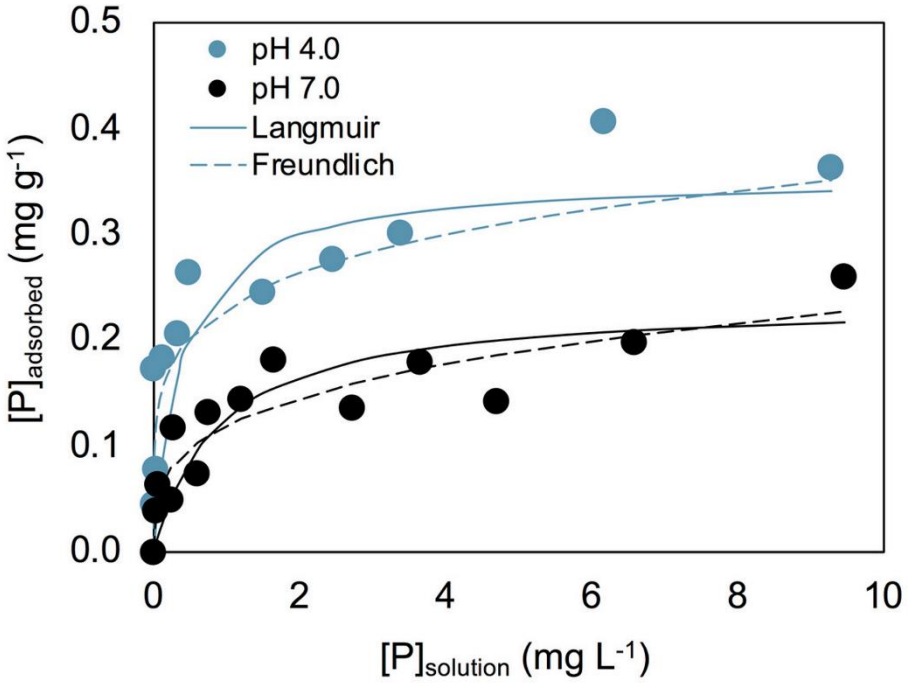

Fig. 4. Isotherm adsorption curves for mine tailings samples collected in 2015 at pH 4.0 (blue points) and 7.0 (black points), adjusted for the Langmuir (solid lines) and Freundlich (dashed lines) models.

6.3.4. Dissolved P contents in estuary water

Regarding the dissolved P in the estuary water, no significant differences were observed between 2015 (on average: 0.920 ± 0.412 mg·L^{-1}) in 2017 (on average: 0.626 ± 0.473 mg·L^{-1}; Fig. 5), however, these values were above the threshold allowed according to Brazilian legislation (0.124 mg·L^{-1}; CONAMA, 2005) and higher than reported in previous studies at the same place by Petrucio et al. (2005) and Venturoti et al. (2015) which found dissolved P contents of 0.128 ± 0.127 mg·L^{-1} and 0.04 ± 0.03 mg·L^{-1} respectively (Fig. 5).

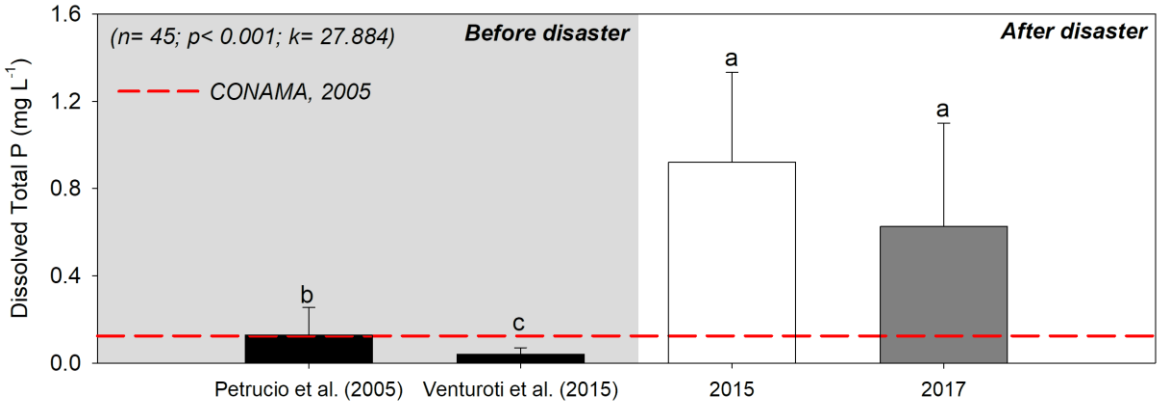

Fig. 5. Total dissolved P in the Rio Doce Estuary water. The red dashed line indicates the total P threshold (0.124 mg·L^{-1}) for water according to Brazilian legislation (CONAMA, 2005). The gray area indicates total P concentration in the estuary water before the mine tailings arrival, whereas the white area indicates the values after the tailings arrival. The same lowercase letters indicate no significant differences among the variables as per the Kruskal–Wallis test at the 5% probability level.

6.4. Discussion

6.4.1. The phosphorus in the Rio Doce estuary: contents and sources

The higher total P content in the estuarine soil soon after the tailings arrival compared to the initial total P content in the tailings from inside the dam suggests that the Fe-rich mine tailings may have, in fact, acted as a carrier of P to the Rio Doce Estuary. Additionally, the strong positive significant correlation (r = 0.936; p < 0.001) between pseudo-total Fe and total P (Fig. 6) corroborates the role of the Fe-rich tailings in transporting P to the estuary soon after the dam collapse.

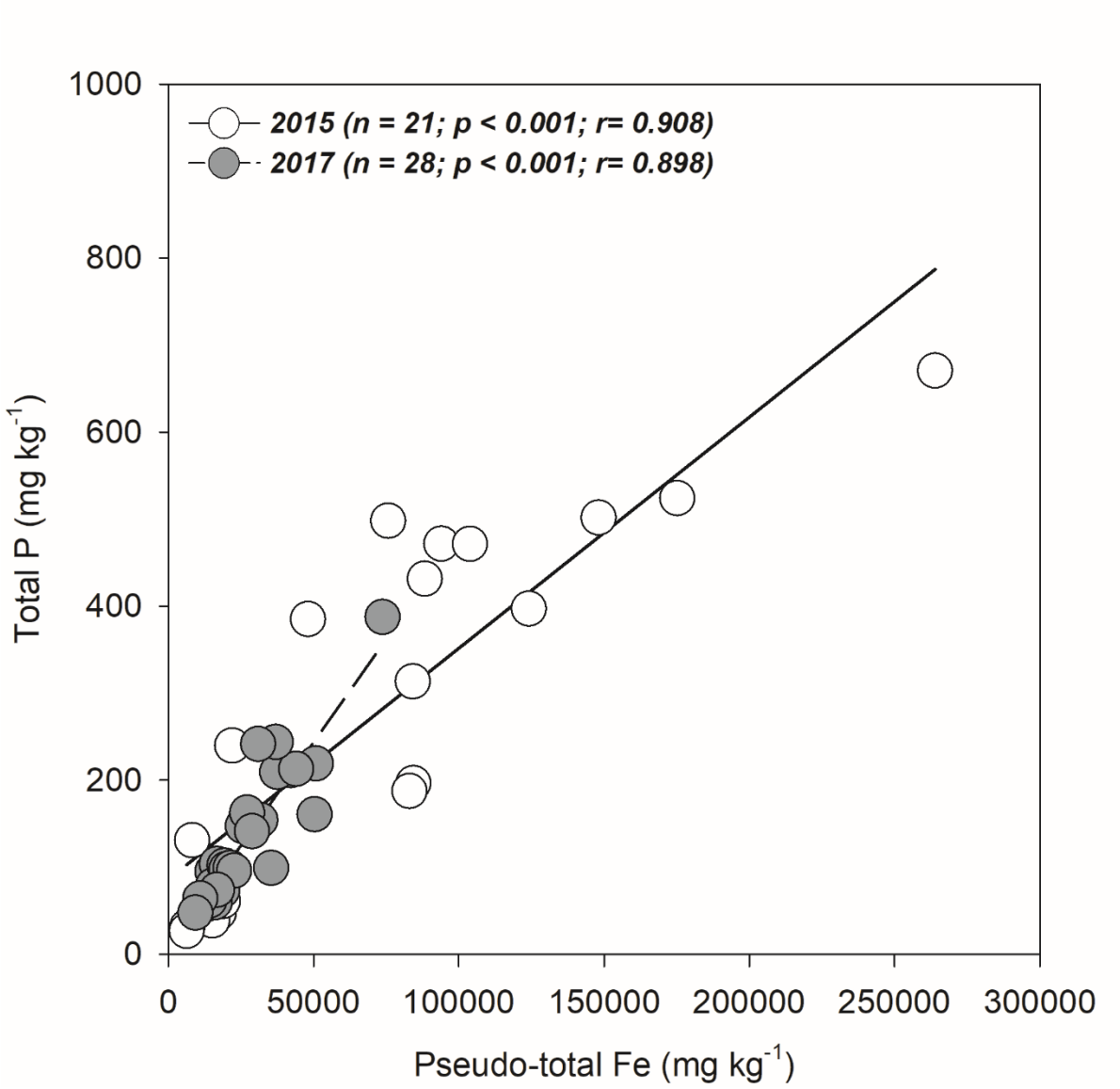

Fig. 6. Spearman correlations between pseudo-total Fe and total P contents in soils for the samples collected in 2015 (solid line) and 2017 (dashed line). *p* values < 0.05 indicate significant correlation.

These mine tailings required 16 d to reach the estuary (Escobar, 2015), traversing 688 km downriver and crossing agricultural farms, cities, and villages throughout the Rio Doce Basin, which covers an area of approximately 84,000 km^2, drains 209 municipalities, and is inhabited by approximately 3.6 million people (BBC, 2016; Phillips, 2016; Pires et al., 2017). In this sense, studies prior to the disaster reported that P sources in the Rio Doce basin upstream from the estuary, are associated with agricultural fertilizers, urban wastes, and sewage which are daily discharged into the Rio Doce basin (Figueiredo et al., 2014; Jardim et al., 2014) which were carried by the wave of tailings towards the estuary, after the Fundão dam rupture. Which

was supported by high contents of dissolved P in 2015 soon after the Fe-rich tailings arrival to the estuary in comparison to values reported in previous studies for the same region (Fig. 8).

In addition, the Fe oxyhydroxides presents in the mine tailings, are known for retaining P, predominantly through the ligand exchange mechanism, as binuclear and bidentate surface complexes, replacing OH groups for P to form bridging, binuclear surface complexes (Cornell and Schwertmann, 2003; Guzman et al., 1994; Queiroz et al., 2018). For instance, Strauss et al. (1997) reported higher and rapid P adsorption rates in poorly crystallized goethite due to its higher charge on external surfaces as a result of the higher surface area compared to hydrothermally treated (i.e., high crystallinity) goethite, leading to strong and partly irreversible P retention. Several studies also reported the role of low crystallinity Fe oxyhydroxides (e.g., ferrihydrite and lepidocrocite) in P adsorption by the formation of bidentate complexes and diffusion into micropores or into aggregates of particles (Kim et al., 2011; Rhoton and Bigham, 2005; Wang et al., 2013a; Wilson et al., 2004). Indeed, we observed significantly positive correlations between both FeLC (r = 0.664; Fig. 7a) and FeCR (r = 0.841; Fig. 7b) and total P in 2015, corroborating P adsorption in both types of Fe oxyhydroxides and thus their participation in controlling the fate of P in the estuarine soils.

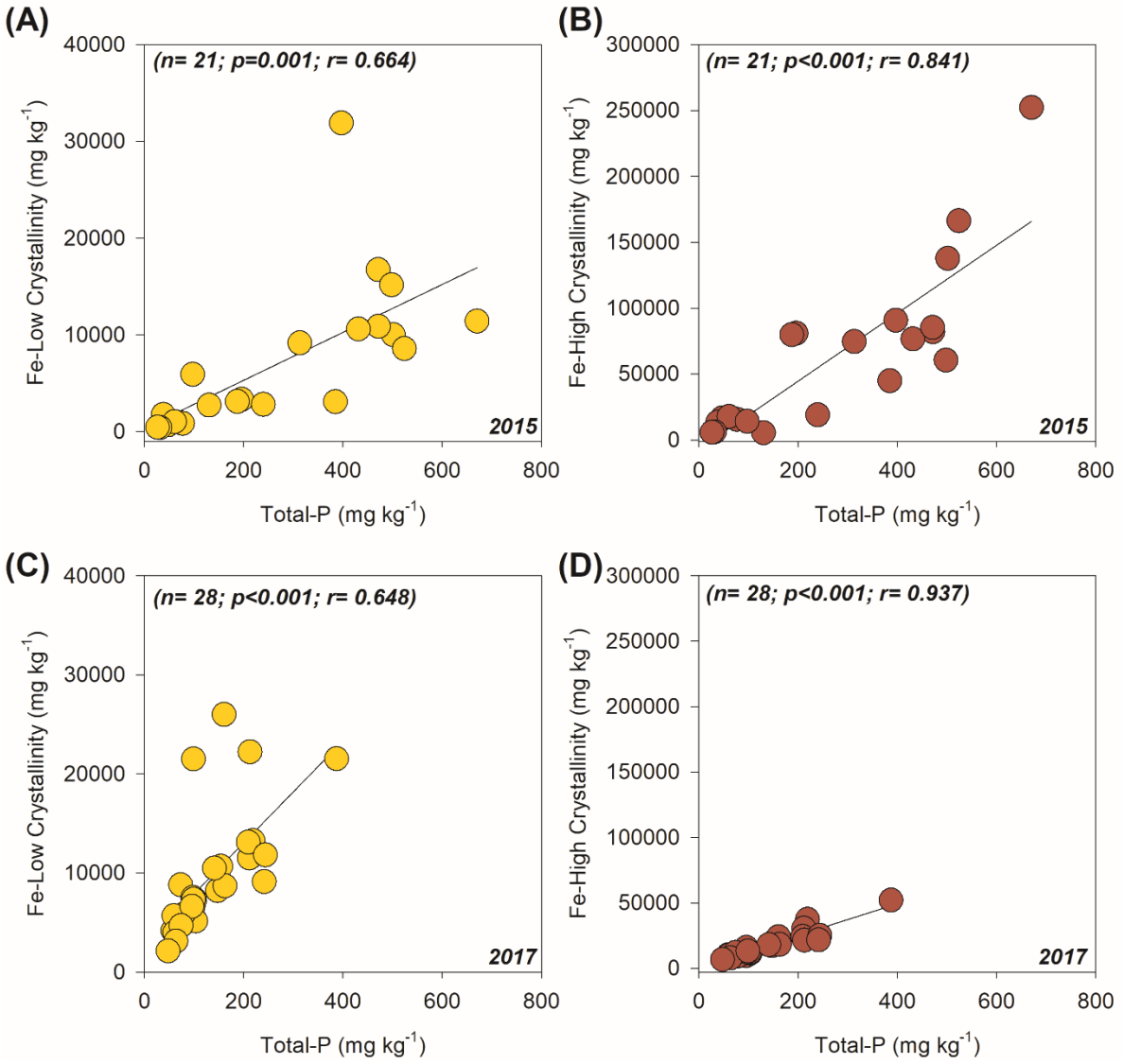

Fig. 7. Spearman correlations between total P and both low (A and C) and high crystallinity (B and D) Fe oxyhydroxides in 2015 and 2017.

Moreover, the affinity of P to the Fe-rich mine tailings was further corroborated by the high slopes of the isotherm curves of adsorption shown in Fig. 4. The sharp initial slope confirms the strong ability of the Fe tailings to adsorb P as result of inner-sphere complexes presence (Ajmal et al., 2018; Chung et al., 2015). The Freundlich isotherm, on the other hand, assumes a nonuniform P adsorption at the mineral surfaces (Fig. 6), indicating the heterogeneity of surface complexes (e.g., the outer-sphere complexes along the mineral surface) (Trazzi et al., 2016; Zhang et al., 2019). In fact, previous studies have reported the role of outer-sphere complexes in P retention on the Fe oxyhydroxide surfaces (Boukemara and Boukhalfa, 2012; Yan et al., 2016). In addition, the isotherms indicated the amount of P retained in the mine tailings varied according to pH, and higher P adsorption took place at pH

4.0 in both isotherm curves. The pH effect is associated with the point of zero charge (PZC) of the Fe oxyhydroxides (for goethite and hematite, the PZC equals approximately 9.0 and 7.4, respectively; Zhu et al., 2019). Here, anions that form inner-sphere complexes, such as PO_4^{3-}, show higher adsorption at pH < 8.3 due to higher presence OH groups on the surface minerals and form covalent ligands (Antelo et al., 2005; Arroyave et al., 2018; Cornell and Schwertmann, 2003). Conversely, the plateau in the curves from 4.0 and 10.0 $mg \cdot L^{-1}$ P might indicate saturation of the OH groups, especially Fe oxyhydroxides, on the mineral surfaces (Lalley et al., 2016). This result points to the maximum capacity of P adsorption in the mine tailings, which can lead to increased P bioavailability due to the absence of, or the reduction in, the number of adsorption sites.

6.4.2. Changes in P availability over time

A comparison of the soil physico–chemical conditions observed in 2017 (mean Eh = −114 mV; mean pH = 7.03) and 2015 (mean Eh = 64 mV; mean pH = 6.98) suggests that Fe oxyhydroxides underwent the dissimilatory Fe(III) reduction process, leading to reductive dissolution (see Fig. 8) (Bonneville et al., 2009; Pan et al., 2016). The riparian vegetation at the Rio Doce Estuary (Figure S1) was dominated by *Eleocharis acutangula*, *Typha domingensis*, and *Hibiscus tiliaceus*, which may have triggered this anaerobic process by promoting continuous organic matter input to the soils coupled with constant flooding by tides which promoting continuous O_2 depletion (Kristensen et al., 2008; Xu et al., 2020; Zhao et al., 2020), may have resulted in decreasing Eh values and the observed suboxic conditions in 2017.

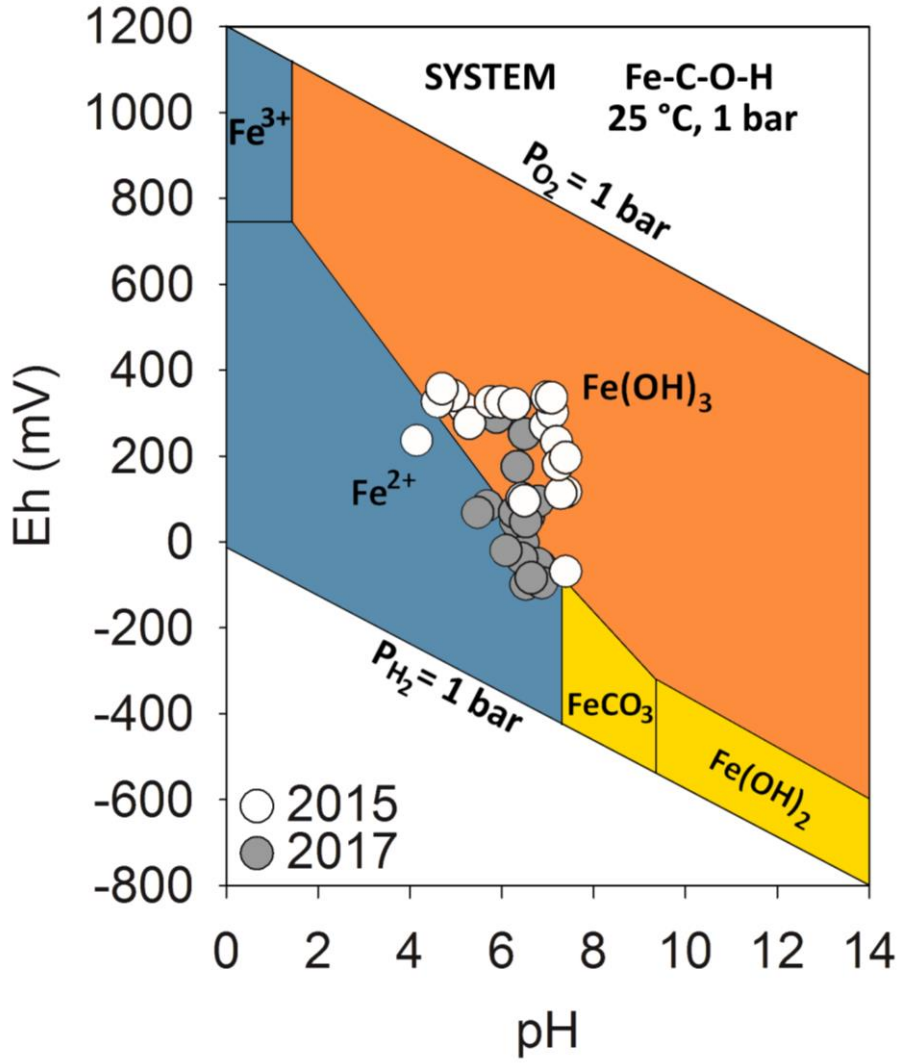

Fig. 8. Eh–pH diagram for the 2015 and 2017 samplings at the Rio Doce Estuary (adapted from Brookins (1988).

In fact, organic matter decomposition in estuarine soils occurs mainly via anaerobic pathways (Canfield et al., 1993). Fe(III) typically serves as the electron acceptor (undergoing dissimilatory Fe(III) reduction), leading to the dissolution of Fe oxyhydroxides at pH values close to neutrality and Eh values below +100 mV (Bücking et al., 2013; Levar et al., 2017; Lovley et al., 2004). Additionally, the generation of organic matter (i.e., electron donor compounds) from plant decay and constant tidal flooding is expected, and the dissolution of Fe oxyhydroxides through dissimilatory Fe reduction is hastened as the redox potential decreases (Du Laing et al., 2009a, 2009b). As a result, the formed Fe^{2+} may be removed from the system by tidal activity since previous studies reported rapid rates of Fe oxyhydroxide dissolution (within hours to weeks), mediated by both biotic and abiotic factors (Davranche et al., 2013; Larsen and Postma, 2001; Weiss et al., 2004).

Indeed, we observed a significantly sharp decrease in the pseudo-total Fe content from 2015 to 2017 (k = 5.400; p = 0.0201; Fig. 2b and Table S2), mostly in the surface layers (0–3 cm), which corroborates the Fe oxyhydroxide reductive dissolution. Also, the XRD spectra indicated a decrease in the peak intensities from 2015 to 2017 of both goethite (d-spacing values = 4.18 and 21.47° 2θ) and hematite (d-spacing values = 3.67 and 24.45° 2θ) (Fig. 3). According to some authors (Velde and Peck, 2002; Wang et al., 2015), this decrease is associated with either changes in mineral abundances or losses of mineral phases (i.e., Fe oxyhydroxides).

The solid-phase fractionation indicated that in addition to Fe losses, the contents of FeCR decreased by 25% from 2015 to 2017 (FeCR: 89.3% to 63.5%; Fig. 2), followed by a significant increase in the percentages of Fe associated with FeLC (2015: 10.3%; 2017: 36.2%; Fig. 2). The dissimilatory Fe reduction process in estuarine soils can dissolve both high and low crystallinity Fe oxyhydroxides (Karimian et al., 2018; Nóbrega et al., 2013; Straub et al., 2000). However, due to the redox oscillations promoted by tidal fluctuations (Keene et al., 2014), plants (Tai et al., 2018), and faunal activity (Araújo Júnior et al., 2016), the solubilized Fe^{2+} may be re-precipitated, leading to newly formed low crystallinity Fe oxyhydroxides (Barcellos et al., 2018; Chen et al., 2018). In these redox oscillating events, especially at the soil–water interface, the dissolved Fe^{2+} in contact with the dissolved O_2 undergoes rapid oxidation and subsequent precipitation, particularly as low crystallinity Fe oxyhydroxides (Charette et al., 2005; Chen et al., 2018).

These Fe transformations are followed by shifts in the crystallinity as well as surface areas and thus the reactivity of the Fe oxyhydroxides toward P, deeply affecting its dynamics (Strauss et al., 1997; Wang et al., 2013b; Yan et al., 2016). Despite the significant losses of Fe, the Fe oxyhydroxides continued to play an important role in P retention in 2017 (Fig. 6), both in the FeLC (r = 0.648; Fig. 7c) and the FeCR (r = 0.937; Fig. 7d) phases.

However, note that FeCR decreased significantly in 2017 (Fig. 2), representing the loss of the Fe fraction most efficient at adsorbing P (Krumina et al., 2016; Luengo et al., 2006). On the other hand, the simultaneous increase in FeLC may have led to a gradual increase in P availability and thus to a more ephemeral control over its dynamics. This interpretation is supported by the higher susceptibility of poorly crystalline Fe oxides to dissolution under redox oscillating environments due to their higher surface areas and amorphous crystal structures (Bhattacharyya et al., 2018; Burdige and Komada, 2020). Thus, as a result of the

significant losses of FeCR (Fig. 2) and the higher instability of FeLC in redox oscillating environments, the role of Fe oxyhydroxides in P retention clearly becomes more ephemeral with time, pointing to the possible release of P to the estuarine waters.

Corroborating this potential P release from the studied estuarine soils, our data showed that the average Exch-P increased significantly from 2015 (2.30 ± 0.41 $mg \cdot kg^{-1}$; Fig. 2e) to 2017 (3.83 ± 1.82 $mg \cdot kg^{-1}$; Fig. 2f), indicating an increase in P bioavailability over time. Moreover, Petrucio et al. (2005) and Venturoti et al. (2015) conducted studies in the same area before the disaster and reported total P dissolved values of 0.128 ± 0.127 $mg \cdot L^{-1}$ and 0.04 ± 0.03 $mg \cdot L^{-1}$, respectively (Fig. 5), which were in accordance with the Brazilian environmental guidelines for water quality (0.124 $mg \cdot L^{-1}$; CONAMA, 2005). On the other hand, in 2015, soon after the deposition of the mine tailings, the dissolved P in the Rio Doce Estuary surpassed this environmental threshold by at least seven times. These results suggest a real risk of eutrophication associated with the mine tailings arrival in the estuary.

In this sense, the riparian vegetation at the Rio Doce Estuary could act on P absorption (Yu et al., 2019), however, the absence of significant differences of dissolved P between 2015 and 2017 (Fig. 5), indicates an ineffective ability of riparian vegetation to uptake P and decrease the values in water. Indeed, *Eleocharis acutangula* and *Typha domingensis*, which are the plants that predominate at Rio Doce estuary, are poorly efficient to absorb P, lowering its role as biofilters (Esteves and Suzuki, 2013; Rejmánková, 2001).

Thus, the similar values of total dissolved P in the estuary water in 2015 and 2017 (Fig. 5) are closely linked to limited capacity of the Fe oxyhydroxides to continue acting as effective sinks for P upon arriving in the estuarine environment (Fig. 5). This finding is related both to the Fe losses by reductive dissolution (mostly of the thermodynamically more stable Fe mineral fraction or FeCR) and the increase in the less stable Fe fraction (i.e., FeLC).

6.4.3. Risks of eutrophication in the estuarine soils of Rio Doce

The high values of dissolved P in the Rio Doce Estuary in 2017 (Fig. 8) and the significant increase in Exch-P from 2015 to 2017 (Fig. 2) suggest a continuous and ongoing eutrophication process at the Rio Doce Estuary, linked to deposited Fe-rich mine tailings which are a continuous and significant source of P loads. The total P content observed in 2015 at Rio Doce estuarine soil was as high as those reported for other urban heavily polluted estuarine soils

worldwide with imminent risk of eutrophication or eutrophicated indeed (Table 1). However, in the reported studies the P sources were anthropic activities known to produce wastes with high P loads such as shrimp farming, agriculture, and sewage discharge (Table 1), which led to a soil enrichment of P labile.

Table 1 - Total P content in the surface soil (depth = 0–3 cm) from the Rio Doce Estuary (2015), and the eutrophication risk in other estuaries worldwide according to the respective total P contents in the soils.

Site	Total P soil ($mg \cdot kg^{-1}$)	P source	Eutrophication risk‡	Reference
This study (2015)†	*430 ± 200*	*Mariana disaster*	-	-
Yangtze River Estuary, China	721 ± 105	Natural water and solid discharge	High	Jin et al. (2013)
Mai Po Marshes, China	1546 ± 550	Shrimp farming	Eutrophicated	Lai and Lam, (2008)
Lake Pontchartrain, USA	455 ± 47	Seasonal runoff	High	Roy et al. (2012)
Yellow River Delta, China	594 ± 56	Agricultural, industrial, and urban sewage	High	Sun et al. (2012)
Bronx River, USA	583 ± 628	Industrial and urban sewage	High	Wang and Pant, (2010)
Han River, South Korea	480 ± 151	Agricultural, fish farming, and seasonal runoff	High	Kim et al. (2003)

† Mean ± Standard Deviation for P contents for 0–3 cm depth, representing deposition of mining tailings. ‡ According to the respective authors.

On another hand, our results suggest that P may be continually added to the estuarine soils via adsorption by Fe oxyhydroxides and gradually released into the estuary waters in response to the rapid geochemical transformations of the Fe forms in environments with Fe enrichments. Additionally, geochemical Fe transformations and its subsequent effect on P availability may vary with seasons (Li et al., 2017; Thibault de Chanvalon et al., 2016). For instance, previous studies reported higher organic carbon, Fe, and P loads during wet seasons as a result of river floods leading to anoxic conditions, enhancing of iron reduction process and P availability (McKee et al., 2000; Monbet et al., 2009; Zwolsman, 1994).

Understanding the P contents and the risks of eutrophication obtained from this study could be applied to other redox-dynamic environments (such as estuaries, lakes, streams, wetlands, and coastal humid areas) receiving large amounts of Fe-rich material associated

with P. Thus, the concerns raised in this study go beyond the Rio Doce estuarine system, since many other cases involving large amounts of Fe-rich tailings discharged into redox-dynamic environments such as rivers and lakes have occurred in other parts of the world e.g., the Shag River in New Zealand where at least 85,000 tons of mine tailings were dumped into the river (Black et al., 2004), the Tinto and Odiel rivers in Spain with large runoff of dissolved Fe into the estuaries (Braungardt et al., 2003), Doñana Park in Spain where a massive amounts of Fe-rich mud was spilled from the accident in Aznalcollar (Grimalt et al., 1999), the Bøkfjorden Estuary in Norway affected by tailing discharges from an Fe ore mine (Brooks et al., 2015), and the Brumadinho Disaster in Brazil which in 2019, approximately 12 million cubic meters of Fe ore tailing were discharged into the Paraopeba River after the Brumadinho dam rupture (Rotta et al., 2020; Thompson et al., 2020).

Thus, for estuaries with Fe enrichment from disaster or from natural flows (e.g., sediment transport) linked to P loads from anthropogenic activities as sewage discharge, agricultural fertilizers, urban waste, or natural sources, leads to changes to P-cycling mechanisms, with soils from estuaries switching from P sinks to sources of P (Jarvie et al., 2005).

6.5. Conclusions

Our study showed that although Fe oxyhydroxides have been widely reported as the key mineral phases for the immobilization of P in soils, they can trigger a rapid release of P in estuarine soils. Our results proved that the high P loads associated with the Fe mine tailings arising from the world's biggest mining disaster to date (i.e., the Mariana disaster in Brazil) mainly constituted highly crystalline Fe oxyhydroxides (goethite and hematite). The redox oscillating conditions in the estuarine soils caused rapid Fe transformations, leading to a large P release in both the soil and water of the estuary. The loss of Fe oxides through this reductive dissolution was followed by a loss of Fe oxide crystallinity, which further increased P availability. Accordingly, a significant release of bioavailable P likely degraded the health of the ecosystem and raised the risk of eutrophication in the Rio Doce Estuary. Thus, long-term monitoring to evaluate the trophic state in the Rio Doce estuary is required as well as strategies for its remediation.

Acknowledgments

This work was funded by grants to AFB and TOF from Fundação de Amparo do Espirito Santo (FAPES Rio Doce 77683544/2017 and Sinapse 81712405/2018), Coordenação de Aperfeiçoamento de Pessoal de Nível Superior CAPES (Finance Code 001), and CNPq (grant numbers 301161/2017-8 and 305996/2018-5 to AFB and TOF, respectively). The authors are also grateful for the financial support provided by the São Paulo Research Foundation (FAPESP; grant numbers 2018/04259-2; 2019/02855-0; 2019/19987-6 and 2018/08408-2 to HMQ, DB, and TOF, respectively), Xunta de Galicia-Consellería de Educación e Ordeanción Universitaria de Galicia (Consolidation of Competitive Groups of Investigation; GRC GI 1574), CRETUS Strategic Group (AGRUP2015/02), and Fundação de Amparo à Pesquisa do Estado do Rio de Janeiro (JCNE grant number FAPERJ E-26/202.757/2019 to GNN).

References

Ajmal, Z., Muhmood, A., Usman, M., Kizito, S., Lu, J., Dong, R., Wu, S., 2018. Phosphate removal from aqueous solution using iron oxides: Adsorption, desorption and regeneration characteristics. J. Colloid Interface Sci. 528, 145–155. https://doi.org/10.1016/j.jcis.2018.05.084

Antelo, J., Avena, M., Fiol, S., López, R., Arce, F., 2005. Effects of pH and ionic strength on the adsorption of phosphate and arsenate at the goethite-water interface. J. Colloid Interface Sci. 285, 476–486. https://doi.org/10.1016/j.jcis.2004.12.032

Araújo Júnior, J.M. de C., Ferreira, T.O., Suarez-Abelenda, M., Nóbrega, G.N., Albuquerque, A.G.B.M., Bezerra, A. de C., Otero, X.L., 2016. The role of bioturbation by Ucides cordatus crab in the fractionation and bioavailability of trace metals in tropical semiarid mangroves. Mar. Pollut. Bull. 111, 194–202. https://doi.org/10.1016/j.marpolbul.2016.07.011

Arias, M., Da Silva-Carballal, J., García-Río, L., Mejuto, J., Núñez, A., 2006. Retention of phosphorus by iron and aluminum-oxides-coated quartz particles. J. Colloid Interface Sci. 295, 65–70. https://doi.org/10.1016/j.jcis.2005.08.001

Arroyave, J.M., Puccia, V., Zanini, G.P., Avena, M.J., 2018. Surface speciation of phosphate on goethite as seen by InfraRed Surface Titrations (IRST). Spectrochim. Acta - Part A Mol. Biomol. Spectrosc. 199, 57–64. https://doi.org/10.1016/j.saa.2018.03.043

Barcellos, D., Cyle, K.T., Thompson, A., 2018. Faster redox fluctuations can lead to higher iron reduction rates in humid forest soils. Biogeochemistry 137, 367–378. https://doi.org/10.1007/s10533-018-0427-0

Barcellos, D., Queiroz, H.M., Nóbrega, G.N., de Oliveira Filho, R.L., Santaella, S.T., Otero, X.L., Ferreira, T.O., 2019. Phosphorus enriched effluents increase eutrophication risks for mangrove systems in northeastern Brazil. Mar. Pollut. Bull. 142, 58–63. https://doi.org/10.1016/j.marpolbul.2019.03.031

BBC, 2016. Samarco dam failure in Brazil "caused by design flaws" - BBC News [WWW Document]. BBC. URL https://www.bbc.com/news/business-37218145 (accessed 11.17.19).

Bhattacharyya, A., Campbell, A.N., Tfaily, M.M., Lin, Y., Kukkadapu, R.K., Silver, W.L., Nico, P.S., Pett-Ridge, J., 2018. Redox Fluctuations Control the Coupled Cycling of Iron and Carbon in Tropical Forest Soils. Environ. Sci. Technol. 52, 14129–14139. https://doi.org/10.1021/acs.est.8b03408

Black, A., Craw, D., Youngson, J.., Karubaba, J., 2004. Natural recovery rates of a river system impacted by mine tailing discharge: Shag River, East Otago, New Zealand. J. Geochemical Explor. 84, 21–34. https://doi.org/10.1016/j.gexplo.2004.02.002

Boeykens, S.P., Piol, M.N., Samudio Legal, L., Saralegui, A.B., Vázquez, C., 2017. Eutrophication decrease: Phosphate adsorption processes in presence of nitrates. J. Environ. Manage. 203, 888–895. https://doi.org/10.1016/j.jenvman.2017.05.026

Bonneville, S., Behrends, T., Van Cappellen, P., 2009. Solubility and dissimilatory reduction kinetics of iron(III) oxyhydroxides: A linear free energy relationship. Geochim. Cosmochim. Acta 73, 5273–5282. https://doi.org/10.1016/j.gca.2009.06.006

Boukemara, L., Boukhalfa, C., 2012. Phosphate removal from aqueous solution by hydrous iron oxide freshly prepared effects of pH, iron concentration and competitive ions. Procedia Eng. 33, 163–167. https://doi.org/10.1016/j.proeng.2012.01.1189

Braungardt, C.B., Achterberg, E.P., Elbaz-Poulichet, F., Morley, N.H., 2003. Metal geochemistry in a mine-polluted estuarine system in Spain. Appl. Geochemistry 18, 1757–1771. https://doi.org/10.1016/S0883-2927(03)00079-9

Brookins, D.G., 1988. Eh-pH diagrams for geochemistry, 1st ed. Springer-Verlag Berlin Heidelberg. https://doi.org/10.1007/978-3-642-73093-1

Brooks, S.J., Harman, C., Hultman, M.T., Berge, J.A., 2015. Integrated biomarker assessment of the effects of tailing discharges from an iron ore mine using blue mussels (Mytilus spp.). Sci. Total Environ. 524–525, 104–114. https://doi.org/10.1016/j.scitotenv.2015.03.135

Bücking, C., Schicklberger, M., Gescher, J., 2013. The Biochemistry of Dissimilatory Ferric Iron and Manganese Reduction in Shewanella oneidensis, in: Gescher, J., Kappler, A. (Eds.), Microbial Metal Respiration. Springer Berlin Heidelberg, Berlin, Heidelberg, pp. 49–82. https://doi.org/10.1007/978-3-642-32867-1_3

Burdige, D.J., Komada, T., 2020. Iron redox cycling, sediment resuspension and the role of sediments in low oxygen environments as sources of iron to the water column. Mar. Chem. 223, 103793. https://doi.org/10.1016/j.marchem.2020.103793

Canfield, D.E., Thamdrup, B., Hansen, J.W., 1993. The anaerobic degradation of organic matter in Danish coastal sediments: Iron reduction, manganese reduction, and sulfate reduction. Geochim. Cosmochim. Acta 57, 3867–3883. https://doi.org/10.1016/0016-7037(93)90340-3

Ceulemans, T., Bodé, S., Bollyn, J., Harpole, S., Coorevits, K., Peeters, G., Van Acker, K., Smolders, E., Boeckx, P., Honnay, O., 2017. Phosphorus resource partitioning shapes phosphorus acquisition and plant species abundance in grasslands. Nat. Plants 3, 16224. https://doi.org/10.1038/nplants.2016.224

Charana Walpola, B., 2012. Prospectus of phosphate solubilizing microorganisms and phosphorus availability in agricultural soils: A review. African J. Microbiol. Res. 6, 6600–6605. https://doi.org/10.5897/ajmr12.889

Charette, M.A., Sholkovitz, E.R., Hansel, C.M., 2005. Trace element cycling in a subterranean estuary: Part 1. Geochemistry of the permeable sediments. Geochim. Cosmochim. Acta 69, 2095–2109. https://doi.org/10.1016/j.gca.2004.10.024

Chen, C., Meile, C., Wilmoth, J., Barcellos, D., Thompson, A., 2018. Influence of pO 2 on Iron Redox Cycling and Anaerobic Organic Carbon Mineralization in a Humid Tropical Forest Soil. Environ. Sci. Technol. 52, 7709–7719. https://doi.org/10.1021/acs.est.8b01368

Chung, H.-K., Kim, W.-H., Park, J., Cho, J., Jeong, T.-Y., Park, P.-K., 2015. Application of Langmuir and Freundlich isotherms to predict adsorbate removal efficiency or required amount of adsorbent. J. Ind. Eng. Chem. 28, 241–246. https://doi.org/10.1016/j.jiec.2015.02.021

Coelho, J.P.P., Flindt, M.R.R., Jensen, H.S.S., Lillebø, A.I.I., Pardal, M.A.A., 2004. Phosphorus speciation and availability in intertidal sediments of a temperate estuary: Relation to eutrophication and annual P-fluxes. Estuar. Coast. Shelf Sci. 61, 583–590. https://doi.org/10.1016/j.ecss.2004.07.001

CONAMA, 2005. Brazilian water quality guidelines. Resolution n. 357 - 2005.

Cornell, R.M., Schwertmann, U., 2003. The Iron Oxides: Structure, Reactions, Occurences and Uses, WILEY-VCH. https://doi.org/10.1002/3527602097.ch1

Cui, H.-J., Wang, M.K., Fu, M.-L., Ci, E., 2011. Enhancing phosphorus availability in phosphorus-fertilized zones by reducing phosphate adsorbed on ferrihydrite using rice straw-derived biochar. J. Soils Sediments 11, 1135–1141. https://doi.org/10.1007/s11368-011-0405-9

Davranche, M., Dia, A., Fakih, M., Nowack, B., Gruau, G., Ona-nguema, G., Petitjean, P., Martin, S., Hochreutener, R., 2013. Organic matter control on the reactivity of Fe(III)-oxyhydroxides and associated As in wetland soils: A kinetic modeling study. Chem. Geol. 335, 24–35. https://doi.org/10.1016/j.chemgeo.2012.10.040

Du Laing, G., Meers, E., Dewispelaere, M., Rinklebe, J., Vandecasteele, B., Verloo, M.G., Tack, F.M.G., 2009a. Effect of Water Table Level on Metal Mobility at Different Depths in Wetland Soils of the Scheldt Estuary (Belgium). Water. Air. Soil Pollut. 202, 353–367. https://doi.org/10.1007/s11270-009-9982-2

Du Laing, G., Rinklebe, J., Vandecasteele, B., Meers, E., Tack, F.M.G., 2009b. Trace metal behaviour in estuarine and riverine floodplain soils and sediments: A review. Sci. Total Environ. 407, 3972–3985. https://doi.org/10.1016/j.scitotenv.2008.07.025

Ekholm, P., Lehtoranta, J., 2012. Does control of soil erosion inhibit aquatic eutrophication? J. Environ. Manage. 93, 140–146. https://doi.org/10.1016/j.jenvman.2011.09.010

Elser, J.J., Bracken, M.E.S., Cleland, E.E., Gruner, D.S., Harpole, W.S., Hillebrand, H., Ngai, J.T., Seabloom, E.W., Shurin, J.B., Smith, J.E., 2007. Global analysis of nitrogen and phosphorus limitation of primary producers in freshwater, marine and terrestrial ecosystems. Ecol. Lett. 10, 1135–1142. https://doi.org/10.1111/j.1461-0248.2007.01113.x

Escobar, H., 2015. Mud tsunami wreaks ecological havoc in Brazil. Science (80-.). 350, 1138–1139. https://doi.org/10.1126/science.350.6265.1138

Esteves, B. dos S., Suzuki, M.S., 2013. Nitrogen and phosphorus resorption efficiency, and N : P ratios in natural populations of Typha domingensis Pers. in a coastal tropical lagoon. Acta Limnol. Bras. 25, 124–130. https://doi.org/10.1590/s2179-975x2013000200003

Figueiredo, J.A. de, Noriega, C.D., Oliveira, E.M.C. de, Rodrigues Neto, R., Barroso, G.F., Araújo Filho, M., 2014. Avaliação biogeoquímica de águas fluviais com ênfase no comportamento dos compostos de nitrogênio e fósforo total para diagnoses provenientes do sistema aquático Bacia do Rio Doce, no Espírito Santo. Geochim. Bras. 28, 215–226. https://doi.org/10.5327/z0102-9800201400020009

Filippelli, G.M., Delaney, M.L., 1994. The oceanic phosphorus cycle and continental weathering during the Neogene. Paleoceanography 9, 643–652. https://doi.org/10.1029/94PA01453

Fink, J.R., Inda, A.V., Tiecher, T., Barrón, V., 2016. Iron oxides and organic matter on soil phosphorus availability. Cienc. e Agrotecnologia 40, 369–379. https://doi.org/10.1590/1413-70542016404023016

Fortin, D., Leppard, G.G., Tessier, A., 1993. Characteristics of lacustrine diagenetic iron oxyhydroxides. Geochim. Cosmochim. Acta 57, 4391–4404. https://doi.org/10.1016/0016-7037(93)90490-N

Gabriel, F.A., Silva, A.G., Queiroz, H.M., Ferreira, T.O., Hauser-Davis, R.A., Bernardino, A.F., 2020. Ecological Risks of Metal and Metalloid Contamination in the Rio Doce Estuary. Integr. Environ. Assess. Manag. 16, 655–660. https://doi.org/10.1002/ieam.4250

Gomes, L.E. de O., Correa, L.B., Sá, F., Neto, R.R., Bernardino, A.F., 2017. The impacts of the Samarco mine tailing spill on the Rio Doce estuary, Eastern Brazil. Mar. Pollut. Bull. 120, 28–36. https://doi.org/10.1016/j.marpolbul.2017.04.056

Grimalt, J.O., Ferrer, M., Macpherson, E., 1999. The mine tailing accident in Aznalcollar. Sci. Total Environ. 242, 3–11. https://doi.org/10.1016/S0048-9697(99)00372-1

Guzman, G., Alcantara, E., Barron, V., Torrent, J., 1994. Phytoavailability of phosphate adsorbed on ferrihydrite, hematite, and goethite. Plant Soil 159, 219–225. https://doi.org/10.1007/BF00009284

Holtan, H., Kamp-Nielsen, L., Stuanes, A.O., 1988. Phosphorus in soil, water and sediment: an overview. Hydrobiologia 170, 19–34. https://doi.org/10.1007/BF00024896

Howard, J., Hoyt, S., Isensee, K., Telszewski, M., Pidgeon, E., Telszewski, M., 2014. Coastal blue carbon: methods for assessing carbon stocks and emissions factors in mangroves, tidal salt marshes, and seagrasses, Conservation International. Conservation International, Intergovernmental Oceanographic Commission of UNESCO, International Union for Conservation of Nature, Arlington, VA, USA, Arlington, VA, USA.

Huerta-Diaz, M.A., Morse, J.W., 1990. A quantitative method for determination of trace metal concentrations in sedimentary pyrite. Mar. Chem. 29, 119–144. https://doi.org/10.1016/0304-4203(90)90009-2

Jardim, F.A., von Sperling, E., Jardim, B.F. de M., Almeida, K.C. de B., 2014. Fatores determinantes das florações de cianobactérias na água do Rio Doce, Minas Gerais, Brasil. Eng. Sanit. e Ambient. 19, 207–218. https://doi.org/10.1590/S1413-41522014019000001026

Jarvie, H.P., Jürgens, M.D., Williams, R.J., Neal, C., Davies, J.J.L., Barrett, C., White, J., 2005. Role of river bed sediments as sources and sinks of phosphorus across two major eutrophic UK river basins: The Hampshire Avon and Herefordshire Wye. J. Hydrol. 304, 51–74. https://doi.org/10.1016/j.jhydrol.2004.10.002

Jiménez-Cárceles, F.J., Álvarez-Rogel, J., 2008. Phosphorus fractionation and distribution in salt marsh soils affected by mine wastes and eutrophicated water: A case study in SE Spain. Geoderma 144, 299–309. https://doi.org/10.1016/j.geoderma.2007.11.024

Jin, X., He, Y., Kirumba, G., Hassan, Y., Li, J., 2013. Phosphorus fractions and phosphate sorption-release characteristics of the sediment in the Yangtze River estuary reservoir. Ecol. Eng. 55, 62–66. https://doi.org/10.1016/j.ecoleng.2013.02.001

Kämpf, N., Schwertmann, N., 1982. Quantitative determination of goethite and hematite in kaolinitic soils by X-ray diffraction. Clay Miner. 17, 359–363. https://doi.org/10.1180/claymin.1982.017.3.08

Karimian, N., Johnston, S.G., Burton, E.D., 2018. Iron and sulfur cycling in acid sulfate soil wetlands under dynamic redox conditions: A review. Chemosphere 197, 803–816. https://doi.org/10.1016/j.chemosphere.2018.01.096

Kim, J., Li, W., Philips, B.L., Grey, C.P., 2011. Phosphate adsorption on the iron oxyhydroxides goethite (α-FeOOH), akaganeite (β-FeOOH), and lepidocrocite (γ-FeOOH): a 31P NMR Study. Energy Environ. Sci. 4, 4298–4305. https://doi.org/10.1039/C1EE02093E

Kim, L.-H., Choi, E., Stenstrom, M.K., 2003. Sediment characteristics, phosphorus types and phosphorus release rates between river and lake sediments. Chemosphere 50, 53–61. https://doi.org/10.1016/S0045-6535(02)00310-7

Kraal, P., Burton, E.D., Rose, A.L., Kocar, B.D., Lockhart, R.S., Grice, K., Bush, R.T., Tan, E., Webb, S.M., 2015. Sedimentary iron–phosphorus cycling under contrasting redox conditions in a eutrophic estuary. Chem. Geol. 392, 19–31. https://doi.org/10.1016/j.chemgeo.2014.11.006

Kristensen, E., Bouillon, S., Dittmar, T., Marchand, C., 2008. Organic carbon dynamics in mangrove ecosystems: A review. Aquat. Bot. 89, 201–219. https://doi.org/10.1016/j.aquabot.2007.12.005

Krumina, L., Kenney, J.P.L., Loring, J.S., Persson, P., 2016. Desorption mechanisms of phosphate from ferrihydrite and goethite surfaces. Chem. Geol. 427, 54–64. https://doi.org/10.1016/j.chemgeo.2016.02.016

LaForce, M.J., Hansel, C.M., Fendorf, S., 2000. Constructing Simple Wetland Sampling Devices. Soil Sci. Soc. Am. J. 64, 809–811. https://doi.org/10.2136/sssaj2000.642809x

Lai, D.Y.F., Lam, K.C., 2008. Phosphorus retention and release by sediments in the eutrophic Mai Po Marshes, Hong Kong. Mar. Pollut. Bull. 57, 349–356. https://doi.org/10.1016/j.marpolbul.2008.01.038

Lalley, J., Han, C., Li, X., Dionysiou, D.D., Nadagouda, M.N., 2016. Phosphate adsorption using modified iron oxide-based sorbents in lake water: Kinetics, equilibrium, and column tests. Chem. Eng. J. 284, 1386–1396. https://doi.org/10.1016/j.cej.2015.08.114

Larsen, O., Postma, D., 2001. Kinetics of reductive bulk dissolution of lepidocrocite, ferrihydrite, and goethite. Geochim. Cosmochim. Acta 65, 1367–1379. https://doi.org/10.1016/S0016-7037(00)00623-2

Levar, C.E., Hoffman, C.L., Dunshee, A.J., Toner, B.M., Bond, D.R., 2017. Redox potential as a master variable controlling pathways of metal reduction by Geobacter sulfurreducens. ISME J. 11, 741–752. https://doi.org/10.1038/ismej.2016.146

Li, R., Xu, J., Li, X., Shi, Z., Harrison, P.J., 2017. Spatiotemporal Variability in Phosphorus Species in the Pearl River Estuary: Influence of the River Discharge. Sci. Rep. 7, 13649. https://doi.org/10.1038/s41598-017-13924-w

Lima, A.T., Bastos, F.A., Teubner, F.J., Neto, R.R., Cooper, A., Barroso, G.F., 2020. Strengths and Weaknesses of a Hybrid Post-disaster Management Approach: the Doce River (Brazil) Mine-Tailing Dam Burst. Environ. Manage. 65, 711–724. https://doi.org/10.1007/s00267-020-01279-4

Liptzin, D., Silver, W.L., 2009. Effects of carbon additions on iron reduction and phosphorus availability in a humid tropical forest soil. Soil Biol. Biochem. 41, 1696–1702. https://doi.org/10.1016/j.soilbio.2009.05.013

Lovley, D.R., Holmes, D.E., Nevin, K.P., 2004. Dissimilatory Fe(III) and Mn(IV) Reduction, in: Advances in Microbial Physiology. pp. 219–286. https://doi.org/10.1016/S0065-2911(04)49005-5

Luengo, C., Brigante, M., Antelo, J., Avena, M., 2006. Kinetics of phosphate adsorption on goethite: Comparing batch adsorption and ATR-IR measurements. J. Colloid Interface Sci. 300, 511–518. https://doi.org/10.1016/j.jcis.2006.04.015

Marques, M.M., Barbosa, F., 2001. Biological quality of waters from an impacted tropical watershed (middle Rio Doce basin, southeast Brazil), using benthic macroinvertebrate communities as an indicator. Hydrobiologia 457, 69–76. https://doi.org/10.1023/A:1012297915323

Marta-Almeida, M., Mendes, R., Amorim, F.N., Cirano, M., Dias, J.M., 2016. Fundão Dam collapse: Oceanic dispersion of River Doce after the greatest Brazilian environmental accident. Mar. Pollut. Bull. 112, 359–364. https://doi.org/10.1016/j.marpolbul.2016.07.039

McKee, L.J., Eyre, B.D., Hossain, S., 2000. Transport and retention of nitrogen and phosphorus in the sub-tropical Richmond River estuary, Australia - A budget approach. Biogeochemistry 50, 241–278. https://doi.org/10.1023/A:1006339910533

Medeiros, A.O., Missagia, B.S., Brandão, L.R., Callisto, M., Barbosa, F.A.R., Rosa, C.A., 2012. Water quality and diversity of yeasts from tropical lakes and rivers from the Rio Doce basin in Southeastern Brazil. Brazilian J. Microbiol. 43, 1582–1594. https://doi.org/10.1590/S1517-83822012000400043

Monbet, P., McKelvie, I.D., Worsfold, P.J., 2009. Dissolved organic phosphorus speciation in the waters of the Tamar estuary (SW England). Geochim. Cosmochim. Acta 73, 1027–1038. https://doi.org/10.1016/j.gca.2008.11.024

Murphy, J., Riley, J.P., 1962. A modified single solution method for the determination of phosphate in natural waters. Anal. Chim. Acta 27, 31–36. https://doi.org/10.1016/S0003-2670(00)88444-5

Nóbrega, G.N., Ferreira, T.O., Romero, R.E., Marques, A.G.B., Otero, X.L., 2013. Iron and sulfur geochemistry in semi-arid mangrove soils (Ceará, Brazil) in relation to seasonal changes and shrimp farming effluents. Environ. Monit. Assess. 185, 7393–7407. https://doi.org/10.1007/s10661-013-3108-4

Nóbrega, G.N., Otero, X.L., Macías, F., Ferreira, T.O., 2014. Phosphorus geochemistry in a Brazilian semiarid mangrove soil affected by shrimp farm effluents. Environ. Monit. Assess. 186, 5749–5762. https://doi.org/10.1007/s10661-014-3817-3

Otero, X.L., De La Peña-Lastra, S., Pérez-Alberti, A., Ferreira, T.O., Huerta-Diaz, M.A., 2018. Seabird colonies as important global drivers in the nitrogen and phosphorus cycles. Nat. Commun. 9. https://doi.org/10.1038/s41467-017-02446-8

Otero, X.L., Ferreira, T.O., Huerta-Díaz, M.A., Partiti, C.S.M., Souza, V., Vidal-Torrado, P., Macías, F., 2009. Geochemistry of iron and manganese in soils and sediments of a mangrove system, Island of Pai Matos (Cananeia — SP, Brazil). Geoderma 148, 318–335. https://doi.org/10.1016/j.geoderma.2008.10.016

Otero, X.L., Tejada, O., Martín-Pastor, M., De La Peña, S., Ferreira, T.O., Pérez-Alberti, A., 2015. Phosphorus in seagull colonies and the effect on the habitats. The case of yellow-legged gulls (Larus michahellis) in the Atlantic Islands National Park (Galicia-NW Spain). Sci. Total Environ. 532, 383–397. https://doi.org/10.1016/j.scitotenv.2015.06.013

Paludan, C., Morris, J.T., 1999. Distribution and speciation of phosphorus along a salinity gradient in intertidal marsh sediments. Biogeochemistry 45, 197–221. https://doi.org/https://doi.org/10.1023/A:1006136621465

Pan, W., Kan, J., Inamdar, S., Chen, C., Sparks, D., 2016. Dissimilatory microbial iron reduction release DOC (dissolved organic carbon) from carbon-ferrihydrite association. Soil Biol. Biochem. 103, 232–240. https://doi.org/10.1016/j.soilbio.2016.08.026

Parsons, C.T., Rezanezhad, F., O'Connell, D.W., Van Cappellen, P., 2017. Sediment phosphorus speciation and mobility under dynamic redox conditions. Biogeosciences 14, 3585–3602. https://doi.org/10.5194/bg-14-3585-2017

Paytan, A., McLaughlin, K., 2007. The oceanic phosphorus cycle. Chem. Rev. 107, 563–576. https://doi.org/10.1021/cr0503613

Petrucio, M.M., Medeiros, A.O., Rosa, C.A., Barbosa, F.A.R., 2005. Trophic state and microorganisms community of major sub-basins of the middle Rio Doce basin, southeast Brazil. Brazilian Arch. Biol. Technol. 48, 625–633. https://doi.org/10.1590/S1516-89132005000500015

Phillips, D., 2016. Samarco dam collapse: one year on from Brazil's worst environmental disaster | Guardian Sustainable Business | The Guardian [WWW Document]. Guard. URL https://www.theguardian.com/sustainable-business/2016/oct/15/samarco-dam-collapse-brazil-worst-environmental-disaster-bhp-billiton-vale-mining (accessed 11.17.19).

Pires, A.P.F., Rezende, C.L., Assad, E.D., Loyola, R., Scarano, F.R., 2017. Forest restoration can increase the Rio Doce watershed resilience. Perspect. Ecol. Conserv. 15, 187–193. https://doi.org/10.1016/j.pecon.2017.08.003

Queiroz, H.M., Nóbrega, G.N., Ferreira, T.O., Almeida, L.S., Romero, T.B., Santaella, S.T., Bernardino, A.F., Otero, X.L., 2018. The Samarco mine tailing disaster: A possible time-bomb for heavy metals contamination? Sci. Total Environ. 637–638, 498–506. https://doi.org/10.1016/j.scitotenv.2018.04.370

Reimann, C., Filzmoser, P., Garrett, R.G., Dutter, R., 2008. Statistical Data Analysis Explained, Statistical Data Analysis Explained: Applied Environmental Statistics with R. John Wiley & Sons, Ltd, Chichester, UK. https://doi.org/10.1002/9780470987605

Reinhard, C.T., Planavsky, N.J., Gill, B.C., Ozaki, K., Robbins, L.J., Lyons, T.W., Fischer, W.W., Wang, C., Cole, D.B., Konhauser, K.O., 2017. Evolution of the global phosphorus cycle. Nature. https://doi.org/10.1038/nature20772

Rejmánková, E., 2001. Effect of experimental phosphorus enrichment on oligotrophic tropical marshes in Belize, Central America. Plant Soil 236, 33–53. https://doi.org/10.1023/A:1011953715153

Rhoton, F.E., Bigham, J.M., 2005. Phosphate Adsorption by Ferrihydrite-Amended Soils. J. Environ. Qual. 34, 890–896. https://doi.org/10.2134/jeq2004.0176

Richardson, A.E., Simpson, R.J., 2011. Soil microorganisms mediating phosphorus availability. Plant Physiol. 156, 989–996. https://doi.org/10.1104/pp.111.175448

Rotta, L.H.S., Alcântara, E., Park, E., Negri, R.G., Lin, Y.N., Bernardo, N., Mendes, T.S.G., Souza Filho, C.R., 2020. The 2019 Brumadinho tailings dam collapse: Possible cause and impacts of the worst human and environmental disaster in Brazil. Int. J. Appl. Earth Obs. Geoinf. 90, 102119. https://doi.org/10.1016/j.jag.2020.102119

Roy, E.D., Nguyen, N.T., Bargu, S., White, J.R., 2012. Internal loading of phosphorus from sediments of Lake Pontchartrain (Louisiana, USA) with implications for eutrophication. Hydrobiologia 684, 69–82. https://doi.org/10.1007/s10750-011-0969-9

Ruttenberg, K.C., 2001. Phosphorus Cycle, in: Encyclopedia of Ocean Sciences. Elsevier, pp. 401–412. https://doi.org/10.1016/B978-012374473-9.00277-0

Santolin, C.V.A., Ciminelli, V.S.T., Nascentes, C.C., Windmöller, C.C., 2015. Distribution and environmental impact evaluation of metals in sediments from the Doce River Basin, Brazil. Environ. Earth Sci. 74, 1235–1248. https://doi.org/10.1007/s12665-015-4115-2

Schendel, E.K., Schreier, H., Lavkulich, L.M., 2004. Linkages between phosphorus index estimates and environmental quality indicators. J. Soil Water Conserv. 59, 243–251.

Singh, B., Gilkes, R.J., 1991. Concentration of iron oxides from soil clays by 5 <scp>m</scp> NaOH treatment: the complete removal of sodalite and kaolin. Clay Miner. 26, 463–472. https://doi.org/10.1180/claymin.1991.026.4.02

Straub, K.L., Benz, M., Schink, B., 2000. Iron metabolism in anoxic environments at near neutral pH. FEMS Microbiol. Ecol. 34, 181–186. https://doi.org/10.1016/S0168-6496(00)00088-X

Strauss, R., Brümmer, G.W., Barrow, N.J., 1997. Effects of crystallinity of goethite: II. Rates of sorption and desorption of phosphate. Eur. J. Soil Sci. 48, 101–114. https://doi.org/10.1111/j.1365-2389.1997.tb00189.x

Sun, J., Xu, G., Shao, H., Xu, S., 2012. Potential Retention and Release Capacity of Phosphorus in the Newly Formed Wetland Soils from the Yellow River Delta, China. CLEAN - Soil, Air, Water 40, 1131–1136. https://doi.org/10.1002/clen.201100739

Tai, Y., Tam, N.F.-Y., Wang, R., Yang, Yang, Lin, J., Wang, J., Yang, Yufen, Li, L., Sun, Y., 2018. Iron plaque formation on wetland-plant roots accelerates removal of water-borne antibiotics. Plant Soil 433, 323–338. https://doi.org/10.1007/s11104-018-3843-y

Tessier, A., Campbell, P.G.C., Bisson, M., 1979. Sequential extraction procedure for the speciation of particulate trace metals. Anal. Chem. 51, 844–851. https://doi.org/10.1021/ac50043a017

Thibault de Chanvalon, A., Mouret, A., Knoery, J., Geslin, E., Péron, O., Metzger, E., 2016. Manganese, iron and phosphorus cycling in an estuarine mudflat, Loire, France. J. Sea Res. 118, 92–102. https://doi.org/10.1016/j.seares.2016.10.004

Thompson, F., de Oliveira, B.C., Cordeiro, M.C., Masi, B.P., Rangel, T.P., Paz, P., Freitas, T., Lopes, G., Silva, B.S., S. Cabral, A., Soares, M., Lacerda, D., dos Santos Vergilio, C., Lopes-Ferreira, M., Lima, C., Thompson, C., de Rezende, C.E., 2020. Severe impacts of the Brumadinho dam failure (Minas Gerais, Brazil) on the water quality of the Paraopeba River. Sci. Total Environ. 705, 135914. https://doi.org/10.1016/j.scitotenv.2019.135914

Torrent, J., Schwertmann, U., Barrón, V., 1992. Fast and Slow Phosphate Sorption by Goethite-Rich Natural Materials. Clays Clay Miner. 40, 14–21. https://doi.org/10.1346/CCMN.1992.0400103

Trazzi, P.A., Leahy, J.J., Hayes, M.H.B., Kwapinski, W., 2016. Adsorption and desorption of phosphate on biochars. J. Environ. Chem. Eng. 4, 37–46. https://doi.org/10.1016/j.jece.2015.11.005

USEPA, 1996. Method 3052, Microwave assisted acid digestion of siliceous and organically based matrices. Usepa 1–20. https://doi.org/10.1017/CBO9781107415324.004

Velde, B., Peck, T., 2002. Clay Mineral Changes in the Morrow Experimental Plots, University of Illinois. Clays Clay Miner. 50, 364–370. https://doi.org/10.1346/000986002760833738

Venturoti, G.P., Veronez, A.C., Salla, R. V., Gomes, L.C., 2015. Variation of limnological parameters in a tropical lake used for tilapia cage farming. Aquac. Reports 2, 152–157. https://doi.org/10.1016/j.aqrep.2015.09.006

Vitousek, P.M., Porder, S., Houlton, B.Z., Chadwick, O.A., 2010. Terrestrial phosphorus limitation: mechanisms, implications, and nitrogen–phosphorus interactions. Ecol. Appl. 20, 5–15. https://doi.org/10.1890/08-0127.1

Wang, F., Sims, J.T., Ma, L., Ma, W., Dou, Z., Zhang, F., 2011. The Phosphorus Footprint of China's Food Chain: Implications for Food Security, Natural Resource Management, and Environmental Quality. J. Environ. Qual. 40, 1081–1089. https://doi.org/10.2134/jeq2010.0444

Wang, J., Pant, H.K., 2010. Enzymatic hydrolysis of organic phosphorus in river bed sediments. Ecol. Eng. 36, 963–968. https://doi.org/10.1016/j.ecoleng.2010.03.006

Wang, X., Li, W., Harrington, R., Liu, F., Parise, J.B., Feng, X., Sparks, D.L., 2013a. Effect of ferrihydrite crystallite size on phosphate adsorption reactivity. Environ. Sci. Technol. 47, 10322–10331. https://doi.org/10.1021/es401301z

Wang, X., Liu, F., Tan, W., Li, W., Feng, X., Sparks, D.L., 2013b. Characteristics of Phosphate Adsorption-Desorption Onto Ferrihydrite. Soil Sci. 178, 1–11. https://doi.org/10.1097/SS.0b013e31828683f8

Wang, X., Zhu, M., Lan, S., Ginder-Vogel, M., Liu, F., Feng, X., 2015. Formation and secondary mineralization of ferrihydrite in the presence of silicate and Mn(II). Chem. Geol. 415, 37–46. https://doi.org/10.1016/j.chemgeo.2015.09.009

Weiss, J. V., Emerson, D., Megonigal, J.P., 2004. Geochemical control of microbial Fe(III) reduction potential in wetlands: Comparison of the rhizosphere to non-rhizosphere soil. FEMS Microbiol. Ecol. 48, 89–100. https://doi.org/10.1016/j.femsec.2003.12.014

Werner, E., Ami, N., 2014. The phosphorus cycle. Aquat. Ecol. 6, 347–363. https://doi.org/10.1007/978-94-017-8944-8_20

Wilson, G. V., Rhoton, F.E., Selim, H.M., 2004. Modeling the impact of ferrihydrite on adsorption-desorption of soil phosphorus. Soil Sci. 169, 271–281. https://doi.org/10.1097/01.ss.0000126841.03965.3a

Xu, C., Wong, V.N.L., Reef, R.E., 2020. Effect of inundation on greenhouse gas emissions from temperate coastal wetland soils with different vegetation types in southern Australia. Sci. Total Environ. 142949. https://doi.org/10.1016/j.scitotenv.2020.142949

Xue, R., Xu, J., Gu, L., Pan, L., He, Q., 2018. Study of Phosphorus Removal by Using Sponge Iron Adsorption. Water, Air, Soil Pollut. 229, 161. https://doi.org/10.1007/s11270-018-3753-x

Yan, J., Jiang, T., Yao, Y., Lu, S., Wang, Q., Wei, S., 2016. Preliminary investigation of phosphorus adsorption onto two types of iron oxide-organic matter complexes. J. Environ. Sci. (China) 42, 152–162. https://doi.org/10.1016/j.jes.2015.08.008

Yu, S., Miao, C., Song, H., Huang, Y., Chen, W., He, X., 2019. Efficiency of nitrogen and phosphorus removal by six macrophytes from eutrophic water. Int. J. Phytoremediation 21, 643–651. https://doi.org/10.1080/15226514.2018.1556582

Zachara, J.M., Fredrickson, J.K., Smith, S.C., Gassman, P.L., 2001. Solubilization of Fe(III) oxide-bound trace metals by a dissimilatory Fe(III) reducing bacterium. Geochim. Cosmochim. Acta 65, 75–93. https://doi.org/10.1016/S0016-7037(00)00500-7

Zhang, H., Elskens, M., Chen, G., Chou, L., 2019. Phosphate adsorption on hydrous ferric oxide (HFO) at different salinities and pHs. Chemosphere 225, 352–359. https://doi.org/10.1016/j.chemosphere.2019.03.068

Zhao, Q., Dunham-Cheatham, S., Adhikari, D., Chen, C., Patel, A., Poulson, S.R., Obrist, D., Verburg, P.S.J., Wang, X., Roden, E.R., Thompson, A., Yang, Y., 2020. Oxidation of soil organic carbon during an anoxic-oxic transition. Geoderma 377, 114584. https://doi.org/10.1016/j.geoderma.2020.114584

Zhu, M., Hu, X., Tu, C., Zhang, H., Song, F., Luo, Y., Christie, P., 2019. Sorption mechanisms of diphenylarsinic acid on ferrihydrite, goethite and hematite using sequential extraction, FTIR measurement and XAFS spectroscopy. Sci. Total Environ. 669, 991–1000. https://doi.org/10.1016/j.scitotenv.2019.03.166

Zwolsman, J.J.G., 1994. Seasonal Variability and Biogeochemistry of Phosphorus in the Scheldt Estuary, South-west Netherlands. Estuar. Coast. Shelf Sci. 39, 227–248. https://doi.org/10.1006/ecss.1994.1061

Supplementary Material

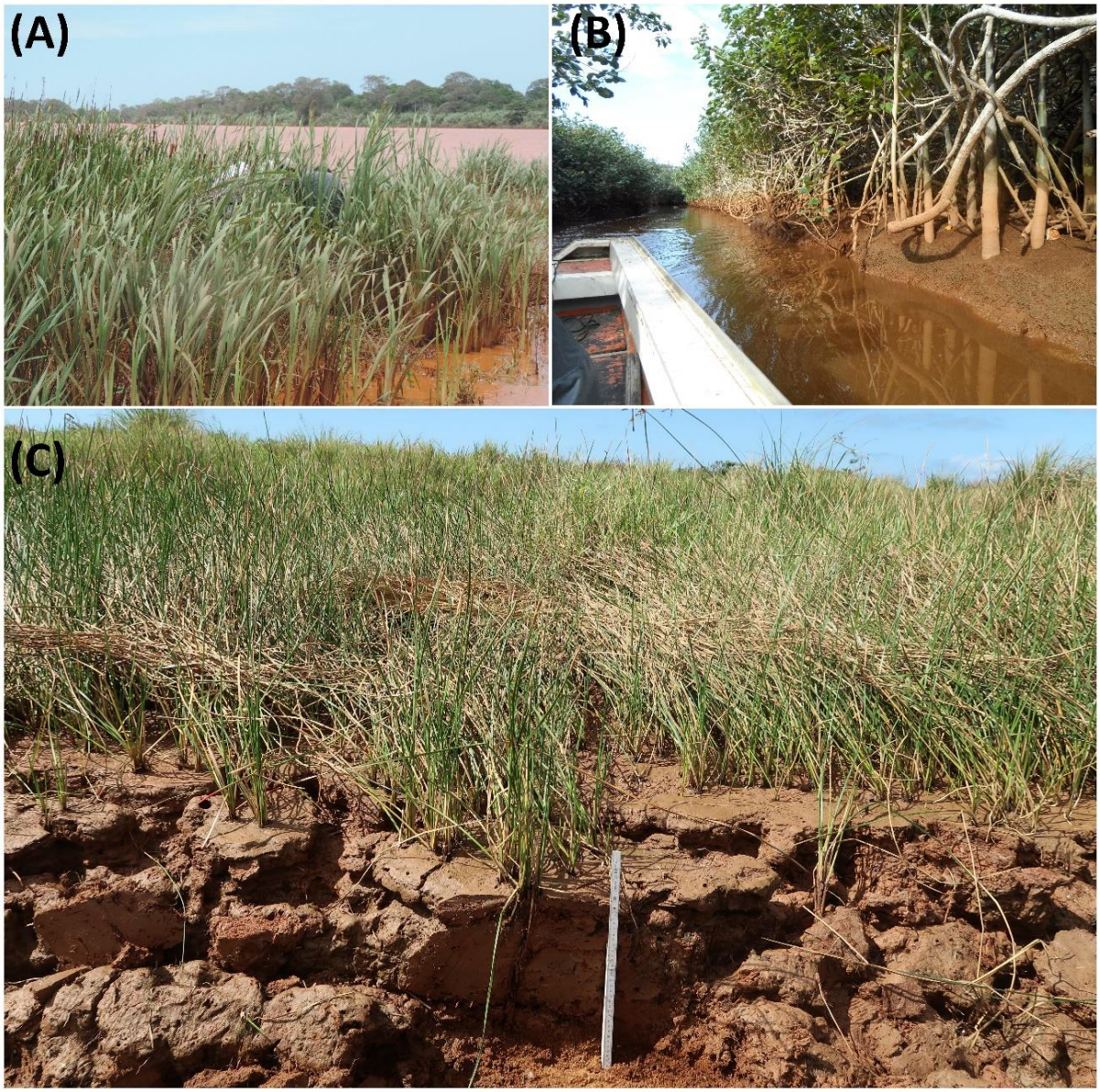

Fig. S1. An overview of predominant vegetations in the Rio Doce estuary: *Typha domingensis* (A; courtesy of Xosé L. Otero), *Hibiscus tiliaceus* (B; courtesy of Hermano M. Queiroz), and *Eleocharis acutangula* (C; courtesy of Youjun Deng).

Table S1 – Description of solid-phase fractionation analysis of iron (Fe) according to Tessier et al. (1979), Huerta-Diaz and Morse (1990), and Fortin et al. (1993).

Iron fraction	Abbreviation	Chemical Extractor/Procedure
Exchangeable and solube Fe	EX	Extracted with a 1 mol L^{-1} $MgCl_2$ solution at pH adjusted to 7
Fe associated with carbonates	CA	Extracted with a 1 mol L^{-1} NaOAc (sodium acetate) solution at pH 5
Fe associated with ferrihydrite and lepidocrocite, i.e, low crystallinity Fe phases	LC	Extracted with a 0.04 mol L^{-1} hydroxylamine + acetic acid 25 % (v/v) solution at 30 °C (ferrihydrite) and 96 °C (lepidocrocite)
Fe associated with hematite and goethite, i.e, high crystallinity Fe phases	CR	Extracted with a 0.25 mol L^{-1} sodium citrate + 0.11 mol L^{-1} sodium bicarbonate solution and 3 g of sodium dithionite at 75 °C
Fe associated to pyrite	PY	Extracted with concentrated HNO_3. Before extraction the samples were subjected to treatment with 10 mol L^{-1} HF to remove phyllosilicates Fe, and concentrated H_2SO_4 was then added to remove Fe associated with organic matter

Table S2 – Kruskal-Wallis non-parametric test summary for Total-P, Total-Fe, and Exch-P variables.

Variable	Average ± SD (mg·kg^{-1})				
	2015	2017	*p* value	*k* (Critical value)	K (Observed value)
Total P	289 ± 201	136 ± 78	0.0347	3.8415	4.4611
Pseudo-total Fe	74892 ± 66577	26726 ± 14849	0.0201	3.8415	5.4000
Exch-P	2.3 ± 0.4	3.8 ± 1.8	< 0.0001	3.8415	35.8311

SD: standard deviation; Exch-P= Exchangeable P; K = Kruskal-Wallis test;

7. IRON-RICH TAILINGS UNDER A REDOX ACTIVE ENVIRONMENT: MINERALOGICAL CHANGES AND POTENTIAL ENVIRONMENTAL CONSEQUENCES

Abstract

Iron (Fe) oxyhydroxides provide many functions in soils especially due to their high surface area and high surface charge density. However, much of the actual reactivity of Fe oxyhydroxides depends on their mineralogical characteristics (e.g., degree of crystallinity, isomorphic substitution, and crystal size). Detailed studies regarding the mineralogical characteristics of Fe oxyhydroxides are essential in predicting their stability and reactivity within the soils and sediments environment. The present study aimed to evaluate the mineralogical changes of an Fe-rich tailing and its potential environmental implications after the world's largest mining disaster. The mineralogical characteristics of the tailings were studied in four different years to assess how an active redox environment affects Fe oxyhydroxides and within which timeframe significant mineralogical changes may occur. Our results indicate an expressive crystallinity decrease in Fe oxyhydroxides which were initially composed (92.6 %) of high crystallinity Fe oxyhydroxides (i.e., goethite and hematite). Within 4 years the mineralogy shifted and poorly crystallinity Fe oxyhydroxides (i.e., lepidocrocite and ferrihydrite) represented 47% of Fe forms in 2019. In addition, SEM micrographs and mean crystal size evidenced a decrease in particle size from 109 nm to 49 nm for goethite at d_{111} plan. The changes in mean crystal size increases the reactivity of Fe oxyhydroxides resulting in a higher interaction with cationic and anionic species. The decreased crystallinity and increased reactivity led to higher susceptibility to reductive dissolution. Overall, our study evidence that the decrease in crystallinity coupled to the higher susceptibility to reductive dissolution of Fe oxyhydroxides can affect the fate of environmentally detrimental elements (e.g., phosphorus and metals) and, thus, increase the concentration of these pollutants in estuarine soils and waters.

Keywords: Samarco, iron oxyhydroxides, crystallinity, Fe minerals

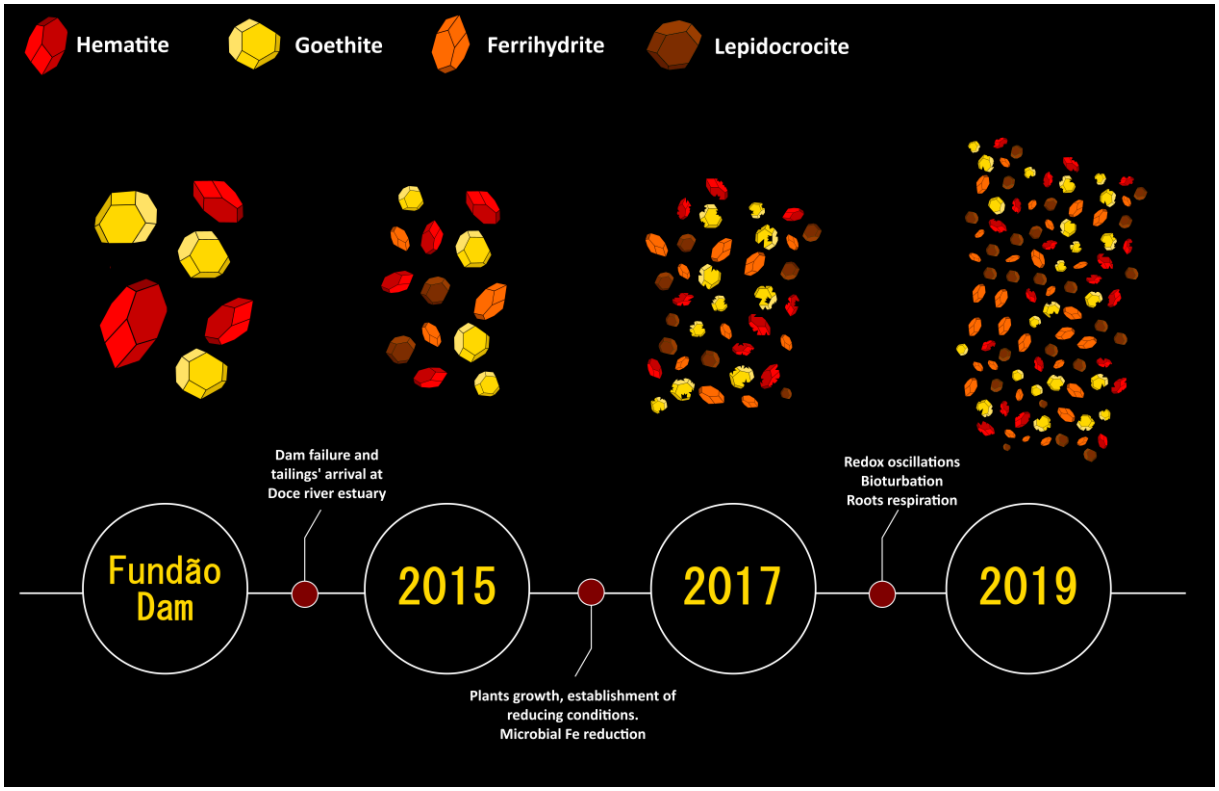

7.1. Introduction

Iron (Fe) ore production is one the most important mining activities worldwide with a production of approximately 3000 Mt a year (Lu 2015). However, Fe mining produces tons of tailings a year which usually are stored in dams (Zheng et al. 2011; Glombitza and Reichel 2014; Lu 2015). These produced tailings are mainly composed of fine particles rich in Fe oxides and hydroxides (e.g., hematite, goethite, maghemite, and magnetite) and minors quantities of quartz, kaolinite, gibbsite, and pyrite (Zhang et al. 2006; Lu 2015; Botha and Soares 2015; Silva et al. 2020).

Fe oxyhydroxides occur commonly as nanoparticles in soils and sediments (Fontes and Weed 1991; Faivre and Frankel 2016). Due to their small particle size (as small as 1 or 2 nanometers), large specific surface area (up to 600 $m^2\ g^{-1}$), high structural defects, they are among the most reactive minerals in terrestrial environments (Schwertmann 1988; Cornell and Schwertmann 2003).

Several Fe oxyhydroxides have been recognized; most of them commonly occur in natural environments (Bigham et al. 2002; Faivre and Frankel 2016). However, only eight are frequently found in soils and sediments e.g., hematite, maghemite, magnetite, ferrihydrite,

green rust, goethite, lepidocrocite, and schwertmannite (Bigham et al. 2002). The structure of Fe oxyhydroxides consists of close-packed arrays of anions, commonly forming three-dimension arrangements such as the octahedral and/or tetrahedral packings (Schwertmann and Taylor 1989). Their high specific surface areas, often > 100 m^2 g^{-1}, and the variability of minerals is a result of the arrangement of $Fe(O/OH)_6$, FeO_6, or FeO_4 (Bigham et al. 2002; Cornell and Schwertmann 2003).

In soils, Fe oxyhydroxides play numerous important functions such as providing sorption sites for nutrients (e.g., phosphorus; Fink et al. 2016), promoting organo-mineral interactions which increase soil organic matter stabilization (Wang et al. 2019), and attenuating the contamination of potentially toxic elements (e.g., metals; Herbert 1996; Rutten and de Lange 2003; Sherameti and Varma 2015). Within the soil environment, Fe oxyhydroxides are poorly soluble in a wide pH range (4–10) and in the absence of complexing (e.g., organic compounds) or reducing environments (e.g., anaerobic media). Under these common soil conditions Fe oxyhydroxides exhibit high stability within most terrestrial soils (Benjamin et al. 1996; Cornell and Schwertmann 2003; Hartley et al. 2004).

Contrastingly, in wetland soils and sediments, the stability of Fe oxyhydroxides experience a stability loss in response to the redox oscillating environment (Schwertmann 1991; Cummings et al. 2000). Under suboxic and/or anoxic soil conditions the reductive dissolution of Fe oxyhydroxides may take place (Lovley 1991; Reddy and DeLaune 2008). This is a conspicuous process in estuarine soils and sediments where these redox conditions are likely attended (Reddy and DeLaune 2008). The reducing of Fe oxyhydroxides promote, not only the mineral dissolution but, the release of the adsorbed cations and anions (Bonneville et al. 2004; Lovley et al. 2004).

In addition to the soil geochemical environment, some intrinsic properties of the different iron oxyhydroxides may affect its dissolution; e.g., surface area, degree of crystallinity, and isomorphic Al-substitution (Fontes and Weed 1991; Cornell and Schwertmann 2003). These characteristics are interrelated and their effects on mineral dissolution are associated with the structural disorder, crystal defects (e.g., vacancies), higher surface interactions resulting in a weakening of the Fe-O bonds and, ultimately, higher susceptibility to dissolution (Ruan and Gilkes 1995; Strauss et al. 1997; Larsen and Postma 2001).

Therefore, detailed studies regarding the mineralogical characteristics of Fe oxyhydroxides are essential in predicting, not only their stability and reactivity in soils and sediments environment, but also, the potential release of associated elements, such as potentially toxic elements (Buekers et al. 2008; Pereira et al. 2008; Harford et al. 2015; Gomes et al. 2017; Cui et al. 2020).

The present study aimed to assess the mineralogical changes in a Fe oxide-rich mine tailing deposited at the Doce River estuarine soils in 2015 after the world's largest mining disaster (Escobar 2015; Carmo et al. 2017). We performed a detailed mineralogical assessment in different years (2015, 2017 and 2020) using X-ray diffraction (XRD), attenuated total reflectance fourier transform infrared (ATR-FTIR), and scanning electron microscopy (SEM) in addition to different chemical analysis, such as total contents and sequential extraction procedures.

The Doce River estuary provides a unique field case to assess how an active redox environment affects iron oxides and within which timeframe significant mineralogical changes may occur. Additionally, previous studies have reported the presence of potentially toxic elements and phosphorus associated with the mine tailings Fe oxyhydroxides (Queiroz et al. 2018; Gabriel et al. 2020a). Thus, the present study is pivotal to determine the actual role of Fe oxyhydroxides in the fate of these environmentally detrimental elements (Queiroz et al. 2018, 2021a; Bernardino et al. 2019).

7.2. Materials and methods

7.2.1. Study site and sampling

The study site is located at the Doce River estuary, SE Brazil (19°38'–19°45'S and 39°45'–39°55'W; Fig. 1) which, in 2015, after the Fundão dam failure, received a large quantity of fine textured Fe-rich mining tailings (Gomes et al. 2017; Queiroz et al. 2018). The estuarine region is characterized by two distinct climate seasons: a dry season from April to September and a wet season from October to March marked by river flooding peaks (Mello et al. 2012; Gabriel et al. 2020a).

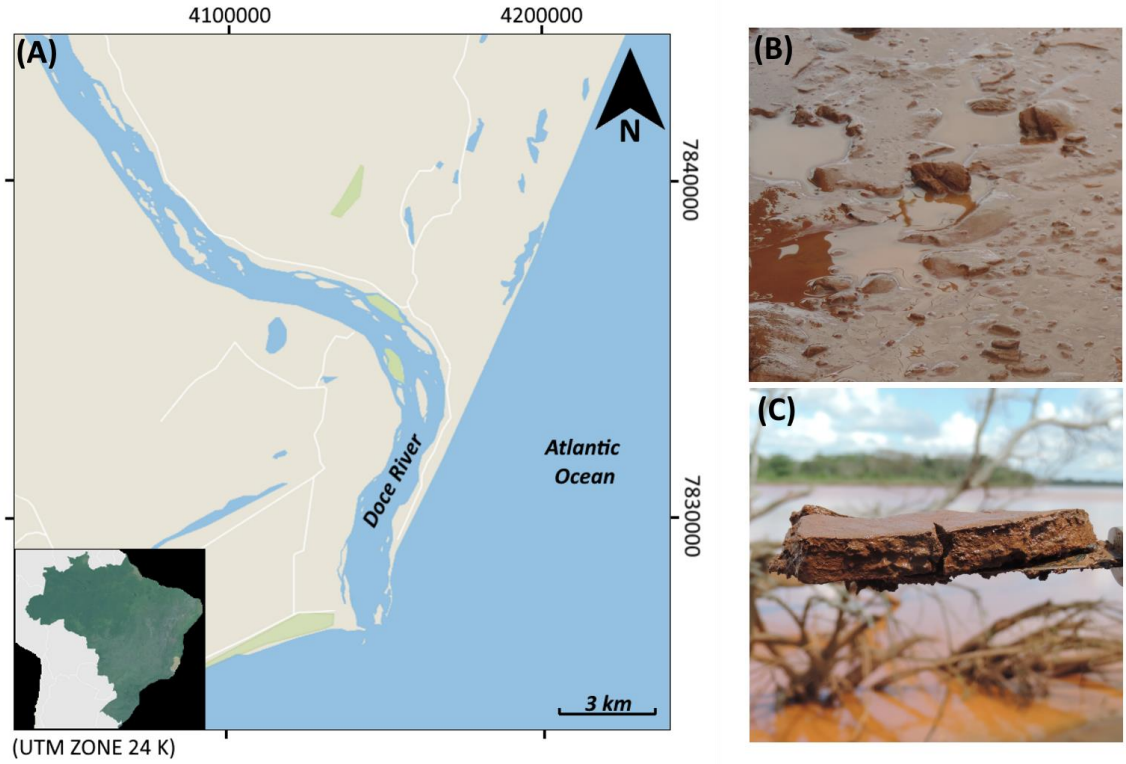

Fig. 1. Location of the studied site at the Doce River estuary, in the municipality of Regência, Espírito Santo state, Brazil (A). In detail, the freshly deposited iron tailings on the estuarine soils in 2015 (B) the ~ 5cm layer of the iron-rich fine textured tailing deposited on the estuary (C).

For the present study four sampling procedures were performed. Firstly, a tailing sample was collected from inside the Fundão dam. This sample was donated by the Brazilian National Mining Agency. At the estuary, three samplings were performed in different field campaigns. The first campaign was performed in 2015, seven days after the tailings' arrival at the estuary. The other two field campaigns were performed in 2017 in 2019; two and four years after the disaster, respectively. The estuarine samples were collected using polyvinyl chloride tubes attached to a waterlogged soil sampler (LaForce et al. 2000; Otero et al. 2009; Howard et al. 2014). All samplings were performed at the same locations to revisit the same sites over time. After collection, the samples were hermetically sealed and transported in the vertical position at a temperature of approximately 4 °C (LaForce et al. 2000; Howard et al. 2014; Nóbrega et al. 2014; Barcellos et al. 2019). In the laboratory the samples were sectioned and collected in the depth of 0–15 cm, which represents the depth most representative of the deposited tailings.

The pH and redox potential (Eh) values from all samples were obtained using portable meters. The pH was obtained using a glass electrode previously calibrated with standard

solutions (pH 4.0 and 7.0). The Eh values were recorded using a platinum electrode and values were adjusted by adding the value for the calomel reference electrode (+244 mV S.H.E.).

7.2.2. X-ray Diffraction and calculating of mean crystal size (MCS)

X-Ray Diffraction of the clay fraction (<2 μm) was obtained in a *Rigaku Miniflex II* device with CuKα radiation. The samples were scanned from 20–60° 2θ, step size of 0.02° 2θ and counting time of 5s step^{-1}. The samples were previously treated using sodium hypochlorite 9% to remove organic matter followed by sand removal by a wet sieving after the dispersion of the suspension with 0.01 mg L^{-1} Na_2CO_3. Clay separation from the silt fraction was performed by the sedimentation method (Stoke's law; Jackson 2005).

The mean crystal size (MCS) was calculated from the width of the half-height of the reflexes for Goethite (d_{110} and d_{111}) and Hematite (d_{104} and d_{110}) using the Scherrer formula (Klug and Alexander 1974) and after correcting the width at half-height using NaCl as an internal standard (Singh and Gilkes 1992).

7.2.3. Attenuated total reflectance Fourier transform infrared (ATR-FTIR)

ATR–FTIR data collection was obtained in PerkinElmer Two FT-IR spectrometer equipped with an N_2 purge gas. A diamond crystal was used for the spectra acquisition (45° angle of incidence). Previously to data collection the samples were macerated in an agate mill. The samples were arranged covering the entire crystal and then were pressed to a constant force of 115 N. The spectra were obtained in a spectral range from 400 cm^{-1} to 4000 cm^{-1}. A total of 50 coadded spectra were obtained for each spectrum with a resolution of 4 cm^{-1} and adjusted using attenuated total reflectance (ATR) method.

7.2.4. Scanning electron microscopy – SEM analysis

Scanning electron microscopy photomicrographs of the samples were obtained using a SU8010 cold field emission scanning electron microscope (FESEM, Hitachi, Japan). The Elemental analysis was carried out using an energy-dispersive X-ray spectroscopy (EDS,

AMETEK-EDAX, USA) attached at the scanning electron microscope. Previously to analysis, the samples were anchored tightly on the surface of the conducting tape after coating with a thin layer (0.5–15 nm) of gold and then transferred directly into the microscope.

7.2.5. Fe sequential chemical extraction

A sequential extraction of Fe was carried out using a combination of methods proposed by Tessier et al. (1979), Huerta-Diaz and Morse (1990), and Fortin et al. (1993). The method enables the determination of six distinct fractions operationally defined as: exchangeable and soluble Fe (EX); Fe bounded to carbonates (FeCA); Fe bounded ferrihydrite (FR), lepidocrocite (LP), crystalline Fe oxyhydroxides (i.e., goethite and hematite, CR); and pyritic Fe (PY).

7.3. Results

7.3.1. Physicochemical conditions

The tailing sample from inside the Fundão dam showed Eh (+360 mV) and pH (6.0) values characteristic of oxidizing conditions (> +300 mV; Reddy and DeLaune 2008) (Fig. 2). At the estuary, in 2015 immediately after the disaster, the Eh and pH values were +64 mV and 7.0, respectively, indicating moderately reducing conditions (0 to +300 mV; Fig. 2). In 2017 the Eh (–114 mV) and pH (7.0) values indicated reduced conditions (Eh values < 0 mV; Fig. 2). In 2019, four years after the tailings' arrival, moderately reducing conditions were registered (Eh= 44 mV; pH= 6.0; Fig. 2).

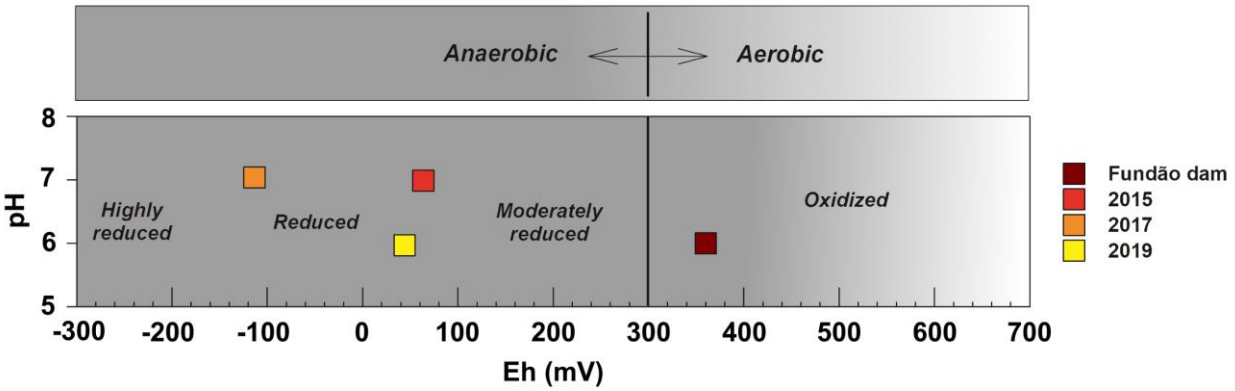

Fig. 2. Eh-pH diagram with the data of the tailing sample from Fundão dam and the samples collected at Doce River estuary in 2015, 2017, and 2019. The Eh-pH diagram and redox condition classification (i.e., highly reduced, reduced, moderately reduced, and oxidized) were adapted from Reddy and DeLaune (2008).

7.3.2. X-ray diffraction and mean crystal size results (MCS)

The clay XRD patterns of the tailing sample showed the presence of goethite (0.160, 0.258, 0.245, 0.338, and 0.418 nm; Fig. 3), hematite (0.169, 0.184, 0.252, and 0.371nm), and kaolinite (0.234, 0.358 nm). In the estuary samples from 2015, 2017, and 2019 the clay XRD patterns showed a similar mineralogical assemblage also with the presence of goethite (0.157, 0.258, 0.245, 0.338, and 0.418 nm; Fig. 3), hematite (0.169, 0.184, 0.252 nm), and kaolinite (0.234, 0.358 nm) (Fig. 3).

In addition, sharper goethite (0.245, 0.269, and 0.418 nm) peaks were observed in the tailing sample and the sharpness gradually decreased in the estuary samples from 2015, 2017, and 2019. For hematite, it was also observed sharper peaks (0.371, 0.296, 0.252, and 0.184 nm; Fig. 3) in the tailing sample, which decreased gradually in the estuary samples from 2015, 2017, and 2019.

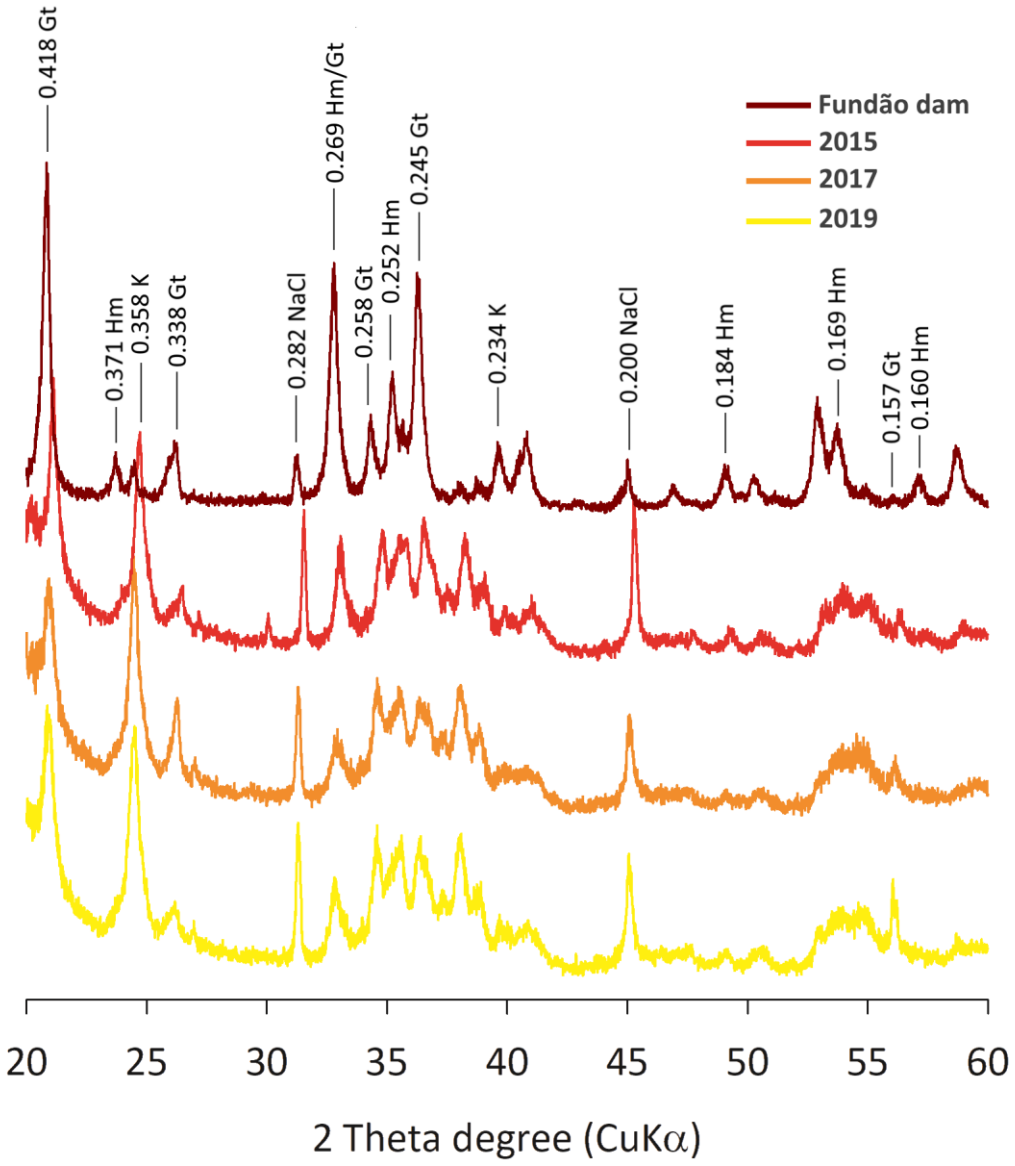

Fig. 3. XRD patterns from the tailing sample and samples collected at the estuary in 2015, 2017 and 2019. Kaolinite (K), Goethite (Gt), Hematite (Hm).

Regarding the mean crystal size (MCS), the d_{110} plan for goethite showed a value of 56.14 for the tailing sample, while the estuary samples from 2015, 2017, and 2019 showed, respectively, values of 86.25, 42.93, and 29.78 nm (Table 1). The MCS for goethite at d_{111} plan were 109.38, 87.50, 61.70, and 48.62 nm for the tailing ante the estuary samples from 2015, 2017, and 2019, respectively (Table 1). The MCS for hematite at d_{104} plan were 41.86, 61.83, and 31.93 nm for the tailing and samples collected in 2015, and 2017, respectively (Table 1). In the tailing sample the MCS for hematite at d_{012} and d_{110} were 54.89 and 82.76 nm, respectively. For the estuary samples from 2015, 2017, and 2019 the MCS for hematite at d_{012}

and d_{110}, and at d_{104} plan (from 2019) were not calculated due to the irregular peak morphology (Fig. 3).

Table 1 – Corrected d-spacing and mean crystal size (MCS) of goethite (Gt) and hematite (Hm) for the clay fraction of the tailing (inside the Fundão dam) and the samples collected at Doce River estuary in 2015, 2017, and 2019.

Sample	d-spacing*					MCS (nm)				
	Gt_{110}	Gt_{111}	Hm_{012}	Hm_{104}	Hm_{110}	Gt_{110}	Gt_{111}	Hm_{012}	Hm_{104}	Hm_{110}
Fundão dam	4.17	2.45	3.67	2.69	2.52	56.14	109.38	54.89	41.86	82.76
2015	4.16	2.45	n.d	2.69	2.52	86.25	87.50	n.d	61.83	n.d
2017	4.16	2.45	n.d	2.69	2.51	42.93	61.70	n.d	31.93	n.d
2019	4.17	2.44	n.d	2.70	2.51	29.78	48.62	n.d	n.d	n.d

*corrected d-spacing using halite as an internal standard. N.d. = not determined

7.3.3. ATR-FTIR results

The tailing showed bands assigned to Fe oxyhydroxides at 3131 to 532 cm^{-1} and the stretching vibration of O–H bonds assigned to goethite at bands 3131, 1650, 1008, and 798 cm^{-1}. The lower stretching band at 532 cm^{-1} was assigned to hematite (Fig. 4; Chukanov 2014).

On the other hand, in the samples collected at the Doce River estuary in 2015, 2017, and 2019, bands of Fe oxyhydroxides were observed at 2985 to 452 cm^{-1} (Fig. 4). The most prominent bands in the estuary samples were at 1003, 793, and 749 cm^{-1} (Fig. 4), which represent the typical bands of goethite and lepidocrocite (Chukanov 2014). In addition, in all the samples from the estuary (i.e., 2015, 2017, and 2019), distinct bands of ferrihydrite were observed at 1026 to 676 cm^{-1} (Fig. 4).

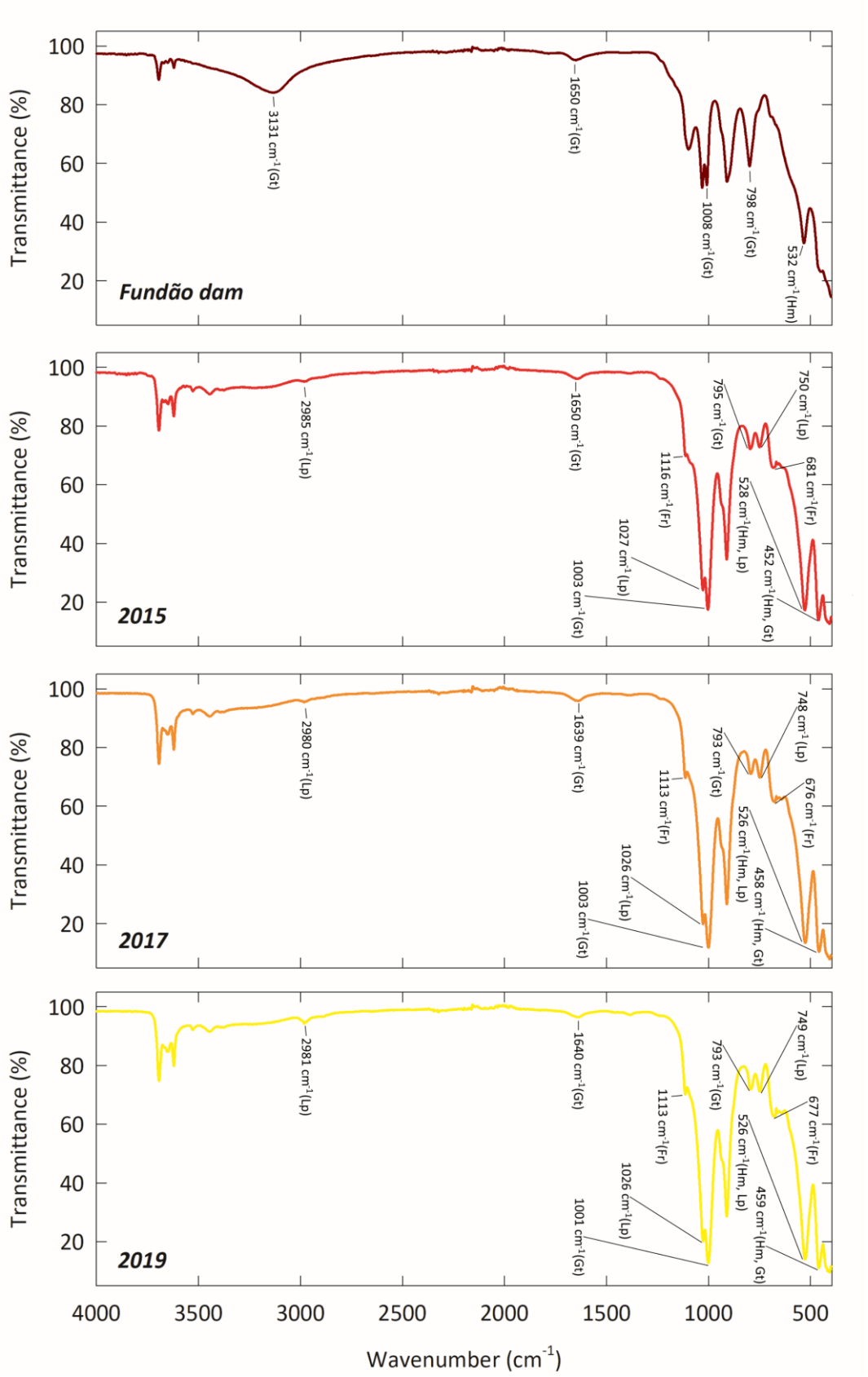

Fig. 4. Attenuated total reflection – Fourier-transform infrared spectroscopy (ATR-FTIR) spectra of the tailing sample and samples collected at Doce River estuary in 2015, 2017 and 2019.

7.3.4. SEM-EDS results from tailings and samples from the Doce River estuary

The SEM micrographs from the tailing samples (Fig. 5A) displayed the presence of Fe oxyhydroxides with a distinct shape that occur naturally in soil and sediments; Bigham et al. 2002). The presence of Fe oxyhydroxides was evidenced by SEM-EDS analyses performed in the central part of the grains that showed a dominant FeO chemical composition (Fig. 5E). The SEM micrographs showed irregular shape in particles from 2015 (Fig. 5B), 2017 (Fig. 5C), and 2019 (Figure 5D) with similar chemical composition (i.e., predominantly FeO; Fig. 5E) also indicating the presence of Fe oxyhydroxides. However, for these years, the SEM micrographs evidenced gradually smaller particle sizes (Fig.5 B, C and D) when compared to the mineral particles observed in the tailing sample (Fig.5A).

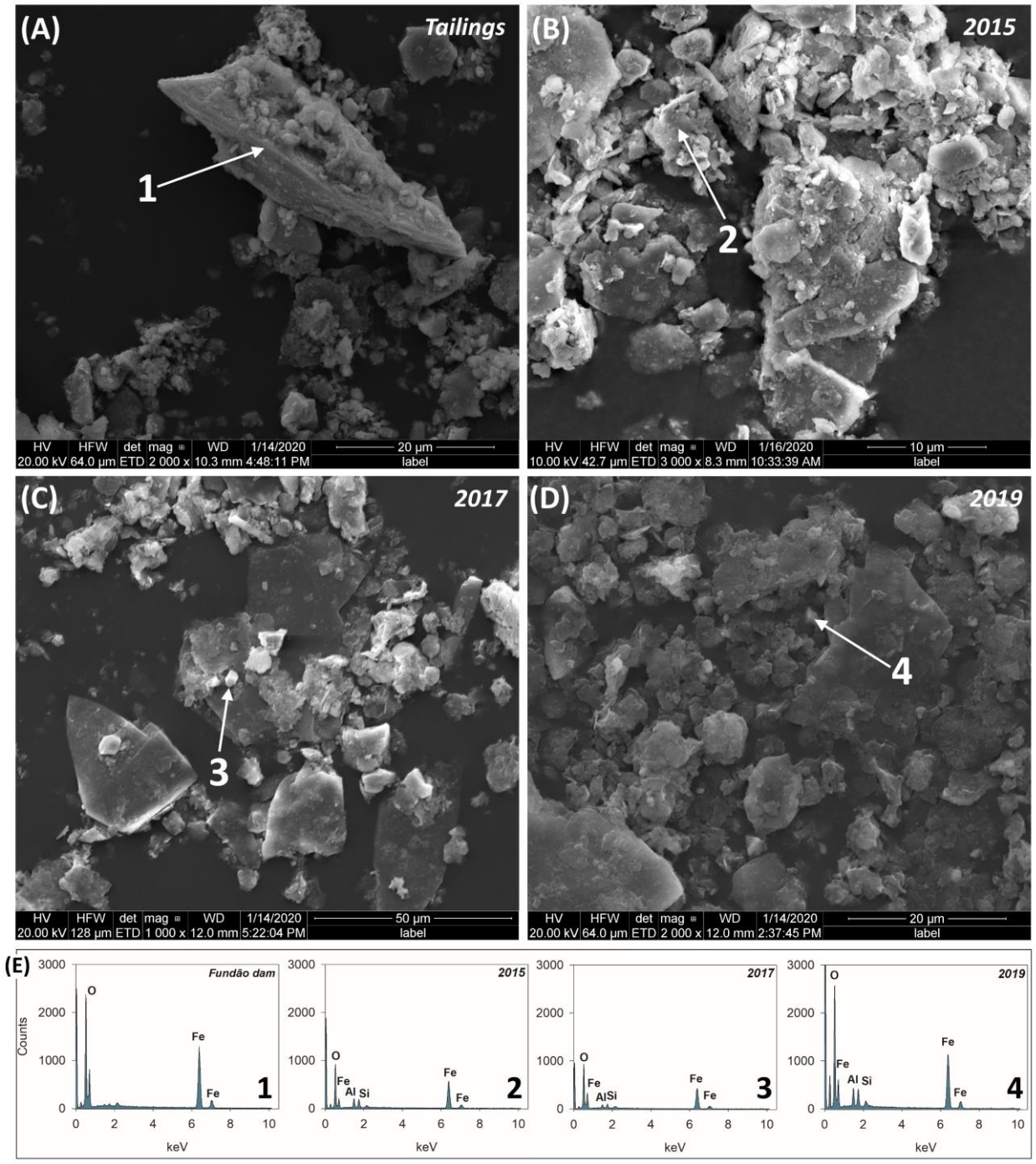

Fig. 5. Scanning electron microscopy (SEM) of the mine tailing from Fundão dam (A) and samples collected at Doce River estuary in 2015 (B), in 2017 (C) and 2019 (D). Chemical composition (E) obtained by energy-dispersive X-ray spectroscopy (EDS) in the analyzed samples.

7.3.5. Sequential extraction of Fe

The Fe sequential extraction showed that in the tailing was mostly associated with crystalline Fe oxides (FeCR: 92.1 Fig. 6) followed by poorly crystalline Fe oxyhydroxides (FeLP:

3.7 % and FeFR: 0.1 %; Fig. 6) and pyritic iron (FePY 4.1 %). Fe associated with FeEX and FeCA accounted for less than 1 % of total Fe, with a small contribution to the total Fe contents.

Samples from the estuary changed significantly over time. Similarly, to the tailings, in 2015, most of the Fe was associated with crystalline oxides (FeCR: 93.1 %), followed by the FeFR (3.4 %) and FeLP (3.3 % Fig. 6). The FeEX, along with FeCA, and FePY also represented less than 1% of total Fe content (Fig. 6).

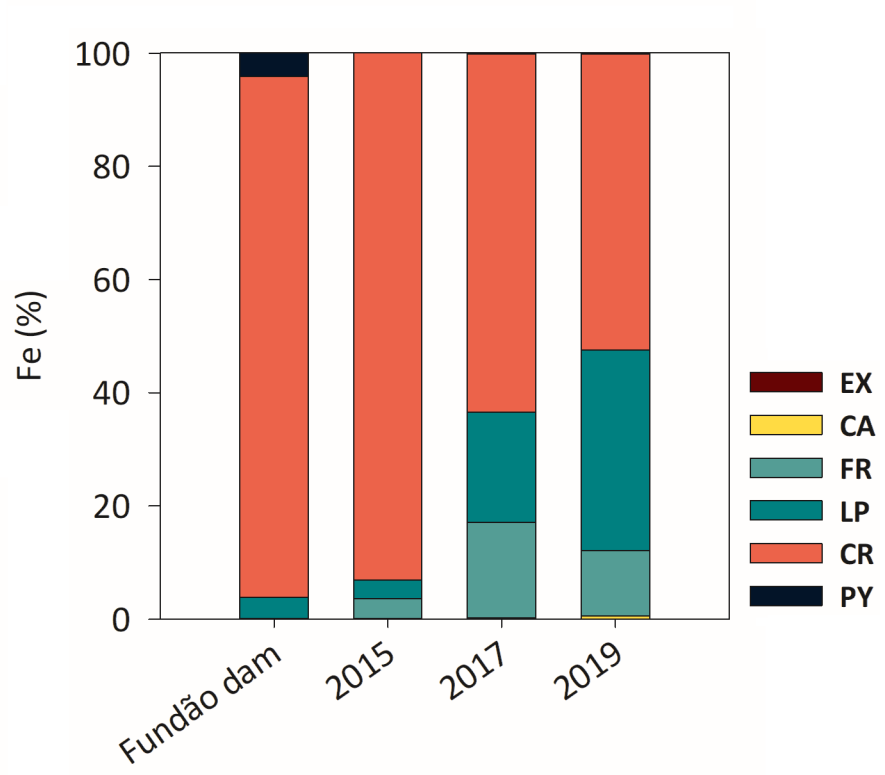

Fig. 6. Percentage of each solid phase fraction in the mine tailing and in samples from the Doce River estuary collected in 2015, 2017, and 2019. EX: exchangeable Fe, CA: Fe bounded to carbonates, FR: Fe bounded to ferrihydrite, LP: Fe bounded to lepidocrocite, CR: Fe associated with high crystallinity oxyhydroxides (i.e., hematite and goethite), and PY: pyritic Fe.

However, in the following years, our data evidenced a sharp change in the crystallinity of Fe oxyhydroxides in the estuary. In the years of 2017 and 2019 FeCR represented, respectively, 63% and 52% of the total Fe contents. Contrastingly, Fe associated with poorly crystallinity oxyhydroxides (i.e., FeFR + FeLP) increased to 37% of total Fe in 2017 and to 47% in 2019 (Fig. 6). Fe associated with the other fractions (i.e., FeEX, FeCA, and FePY) remained in small percentages representing less than 1% of the total Fe (0.2 ± 0.2 %), both in 2017 and 2019.

7.4. Discussion

7.4.1. The physicochemical changes

The physicochemical conditions of the tailings inside the Fundão dam indicated the existence of oxidizing conditions. However, in 2015 the soil physicochemical conditions evidenced a change to a moderately reduced environment, commonly reported in soils and sediments at estuarine environments. In 2017, the physicochemical conditions became further reduced and favorable to the microbial Fe reduction (Eh < 0 mV; Reddy and DeLaune 2008). Thus, our results evidenced a clear redox oscillating environment at the Doce River estuary.

The more reduced physicochemical environment in the estuary is related to organic matter inputs due to the growth of estuarine plants at Doce River (i.e., *Eleocharis acutangula* and *Typha domingensis* (Queiroz et al. 2021b). In fact, after the deposition in the estuary plants colonized the tailings, promoting the organic matter inputs (e.g., litterfall and dead roots). The plant growth coupled with tidal flooding and low O_2 diffusion, would have triggered the decay in Eh values (Queiroz et al. 2021a) and the anaerobic respiration pathways (e.g., microbial Fe reduction) .

The higher Eh values registered in 2019 may also be credited to the effects of plant growth and roots respiration (Rehman et al. 2017). Moreover, the vegetation growth stimulate the presence and activity of fauna (e.g., bioturbation by crabs) in estuarine soils which further enhance oxygen diffusion into the estuarine soils (Fondo and Martens 1998; Sarker et al. 2020). Crabs' burrows and bioturbation promote soil aeration the increase in Eh values and, thus, the oxidation of Fe (Fe^{2+}); which re-precipitates as poorly crystallinity Fe oxyhydroxides (Nielsen et al. 2003; Ferreira et al. 2007; Alongi 2010).

7.4.2. Mineralogical changes over time

The tailing mineralogical assemblage was predominantly composed of Fe oxides and thus clearly associated with the mined Fe-rich ore in the Germano mine (Minas Gerais, SE Brazil). The mine is located in the "*Quadrilátero Ferrífero*" a geological formation of Palaeoproterozoic banded iron formation (Itabirite) mainly composed of the identified iron oxides (e.g., hematite, goethite; Cabral et al. 2002; Silva et al. 2017; Gama et al. 2019). The XRD spectra showed greater intensities and sharper peaks for the hematite and goethite in

the tailings which indicate a higher crystallinity when compared to the surface samples from the Doce River estuary (Schulze 1981; Schwertmann et al. 1982).

In fact, the higher MCS values (Table 1) for both hematite (d_{012} plan: 54.89 nm; d_{104} plan: 41.86 nm; d_{110} plan: 82.76 nm) and goethite (d_{110} plan: 56.14 nm, d_{111} plan: 109.38 nm) in the tailing sample when compared with the MCS values of the estuary samples (i.e., 2015 to 2019) corroborate the higher crystal growth and crystallinity in the tailing (Singh and Gilkes 1992; Camêlo et al. 2017). According to Fontes (1991), well crystalline goethite with a greater crystal development exhibits higher MCS values at d_{111} plan than at d_{110} plan indicating a preferential growth in the z direction. Similarly, for hematite, higher MCS at d_{110} plan also indicates a greater crystal development (Melo et al. 2001).

On the other hand, the samples from the different studied years (i.e., 2015, 2017, and 2019; Fig. 3) showed XRD spectra suggesting a mineral assemblage mainly composed of lower crystallinity Fe oxides with structural disorders which led to less intense and broad peaks (Cornell and Schwertmann 2003; Camêlo et al. 2018). Thus, the lower intensity and less sharp peaks of hematite (0.371, 0.296, 0.252, and 0.184 nm) and goethite (0.245, 0.269, and 0.418 nm) in samples from 2015, 2017, and 2019 (Fig. 3) are probably associated with a decreased crystallinity degree and/or losses of mineral phases (see Velde and Peck 2002; Wang et al. 2015).

Previous studies reported that a decrease in crystallinity degree and/or losses of mineral phases results in lower values of MCS, more structural defects, and lower intensity and sharpness of XRD peaks (Fontes and Weed 1991; Melo et al. 2001; Wang et al. 2015; Camêlo et al. 2018). Moreover, the decrease in crystallinity may reflect on a higher susceptibility of Fe oxyhydroxides to experience a reductive dissolution due to an increase both in surface area and structural disorder (see Larsen and Postma 2001; Cornell and Schwertmann 2003).

The lower MCS values in samples from 2015, 2017 and 2017 are supported by SEM micrographs (Fig. 5) that showed evident smaller grain sizes in these years (< 20 nm). In addition, the SEM micrographs of samples from 2015, 2017, and 2019, did not present the typical morphology of goethite (acicular; Bigham et al. 2002) or hematite (hexagonal and rhombohedral; Schwertmann et al. 2000) showing irregular particle morphologies which also evidences a particle size narrowing and an ordination decaying (see Schwertmann and Fitzpatrick 1992; Gao and Schulze 2010; Das and Hendry 2014).

This structural disorder in the estuary samples was further corroborated by the ATR-FTIR results (Fig. 4). The greater and sharper goethite bands at 795 cm^{-1} and 1001 cm^{-1} are associated with higher bending vibrations of OH that may be a result of a structural disorder promoted by Al-substitution or by partial mineral dissolution that leads to Fe displacement and more bonding OH groups (Ruan et al. 2002; Cornell and Schwertmann 2003; Faivre and Frankel 2016). Additionally, the broadening and stretching of bands at 748 cm^{-1}, and at 681 to 676 cm^{-1}, and at 1026 cm^{-1} (in 2015, 2017, and 2019; Fig. 4) also result from the OH stretching vibration, typical of poorly crystalline Fe oxyhydroxides (Bazilevskaya et al. 2011, 2012). On the other hand, the smaller and slightly stretched bands of goethite and hematite at 3131 to 798 cm^{-1} and at 532 cm^{-1} (Fig. 4) in the tailing sample indicate a lower presence of OH surface groups which corroborate the higher crystallinity observed in the XRD spectra (Fig. 3). In Fact, Ruan et al., (2002) reported a systematic decrease in the width of hematite and goethite bands resulting from hydroxyl liberation and the changes in Fe-OH to FeO bonding after thermal dihydroxylation which led to crystallization and crystal growth.

The hydroxylation of Fe oxyhydroxides in wetland soils occurs due to natural processes, mainly mediated by microorganisms and redox oscillation (Randall et al. 1999; Jolivet et al. 2004; Kosolapov et al. 2004). In fact, the Fe fractionation showed a significant and rapid shift in the distribution of Fe oxides within few years at the Doce River estuary. The data showed a marked increase in the poorly crystalline Fe oxyhydroxides (i.e., FeFR+FeLP) from 2015 (6.8%) to 2017 (36.3%) and 2019 (47%; Fig. 6). The clear loss in crystallinity is related to the active redox environment found in the studied estuary, which oscillated between reduced to moderately reduced conditions (see Fig. 2). These redox oscillations occur due to tidal flooding (Seybold et al. 2002), plants activity (Rehman et al. 2017), organic matter inputs into soil (Reddy and DeLaune 2008), O_2 depletion (Du Laing et al. 2009), and fauna activity (i.e., bioturbation; Otero et al. 2020). This active redox environment favor the microbial Fe reduction (Lovley 1991) and the subsequent oxidation of Fe^{2+} to Fe^{III}, and thus, its re-precipitation as poorly crystallinity Fe oxyhydroxides (Lindsay 1991; Zachara et al. 2001; Johnston et al. 2011).

The Fe reduction consume both the high and poorly crystalline Fe oxyhydroxides (Kukkadapu et al. 2001; Pan et al. 2016). Upon O_2 reentry, due to lowering tides, fauna activity, or roots respiration, the re-precipitation of Fe may occur rapidly in the system (Chen et al. 2018). This reoxidation usually favor the formation of poorly crystalline Fe oxyhydroxides due

to low interfacial energies of nucleation of these Fe minerals (Stumm and Morgan 1996; Barcellos et al. 2018; Chen et al. 2018). Our results agree with those reported by Winkler et al. (2018) and Thompson et al. (2011) which showed a decreased crystallinity of Fe oxyhydroxides with time after redox cycles. However, these authors evidenced these mineralogical changes in a paddy soil and often waterlogged forest soils after several decades of exposition to redox fluctuations.

The stability of the re-precipitated poorly crystalline Fe oxyhydroxides may be enhanced in the Al presence during the crystallization process (isomorphic Al-substitution; Schwertmann 1991; Violante et al. 2003). Masue-Slowey et al., (2011) reported that Al-substitution in low crystallinity Fe oxyhydroxides increased the mineral stability against the reductive dissolution. This higher stability is associated with changes in structural ordering with the fortification of hydrogen bonds (Cornell and Schwertmann 2003). Thus, despite the active redox environment, Al-substitution may contribute to the maintenance of poorly crystalline Fe oxyhydroxides in the soil over time.

7.4.3. Potential environmental implications

The clear shifts in the mineralogical characteristics of Fe oxyhydroxides may have several important environmental implications for the estuarine environment in the future. Iron oxyhydroxides are known for their role in metals retention (Hochella et al. 2005) due to their low particle size, high surface areas, and, thus, high reactivity (Herbert 1996; Buerge-Weirich et al. 2002). Under oxic conditions Fe oxyhydroxides may retain heavy metals due to the formation of inner or surface complexes such as monodentate surface hydroxo-complexes or by bi-nuclear internal complexes (Grossl et al. 1994; Cornell and Schwertmann 2003). These complexes are strongly stable, virtually irreversible , and guarantee the low bioavailability of metals (Rose and Bianchi-Mosquera 1993; Trivedi and Axe 2001). However under transitory/cyclic anoxic conditions Fe oxyhydroxides experience a reductive dissolution which leads to a decrease in their stability and in their capacity to retain metals (Herbert 1996; Queiroz et al. 2021b).

Due to their smaller size (2–6 nm) and higher surface area (200 to 600 $m^2\ g^{-1}$), the poorly crystalline Fe oxyhydroxides, (Roden and Zachara 1996; Randall et al. 1999; Manceau et al. 2000) have a greater potential to adsorb and immobilize both cationic and anionic

species. Indeed, several studies reported the great capacity of poorly crystalline Fe oxyhydroxides (e.g., ferrihydrite and lepidocrocite) in promoting the immobilization of heavy metals in different soils (Martínez 1998; Manceau et al. 2000; Cornell and Schwertmann 2003; Tack et al. 2006; Komárek et al. 2013; Baleeiro et al. 2018). Similarly, P retention in poorly crystallinity Fe oxyhydroxides is also widely reported and a well-recognized phenom (Slomp et al. 1996; Arai and Sparks 2001; Wang et al. 2013; Liao et al. 2020) which plays an important role in the eutrophication process (Wilson et al. 2004; Kraal et al. 2015; Queiroz et al. 2021a).

These low crystalline Fe oxyhydroxides present short-range-ordering, surface imperfections, weak Fe-OH bonds, which favor edges dissolution (Cornell and Schwertmann 2003). With further dissolution, the crystals are made gradually smaller with a higher surface area (Larsen and Postma 2001). These characteristics are accountable for an intense dissolution rate (Bonneville et al. 2004). In response to these characteristics, the associated metals and phosphorus are made bioavailable (Schwertmann 1991; Larsen and Postma 2001; Queiroz et al. 2021b) posing severe environmental risks to the Doce River estuary. In fact, previous studies reported a high concentrations of metals (Queiroz et al. 2018, 2021a) and phosphorus (Queiroz et al. 2021b) associated with the estuary Fe oxyhydroxides. Thus, the mineralogical changes caused by the active redox environment such as smaller particles size observed in SEM micrographs (Fig. 5), lower MCS (Table1), and decreased crystallinity (Fig. 4; Fig. 6), corroborate the higher mineral dissolution susceptibility at the Doce River estuarine soil. These mineral changes may lead to an increase in the concentration of pollutants (e.g., metals and phosphorus) in the soil and water from Doce River estuary in the near future. In fact, Queiroz et al. (2021a, b) recently reported an increase in phosphorus and metals bioavailability associated with soil Fe losses due to reductive dissolution.

7.5. Conclusions

Initially, the tailings from inside Fundão dam were composed predominantly of high crystalline Fe oxyhydroxides (e.g., goethite and hematite). In 2015 after the dam failure, the tailing was exposed to a redox oscillating environment at Doce River estuary. The new biogeochemical conditions decreased the crystallinity of Fe oxyhydroxides from 2015 through 2019. Our results reveal a rapid mineralogical assemblage change within four years. The mineralogical shifts were driven by the microbial-mediated reductive dissolution, plant

growth and roots respiration, and fauna activity. Within this period, our data evidence a change from a dominance (92%) of highly crystalline Fe oxyhydroxides (goethite and hematite) to a higher presence (47%) of poorly crystallinity Fe oxyhydroxides (e.g., lepidocrocite and ferrihydrite) with smaller particle size (from 109 nm to 49 nm for goethite at d_{111} plan) and higher reactivity.

The decreased crystallinity of Fe oxyhydroxides was followed by a higher susceptibility to mineral dissolution. Such case decreases the capacity of these minerals in retaining both cationic and anionic potentially pollutant elements (e.g., metals and phosphorus) and, thus, may increase the concentration of these pollutants in estuarine soils and waters.

Acknowledgments

This work received financial support provided by the Fundação de Amparo à Pesquisa e Inovação do Espírito Santo (FAPES, grant number 77683544), Coordenação de Aperfeiçoamento de Pessoal de Nível Superior CAPES (Finance Code 001), Conselho Nacional de Desenvolvimento Científico e Tecnológico (CNPq, grants number 301161/2017-8 and 305996/2018-5 to AFB and TOF, respectively), São Paulo Research Foundation (FAPESP, grants number 2018/04259-2, 2018/08408-2, 2019/18324-3, 2019/17413-2, 2019/14800-5, and 2019/19987-6), and Xunta de Galicia-Consellería de Educación e Ordeanción Universitaria de Galicia (Consolidation of competitive groups of investigation; GRC GI 1574).

References

Alongi DM (2010) Dissolved iron supply limits early growth of estuarine mangroves. Ecology 91:3229–3241. https://doi.org/10.1890/09-2142.1

Arai Y, Sparks DL (2001) ATR–FTIR Spectroscopic Investigation on Phosphate Adsorption Mechanisms at the Ferrihydrite–Water Interface. J Colloid Interface Sci 241:317–326. https://doi.org/10.1006/jcis.2001.7773

Baleeiro A, Fiol S, Otero-Fariña A, Antelo J (2018) Surface chemistry of iron oxides formed by neutralization of acidic mine waters: Removal of trace metals. Appl Geochemistry 89:129–137. https://doi.org/10.1016/j.apgeochem.2017.12.003

Barcellos D, Cyle KT, Thompson A (2018) Faster redox fluctuations can lead to higher iron reduction rates in humid forest soils. Biogeochemistry 137:367–378. https://doi.org/10.1007/s10533-018-0427-0

Barcellos D, Queiroz HM, Nóbrega GN, et al (2019) Phosphorus enriched effluents increase eutrophication risks for mangrove systems in northeastern Brazil. Mar Pollut Bull 142:58–63. https://doi.org/10.1016/j.marpolbul.2019.03.031

Bazilevskaya E, Archibald DD, Aryanpour M, et al (2011) Aluminum coprecipitates with Fe (hydr)oxides: Does isomorphous substitution of Al3+ for Fe3+ in goethite occur? Geochim Cosmochim Acta 75:4667–4683. https://doi.org/10.1016/j.gca.2011.05.041

Bazilevskaya E, Archibald DD, Martínez CE (2012) Rate constants and mechanisms for the crystallization of Al nano-goethite under environmentally relevant conditions. Geochim Cosmochim Acta 88:167–182. https://doi.org/10.1016/j.gca.2012.04.026

Benjamin MM, Sletten RS, Bailey RP, Bennett T (1996) Sorption and filtration of metals using iron-oxide-coated sand. Water Res 30:2609–2620. https://doi.org/10.1016/S0043-1354(96)00161-3

Bernardino AF, Pais FS, Oliveira LS, et al (2019) Chronic trace metals effects of mine tailings on estuarine assemblages revealed by environmental DNA. PeerJ 7:e8042. https://doi.org/10.7717/peerj.8042

Bigham JM, Fitzpatrick RW, Schulze DG (2002) Iron Oxides. In: Soil Mineralogy with Environmental Applications. Soil Science Society of America, Madison, Wisconsin, pp 323–366

Bonneville S, Van Cappellen P, Behrends T (2004) Microbial reduction of iron(III) oxyhydroxides: Effects of mineral solubility and availability. Chem Geol 212:255–268. https://doi.org/10.1016/j.chemgeo.2004.08.015

Botha L, Soares JBP (2015) The Influence of Tailings Composition on Flocculation. Can J Chem Eng 93:1514–1523. https://doi.org/10.1002/cjce.22241

Buekers J, Amery F, Maes A, Smolders E (2008) Long-term reactions of Ni, Zn and Cd with iron oxyhydroxides depend on crystallinity and structure and on metal concentrations. Eur J Soil Sci 59:706–715. https://doi.org/10.1111/j.1365-2389.2008.01028.x

Buerge-Weirich D, Hari R, Xue H, et al (2002) Adsorption of Cu, Cd, and Ni on goethite in the presence of natural groundwater ligands. Environ Sci Technol 36:328–336. https://doi.org/10.1021/es010892i

Cabral AR, Lehmann B, Kwitko R, et al (2002) Palladseite and its oxidation: evidence from Au-Pd vein-type mineralization (jacutinga), Cauê iron-ore mine, Quadrilátero Ferrífero, Minas Gerais, Brazil. Mineral Mag 66: 327–336. https://doi.org/10.1180/0026461026620033

Camêlo D de L, Ker JC, Fontes MPF, et al (2017) Pedogenic iron oxides in iron-rich oxisols developed from mafic rocks. Rev Bras Cienc do Solo 41:1–16. https://doi.org/10.1590/18069657rbcs20160379

Camêlo D de L, Ker JC, Fontes MPF, et al (2018) Mineralogy, magnetic susceptibility and geochemistry of fe-rich oxisols developed from several parent materials. Sci Agric 75:410–419. https://doi.org/10.1590/1678-992x-2017-0087

Carmo FF do, Kamino LHY, Junior RT, et al (2017) Fundão tailings dam failures: the environment tragedy of the largest technological disaster of Brazilian mining in global context. Perspect Ecol Conserv 15: 145–151. https://doi.org/10.1016/j.pecon.2017.06.002

Chen C, Meile C, Wilmoth J, et al (2018) Influence of pO 2 on Iron Redox Cycling and Anaerobic Organic Carbon Mineralization in a Humid Tropical Forest Soil. Environ Sci Technol 52:7709–7719. https://doi.org/10.1021/acs.est.8b01368

Chukanov N V. (2014) Infrared spectra of mineral species. Springer Geochemistry/Mineralogy, Chernogolovka, Russia

Cornell RM, Schwertmann U (2003) The Iron Oxides: Structure, Reactions, Occurences and Uses

Cui H, Zhang X, Wu Q, et al (2020) Hematite enhances the immobilization of copper, cadmium and phosphorus in soil amended with hydroxyapatite under flooded conditions. Sci Total Environ 708:134590. https://doi.org/10.1016/j.scitotenv.2019.134590

Cummings DE, March AW, Bostick B, et al (2000) Evidence for microbial Fe(III) reduction in anoxic, mining-impacted lake sediments (Lake Coeur d'Alene, Idaho). Appl Environ Microbiol 66:154–62

Das S, Hendry MJ (2014) Characterization of hematite nanoparticles synthesized via two different pathways. J Nanoparticle Res 16:2535. https://doi.org/10.1007/s11051-014-2535-7

Du Laing G, Rinklebe J, Vandecasteele B, et al (2009) Trace metal behaviour in estuarine and riverine floodplain soils and sediments: A review. Sci Total Environ 407:3972–3985. https://doi.org/10.1016/j.scitotenv.2008.07.025

Escobar H (2015) Mud tsunami wreaks ecological havoc in Brazil. Science (80-) 350:1138–1139. https://doi.org/10.1126/science.350.6265.1138

Faivre D, Frankel RB (2016) Iron Oxides: From Nature to Applications, 1st edn. Wiley-VCH, Weinheim, Germany

Ferreira TO, Otero XL, Vidal-Torrado P, Macías F (2007) Effects of bioturbation by root and crab activity on iron and sulfur biogeochemistry in mangrove substrate. Geoderma 142:36–46. https://doi.org/10.1016/j.geoderma.2007.07.010

Fink JR, Inda AV, Tiecher T, Barrón V (2016) Iron oxides and organic matter on soil phosphorus availability. Cienc e Agrotecnologia 40:369–379. https://doi.org/10.1590/1413-70542016404023016

Fondo EN, Martens EE (1998) Effects of mangrove deforestation on macrofaunal densities, Gazi Bay, Kenya. Mangroves Salt Marshes 2: 75–83. https://doi.org/10.1023/A:1009982900931

Fontes MPF, Weed SB (1991) Iron Oxides in Selected Brazilian Oxisols: I. Mineralogy. Soil Sci Soc Am J 55:1143–1149. https://doi.org/10.2136/sssaj1991.03615995005500040040x

Fortin D, Leppard GG, Tessier A (1993) Characteristics of lacustrine diagenetic iron oxyhydroxides. Geochim Cosmochim Acta 57:4391–4404. https://doi.org/10.1016/0016-7037(93)90490-N

Gabriel FA, Silva AG, Queiroz HM, et al (2020) Ecological Risks of Metal and Metalloid Contamination in the Rio Doce Estuary. Integr Environ Assess Manag 16:655–660. https://doi.org/10.1002/ieam.4250

Gama FF, Paradella WR, Mura JC, de Oliveira CG (2019) Advanced DINSAR analysis on dam stability monitoring: A case study in the Germano mining complex (Mariana, Brazil) with SBAS and PSI techniques. Remote Sens Appl Soc Environ 16: https://doi.org/10.1016/j.rsase.2019.100267

Gao X, Schulze DG (2010) Precipitation and transformation of secondary Fe oxyhydroxides in a Histosol impacted by runoff from a lead smelter. Clays Clay Miner 58: 377–387. https://doi.org/10.1346/CCMN.2010.0580308

Glombitza F, Reichel S (2014) Metal-Containing Residues from Industry and in the Environment: Geobiotechnological Urban Mining. Adv Biochem Eng Biotechnol 141:49–107. https://doi.org/10.1007/10_2013_254

Gomes LE de O, Correa LB, Sá F, et al (2017) The impacts of the Samarco mine tailing spill on the Rio Doce estuary, Eastern Brazil. Mar Pollut Bull 120: 28–36. https://doi.org/10.1016/j.marpolbul.2017.04.056

Grossl PR, Sparks DL, Ainsworth CC (1994) Rapid Kinetics of Cu(II) Adsorption/Desorption on Goethite. Environ Sci Technol 28:1422–1429. https://doi.org/10.1021/es00057a008

Harford AJ, Mooney TJ, Trenfield MA, van Dam RA (2015) Manganese toxicity to tropical freshwater species in low hardness water. Environ Toxicol Chem 34:2856–2863. https://doi.org/10.1002/etc.3135

Hartley W, Edwards R, Lepp NW (2004) Arsenic and heavy metal mobility in iron oxide-amended contaminated soils as evaluated by short- and long-term leaching tests. Environ Pollut 131:495–504. https://doi.org/10.1016/j.envpol.2004.02.017

Herbert RB (1996) Metal retention by iron oxide precipitation from acidic ground water in Dalarna, Sweden. Appl Geochemistry 11:229–235. https://doi.org/10.1016/0883-2927(95)00070-4

Hochella MF, Kasama T, Putnis A, et al (2005) Environmentally important, poorly crystalline Fe/Mn hydrous oxides: Ferrihydrite and a possibly new vernadite-like mineral from the Clark Fork River Superfund Complex. Am Mineral 90: 718–724. https://doi.org/10.2138/am.2005.1591

Howard J, Hoyt S, Isensee K, et al (2014) Coastal blue carbon: methods for assessing carbon stocks and emissions factors in mangroves, tidal salt marshes, and seagrasses. Conservation International, Intergovernmental Oceanographic Commission of UNESCO, International Union for Conservation of Nature, Arlington, VA, USA, Arlington, VA, USA

Huerta-Diaz MA, Morse JW (1990) A quantitative method for determination of trace metal concentrations in sedimentary pyrite. Mar Chem 29: 119–144. https://doi.org/10.1016/0304-4203(90)90009-2

Jackson ML (2005) Soil Chemical Analysis: Advanced Course, 2nd edn. UW-Madison Libraries Parallel Press, Madison, Wisconsin

Johnston SG, Keene AF, Bush RT, et al (2011) Iron geochemical zonation in a tidally inundated acid sulfate soil wetland. Chem Geol 280: 257–270. https://doi.org/10.1016/j.chemgeo.2010.11.014

Jolivet JP, Chanéac C, Tronc E (2004) Iron oxide chemistry. From molecular clusters to extended solid networks. Chem Commun 4:477–483. https://doi.org/10.1039/b304532n

Klug HP, Alexander LE (1974) X-Ray Diffraction Procedures: For Polycrystalline and Amorphous Materials, 2nd edn. Wiley, New York

Komárek M, Vaněk A, Ettler V (2013) Chemical stabilization of metals and arsenic in contaminated soils using oxides - A review. Environ Pollut 172: 9–22. https://doi.org/10.1016/j.envpol.2012.07.045

Kosolapov BDB, Kuschk P, Vainshtein MB, et al (2004) Review Microbial Processes of Heavy Metal Removal from Carbon-Deficient Effluents in Constructed Wetlands. 403–411. https://doi.org/10.1002/elsc.200420048

Kraal P, Burton ED, Rose AL, et al (2015) Sedimentary iron–phosphorus cycling under contrasting redox conditions in a eutrophic estuary. Chem Geol 392:19–31. https://doi.org/10.1016/j.chemgeo.2014.11.006

Kukkadapu RK, Zachara JM, Smith SC, et al (2001) Dissimilatory bacterial reduction of Al-substituted goethite in subsurface sediments. Geochim Cosmochim Acta 65:2913–2924. https://doi.org/10.1016/S0016-7037(01)00656-1

LaForce MJ, Hansel CM, Fendorf S (2000) Constructing Simple Wetland Sampling Devices. Soil Sci Soc Am J 64:809–811. https://doi.org/10.2136/sssaj2000.642809x

Larsen O, Postma D (2001) Kinetics of reductive bulk dissolution of lepidocrocite, ferrihydrite, and goethite. Geochim Cosmochim Acta 65:1367–1379. https://doi.org/10.1016/S0016-7037(00)00623-2

Liao S, Wang X, Yin H, et al (2020) Effects of Al substitution on local structure and morphology of lepidocrocite and its phosphate adsorption kinetics. Geochim Cosmochim Acta 276:109–121. https://doi.org/10.1016/j.gca.2020.02.027

Lindsay WL (1991) Iron oxide solubilization by organic matter and its effect on iron availability. Plant Soil 130:27–34. https://doi.org/10.1007/BF00011852

Lovley DR (1991) Dissimilatory Fe(III) and Mn(IV) Reduction. Microbiol Rev 55:259–287

Lovley DR, Holmes DE, Nevin KP (2004) Dissimilatory Fe(III) and Mn(IV) Reduction. In: Advances in Microbial Physiology. pp 219–286

Lu L (2015) Iron Ore: Mineralogy, Processing and Environmental Sustainability, 1st edn. Elsevier, Sawston

Manceau A, Nagy KL, Spadini L, Ragnarsdottir KV (2000) Influence of anionic layer structure of Fe-oxyhydroxides on the structure of Cd surface complexes. J Colloid Interface Sci 228:306–316. https://doi.org/10.1006/jcis.2000.6922

Martínez CE (1998) Coprecipitates of Cd, Cu, Pb and Zn in Iron Oxides: Solid Phase Transformation and Metal Solubility after Aging and Thermal Treatment. Clays Clay Miner 46:537–545. https://doi.org/10.1346/CCMN.1998.0460507

Masue-Slowey Y, Loeppert RH, Fendorf S (2011) Alteration of ferrihydrite reductive dissolution and transformation by adsorbed As and structural Al: Implications for As retention. Geochim Cosmochim Acta 75:870–886. https://doi.org/10.1016/j.gca.2010.11.016

Mello CR de, Viola MR, Curi N, Silva AM da (2012) Distribuição espacial da precipitação e da erosividade da chuva mensal e anual no Estado do Espírito Santo. Rev Bras Ciência do Solo 36:1878–1891. https://doi.org/10.1590/S0100-06832012000600022

Melo VF, Fontes MPF, Novais RF, et al (2001) Características dos óxidos de ferro e de alumínio de diferentes classes de solos. Rev Bras Ciência do Solo 25: 19–32. https://doi.org/10.1590/s0100-06832001000100003

Nielsen OI, Kristensen E, Macintosh DJ (2003) Impact of fiddler crabs (Uca spp.) on rates and pathways of benthic mineralization in deposited mangrove shrimp pond waste. J Exp Mar Bio Ecol. https://doi.org/10.1016/S0022-0981(03)00041-8

Nóbrega GN, Otero XL, Macías F, Ferreira TO (2014) Phosphorus geochemistry in a Brazilian semiarid mangrove soil affected by shrimp farm effluents. Environ Monit Assess 186:5749–5762. https://doi.org/10.1007/s10661-014-3817-3

Otero XL, Araújo JMC, Barcellos D, et al (2020) Crab bioturbation and seasonality control nitrous oxide emissions in semiarid mangrove forests (Ceará, Brazil). Appl Sci 10:. https://doi.org/10.3390/app10072215

Otero XL, Ferreira TO, Huerta-Díaz MA, et al (2009) Geochemistry of iron and manganese in soils and sediments of a mangrove system, Island of Pai Matos (Cananeia — SP, Brazil). Geoderma 148:318–335. https://doi.org/10.1016/j.geoderma.2008.10.016

Pan W, Kan J, Inamdar S, et al (2016) Dissimilatory microbial iron reduction release DOC (dissolved organic carbon) from carbon-ferrihydrite association. Soil Biol Biochem 103:232–240. https://doi.org/10.1016/j.soilbio.2016.08.026

Pereira AA, Van Hattum B, Brouwer A, et al (2008) Effects of iron-ore mining and processing on metal bioavailability in a tropical coastal lagoon. J Soils Sediments 8: 239–252. https://doi.org/10.1007/s11368-008-0017-1

Queiroz HM, Ferreira TO, Barcellos D, et al (2021a) From sinks to sources: The role of Fe oxyhydroxide transformations on phosphorus dynamics in estuarine soils. J Environ Manage 278:111575. https://doi.org/10.1016/j.jenvman.2020.111575

Queiroz HM, Nóbrega GN, Ferreira TO, et al (2018) The Samarco mine tailing disaster: A possible time-bomb for heavy metals contamination? Sci Total Environ 637–638:498–506. https://doi.org/10.1016/j.scitotenv.2018.04.370

Queiroz HM, Ying SC, Abernathy M, et al (2021b) Manganese: The overlooked contaminant in the world largest mine tailings dam collapse. Environ Int 146: 106284. https://doi.org/10.1016/j.envint.2020.106284

Randall SR, Sherman DM, Ragnarsdottir K V., Collins CR (1999) The mechanism of cadmium surface complexation on iron oxyhydroxide minerals. Geochim Cosmochim Acta 63:2971–2987. https://doi.org/10.1016/S0016-7037(99)00263-X

Reddy KR, DeLaune RD (2008) Biogeochemistry of wetlands: science and applications, 1st edn. CRC Press

Rehman F, Pervez A, Khattak BN, Ahmad R (2017) Constructed Wetlands: Perspectives of the Oxygen Released in the Rhizosphere of Macrophytes. CLEAN - Soil, Air, Water 45:. https://doi.org/10.1002/clen.201600054

Roden EE, Zachara JM (1996) Microbial Reduction of Crystalline Iron(III) Oxides: Influence of Oxide Surface Area and Potential for Cell Growth. Environ Sci Technol 30: 1618–1628. https://doi.org/10.1021/es9506216

Rose AW, Bianchi-Mosquera GC (1993) Adsorption of Cu, Pb, Zn, Co, Ni, and Ag on goethite and hematite; a control on metal mobilization from red beds into stratiform copper deposits. Econ Geol 88:1226–1236. https://doi.org/10.2113/gsecongeo.88.5.1226

Ruan HD, Frost RL, Kloprogge JT, Duong L (2002) Infrared spectroscopy of goethite dehydroxylation: III. FT-IR microscopy of in situ study of the thermal transformation of goethite to hematite. Spectrochim Acta - Part A Mol Biomol Spectrosc 58:967–981. https://doi.org/10.1016/S1386-1425(01)00574-1

Ruan HD, Gilkes RJ (1995) Dehydroxylation of Aluminous Goethite: Unit Cell Dimensions, Crystal Size and Surface Area. Clays Clay Miner 43: 196–211. https://doi.org/10.1346/CCMN.1995.0430207

Rutten A, de Lange GJ (2003) Sequential extraction of iron, manganese and related elements in S1 sapropel sediments, eastern Mediterranean. Palaeogeogr Palaeoclimatol Palaeoecol 190:79–101. https://doi.org/10.1016/S0031-0182(02)00600-4

Sarker S, Masud-Ul-Alam M, Hossain MS, et al (2020) A review of bioturbation and sediment organic geochemistry in mangroves. Geol J gj.3808. https://doi.org/10.1002/gj.3808

Schulze DG (1981) Identification of Soil Iron Oxide Minerals by Differential X-ray Diffraction. Soil Sci Soc Am J 45: 437–440. https://doi.org/10.2136/sssaj1981.03615995004500020040x

Schwertmann U (1988) Occurrence and Formation of Iron Oxides in Various Pedoenvironments. In: Iron in Soils and Clay Minerals. Springer Netherlands, Dordrecht, pp 267–308

Schwertmann U (1991) Solubility and dissolution of iron oxides. Plant Soil. https://doi.org/10.1007/BF00011851

Schwertmann U, Fitzpatrick RW (1992) Iron minerals in surface environments. Catena Suppl 21:7–30

Schwertmann U, Friedl J, Stanjek H, Schulze DG (2000) The Effect of Al on Fe Oxides. XIX. Formation of Al-Substituted Hematite from Ferrihydrite at 25°C and pH 4 To 7. Clays Clay Miner 48:159–172. https://doi.org/10.1346/CCMN.2000.0480202

Schwertmann U, Schulze DG, Murad E (1982) Identification of Ferrihydrite in Soils by Dissolution Kinetics, Differential X-ray Diffraction, and Mössbauer Spectroscopy. Soil Sci Soc Am J 46:869–875. https://doi.org/10.2136/sssaj1982.03615995004600040040x

Schwertmann U, Taylor RM (1989) Iron Oxides. In: Minerals in Soil Environments, 2nd edn. Soil Science Society of America, Madison, Wisconsin, pp 379–438

Seybold CA, Mersie W, Huang J, McNamee C (2002) Soil redox, pH, temperature, and water-table patterns of a freshwater tidal wetland. Wetlands 22: 149–158. https://doi.org/https://doi.org/10.1672/0277-5212(2002)022[0149:SRPTAW]2.0.CO;2

Sherameti I, Varma A (2015) Heavy Metal Contamination of Soils. Springer International Publishing, Cham

Silva AC, Cavalcante LCD, Fabris JD, et al (2017) Características químicas, mineralógicas e físicas do material acumulado em terraços fluviais, originado do fluxo de lama proveniente do rompimento de barragem de rejeitos de mineração de ferro em Bento Rodrigues, Minas Gerais, Brasil. Rev Espinhaço | UFVJM; Rev Espinhaço #9

Silva RCF, Ardisson JD, Cotta AAC, et al (2020) Use of iron mining tailings from dams for carbon nanotubes synthesis in fluidized bed for 17α-ethinylestradiol removal. Environ Pollut 260:. https://doi.org/10.1016/j.envpol.2020.114099

Singh B, Gilkes RJ (1992) Properties and distribution of iron oxides and their association with minor elements in the soils of south-western Australia. J Soil Sci 43: 77–98. https://doi.org/10.1111/j.1365-2389.1992.tb00121.x

Slomp CP, Van Der Gaast SJ, Van Raaphorst W (1996) Phosphorus binding by poorly crystalline iron oxides in North Sea sediments. Mar Chem 52:55–73. https://doi.org/10.1016/0304-4203(95)00078-X

Strauss R, Brummer GW, Barrow NJ (1997) Effects of crystallinity of goethite: II. Rates of sorption and desorption of phosphate. Eur J Soil Sci 48: 101–114. https://doi.org/10.1111/j.1365-2389.1997.tb00189.x

Stumm W, Morgan JJ (1996) Aquatic Chemistry: Chemical Equilibria and Rates in Natural Waters, 3rd edn. John Wiley & Sons, Inc., Danvers

Tack FMG, Van Ranst E, Lievens C, Vandenberghe RE (2006) Soil solution Cd, Cu and Zn concentrations as affected by short-time drying or wetting: The role of hydrous oxides of Fe and Mn. Geoderma 137:83–89. https://doi.org/10.1016/j.geoderma.2006.07.003

Tessier A, Campbell PGC, Bisson M (1979) Sequential extraction procedure for the speciation of particulate trace metals. Anal Chem 51: 844–851. https://doi.org/10.1021/ac50043a017

Thompson A, Rancourt DG, Chadwick OA, Chorover J (2011) Iron solid-phase differentiation along a redox gradient in basaltic soils. Geochim Cosmochim Acta 75: 119–133. https://doi.org/10.1016/j.gca.2010.10.005

Trivedi P, Axe L (2001) Ni and Zn Sorption to Amorphous versus Crystalline Iron Oxides: Macroscopic Studies. J Colloid Interface Sci 244: 221–229. https://doi.org/10.1006/jcis.2001.7970

Velde B, Peck T (2002) Clay Mineral Changes in the Morrow Experimental Plots, University of Illinois. Clays Clay Miner 50:364–370. https://doi.org/10.1346/000986002760833738

Violante A, Barberis E, Pigna M, Boero V (2003) Factors affecting the formation, nature, and properties of iron precipitation products at the soil-root interface. J Plant Nutr 26:1889–1908. https://doi.org/10.1081/PLN-120024252

Wang P, Wang J, Zhang H, et al (2019) The role of iron oxides in the preservation of soil organic matter under long-term fertilization. J Soils Sediments 19: 588–598. https://doi.org/10.1007/s11368-018-2085-1

Wang X, Li W, Harrington R, et al (2013) Effect of Ferrihydrite Crystallite Size on Phosphate Adsorption Reactivity. Environ Sci Technol 47: 10322–10331. https://doi.org/10.1021/es401301z

Wang X, Zhu M, Lan S, et al (2015) Formation and secondary mineralization of ferrihydrite in the presence of silicate and Mn(II). Chem Geol 415: 37–46. https://doi.org/10.1016/j.chemgeo.2015.09.009

Wilson G V., Rhoton FE, Selim HM (2004) Modeling the impact of ferrihydrite on adsorption-desorption of soil phosphorus. Soil Sci 169: 271–281. https://doi.org/10.1097/01.ss.0000126841.03965.3a

Winkler P, Kaiser K, Thompson A, et al (2018) Contrasting evolution of iron phase composition in soils exposed to redox fluctuations. Geochim Cosmochim Acta 235: 89–102. https://doi.org/10.1016/j.gca.2018.05.019

Zachara JM, Fredrickson JK, Smith SC, Gassman PL (2001) Solubilization of Fe(III) oxide-bound trace metals by a dissimilatory Fe(III) reducing bacterium. Geochim Cosmochim Acta 65:75–93. https://doi.org/10.1016/S0016-7037(00)00500-7

Zhang S, Xue X, Liu X, et al (2006) Current situation and comprehensive utilization of iron ore tailing resources. J Min Sci 42:403–408. https://doi.org/10.1007/s10913-006-0069-9

Zheng X, Xu X, Xu K (2011) Study on the risk assessment of the tailings dam break. Procedia Eng 26:2261–2269. https://doi.org/10.1016/j.proeng.2011.11.2433

8. FROM MUD TO SOILS: EARLY PEDOGENESIS OF ANTHROPOGENIC SOILS PRODUCED BY THE WORLD LARGEST MINING DISASTER

Abstract
Mining wastes represent an environmental liability to companies since as they can accidentally contaminate ecosystems. As a result, there has been numerous efforts to determine ways for proper storage or reuse of mine wastes by the mining industry. Amongst the innovative solutions, constructed soils from mine wastes may represent a safe fate for overburden, waste rocks, dumps, and tailings. However, the knowledge on the pedogenetic processes that govern these Anthropogenic soils' functioning is still scarce, limiting the assessment of their potential for providing ecosystem services usually ensured by natural soils. In this sense, the Fundão dam disaster offers a unique opportunity to evaluate the early pedogenesis on the Fe-rich deposited tailings at Doce River estuarine system. We aimed to study anthropogenic estuarine soil's pedogenesis at Doce River estuary and assess how the newly formed soils may provide ecosystem services or affect the overall ecosystem quality. Thus, we studied soils formed from deposited Fe-rich tailings and contrasted them to the bare mine tailings deposited on the estuary and tailings before its deposition. Within four years of pedogenesis, the fine particle accumulation (tailings), fast plant colonization, and the coupled Fe dynamic to the formation of a (Stagnic) Tidalic Spolic Technosol (or Anthropic Typic Hydraquent). Our data evidence the occurrence of different pedogenetic processes (development upbuilding, melanization, incipient paludization, bioturbation, gleization) that were responsible for the formation of an Anthropogenic soil but also for providing ecosystem services (i.e., carbon sequestration, nutrient cycling) previous unprovided. This study sheds new light on the time frame for soil formation, the resilience of tropical estuarine ecosystems, and the unwinding of the world's largest mining disaster.

Keywords: mine tailings, hydromorphic technosol, estuarine technosol, mining, Samarco

8.1. Introduction

The mining industry has been confronting a global crisis over the fate of mine wastes and tailing dams, which are extensively produced by mining companies (Cornwall, 2020). In recent years, dam failures have killed thousands of people worldwide, impacted vast landscapes, and thus, have imposed scientists, miners, and environmentalists to find feasible solutions to mine waste management (Cornwall, 2020; Gomes et al., 2017; Service, 2020). However, mining activity produces tons of a great variety of tailings a year, and finding a suitable fate for these materials is both technically and environmentally complex (Bagatto and Shorthouse, 2000; Rico et al., 2008).

In light of solutions, human-made/modified soils have been reported as a promising alternative, not only to remediate the environmental impacts from mining companies, but

also as an alternative fate for mine tailings (Asensio et al., 2019; Huot et al., 2014, 2013; Santini and Fey, 2016). For instance, recent studies in Brazil reported that Technosols constructed with wastes from mining activities were efficient in both promoting a nutrient-rich environment for plant growth and in providing different ecosystem services (e.g., provision of energy and food), in a similar manner, or even more efficiently, than natural soils (Ruiz et al., 2020a).

The Technosols, a Soil Group according to the World Reference Base for Soil Resources (IUSS Working Group WRB, 2014), are included in the concept of "Anthropogenic soils" (according to Soil Taxonomy; USDA, 2015), since their pedogenesis and properties are deeply affected by the artificial parent material (i.e., artefacts as: mine spoil, industrial waste, bricks, pottery, crushed stone), human-altered material, or human-transported material. Most studies have focused on constructed Technosols as a novel strategy for waste management, immobilization of contaminants, and thus, as allies to land reclamation (Pey et al., 2013; Ruiz et al., 2020a; Šimonovičová et al., 2017; Weiler et al., 2020). However, the process of soil pedogenesis has been rarely assessed; preventing a full understanding of the functioning of these human-made soils and their potential for providing ecosystem regulating (e.g., water purification, climate regulation), provisioning (e.g., food, freshwater, wood), and supporting services (e.g., nutrient cycling, primary production) (Huot et al., 2013; Ruiz et al., 2020b; Séré et al., 2012). Moreover, understanding soil pedogenesis in man produced Technosols provides applicable knowledge not only for the intentionally constructed Technosols but also for those resulting from environmental human-caused disasters (Huot et al., 2014).

The "Fundão" dam collapse (from the Samarco mining company) is recognized as the world largest mining disaster (Gomes et al., 2017; Queiroz et al., 2018; Gabriel et al., 2020a; Queiroz et al., 2021) (Escobar, 2015). It is one of the most emblematic examples of how mining activities have a great driving force capable of profoundly modifying the environment and of how the mine tailings may endanger vast ecosystems (Queiroz et al., 2021). The disaster took place in November 2015 at the Mariana municipality (SE Brazil; Hatje et al., 2017) when a mining dam collapsed and spilled more than 60 million m^3 of iron-ore tailings into the Doce River basin impacting over 600 km of terrestrial, freshwater and estuarine ecosystems (Gomes et al., 2017; Magris et al., 2019; Queiroz et al., 2021). Besides the initial and acute social and environmental impacts to multiple ecosystems, the mine tailings caused long term damage to aquatic organisms and offer a great ecological risk to human communities through soil and

water pollution (Bernardino et al., 2019; Cionek et al., 2019; Gabriel et al., 2020; Queiroz et al., 2021, 2018) . Since then, several efforts have been made by research groups, government agencies, environmentalists to reach solutions to the damages caused (Ferreira et al., 2021; Santana et al., 2020; Santos et al., 2019).

The deposited tailings at the Doce River estuary are mainly composed of iron (Fe) oxyhydroxides of different crystallinities (Queiroz et al., 2018). Iron is a valuable indicator for pedogenesis since its redox transformations play an important role in many processes in soil formation (i.e *ferrolysis*, *gleization*, *laterization*, and *pyritization*) which are responsible for producing a plethora of unique morphological features (Duball et al., 2020; Schwertmann, 1958), sometimes within short periods of time (Wiederhold et al., 2007). Thus, in the present work we hypothesize that four years (reflecting the Time as a soil-forming factor) are enough to trigger pedogenetic processes in the deposited Fe-rich tailings (Parent material) in response to the activity of biota (Organism factor) and seasonal flooding (Relief and Climate factors). To test this hypothesis, we studied soils formed from the deposited Fe-rich tailings and contrasted them to the bare mine tailings deposited on the estuary and to the tailings from inside the dam.Currently, the pedogenesis of estuarine Anthropogenic soils (i.e., Technosols; Donohue et al., 2009) is only reported from a number of sites globally, and this is the first study to report this process on a tropical estuarine ecosystem significantly impacted by Fe-rich mine tailings.

8.2. Materials and methods

8.2.1. Site description

The study site is located at the Doce River estuary is located on SE Brazil, which is a tropical region characterized by two distinct seasons (a dry winter and a wet summer), with a humid subtropical (Cfa), according to the Köppen classification (Alvares et al., 2013). The annual average rainfall is 1400 mm and the mean annual temperature is 22 °C. The fluvial regime is characterized by floods from December to March, and droughts from August to September (Mello et al., 2012).

The Doce River estuary is characterized by the presence of bare sandy islands (Fig. 1A) as a result of the fluvial activity and the sedimentation of coarse sediment carried from the

sedimentary basin (Quaternary age), mainly composed of sandy deposits from the Barreiras Geological Group (Coelho, 2009; Cohen et al., 2014). The mine tailing disaster in 2015 released massive amounts of tailings characterized by fine particles which were deposited on the top of the sandy banks and islands (Fig. 1B, C; Queiroz et al., 2018). After the disaster, riparian ecosystems in the Doce River estuary have seen the establishment and growth of dense *Eleocharis acutangula* (spikerush) stands over time (Fig. 1D).

8.2.2. Field work: sampling, soil description, and in situ measurements

Immediately after the disaster in November 2015, we sampled newly deposited tailings on the Doce River estuary (Fig. 1B). Four years later (2019), we sampled a soil profile at the same place colonized by *Eleocharis acutangula* (spikerush) (coordinates 19°38'14.58"S, 39°49'1.45"W; Fig. 1D). The sampled tailings in 2015 and the soil profile sampled in 2019 were morphologically described according to Soil Survey Manual (USDA, 2017). The soil profile was classified according to the Soil Taxonomy (USDA, 2015) and the World Reference Base – WRB (IUSS Working Group WRB, 2014).

Based on the Munsell color parameters of the studied materials, both the redness rating (RR) (Equation. 1) (Torrent et al., 1983) and the reduction intensity (rH) (Equation 2) (Munch and Ottow, 1983) were determined in all soil samples and on the bare mine tailings (from 2015).

$$RR = (10 - hue) \times \frac{chroma}{value} \qquad \text{(Equation 1)}$$

$$rH = \frac{Eh\ (mV)}{29} + 2pH \qquad \text{(Equation 2)}$$

For RR, chroma and value are numerical values from the Munsell Soil Color Chart, and the hue is the number preceding the indication of the dominant wavelength (e.g., YR) in the Color Chart, so that for 10YR the hue value is 10 and for 10R is 0 (Torrent et al., 1983). Regarding the rH, values = 0 indicate fully reduced conditions whereas rH ≥ 42.2 indicates entirely oxidized conditions (Munch and Ottow, 1983).

The soil pH and redox potential (Eh) were determined in situ using portable electrodes. A glass electrode previously calibrated with standard solutions (pH 4.0 and 7.0) was used for

pH determination, whereas the Eh values were recorded using a platinum electrode. The obtained values were adjusted by adding the value for the calomel reference electrode (+244 mV S.H.E.). To identify and study active pedogenetic processes, the soil samples collected in 2019 were compared with the newly deposited bare mine tailings of 2015 (i.e., days after the tailing arrival in the estuary) and to the buried sandy sediments of the previously bare sandy islands (buried at the bottom of the soil profile; Fig. 1).

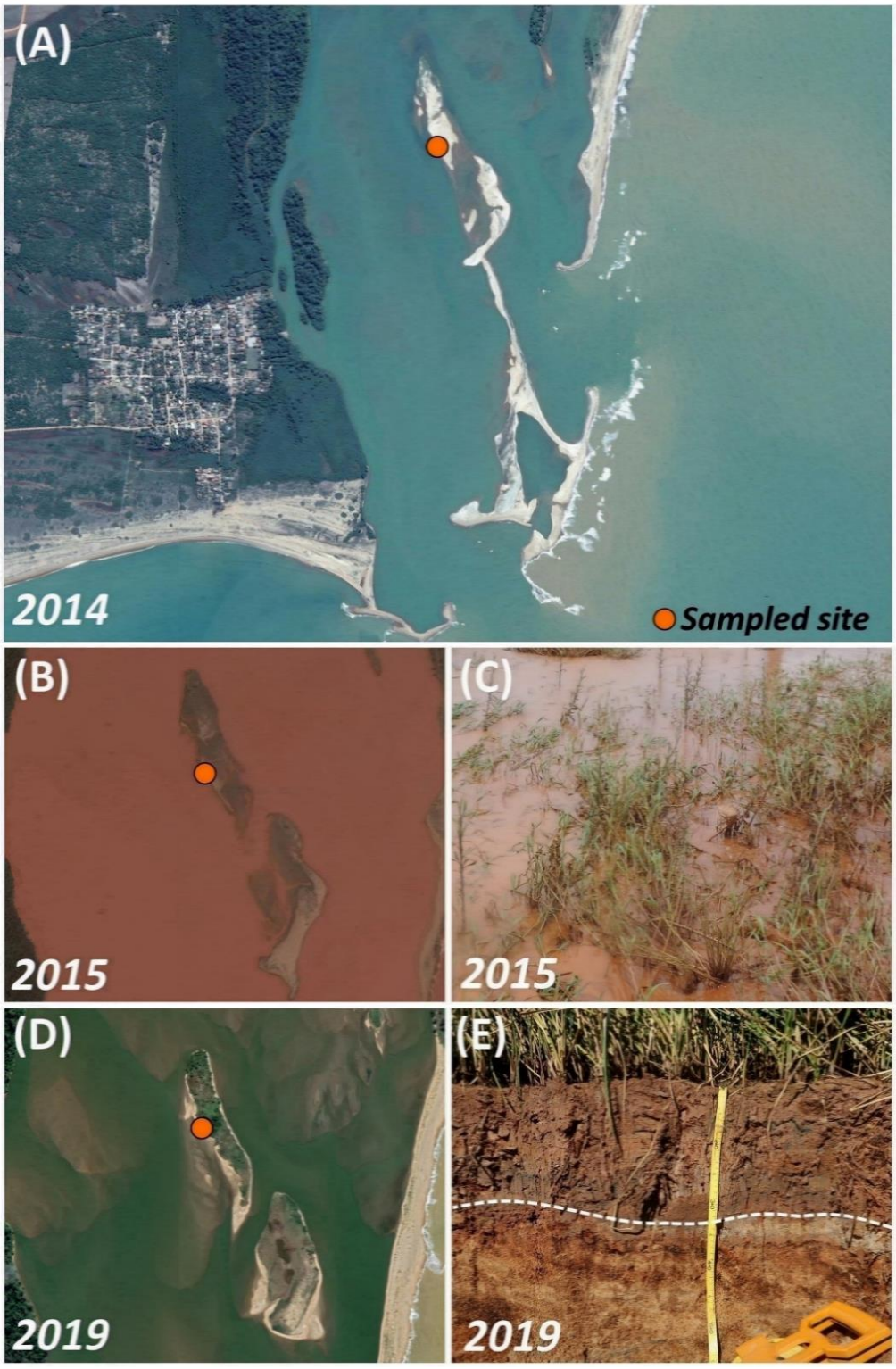

Fig. 1. The bare sandbanks and islands at the Doce River estuary in 2014 before the disaster (A) detailed image of the same island in 2015 soon after the disaster (B) detailed image highlighting both the tailings deposition and the colonization by plants in 2015 (C). Image of the same island four years after the disaster (in 2019) evidencing the dense colonization by *Eleocharis acutangula* (Spikerush) (D) a detailed image of 2019 highlighting the soil profile and the dense stand of *Eleocharis acutangula* (Spikerush) contrasting with the sandy material (bellow the white dashed line; E) from the buried bare sandy material of prior the disaster. The satellite images were obtained from Google™ Earth.

8.2.3. Physical, chemical, and mineralogical analysis of soil and tailing samples

Soil Organic carbon (OC) was determined by combustion oxidation using a Vario TOC Elementar (Langenselbold, German). Grain size distribution was performed using the pipette method (Gee and Bauder, 1986) after previous treatment using 6% (wt/wt) NaClO at pH 8.0 to remove soil organic matter (Mikutta et al., 2005). The Fe fractionation was performed by a combined method (Ferreira et al., 2007a; Otero et al., 2009) where six operationally different fractions were obtained: soluble and exchangeable Fe (EX); Fe associated with carbonates (CA); Fe associated with ferrihydrite (FR); Fe associated with lepidocrocite (LP); Fe associated with high crystalline oxides (i.e., hematite and goethite; CR); pyritic Fe (PY).

The mineralogical composition of soil samples and the iron tailing was performed by X-ray diffraction (XRD) on bulk samples analyzed as powder mounts. XRD analysis was performed in samples of the bare deposited tailings (collected in 2015) and soil samples from the horizons at the depths of 6–20 cm and 42+ cm (collected in 2019). These soil depths represent, respectively, the upper soil horizons (developed directly from the deposited Fe-rich tailings) and the buried sandbank from before the disaster (now at the bottom of the soil profile). The XRD patterns were obtained in a *Bruker D8 ADVANCE* device with CuKα radiation. The samples were scanned from 2–70° 2θ, step size of 0.05° 2θ and counting time of 5s $step^{-1}$.

8.3. Results

8.3.1. Mine tailings

The tailings deposited over the bare sand islands and banks in 2015 after the disaster Fig. 2) presented a clay loam texture (43 % of clay; Fig. 3A) with a massive structure, and colors (hues) characteristic of a Fe-oxide rich (red, 2.5 YR 5/6; Table 1) carbon-poor material (0.37% of carbon Fig. 3B).

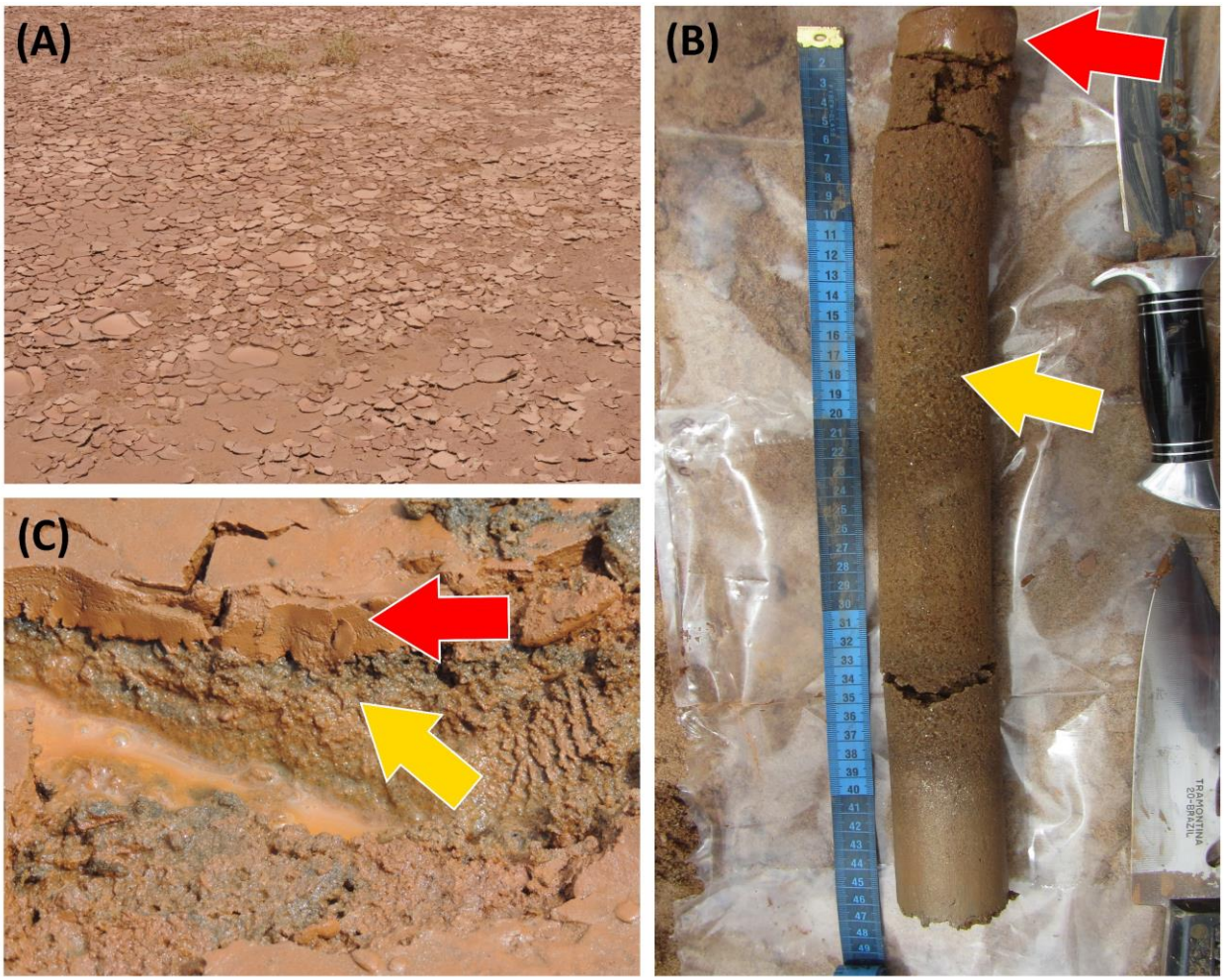

Fig. 2. The deposited tailings at the Doce River estuary in 2015 and the absence of vegetation (A). In detail, the newly deposited tailings (red arrow) over the sandy material deposited before the disaster (yellow arrow) highlighting the texture difference between both materials (B and C).

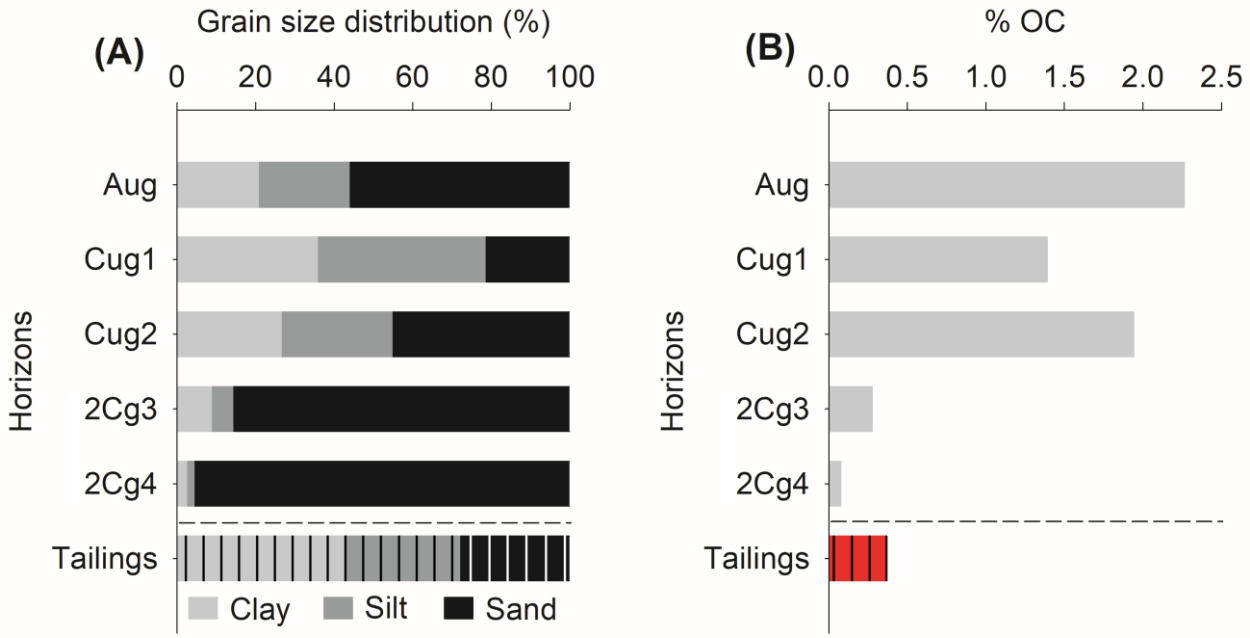

Fig. 3. Grain size distribution (A) and organic carbon contents (B) in the soil profile at Doce River estuary in comparison with the freshly deposited bare tailings of 2015 (below the dashed lines).

The XRD analysis corroborates that the deposited tailings were mainly composed of hematite, goethite, and kaolinite (Fig. 4), commonly associated with the mined Fe-rich ores of the region (e.g., Itabirite rocks; Silva et al., 2017). The Cug1 horizon was representative of the uppermost soil horizons (6–20 cm), and presented a mineralogical assemblage dominated by hematite, goethite, and kaolinite (Fig. 3). Contrastingly, the Cg4 horizon was the lowermost horizon (42+ cm) and was essentially composed of quartz (Fig. 4).

The Eh (+360 mV), pH (6.0), and calculated rH values (24.4; Table 1) indicated the predominance of slightly oxic conditions soon after the mine tailings deposition in 2015 (see Essington, 2015). The Fe fractionation of the bare tailings indicated that 93% of the Fe content was associated with high crystalline Fe oxides (hematite and goethite), followed by poorly crystalline Fe oxyhydroxides (FeLP: 3% and FeFR: 3%). The other fractions (FeEX, FeCA, and FePY) represented ~ 1% of the Fe content.

Table 1 – Main morphological attributes and physicochemical properties of the Anthropogenic soil profile and the bare deposited tailings in Doce River estuary

Horizon	Depth (cm)	Matrix Color†	Soil Color	RR	Struct.	Text.	pH	Eh (mV)	rH	Observations
Bare deposited tailing (2015)										
Tailings	-	2.5 YR 5/6	red	9.0	MA	CL	6.0	+360	24.4	-
Anthropogenic soil profile (2019)										
Aug	0–6	5YR 5/4	reddish-brown	5.0	GR	SCL	5.0	+132	14.6	Common quantities of roots
Cug1	6–20	5YR 5/6	yellowish-red	6.0	MA	CL	5.2	+316	21.3	Moderately few quantities of roots, presence of grayish mottled (5YR 4/1)
Cug2	20–30	5YR 5/2	reddish-gray	2.5	MA	LS	6.0	+47	13.6	Presence of grayish mottled (5YR 5/1)
2Cg3	30–42	5YR 5/3	reddish-brown	2.9	SG	S	5.9	+218	19.3	Presence of reddish mottled (5YR 4/4)
2Cg4	42+	7,5 YR 7/6	reddish-yellow	2.1	SG	S	5.8	+322	22.7	Presence of reddish mottled (5YR 4/5)

†Colors were obtained from wet samples; RR: redness rating; Struct: soil structure; Text: soil texture; Eh: redox potential; rH: reduction intensity; GR: granular; MA: massive; SG: single grain; S: sand; LS: loamy sand; SCL: sand clay loam; CL: clay loam.

8.3.2. Anthropogenic soil

The Anthropogenic soil profile sampled in 2019, four years after the disaster, exhibited five horizons: Aug, Cug1, Cug2, 2Cg3, and 2Cg4 (Fig. 4A). The first three horizons (i.e., Aug, Cug1, and Cug2) differed significantly (Fig. 5D) from the 2Cg3 and 2Cg4 horizons (Fig. 5G), especially with respect to their grain size distribution (Fig. 3A). The three first horizons were composed on average by 30 ± 9 % of fine particles (i.e., clay + silt), with the higher amounts observed in the Cug1 and Cug2 horizons (39% and 27%, respectively; Fig. 3A). Contrarily, the contents of fine particles in 2Cg3 and 2Cg4 were, on average, below 5%, evidencing a coarse texture.

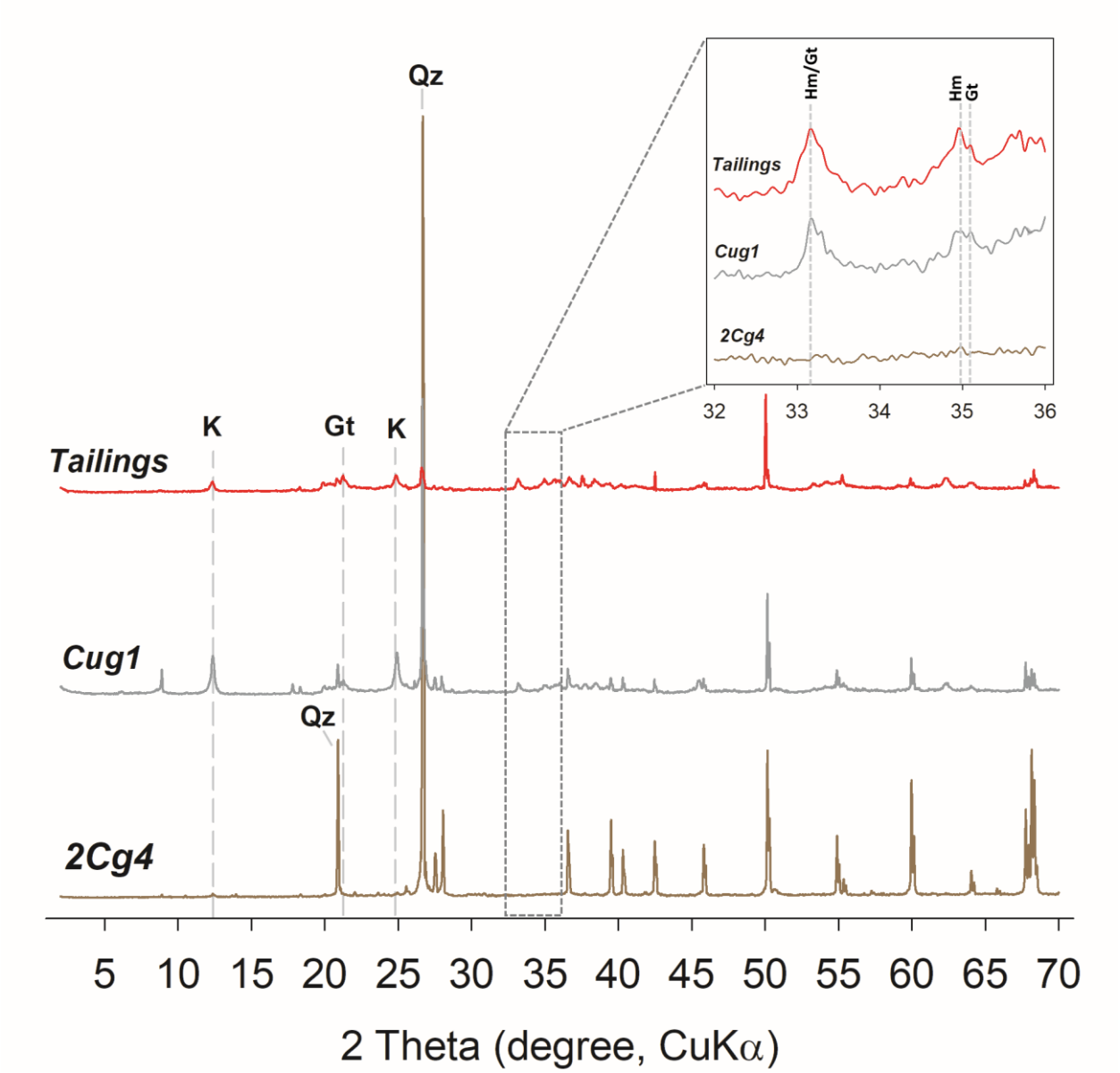

Fig. 4. XRD analysis of a non-oriented sample of the deposited tailings (2015) and of the Cug1 (6–20 cm) and 2Cg4 horizons (42+ cm); collected in 2019. Gt: Goethite; Hm: Hematite; K: Kaolinite; Qz: Quartz.

The surface Aug horizon (0–6 cm) presented a sandy clay loam soil texture, a granular structure (Fig. 4B), common roots (Table 1), OC content of 2.3 % (Fig. 3B), and reddish-brown colors. On the other hand, the two underlying subsurface horizons (Cug1 and Cug2) presented massive structures (i.e., absence or low degree of pedalization; Table 1; Fig. 5C), moderately few roots, and OC contents of 1.4% and 1.9%, respectively (Fig. 3B). The Cug2 horizon was also marked by the presence of grayish mottles (Table 1; Fig 5D).

The two bottom horizons were identified as 2Cg3 and 2Cg4 due to a contrasting change in texture to a sandy, light-colored, and single-grained horizon (Table 1). The 2Cg3 horizon

showed expressive reddish mottling within its sandy matrix. Both sandy soil horizons (Fig. 1E) also presented significantly lower carbon contents (2Cg3 = 0.3% and 2Cg4 = 0.1%).

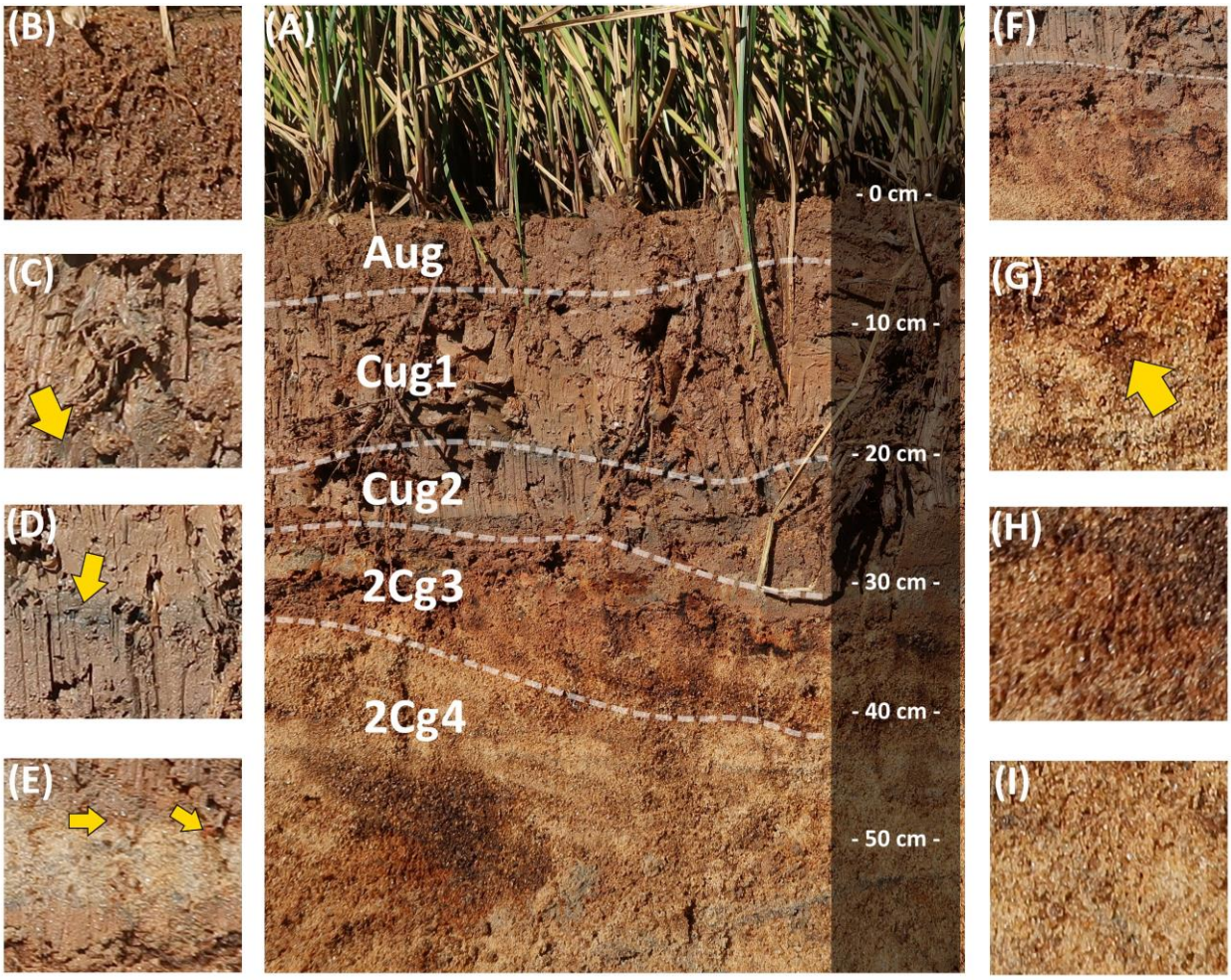

Fig. 5. The Anthropogenic soil profile sampled at the Doce River estuary in 2019, four years after the mine tailing arrival (A). In details, the abundance of roots and the granular structure in the Aug horizon (B); the massive soil structure with moderately few quantities of roots in the Cug1 horizon (C); the gray colors in the soil matrix in Cug2 horizon (D); the reddish mottles in the 2Cg3 (E); the contrasting gray colors within Cug2 (above the dashed line) horizon in comparison with the reddish mottling within the sandy matrix of the 2Cg3 horizon (below the dashed line) (F); detail of the reddish mottling the 2Cg3 horizon (G); detail of the abundance of reddish mottles within the sandy matrix of 2Cg3 (H); detail of the absent soil structure (single grained) within the whitish sandy matrix of horizon 2Cg4.

The soil profile's physicochemical conditions showed pH values ranging from 5.0 to 6.0, indicative of very strongly to moderately acid conditions (USDA, 2017). The lowest pH value (5.0) was recorded in the Aug horizon (Table 1). The Eh values ranged from +47 to +360 mV, with the lowest Eh value recorded in the Cug2 (Table 1). On the other hand, the highest Eh

value was determined in the 2Cg4 (+322 mV) horizon. The rH values were 14.6, 21.3, 13.6, 19.3, and 22.7 for the Aug, Cug1, Cug2, 2Cg3, and 2Cg4, respectively (Table 1).

For the soil profile, the sequential extraction also showed a dominance of Fe oxyhydroxides in all horizons, however with significant changes when compared to the bare tailings. On average, the poorly crystalline Fe oxyhydroxides (FeFR and FeLP) increased to 32%, whereas the crystalline Fe oxides (FeCR) decreased to 67% (Fig. 6). Additionally, the higher Fe contents were observed in the first three horizons (14,687 ± 2,923 mg kg^{-1}), whereas in the bottom sandy horizons the Fe contents were, on average, 4,973 ± 5200 mg kg^{-1} (Fig. 6).

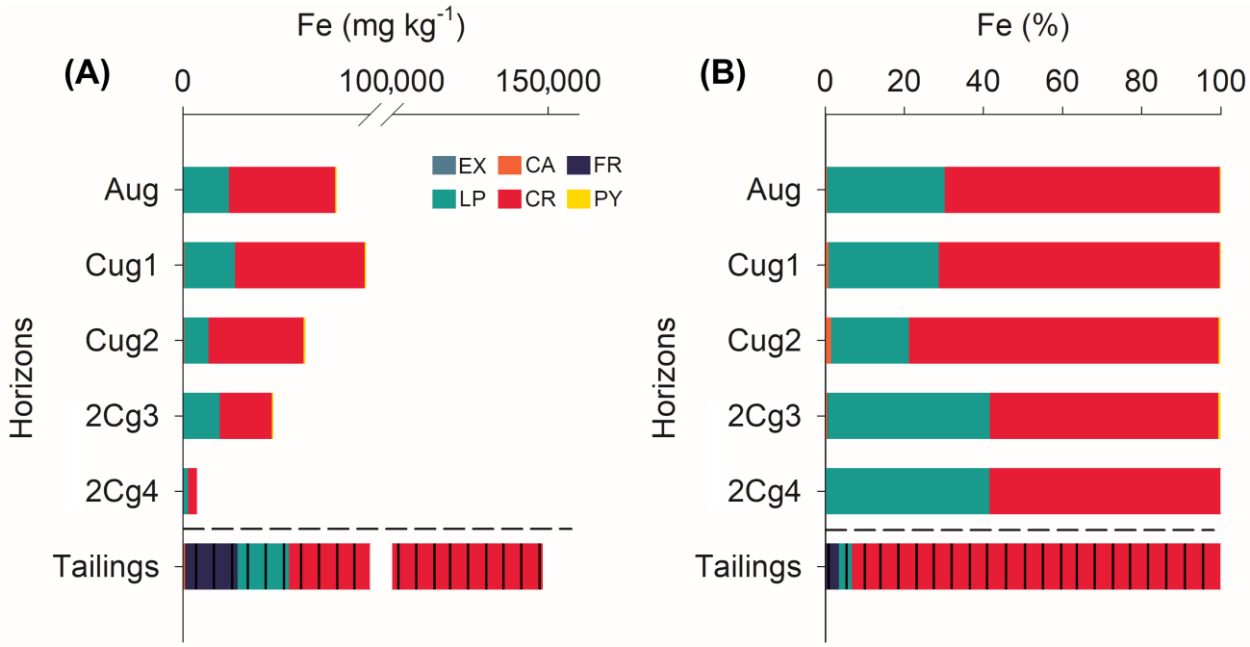

Fig. 6. Fe solid phase fractionation (A) and the percentages of each Fe fraction (B) in the Anthropogenic soil profile (from 2019) and in the bare tailings (from 2015; below the dashed lines). EX: exchangeable Fe; CA: Fe associated with carbonate; FR: Fe associated with ferrihydrite; LP: Fe associated with lepidocrocite; and PY: Fe-pyrite. The percentage of each fraction was determined based on the sum of all fractions, i.e., pseudo-total content.

8.4. Discussion

The tailings' clay texture results from the long-distance traveled (600 km) by the tailings' plume towards the estuary prior to its deposition (Gomes et al., 2017). The transport down river likely selected finer tailing particles which gradually accumulate in the estuary (Fig. 2.; Deletic, 2005). Thus, the grain size distribution of the first three upper soil horizons (i.e., Aug, Cug1, and Cug2) differed significantly (Fig. 4D) from the 2Cg3 and 2Cg4 horizons (Fig. 3A; Fig. 5G). The XRD results and the particle size distribution support the similarity between the Cug1 horizon and the tailings (e.g., clay; Fig. 3A), which present a similar mineralogical assemblage composed of hematite, goethite, and kaolinite (Fig. 4). The sandy texture in the bottom horizons (30 cm downwards) that contrast with the overlying horizons (Fig. 5F), represents a lithological discontinuity (Ahr et al., 2017). The diffractograms corroborate the lithological discontinuity at 30 cm at the boundary between the Cug2 and 2Cg3 horizons since they show a dominance of quartz in the 2Cg4 horizon. Both horizons are related to the preexisting sand banks before the disaster, which were subsequently buried by the Fe-rich tailings.

After the dam rupture, the deposition of fine particles in some areas likely created favorable conditions for the settlement and growth of E. *acutangula* (Fig. 5A; Fig. 7). In fact, different studies have suggested that plant propagules are more easily washed away by tides in bare sandy sites, which may remain uncolonized for long periods of time (Balke et al., 2013). On the other hand, the continuous deposition of fine particles can provide propagules from being washed out since they anchor rapidly upon stranding (Barko and Smart, 1978; Di Nitto et al., 2008) and, thus, resist the disturbance by tidal and other forces (Balke et al., 2011).

Fig. 7. The expressive *Eleocharis acutangula* colonization on the deposited tailings at Doce River estuary forming the Anthropogenic soil in 2019.

The colonization by plants also promoted an increased organic carbon input into the soil (Fig. 3B). This is supported by the 5 to 10-fold increase in mean OC contents in the first three horizons (1.9 ± 0.4% of OC) when compared to the OC contents of the tailings (0.4%; Fig. 3B), and the bottom horizons (i.e., 2Cg3 and 2Cg4; 0.2%). Previous studies have showed the ability of *Eleocharis acutangula* in incorporating high amounts of organic carbon into the soil by roots growth (Fig. 5B, C), decomposition of dead roots, and litter deposition (Alongi, 2012; Ferreira et al., 2019; Stagg et al., 2018), which would lead to the formation of an Aug horizon enriched in organic matter. The effect of plants in the genesis of the Aug horizon's is also corroborated by the presence of roots and by the higher degree of pedalization (i.e., aggregates presence) evidenced by the granular structure (Fig. 5B; Table 1).

The high OC contents in the Aug horizon may indicate an incipient paludization, a pedogenetic process related to the accumulation of organic matter under anaerobic conditions, which has been widely reported in wetland soils from estuarine ecosystems (Ferreira et al., 2007b; Gomes et al., 2016; Schaetzl and Thompson, 2015). The high potential of wetlands to accumulate carbon is globally recognized (Macreadie et al., 2019; Nahlik and

Fennessy, 2016). In fact, these ecosystems are recognized as one of the largest components of the terrestrial carbon pool, especially due to their soils (Chmura et al., 2003; Mitsch et al., 2013).

This higher OC resulted in the darkening of the mineral material in the Aug horizon which presented reddish-brown colors (Table 1). The darkening of the soil material by the admixture of organic matter and humus is indicative of a melanization process (Schaetzl and Thompson, 2015). In this case, both the plant roots and fauna bioturbation may have an important role in incorporating carbon into the studied soil (Bernardino et al., 2020; Sarker et al., 2020; Vidal-Torrado et al., 2010). In fact, several crab (*Minuca rapax*) burrows were observed in the study site (Fig. 8). Additionally, many works have evidenced that the soil mixing by fauna bury litterfall, increase the carbon contents, improve the soil structure, and favors the soil darkening (Bernardino et al., 2020; Sarker et al., 2020; Wang et al., 2010).

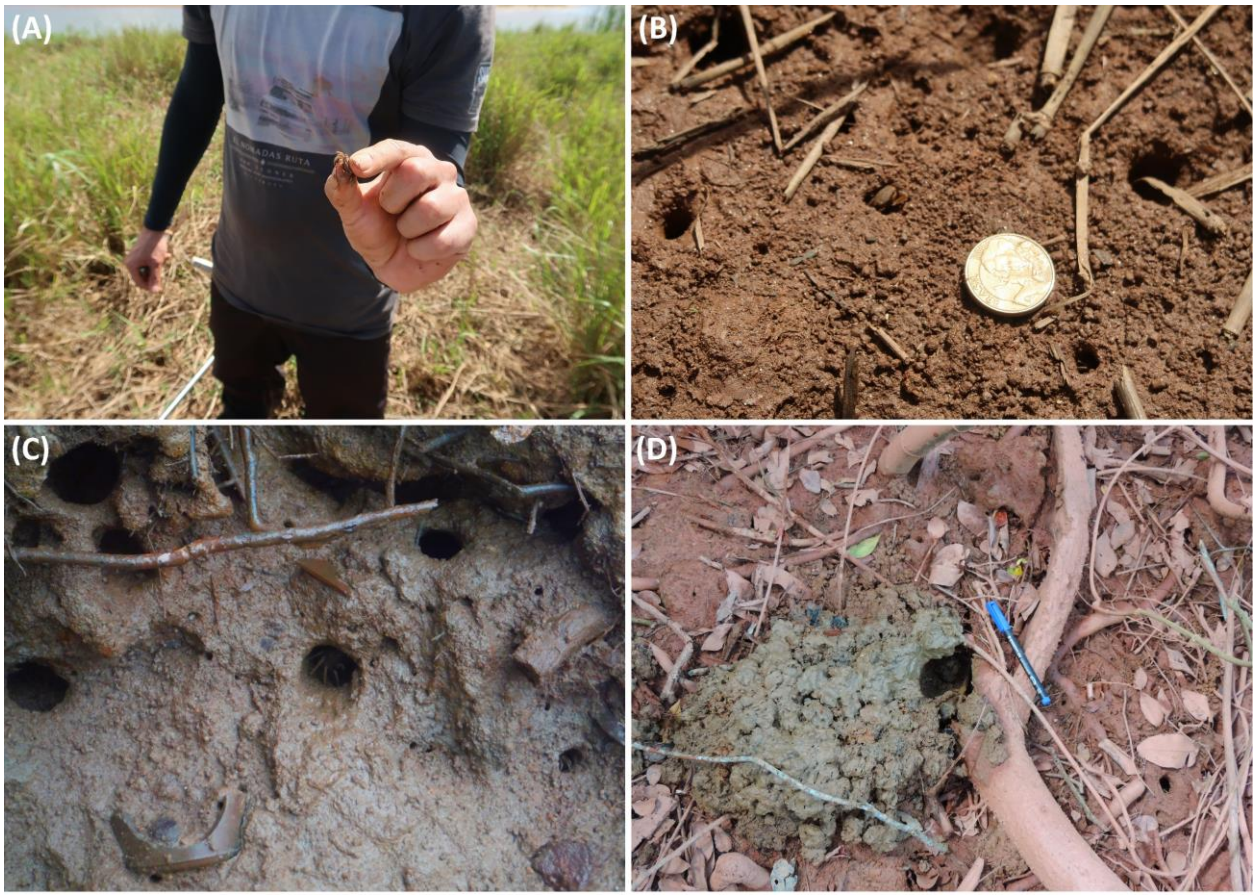

Fig. 8. The presence of crab (Minuca rapax) at the Doce River estuarine soils (A); the effect of soil fauna contributing to soil structure (granular structure) (B). In detail, the crab (M. rapax) burrows (C); and the red Fe-rich mine tailings bioturbated by the local fauna (D) at the Doce River estuary.

Besides its effects on the OC contents, the vegetation has probably enhanced the trapping of fine particles through their stems, by decreasing the turbulence kinetics and promoting the accumulation of clay particles (Jay et al., 2007; Mudd et al., 2010). The result was the thickening of the Anthropogenic soil profile towards the surface (i.e., a developmental upbuilding or a cumulization process; see Almond and Tonkin, 1999; Inoue et al., 2011) by additions of mineral particles to the surface of the soil. This developmental upbuilding promoted by slow additions that can be incorporated by pedogenesis may have improved the carbon contents since Fe oxyhydroxides establish organo-mineral associations that stabilize soil organic matter (Giannetta et al., 2020; Kida and Fujitake, 2020; Seyfferth et al., 2020). A continued deposition of mine tailings at the estuary will probably occur due to the enormous quantity of tailings that are yet accumulated on the river basin (Hatje et al., 2017; Palu and Julien, 2019). Thus, the seasonal flooding, wind, and river currents that constantly transport tailings and suspended fine particles towards the estuary will maintain of the developmental soil upbuilding in the following years. The lowest pH in the Aug horizon is also an effect of the plant colonization and the release of organic acids (e.g., oxalate, acetate, lactate) from roots, which may decrease the pH in wetland soils (Blossfeld et al., 2011).

The Eh and the rH values < 20 (Table 1) evidenced the marked reduced conditions within the Aug and Cug2 horizons, moderate reducing conditions in Cug1 and 2Cg3 horizons, and slightly oxic conditions within the 2Cg4 horizon (Table 1; see Essington, 2015). Therefore, the mottles (i.e., redoximorphic features; Fig. 5D, E) observed throughout the entire soil profile indicate redox conditions that favor both the mobilization (reductive dissolution) and reprecipitation of Fe forms (i.e., $Fe^{2+} \leftrightarrow Fe^{3+}$; Fig. 6). These redoximorphic features are produced by the frequent waterlogging from daily tides and matched the criteria for the gleyed horizons (i.e., suffix g) (Fiedler and Sommer, 2004; Nóbrega et al., 2018; USDA, 2017). Plants may also have contributed to Fe mobilization within the soil profile by releasing Fe-complexing organic acids from roots, further favoring the genesis of the gley horizons and the redoximorphic features (Lee et al., 2008; Lindsay, 1991; Zhou et al., 2011).

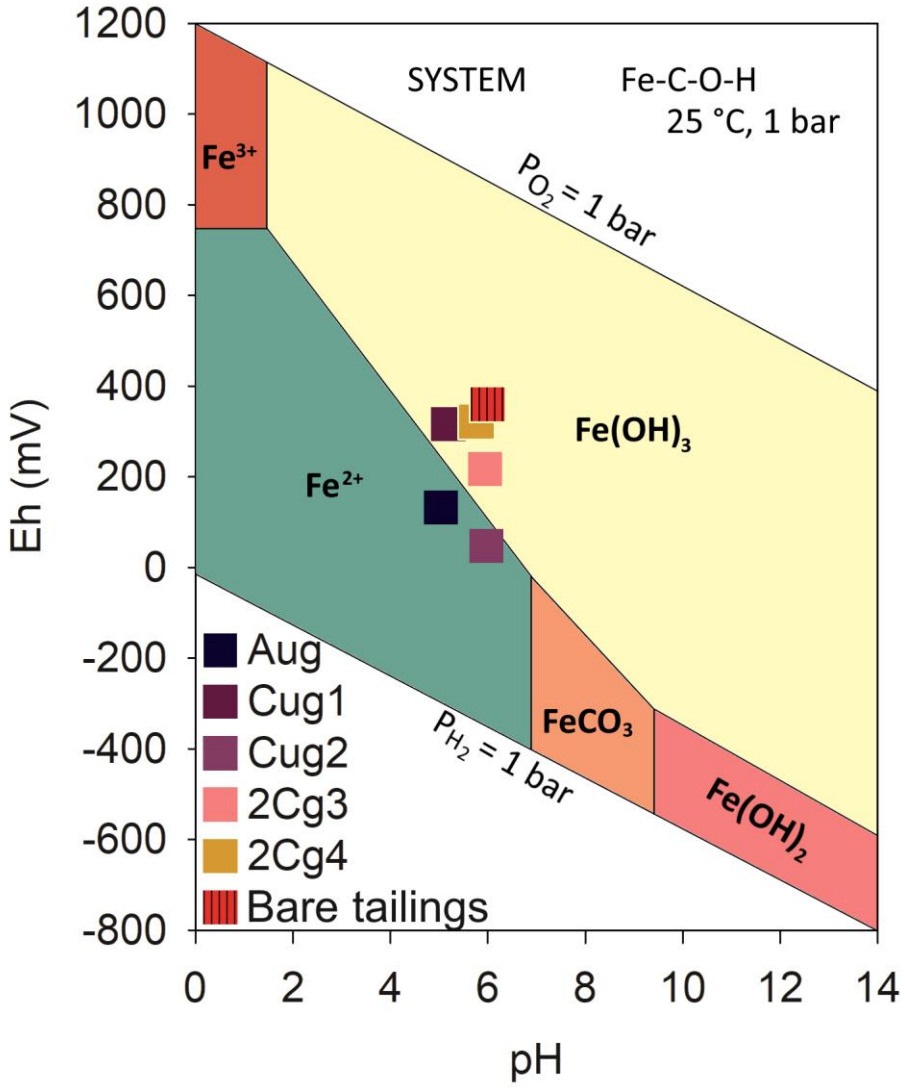

Fig. 9. Eh–pH diagram (adapted from Brookins, 1988) with data from all the studied horizons of the Anthropogenic soil (2019) and the deposited tailings (2015). The plots highlight the favorable conditions to Fe^{2+} within Aug and Cug2 horizons in contrast to the strongly favorable conditions to Fe oxidized forms (i.e., oxyhydroxides) in the deposited tailings and in the bottom sandy horizons (2Cg3 and 2Cg4).

The tailings' deposition produced the higher Fe contents observed in the Aug (Fe: 1,4755 mg kg^{-1}), Cug1 (Fe: 1,7575 mg kg^{-1}), and Cug2 (Fe: 1,1731 mg kg^{-1}) horizons (Fig. 6). However, the Fe contents of these horizons were on average 562% lower than the Fe contents found in the deposited tailings of 2015 (148,114 mg kg^{-1}; Fig. 6). These results evidence a massive Fe loss within four years (Fig. 6). This is the result of a gleization process where the

Fe^{III} present in the Fe oxyhydroxides of tailings (Lovley et al., 2004; Schaetzl and Thompson, 2015) is transformed to Fe^{2+} by microorganisms during the anaerobic organic matter decomposition under the reducing conditions (Fig. 9). Additionally, the lowest pH values in the superficial horizons may also have favored the iron losses (Kraemer, 2004; Lindsay and Schwab, 1982). Finally, the fast plant colonization and the release of organic acids from roots may enhanced Fe losses due to Fe complexation (Blossfeld et al., 2011; Tombácz et al., 2004) or to Fe uptake. In fact, many studies have shown that estuarine plant species uptake and store Fe in minor amounts since it is a micronutrient which occurs in low concentrations and has low bioavailability in soils (Prade et al., 1993; Singh and Rai, 2016; Taylor and Crowder, 1983). As a result of the gleization process, Fe can reach coastal waters where it is a key element for primary productivity, phytoplankton growth, and the biogeochemical cycles of N, C, P and Si (Hutchins and Boyd, 2016; Martin, 1990; Tagliabue et al., 2017).

The gleization process in the Anthropogenic soil profile produced clear morphological evidence by producing grayish soil colors (Schaetzl and Thompson, 2015; Veneman et al., 2015) in the Cug2 horizon (Fig. 5D). In fact, the physicochemical conditions (i.e., pH and Eh; Table 1; Fig. 9), and the rH values observed in the Aug and Cug2 horizons (Table 1) corroborate the favorable conditions to Fe reduction (Fig. 8) (Essington, 2015; Reddy and DeLaune, 2008).

The Fe losses were significantly more pronounced in the Cug2 horizon (Fig. 9A) and mostly related to the poorly crystalline Fe oxyhydroxides (i.e., FR and LP), which decreased on average 53% in comparison to the overlying horizon (i.e., Cug1 Fig. 9A). Indeed, poorly crystalline Fe oxyhydroxides are more susceptible to reductive dissolution under redox active environments mediated-microbial Fe reduction (Bhattacharyya et al., 2018; Larsen and Postma, 2001; Zhao et al., 2020). In this case, the gleization process decreased the redness rating in the Cug2 horizon (RR: 2.5), especially when compared to the color of the newly deposited tailings of 2015 (RR: 9), further corroborating the fast action of the gleization process in the Anthropogenic soil profile.

On the other hand, the sandy 2Cg3 horizon showed redder colors and higher RR (2.9) than the 2Cg4 (RR: 2.1) horizon (Fig. 4H; Table 1). Despite the sandy texture, there was an increase by 20% in the poorly crystalline Fe oxides (FR and LP; Fig. 9B) in the 2Cg3 horizon when compared to the Cug2 horizon, that presents a finer texture (loamy sand). In addition, the content of clay in the 2Cg3 horizon was 9-fold higher than the underlying 2Cg4 horizon (Fig. 3A). These results evidence both the mobilization and reprecipitation of Fe within the

Anthropogenic soil profile. In this case, the released Fe^{2+} from the reduction of Fe oxyhydroxides in the overlying horizons (Cug1 and Cug2) was probably translocated in soil solution during lowering tides to the sandier texture of the 2Cg3 horizon. In this coarser soil horizon, redox conditions (Fig. 9) favor Fe^{2+} oxidation and its reprecipitation as the low-crystalline Fe oxyhydroxides in 2Cg3 (Azoor et al., 2019; Yin et al., 2019). The sandy texture promotes fast drainage and rapid downward flux of water during low tides and, thus, a rapid O_2 diffusion through soil pores (Anschutz et al., 2019; Sartor et al., 2018). In fact, Fe^{2+} can be rapidly oxidized (within hours; Barcellos et al., 2018) and precipitate as low-crystalline Fe oxides under geochemical environments characterized by Eh values above +100 mV and circumneutral pH (Albuquerque et al., 2014; Anschutz et al., 2019; Sartor et al., 2018). Accordingly, the higher Eh values observed in the 2Cg3 (+218 mV) corroborate the favorable conditions to Fe^{2+} oxidation, which also led to the formation of the described redoximorphic features (e.g., reddish mottles; Fig. 5G, H).

Based on the morphological, physical, chemical and mineralogical data, the studied soil profile was classified as Anthropic Typic Hydraquent according to Soil Taxonomy (USDA, 2015) and as a (Stagnic) Tidalic Spolic Technosol (Fig. 5A), according to World Reference Base for Soil Resources (IUSS Working Group WRB, 2014). In the latter, the primary qualifier “Tidalic” indicates that the soil profile is affected by tidal water flux while the “Spolic” indicates that the soil has been developed from artifacts i.e., industrial spoil (tailings, from the mine disaster). On the other hand, both the “Stagnic” supplementary qualifier (IUSS Working Group WRB, 2014) and the Hydraquent group (USDA, 2015) indicate an intense influence of water on the soil properties. Stagnic properties, according to IUSS Working Group WRB (2014), are defined as soil materials saturated with surface water (in this case, tidal water) for a period long enough that allows reducing conditions to occur; corroborated in this study by the Eh < +120 mV and the rH < 20 (Table 1). Additionally, the Fe-rich mine tailings are considered artifacts (i.e., mine spoils) that occupies ≥ 20 % of soil volume, which also allow the classification of an Anthropogenic soil according to Soil Taxonomy (USDA, 2015) and a Technosol according to IUSS Working Group WRB (2014).

During the four years following the disaster, both the developmental upbuilding produced by the tailings’ deposition (Fig. 5) and the fast vegetation growth triggered a fast pedogenetic process leading to the formation of an Anthropogenic soil formation. In this sense, we propose a model for the soil formation at the Doce River estuary after the Fe-rich

tailing arrival in 2015 (Fig. 10). Initially, the estuary was characterized by the presence of natural riparian ecosystems with bare sandy islands and banks. In 2015, the Fe-rich muddy tailings composed mainly of iron oxides were deposited over these sandbanks. The fine particle deposition led to favorable conditions to the settlement and growth of E. *acutangula* over time promoted high organic carbon inputs into the soil, the formation of granular soil structure, and the darkening of the surface horizons. Over time, the plant development further enhanced the trapping of more clay particles and organic carbon inputs. The increase OC deposition led to more anoxic conditions favorable to Fe reduction, promoting both Fe losses from the soil and its remobilization within the profile. The Fe mobilization and reprecipitation into the soil profile resulted in the numerous redoximorphic features with gray or whitish-gray colors and reddish mottles within clayey horizons. Fe reprecipitation as poorly crystalline Fe oxyhydroxides led to the formation of reddish mottles in the sandy horizons.

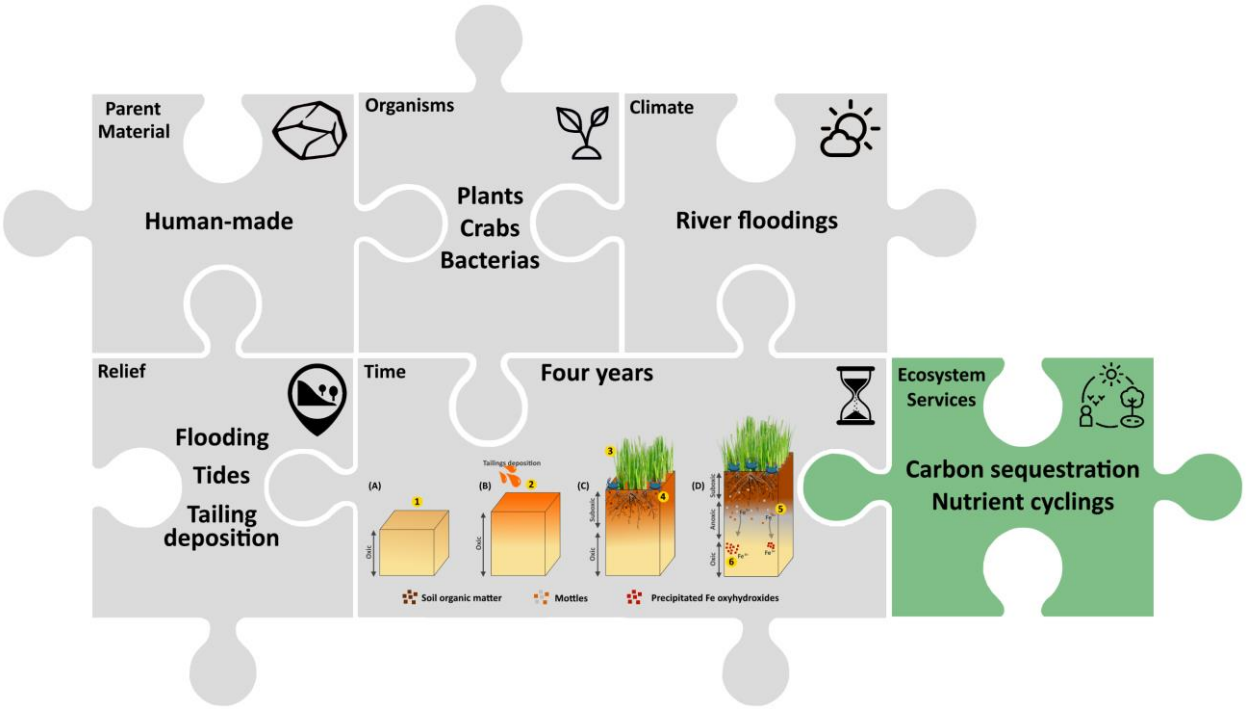

Fig. 10. (A) A schematic conceptual model illustrating the action of the soil-forming factors and the sequence of events leading to the pedogenesis of the Anthropogenic soil at the Doce River estuary after the disaster (order provided in yellow circles); (1) bare sandy islands/banks; (2) deposition of the Fe-rich tailings; (3) colonization by E. *acutangula*; (4) organic carbon inputs into the soil; (5) establishment of anoxic conditions leading to iron reduction and mobilization; (6) reprecipitation of Fe in the mottled sandy horizons. (B) The newly formed estuarine Anthropogenic soil provides the new ecosystem services (e.g., carbon sequestration and nutrient cycling, i.e., iron).

8.5. Conclusions

Our findings reveal that within four years a bare clayey Fe-rich tailing developed into an anthropogenic soil with marked soil forming processes including the developmental upbuilding or cumulization, melanization, bioturbation, incipient paludization and gleization. This study brings the first pedological record of an Anthropogenic soil profile formed in a tropical estuarine ecosystem and supports the role of the soil forming factors (e.g., Climate, Organisms, Relief, Parent material, and Time) on its early pedogenesis and on the resilience of an impacted estuarine environment. Additionally, the rapid soil formation resulted in a significant accumulation of organic carbon, suggesting a high potential for carbon sequestration of this newly formed Anthropogenic soil. Moreover, the significant iron losses may supply the estuarine plants and coastal waters with this crucial micronutrient. Thus, our findings reveal that, despite all the impacts caused by the dam failure, the Doce River estuarine Anthropogenic soil may reach a biogeochemical equilibrium within the estuarine environment and provide ecosystem services that were previously unprovided (e.g., carbon sequestration, nutrient cycling), this possibility must be further explored and monitored in the following years.

Acknowledgments

This work received financial support provided by the Fundação de Amparo à Pesquisa e Inovação do Espírito Santo (FAPES, grant number 77683544), Coordenação de Aperfeiçoamento de Pessoal de Nível Superior CAPES (Finance Code 001), Conselho Nacional de Desenvolvimento Científico e Tecnológico (CNPq, grants number 301161/2017-8 and 305996/2018-5 to AFB and TOF, respectively), São Paulo Research Foundation (FAPESP, grants number 2018/04259-2, 2018/08408-2, 2019/18324-3, 2019/17413-2, 2019/14800-5, and 2019/19987-6), Fundação Carlos Chagas Filho de Amparo à Pesquisa do Estado do Rio de Janeiro (GNN, JCNE Grant E-26/202.757/2019), and Xunta de Galicia-Consellería de Educación e Ordeanción Universitaria de Galicia (Consolidation of competitive groups of investigation; GRC GI 1574), and CRETUS strategic group (AGRUP2015/02).

References

Ahr, S.W., Nordt, L.C., Schaetzl, R.J., 2017. Lithologic Discontinuities in Soils. Int. Encycl. Geogr. People, Earth, Environ. Technol. 1–8. https://doi.org/10.1002/9781118786352.wbieg0816

Albuquerque, A.G.B.M., Ferreira, T.O., Nóbrega, G.N., Romero, R.E., Júnior, V.S.S.S., Meireles, A.J.A.A., Otero, X.L., 2014. Soil genesis on hypersaline tidal flats (apicum ecosystem) in a tropical semi-arid estuary (Ceará, Brazil). Soil Res. 52, 140. https://doi.org/10.1071/SR13179

Almond, P.C., Tonkin, P.J., 1999. Pedogenesis by upbuilding in an extreme leaching and weathering environment, and slow loess accretion, south Westland, New Zealand. Geoderma 92, 1–36. https://doi.org/10.1016/S0016-7061(99)00016-6

Alongi, D.M., 2012. Carbon sequestration in mangrove forests. Carbon Manag. 3, 313–322. https://doi.org/10.4155/cmt.12.20

Alvares, C.A., Stape, J.L., Sentelhas, P.C., de Moraes Gonçalves, J.L., Sparovek, G., 2013. Köppen's climate classification map for Brazil. Meteorol. Zeitschrift 22, 711–728. https://doi.org/10.1127/0941-2948/2013/0507

Anschutz, P., Bouchet, S., Abril, G., Bridou, R., Tessier, E., Amouroux, D., 2019. In vitro simulation of oscillatory redox conditions in intertidal sediments: N, Mn, Fe, and P coupling. Cont. Shelf Res. 177, 33–41. https://doi.org/10.1016/j.csr.2019.03.007

Asensio, V., Flórido, F.G., Ruiz, F., Perlatti, F., Otero, X.L., Oliveira, D.P., Ferreira, T.O., 2019. The potential of a Technosol and tropical native trees for reclamation of copper-polluted soils. Chemosphere 220, 892–899. https://doi.org/10.1016/j.chemosphere.2018.12.190

Azoor, R.M., Deo, R.N., Birbilis, N., Kodikara, J., 2019. On the optimum soil moisture for underground corrosion in different soil types. Corros. Sci. 159, 108116. https://doi.org/10.1016/j.corsci.2019.108116

Bagatto, G., Shorthouse, J.D., 2000. Evaluation of municipal solid waste (MSW) compost as a soil amendment for acidic, metalliferous mine tailings. Int. J. Surf. Mining, Reclam. Environ. 14, 205–214. https://doi.org/10.1080/13895260008953324

Balke, T., Bouma, T., Horstman, E., Webb, E., Erftemeijer, P., Herman, P., 2011. Windows of opportunity: thresholds to mangrove seedling establishment on tidal flats. Mar. Ecol. Prog. Ser. 440, 1–9. https://doi.org/10.3354/meps09364

Balke, T., Webb, E.L., den Elzen, E., Galli, D., Herman, P.M.J., Bouma, T.J., 2013. Seedling establishment in a dynamic sedimentary environment: a conceptual framework using mangroves. J. Appl. Ecol. 50, 740–747. https://doi.org/10.1111/1365-2664.12067

Barcellos, D., Cyle, K.T., Thompson, A., 2018. Faster redox fluctuations can lead to higher iron reduction rates in humid forest soils. Biogeochemistry 137, 367–378. https://doi.org/10.1007/s10533-018-0427-0

Barko, J.W., Smart, R.M., 1978. The growth and biomass distribution of two emergent freshwater plants, Cyperus esculentus and Scirpus validus, on different sediments. Aquat. Bot. 5, 109–117. https://doi.org/10.1016/0304-3770(78)90054-2

Bernardino, A.F., Pais, F.S., Oliveira, L.S., Gabriel, F.A., Ferreira, T.O., Queiroz, H.M., Mazzuco, A.C.A., 2019. Chronic trace metals effects of mine tailings on estuarine assemblages revealed by environmental DNA. PeerJ 2019. https://doi.org/10.7717/peerj.8042

Bernardino, A.F., Sanders, C.J., Bissoli, L.B., Gomes, L.E. de O., Kauffman, J.B., Ferreira, T.O., 2020. Land use impacts on benthic bioturbation potential and carbon burial in Brazilian mangrove ecosystems. Limnol. Oceanogr. 65, 2366–2376. https://doi.org/10.1002/lno.11458

Bhattacharyya, A., Campbell, A.N., Tfaily, M.M., Lin, Y., Kukkadapu, R.K., Silver, W.L., Nico, P.S., Pett-Ridge, J., 2018. Redox Fluctuations Control the Coupled Cycling of Iron and Carbon in Tropical Forest Soils. Environ. Sci. Technol. 52, 14129–14139. https://doi.org/10.1021/acs.est.8b03408

Blossfeld, S., Gansert, D., Thiele, B., Kuhn, A.J., Lösch, R., 2011. The dynamics of oxygen concentration, pH value, and organic acids in the rhizosphere of Juncus spp. Soil Biol. Biochem. 43, 1186–1197. https://doi.org/10.1016/j.soilbio.2011.02.007

Brookins, D.G., 1988. Eh-pH diagrams for geochemistry, 1st ed. Springer-Verlag Berlin Heidelberg. https://doi.org/10.1007/978-3-642-73093-1

Chmura, G.L., Anisfeld, S.C., Cahoon, D.R., Lynch, J.C., 2003. Global carbon sequestration in tidal, saline wetland soils. Global Biogeochem. Cycles 17, 1111. https://doi.org/10.1029/2002GB001917

Cionek, V.M., Alves, G.H.Z., Tófoli, R.M., Rodrigues-Filho, J.L., Dias, R.M., 2019. Brazil in the mud again: lessons not learned from Mariana dam collapse. Biodivers. Conserv. 28, 1935–1938. https://doi.org/10.1007/s10531-019-01762-3

Coelho, A.L.N., 2009. Bacia hidrográfica do Rio Doce (MG/ES): Uma análise socioambiental integrada. Geografares 7, 131–146. https://doi.org/10.7147/GEO00.0000

Cohen, M.C.L., França, M.C., de Fátima Rossetti, D., Pessenda, L.C.R., Giannini, P.C.F., Lorente, F.L., Junior, A.Á.B., Castro, D., Macario, K., 2014. Landscape evolution during the late Quaternary at the Doce River mouth, Espírito Santo State, Southeastern Brazil. Palaeogeogr. Palaeoclimatol. Palaeoecol. 415, 48–58. https://doi.org/10.1016/j.palaeo.2013.12.001

Cornwall, W., 2020. A dam big problem. Science (80-.). 369, 906–909. https://doi.org/10.1126/science.369.6506.906

Deletic, A., 2005. Sediment transport in urban runoff over grassed areas. J. Hydrol. 301, 108–122. https://doi.org/10.1016/j.jhydrol.2004.06.023

Di Nitto, D., Dahdouh-Guebas, F., Kairo, J., Decleir, H., Koedam, N., 2008. Digital terrain modelling to investigate the effects of sea level rise on mangrove propagule establishment. Mar. Ecol. Prog. Ser. 356, 175–188. https://doi.org/10.3354/meps07228

Donohue, S.W., Stolt, M.H., Gold, A., Groffman, P., 2009. Human-Transported Material Soils of Urbanizing Estuarine Landscapes. Soil Sci. Soc. Am. J. 73, 1587–1596. https://doi.org/10.2136/sssaj2008.0218

Duball, C., Vaughan, K., Berkowitz, J.F., Rabenhorst, M.C., VanZomeren, C.M., 2020. Iron monosulfide identification: Field techniques to provide evidence of reducing conditions in soils. Soil Sci. Soc. Am. J. 84, 303–313. https://doi.org/10.1002/saj2.20044

Escobar, H., 2015. Mud tsunami wreaks ecological havoc in Brazil. Science (80-.). 350, 1138–1139. https://doi.org/10.1126/science.350.6265.1138

Essington, M.E., 2015. Soil and Water Chemistry: An Integrative Approach, Second Edition, 2nd ed. CRC Press, Boca Raton, FL.

Ferreira, A.D., Queiroz, H.M., Kaneagae, M.P., Nóbrega, G.N., Otero, X.L., Bernardino, Â.F., Ferreira, T.O., 2021. Gypsum amendment induced rapid pyritization in fe-rich mine tailings from doce river estuary after the fundão dam collapse. Minerals 11. https://doi.org/10.3390/min11020201

Ferreira, A.D., Viana, D.G., Egreja Filho, F.B., Pires, F.R., Bonomo, R., Martins, L.F., Pinto Nascimento, M.C., Silva Cruz, L.B., 2019. Phytoremediation in flooded environments: Dynamics of barium absorption and translocation by Eleocharis acutangula. Chemosphere 219, 836–844. https://doi.org/10.1016/j.chemosphere.2018.12.074

Ferreira, T.O., Otero, X.L., Vidal-Torrado, P., Macías, F., 2007a. Redox Processes in Mangrove Soils under Rhizophora mangle in Relation to Different Environmental Conditions. Soil Sci. Soc. Am. J. 71, 484–491. https://doi.org/10.2136/sssaj2006.0078

Ferreira, T.O., Vidal-Torrado, P., Otero, X.L., Macías, F., 2007b. Are mangrove forest substrates sediments or soils? A case study in southeastern Brazil. CATENA 70, 79–91. https://doi.org/10.1016/j.catena.2006.07.006

Fiedler, S., Sommer, M., 2004. Water and Redox Conditions in Wetland Soils-Their Influence on Pedogenic Oxides and Morphology. Soil Sci. Soc. Am. J. 68, 326–335. https://doi.org/10.2136/sssaj2004.3260

Gabriel, F.A., Silva, A.G., Queiroz, H.M., Ferreira, T.O., Hauser-Davis, R.A., Bernardino, A.F., 2020. Ecological Risks of Metal and Metalloid Contamination in the Rio Doce Estuary. Integr. Environ. Assess. Manag. 16, 655–660. https://doi.org/10.1002/ieam.4250

Gee, G.W., Bauder, J.W., 1986. Particle-size analysis, in: Methods of Soil Analysis: Part 1—Physical and Mineralogical Methods. Soil Science Society of America, American Society of Agronomy, pp. 383–411.

Giannetta, B., Siebecker, M.G., Zaccone, C., Plaza, C., Rovira, P., Vischetti, C., Sparks, D.L., 2020. Iron(III) fate after complexation with soil organic matter in fine silt and clay fractions: An EXAFS spectroscopic approach. Soil Tillage Res. 200, 104617. https://doi.org/10.1016/j.still.2020.104617

Gomes, F.H., Ker, J.C., Ferreira, T.O., Moreau, A.M.S. dos S., Moreau, M.S., 2016. Characterization and pedogenesis of mangrove soils from Ilhéus - BA, Brazil. Rev. Ciência Agronômica 47, 599–608. https://doi.org/10.5935/1806-6690.20160072

Gomes, L.E. de O., Correa, L.B., Sá, F., Neto, R.R., Bernardino, A.F., 2017. The impacts of the Samarco mine tailing spill on the Rio Doce estuary, Eastern Brazil. Mar. Pollut. Bull. 120, 28–36. https://doi.org/10.1016/j.marpolbul.2017.04.056

Hatje, V., Pedreira, R.M.A., de Rezende, C.E., Schettini, C.A.F., de Souza, G.C., Marin, D.C., Hackspacher, P.C., 2017. The environmental impacts of one of the largest tailing dam failures worldwide. Sci. Rep. 7, 10706. https://doi.org/10.1038/s41598-017-11143-x

Huot, H., Simonnot, M.O., Marion, P., Yvon, J., De Donato, P., Morel, J.L., 2013. Characteristics and potential pedogenetic processes of a Technosol developing on iron industry deposits. J. Soils Sediments 13, 555–568. https://doi.org/10.1007/s11368-012-0513-1

Huot, H., Simonnot, M.O., Watteau, F., Marion, P., Yvon, J., De Donato, P., Morel, J.L., 2014. Early transformation and transfer processes in a Technosol developing on iron industry deposits. Eur. J. Soil Sci. 65, 470–484. https://doi.org/10.1111/ejss.12106

Hutchins, D.A., Boyd, P.W., 2016. Marine phytoplankton and the changing ocean iron cycle. Nat. Clim. Chang. https://doi.org/10.1038/nclimate3147

Inoue, Y., Hiradate, S., Sase, T., Hosono, M., Morita, S., Matsuzaki, H., 2011. Using 14C dating of stable humin fractions to assess upbuilding pedogenesis of a buried Holocene humic soil horizon, Towada volcano, Japan. Geoderma 167–168, 85–90. https://doi.org/10.1016/j.geoderma.2011.08.011

IUSS Working Group WRB, 2014. World reference base for soil resources 2014. International soil classification system for naming soils and creating legends for soil maps, World Soil Resources Reports No. 106. FAO, Rome.

Jay, D.A., Orton, P.M., Chisholm, T., Wilson, D.J., Fain, A.M.V., 2007. Particle trapping in stratified estuaries: Consequences of mass conservation. Estuaries and Coasts 30, 1095–1105. https://doi.org/10.1007/BF02841399

Kida, M., Fujitake, N., 2020. Organic Carbon Stabilization Mechanisms in Mangrove Soils: A Review. Forests 11, 981. https://doi.org/10.3390/f11090981

Kraemer, S.M., 2004. Iron oxide dissolution and solubility in the presence of siderophores. Aquat. Sci. - Res. Across Boundaries 66, 3–18. https://doi.org/10.1007/s00027-003-0690-5

Larsen, O., Postma, D., 2001. Kinetics of reductive bulk dissolution of lepidocrocite, ferrihydrite, and goethite. Geochim. Cosmochim. Acta 65, 1367–1379. https://doi.org/10.1016/S0016-7037(00)00623-2

Lee, R.Y., Porubsky, W.P., Feller, I.C., McKee, K.L., Joye, S.B., 2008. Porewater biogeochemistry and soil metabolism in dwarf red mangrove habitats (Twin Cays, Belize). Biogeochemistry. https://doi.org/10.1007/s10533-008-9176-9

Lindsay, W.L., 1991. Iron oxide solubilization by organic matter and its effect on iron availability. Plant Soil 130, 27–34. https://doi.org/10.1007/BF00011852

Lindsay, W.L., Schwab, A.P., 1982. The chemistry of iron in soils and its availability to plants. J. Plant Nutr. 5, 821–840. https://doi.org/10.1080/01904168209363012

Lovley, D.R., Holmes, D.E., Nevin, K.P., 2004. Dissimilatory Fe(III) and Mn(IV) Reduction, in: Advances in Microbial Physiology. pp. 219–286. https://doi.org/10.1016/S0065-2911(04)49005-5

Macreadie, P.I., Anton, A., Raven, J.A., Beaumont, N., Connolly, R.M., Friess, D.A., Kelleway, J.J., Kennedy, H., Kuwae, T., Lavery, P.S., Lovelock, C.E., Smale, D.A., Apostolaki, E.T., Atwood, T.B., Baldock, J., Bianchi, T.S., Chmura, G.L., Eyre, B.D., Fourqurean, J.W., Hall-Spencer, J.M., Huxham, M., Hendriks, I.E., Krause-Jensen, D., Laffoley, D., Luisetti, T., Marbà, N., Masque, P., McGlathery, K.J., Megonigal, J.P., Murdiyarso, D., Russell, B.D., Santos, R., Serrano, O., Silliman, B.R., Watanabe, K., Duarte, C.M., 2019. The future of Blue Carbon science. Nat. Commun. 10, 1–13. https://doi.org/10.1038/s41467-019-11693-w

Magris, R.A., Marta-Almeida, M., Monteiro, J.A.F., Ban, N.C., 2019. A modelling approach to assess the impact of land mining on marine biodiversity: Assessment in coastal catchments experiencing catastrophic events (SW Brazil). Sci. Total Environ. 659, 828–840. https://doi.org/10.1016/j.scitotenv.2018.12.238

Marta-Almeida, M., Mendes, R., Amorim, F.N., Cirano, M., Dias, J.M., 2016. Fundão Dam collapse: Oceanic dispersion of River Doce after the greatest Brazilian environmental accident. Mar. Pollut. Bull. 112, 359–364. https://doi.org/10.1016/j.marpolbul.2016.07.039

Martin, J.H., 1990. Glacial-interglacial CO2 change: The Iron Hypothesis. Paleoceanography. https://doi.org/10.1029/PA005i001p00001

Mello, C.R. de, Viola, M.R., Curi, N., Silva, A.M. da, 2012. Distribuição espacial da precipitação e da erosividade da chuva mensal e anual no Estado do Espírito Santo. Rev. Bras. Ciência do Solo 36, 1878–1891. https://doi.org/10.1590/S0100-06832012000600022

Mikutta, R., Kleber, M., Kaiser, K., Jahn, R., 2005. Review: Organic matter removal from soils using hydrogen peroxide, sodium hypochlorite, and disodium peroxodisulfate. Soil Sci. Soc. Am. J. 69, 120–135. https://doi.org/10.2136/sssaj2005.0120

Mitsch, W.J., Bernal, B., Nahlik, A.M., Mander, Ü., Zhang, L., Anderson, C.J., Jørgensen, S.E., Brix, H., 2013. Wetlands, carbon, and climate change. Landsc. Ecol. 28, 583–597. https://doi.org/10.1007/s10980-012-9758-8

Mudd, S.M., D'Alpaos, A., Morris, J.T., 2010. How does vegetation affect sedimentation on tidal marshes? Investigating particle capture and hydrodynamic controls on biologically mediated sedimentation. J. Geophys. Res. Earth Surf. 115, 1–14. https://doi.org/10.1029/2009JF001566

Munch, J.C., Ottow, J.C.G., 1983. Reductive Transformation Mechanism of Ferric Oxides in Hydromorphic Soils. Ecol. Bull. 383–394.

Nahlik, A.M., Fennessy, M.S., 2016. Carbon storage in US wetlands. Nat. Commun. 7, 1–9. https://doi.org/10.1038/ncomms13835

Nóbrega, G.N., Romero, D.J., Otero, X.L., Ferreira, T.O., 2018. Pedological Studies of Subaqueous Soils as a Contribution to the Protection of Seagrass Meadows in Brazil. Rev. Bras. Ciência do Solo 42, 1–12. https://doi.org/10.1590/18069657rbcs20170117

Otero, X.L., Ferreira, T.O., Huerta-Díaz, M.A., Partiti, C.S.M., Souza, V., Vidal-Torrado, P., Macías, F., 2009. Geochemistry of iron and manganese in soils and sediments of a mangrove system, Island of Pai Matos (Cananeia — SP, Brazil). Geoderma 148, 318–335. https://doi.org/10.1016/j.geoderma.2008.10.016

Palu, M.C., Julien, P.Y., 2019. Modeling the Sediment Load of the Doce River after the Fundão Tailings Dam Collapse, Brazil. J. Hydraul. Eng. 145, 05019002. https://doi.org/10.1061/(asce)hy.1943-7900.0001582

Pey, B., Cortet, J., Watteau, F., Cheynier, K., Schwartz, C., 2013. Structure of earthworm burrows related to organic matter of a constructed Technosol. Geoderma 202–203, 103–111. https://doi.org/10.1016/j.geoderma.2013.03.010

Prade, K., Ottow, J.C.G., Jacq, V., 1993. Excessive iron uptake (iron toxicity) by wetland rice (Oryza sativa L.) on an acid sulphate soil in the Casamance/Senegal. Int. Inst. L. Reclam. Improv. Wageningen, Netherlands. ILRI Publ. 44, 150–162.

Queiroz, H.M., Nóbrega, G.N., Ferreira, T.O., Almeida, L.S., Romero, T.B., Santaella, S.T., Bernardino, A.F., Otero, X.L., 2018. The Samarco mine tailing disaster: A possible time-bomb for heavy metals contamination? Sci. Total Environ. 637–638, 498–506. https://doi.org/10.1016/j.scitotenv.2018.04.370

Queiroz, H.M., Ying, S.C., Abernathy, M., Barcellos, D., Gabriel, F.A., Otero, X.L., Nóbrega, G.N., Bernardino, A.F., Ferreira, T.O., 2021. Manganese: The overlooked contaminant in the world largest mine tailings dam collapse. Environ. Int. 146, 106284. https://doi.org/10.1016/j.envint.2020.106284

Reddy, K.R., DeLaune, R.D., 2008. Biogeochemistry of wetlands: science and applications, 1st ed. CRC Press.

Rico, M., Benito, G., Salgueiro, A.R., Díez-Herrero, A., Pereira, H.G., 2008. Reported tailings dam failures. A review of the European incidents in the worldwide context. J. Hazard. Mater. 152, 846–852. https://doi.org/10.1016/j.jhazmat.2007.07.050

Ruiz, F., Cherubin, M.R., Ferreira, T.O., 2020a. Soil quality assessment of constructed Technosols: Towards the validation of a promising strategy for land reclamation, waste management and the recovery of soil functions. J. Environ. Manage. 276. https://doi.org/10.1016/j.jenvman.2020.111344

Ruiz, F., Resmini Sartor, L., de Souza Júnior, V.S., Cheyson Barros dos Santos, J., Osório Ferreira, T., 2020b. Fast pedogenesis of tropical Technosols developed from dolomitic limestone mine spoils (SE-Brazil). Geoderma 374, 114439. https://doi.org/10.1016/j.geoderma.2020.114439

Santana, P.H.L., Burak, D.L., Thiengo, C.C., Peçanha, A.L., Neves, M.A., Mendonça, E. de S., 2020. Jack beans and vetiver grass growth on iron ore tailing sediments from the Doce River dam disaster in Brazil: plant growth regulator effects under different edaphic conditions. J. Soils Sediments 20, 4103–4110. https://doi.org/10.1007/s11368-020-02774-1

Santini, T.C., Fey, M. V., 2016. Assessment of Technosol formation and in situ remediation in capped alkaline tailings. CATENA 136, 17–29. https://doi.org/10.1016/j.catena.2015.08.006

Santos, E.S., Abreu, M.M., Macías, F., 2019. Rehabilitation of mining areas through integrated biotechnological approach: Technosols derived from organic/inorganic wastes and autochthonous plant development. Chemosphere 224, 765–775. https://doi.org/10.1016/j.chemosphere.2019.02.172

Sarker, S., Masud-Ul-Alam, M., Hossain, M.S., Rahman Chowdhury, S., Sharifuzzaman, S., 2020. A review of bioturbation and sediment organic geochemistry in mangroves. Geol. J. gj.3808. https://doi.org/10.1002/gj.3808

Sartor, L.R., Graham, R.C., Ying, S.C., Otero, X.L., Montes, C.R., Ferreira, T.O., 2018. Role of Redox Processes in the Pedogenesis of Hypersaline Tidal Flat Soils on the Brazilian Coast. Soil Sci. Soc. Am. J. 82, 1217. https://doi.org/10.2136/sssaj2018.01.0023

Schaetzl, R.J., Thompson, M.L., 2015. Soils: Genesis and Geomorphology, 2nd ed. Cambridge University Press, New York, NY.

Schwertmann, U., 1958. The Effect of Pedogenic Environments on Iron Oxide Minerals. Springer, New York, NY, pp. 171–200. https://doi.org/10.1007/978-1-4612-5046-3_5

Séré, G., Ouvrard, S., Magnenet, V., Pey, B., Morel, J.L., Schwartz, C., 2012. Predictability of the Evolution of the Soil Structure using Water Flow Modeling for a Constructed Technosol. Vadose Zo. J. 11. https://doi.org/10.2136/vzj2011.0069

Service, R.F., 2020. Red alert. Science (80-.). 369, 910–911. https://doi.org/10.1126/science.369.6506.910

Seyfferth, A.L., Bothfeld, F., Vargas, R., Stuckey, J.W., Wang, J., Kearns, K., Michael, H.A., Guimond, J., Yu, X., Sparks, D.L., 2020. Spatial and temporal heterogeneity of geochemical controls on carbon cycling in a tidal salt marsh. Geochim. Cosmochim. Acta 282, 1–18. https://doi.org/10.1016/j.gca.2020.05.013

Silva, A.C., Cavalcante, L.C.D., Fabris, J.D., Júnior, R.F., Barral, U.M., Farnezi, M.M. de M., Viana, A.J.S., Ardisson, J.D., Fernandez-Outon, L.E., Lara, L.R.S., Stumpf, H.O., Barbosa, J.B.S., Silva, L.C. da, 2017. Características químicas, mineralógicas e físicas do material acumulado em terraços fluviais, originado do fluxo de lama proveniente do rompimento de barragem de rejeitos de mineração de ferro em Bento Rodrigues, Minas Gerais, Brasil. Rev. Espinhaço | UFVJM; Rev. Espinhaço #9.

Šimonovičová, A., Ferianc, P., Vojtková, H., Pangallo, D., Hanajík, P., Kraková, L., Feketeová, Z., Čerňanský, S., Okenicová, L., Žemberyová, M., Bujdoš, M., Pauditšová, E., 2017. Alkaline Technosol contaminated by former mining activity and its culturable autochthonous microbiota. Chemosphere 171, 89–96. https://doi.org/10.1016/j.chemosphere.2016.11.131

Singh, M.M., Rai, P.K., 2016. A microcosm investigation of fe (iron) removal using macrophytes of ramsar lake: A phytoremediation approach. Int. J. Phytoremediation 18, 1231–1236. https://doi.org/10.1080/15226514.2016.1193471

Stagg, C.L., Baustian, M.M., Perry, C.L., Carruthers, T.J.B., Hall, C.T., 2018. Direct and indirect controls on organic matter decomposition in four coastal wetland communities along a landscape salinity gradient. J. Ecol. 106, 655–670. https://doi.org/10.1111/1365-2745.12901

Tagliabue, A., Bowie, A.R., Boyd, P.W., Buck, K.N., Johnson, K.S., Saito, M.A., 2017. The integral role of iron in ocean biogeochemistry. Nature 543, 51–59. https://doi.org/10.1038/nature21058

Taylor, G.J., Crowder, A.A., 1983. Uptake and accumulation of heavy metals by Typha latifolia in wetlands of the Sudbury, Ontario region. Can. J. Bot. 61, 63–73. https://doi.org/10.1139/b83-005

Tombácz, E., Libor, Z., Illés, E., Majzik, A., Klumpp, E., 2004. The role of reactive surface sites and complexation by humic acids in the interaction of clay mineral and iron oxide particles. Org. Geochem. 35, 257–267. https://doi.org/10.1016/j.orggeochem.2003.11.002

Torrent, J., Schwertmann, U., Fechter, H., Alferez, F., 1983. Quantitative relationships between soil color and hematite content. Soil Sci. 136, 354–358. https://doi.org/10.1097/00010694-198312000-00004

USDA, 2017. Soil Survey Manual Agriculture. Handbook 18. USDA, Nat. Resour. Conserv. Serv. 18, 483.

USDA, U.S.D. of A., 2015. Soil Taxonomy, version 2. ed, Illustrated Guide to Soil Taxonomy. Soil Survey Staff - Natural Resources Conservation Service Soil, Lincoln, Nebraska. https://doi.org/10.2134/jae.1982.0003

Veneman, P.L.M., Spokas, L.A., Lindbo, D.L., 2015. Soil Moisture and Redoximorphic Features: A Historical Perspective, in: Quantifying Soil Hydromorphology. pp. 1–23. https://doi.org/10.2136/sssaspecpub54.c1

Vidal-Torrado, P., Ferreira, T.O., Otero, X.L., Souza-Júnior, V.S., Ferreira, F.P., Andrade, G.R.P., Macías, F., 2010. Pedogenetic processes in mangrove soils, in: Biogeochemistry and Pedogenetic Process in Saltmarsh and Mangrove Systems. pp. 27–56.

Wang, J.Q., Zhang, X.D., Jiang, L.F., Bertness, M.D., Fang, C.M., Chen, J.K., Hara, T., Li, B., 2010. Bioturbation of Burrowing Crabs Promotes Sediment Turnover and Carbon and Nitrogen Movements in an Estuarine Salt Marsh. Ecosystems 13, 586–599. https://doi.org/10.1007/s10021-010-9342-5

Weiler, J., Firpo, B.A., Schneider, I.A.H., 2020. Technosol as an integrated management tool for turning urban and coal mining waste into a resource. Miner. Eng. 147, 106179. https://doi.org/10.1016/j.mineng.2019.106179

Wiederhold, J.G., Teutsch, N., Kraemer, S.M., Halliday, A.N., Kretzschmar, R., 2007. Iron Isotope Fractionation during Pedogenesis in Redoximorphic Soils. Soil Sci. Soc. Am. J. 71, 1840–1850. https://doi.org/10.2136/sssaj2006.0379

Yin, S., Bai, J., Wang, W., Zhang, G., Jia, J., Cui, B., Liu, X., 2019. Effects of soil moisture on carbon mineralization in floodplain wetlands with different flooding frequencies. J. Hydrol. 574, 1074–1084. https://doi.org/10.1016/j.jhydrol.2019.05.007

Zhao, Q., Dunham-Cheatham, S., Adhikari, D., Chen, C., Patel, A., Poulson, S.R., Obrist, D., Verburg, P.S.J., Wang, X., Roden, E.R., Thompson, A., Yang, Y., 2020. Oxidation of soil organic carbon during an anoxic-oxic transition. Geoderma 377, 114584. https://doi.org/10.1016/j.geoderma.2020.114584

Zhou, Y. wu, Peng, Y. sheng, Li, X. lin, Chen, G. zhu, 2011. Accumulation and partitioning of heavy metals in mangrove rhizosphere sediments. Environ. Earth Sci. 64, 799–807. https://doi.org/10.1007/s12665-011-0904-4

9. FINAL CONSIDERATIONS

Each year new approaches emerge in the way Earth surface systems are studied by geochemists. Geochemistry pursuits the relationships between elements and at the same time their behavior and interactions in different terrestrial environments. In this context, iron (Fe) has always been an intriguing element reported in many geochemical studies on Earth's ecosystems. Its great abundance is directly proportional to its importance on a variety of biogeochemical cycles. This perspective brings Fe to the central stage of the biogeochemical cycles in an era of disturbances driven by humanity and climate change.

In this study, a great range of analytical techniques were employed to the understanding of Fe geochemistry in tropical estuarine soils affected by both anthropic and natural impacts and to assess its control over the dynamic of other important elements (i.e., metals, P, S, and C).

Our results revealed a great sensibility of the Fe biogeochemical cycle in mangrove forests against a future scenario of climate change exhibiting a lowered capacity for metals immobilization and carbon sequestration. These changes were driven by a massive mangrove forest loss. Under this condition decreases in SCS up to 33% and Fe losses of up to 50% were reported. Such a case affected the biogeochemistry and the dynamic of other elements (e.g., S and C). As a result, the dead mangrove soils showed a decreased ability to provide carbon sequestration and immobilization of potentially toxic elements (e.g., metals). Moreover, a loss of 170 tons of Fe from dead mangrove forests to estuarine water and ocean were estimated.

In a different scenario, the Samarco mine disaster involved the spillage of millions of tons of Fe-enriched tailings into the Doce River estuary. The dominant crystalline Fe forms that settled in the estuarine wetland soils were found to be closely associated with trace metals and a large P load. The transitory/cyclic anoxic conditions (common in estuarine soils) solubilized the Fe oxyhydroxides, releasing the associated metals and leading to a chronic contamination. Indeed, as predicted, the tailings' deposition favored the establishment and growth of plants which promoted a soil C input favoring the reductive dissolution of Fe oxyhydroxides.

Once these minerals were solubilized, metals, especially manganese (Mn), and a large amount of P were also made available. The increase in Mn bioavailability led to an increase in Mn levels in fish tissues which are commonly consumed by the local population. The Mn

bioavailability increased in response to the ephemeral control exerted by Fe oxyhydroxides on Mn bioavailability. These minerals were gradually solubilized and replaced by poorly crystalline Fe oxides which are easily reduced. Moreover, the redox conditions observed in the estuarine soil were highly conducive to the reductive dissolution of Mn^{III} and Mn^{IV} containing poorly crystalline oxides, which led to the continued increase in dissolved Mn. For phosphorus, the dissimilatory Fe reduction led to an increase of readily available P in the estuarine soils and water posing a eutrophication risk. Although Fe oxyhydroxides have been widely known to play a key role in the immobilization of P in soils, they actually triggered a rapid release of P in the studied estuarine soils.

The Fe geochemistry approach also revealed another face of the disaster. Within four years fast plant colonization coupled with Fe dynamic led to the formation of an Anthropogenic estuarine soil (i.e., a *Tidalic Spolic Technosol*). This soil seems to provide ecosystem services (i.e., carbon sequestration, nutrient cycling) previous unprovided by the estuarine soils. This study sheds new light on the time frame for soil formation, the resilience of tropical estuarine ecosystems, and to the unwinding of the world's largest mining disaster.

This study brings new insights on how Fe biogeochemistry in estuarine soils may regulate the fate of elements such as S, Fe, C, P, and metals in response to future climate changes and anthropogenic impacts. Certainly, these findings bring Fe to the center for future long-term studies in order to monitor the evolution of impacts caused by anthropic or natural disasters in estuarine ecosystems.